Second Series *October, 1927* *Vol. 30, No. 4*

THE

PHYSICAL REVIEW

THE DETERMINATION OF CERTAIN OUTER X-RAY ENERGY LEVELS FOR THE ELEMENTS FROM ANTIMONY (51) TO SAMARIUM (62)

By Katherine Chamberlain and George A. Lindsay

Abstract

X-ray L absorption edges and corresponding emission lines for elements Sb(51) to Sa(62).—The three L absorption edges and certain adjacent emission lines of the same element were photographed for series of ten elements from antimony to samarium. Thus a direct measurement of the distances on the photographic plates from the $L\beta_2$ line to the L_{III} edge, from $L\gamma_1$ to L_{II}, and from $L\gamma_4$ to L_I made possible the determination of the N_{IV}, N_V, and O_{II-III} energy levels respectively. In certain cases the edge and line were obtained on separate plates having the same reference line. The method seems to be an advantageous one in cases in which the energy of the desired level is so small that a slight error in the wave-length of either absorption edge or emission line would make a considerable error when computations are based upon determinations of these by different investigators. Particulars are given concerning the making of *absorbing screens containing free antimony, tellurium and iodine.* With these screens the L_I absorption edges for Sb(51), Te(52), and I(53) were found at 2631.7, 2503.9 and 2383.9 x-units; L_{II} edges at 2821.9, 2679.3 and 2547.5 x-units; and L_{III} edges at 2990.7, 2845.7 and 2713.9 x-units, respectively.

Variation with atomic number of the values of the N_{IV}, N_V and O_{II-III} energy levels.—The N_{IV} and N_V levels, which form a relativity doublet, are very close together in the case of the lower elements studied and show a slightly greater separation for the higher elements. All the curves showing the variation of energy level with atomic number show a distinct bend at lanthanum (57) as is to be expected according to the existing theory, for the next element, cerium, marks the beginning of the rare-earth group. The O_{II-III} curve for antimony, tellurium and iodine runs nearly horizontal, and as this level represents the outermost occupied orbit in these elements, the values obtained should be related to the ionizing potential. The values so computed are of the proper relative order of magnitude but are somewhat lower than the values obtained by other methods. This would indicate that the beginning of the absorption edge represents transitions to optical orbits rather than to infinity.

THE present work was undertaken in the attempt to increase the accuracy of the values of the outer energy levels of ten elements from antimony (51) to samarium (62) by photographing the L absorption spectra and emission lines of the same element that fell near the edge on the same plate. Thus, a direct measurement of the distance from the absorption edge to an emission line emitted when electron transitions take place between an N or an O level and the L level in question was made possible and promised to

afford a more accurate determination of these N and O levels than was to be expected when the calculations were based upon experimental data in which the emission lines have been measured by one investigator and the absorption limits by another.

Only one emission line was used for each edge, the $L\beta_2$ line for the L_{III} edge, $L\gamma_1$ for L_{II}, and $L\gamma_4$ for L_I. The difference in ν/R between the edge and the reference line in the three cases gave ν/R for the N_V level, the N_{IV}, and O_{II-III} respectively. It is apparent that small errors in the wave-length of the reference lines would not have an appreciable effect upon the computations involved in these outer levels. From the Bragg formula, a small difference, $\Delta\lambda$, is very approximately given by $\Delta\lambda = 2d\cos\theta\Delta\theta = (d/r)\cos\theta\Delta s$ where d is the grating constant, r the radius of the spectrograph, and Δs the distance on the plate between absorption edge and reference line. This last distance was never much more than 2 mm so that an error of two or three x-units in the reference line would have no appreciable effect upon the value of ν/R for the outer level under consideration. The angle $\Delta\theta$ corresponding to Δs, calculated from the plate measurements and subtracted from the angle θ for the reference line, gave us the angle θ corresponding to the edge with reference to the emission line. Other levels might have been determined in the same way but it was not apparent that the method would present any particular advantage unless the line fell close to the edge concerned. The elements used seemed of especial interest, as they represent an important region in the Periodic Table. It is worthy of mention that the L absorption limits obtained here for antimony, tellurium and iodine represent the *free* element and thus give the energy level values most characteristic of the element concerned.

The L_I edge and the γ_4 line fall so close to each other that it was thought best to photograph them upon alternate horizontal portions of the same plate so that they would not be superposed. In some cases, they were photographed on separate plates together with a common reference line. It was also essential to remove all traces of the elements concerned from the target and focussing cylinder before making an L_I absorption edge, for traces of the γ_4 line might have been mistaken for this faint edge. It seemed conclusive that this had not occurred when the stronger $\gamma_{2,3}$ lines did not appear on the portion of the plate carrying the absorption. The exposures for the absorption edges were from two to four hours in length and for the emission lines from ten minutes for γ_1 or β_2, to an hour for γ_4.

Description of Apparatus

A Siegbahn precision vacuum spectrograph with a radius of approximately 18 cm was employed. The fore-pump used was a large two-stage oil pump. For the earlier part of the work, a Gaede molecular pump was used as a finishing pump and for the last part a mercury diffusion pump with liquid air. Transformers were used as the source of high potential with voltage regulation by means of rheostats in the primary circuits. The crystal was calcite.

Preparation of the Absorbing Screens

As mentioned previously, the free elements were used in making the absorbing screens containing iodine, tellurium and antimony. Above xenon, the screens were prepared with the following compounds.

$$CsCl,\ BaCl_2,\ La(NO_3)_3,\ Ce(NO_3)_3,\ Pr_2(SO_4)_3,$$
$$Nd(NO_3)_3 \cdot 2NH_4NO_3 \cdot 4H_2O,\ Sm_2(SO_4)_3$$

All of the salts used were soluble either in water or in an acid solution sufficiently dilute so that it did not destroy the paper of the absorbing screen. The screens were prepared by soaking a piece of paper in the solution and drying it rapidly over a Bunsen flame. In general, a satisfactory screen contained from 3 to 8 mg of the compound per cm^2.

In the case of antimony, tellurium and iodine, the conditions for securing satisfactory absorption edges seem much more critical than is the case with the elements investigated above xenon and the increase in difficulty would appear to be too abrupt to be due merely to the increase in wave-length of the absorption edges. It is suggested that this may be at least partly due to the multi-valent nature of these elements. Coster has shown[1] that their different valence forms have L_{III} absorption edges differing from one another by one or two x-units. Moreover, it has been shown by one of the writers[2] that the x-ray beam may exert an appreciable reducing or oxidizing action upon a portion of the material in the absorbing screen. Thus, we could expect a superposition of the absorption edges of the different valence forms that would tend to reduce the sharpness of the main edge. The free element has the absorption edge of longest wave-length so that it would seem likely that the above difficulty would be minimized by using the free element to make the absorbing screen. Then, if secondary edges were produced because of change in valence of part of the material on the absorbing screen, they would fall on the short wave-length side of the main edge, i.e. in the region in which absorption is most marked and so would not have a tendency to obliterate the main edge by being partly superposed over it.

Some difficulty was experienced in producing screens containing the free element that were sufficiently thin and homogeneous to give satisfactory absorption since the usual method of soaking a paper in a solution of the substance was inapplicable. Tellurium was ground finely in an agate mortar and rubbed on paper in the dry state. For antimony, however, this method was not entirely satisfactory.

A very much finer form of metallic antimony was secured by a chemical precipitation. Hydrochloric acid was added to a water solution of potassium antimony tartrate until the precipitate first formed dissolved and a sheet of pure zinc was then placed in it. The zinc displaced the antimony from the solution of its salt and the latter collected as a very finely divided precipitate on the surface of the zinc. This precipitate was scraped off, washed repeatedly by decantation and filtered and in this way metallic antimony was

[1] Coster, Zeits. f. Physik **25**, 83 (1924).
[2] Chamberlain, Phys. Rev. **26**, 525 (1925).

secured having physical characteristics not unlike those of very finely powdered graphite. A very thin layer of this wet precipitate was spread over both sides of a piece of gold-beater's skin that had been previously weighed, and the whole was dried rapidly, after which it was weighed again and found to have about 1.5 mg of antimony per cm². For the L_{III} edge, two layers, for the L_{II} edge four layers, and for the L_I edge six layers of the absorbing screen were used representing approximately 3, 6 and 9 mg of the metal per cm² respectively. With these screens satisfactory plates were obtained for all three absorption edges without difficulty.

A difficulty presented by free iodine is its tendency to sublime, for unless it is enclosed in an air-tight envelope, the iodine will all leave the absorbing screen in a very short time, particularly if it is in an extremely finely divided state. Iodine was precipitated by adding a water solution of potassium iodide to one of an excess of iodic acid and the precipitate of free iodine was washed, filtered, dried and spread in a very thin layer on gold-beater's skin. It was immediately sealed in an envelope of gold-beater's skin with collodion and kept in a desiccator in the presence of excess of iodine. This screen contained approximately 6 mg of iodine per cm² and the L_{III} edge was obtained with it without pumping out the spectrograph chamber.

It was apparent that a screen made by dissolving iodine in collodion would fulfill the condition of having the absorbing substance in an extremely finely divided state and could be used more satisfactorily in a vacuum. Iodine forms complexes, however, when dissolved in alcohol and if these were not destroyed when the alcohol in the collodion evaporated, the absorption edge might represent the compound instead of the free element. It seemed important that it should not do so, for slight variations in the wave-length of the absorption edge from this cause might produce a difference by no means negligible in the O_{II-III} energy level. A weighed amount of iodine was dissolved in alcohol in a small vial, about one cc of collodion added and the whole spread in a thin layer on the bottom of a glass dish after mixing thoroughly. The collodion film obtained contained approximately one-third mg of iodine per cm² and six layers were used for the absorbing screen. The film appeared light brown in color and perfectly homogeneous but it is essential not to dissolve too much iodine in a given amount of collodion or it will form crystalline patterns on the surface of the later with a consequent loss of homogeneity of the screen.

A comparison of the plates made of the L_{III} edge with the precipitated iodine screen and the collodion screen showed no appreciable shift of the absorption edge so it seemed safe to assume that any complexes formed by the alcohol were destroyed again or that the absorption edge of the complex did not differ appreciably from that of the free element. The collodion screen was therefore used for the remainder of the iodine edges and proved entirely satisfactory in a vacuum. The edges obtained, including L_I, were reasonably sharp and showed excellent contrast.

Table I contains the wave-lengths of the L absorption edges for free antimony, tellurium and iodine as computed from our measurements, together with the values of ν/R.

TABLE I

Wave-lengths of the L absorption edges for free antimony, tellurium and iodine.

Element	Absorption edge	Wave-length	ν/R	Reference line
51 Sb	L_I	2631.7 x-units	346.3	Sb $L\gamma_4$
	L_{II}	2821.9	322.9	Sb $L\gamma_1$
	L_{III}	2990.7	304.7	Sb $L\beta_2$
52 Te	L_I	2503.9	363.9	Te $L\gamma_4$
	L_{II}	2679.3	340.1	Te $L\gamma_1$
	L_{III}	2845.7	320.2	Te $L\beta_2$
53 I	L_I	2383.9	382.3	I $L\gamma_4$
	L_{II}	2547.5	357.7	I $L\gamma_1$
	L_{III}	2713.9	335.8	I $L\beta_2$

The values for the reference lines are taken from Coster's[3] and Nishina's[4] tables.

Table II gives the values of ν/R for the energy levels considered here.

TABLE II

Values of the energy levels, ν/R

	Sb	Te	I	Cs	Ba	La	Ce	Pr	Nd	Sm
N_{IV}	2.61	3.42	4.16	6.04	7.09	8.08	8.51	9.01	9.28	10.07
N_V	2.61	3.39	3.91	5.73	6.70	7.83	8.36	8.83	9.08	9.40
O_{II-III}	0.25	0.26	0.38	1.08	1.56	2.34	2.41	2.55	2.67	2.53

TABLE III

The square root of the values of the energy levels, $(\nu/R)^{1/2}$.

	Sb	Te	I	Cs	Ba	La	Ce	Pr	Nd	Sm
N_{IV}	1.62	1.85	2.04	2.46	2.66	2.84	2.92	3.00	3.05	3.17
N_V	1.62	1.84	1.98	2.39	2.59	2.80	2.89	2.98	3.01	3.07
O_{II-III}	0.50	0.51	0.62	1.04	1.25	1.53	1.55	1.60	1.63	1.59

TABLE IV

Energy levels in equivalent volts.

	Sb	Te	I	Cs	Ba	La	Ce	Pr	Nd	Sm
N_{IV}	35.4	46.3	56.3	81.8	96.0	109.4	115.3	122.0	125.7	136.4
N_V	35.3	45.9	53.0	77.6	90.7	106.1	113.2	119.6	123.0	127.3
O_{II-III}	3.4	3.5	5.2	14.6	21.1	31.8	32.6	34.5	36.2	34.3

DISCUSSION OF RESULTS

Figure 1 is a graph of the N_{IV}, N_V and O_{II-III} energy level diagrams obtained by plotting $(\nu/R)^{1/2}$ against the atomic number. Graphs obtained in this way are usually approximately straight lines that rise gradually with increasing atomic number. At the points at which electrons begin to be inserted again in groups previously in a state of temporary completion, the increase in energy is less because of shielding so that the level diagrams show a bend at the element before which this has occurred. Succeeding values lie in the new direction and the graph continues approximately linear. All three of our graphs are represented by two such portions that meet at lan-

[3] Coster, Phil. Mag. **43**, 1070 (1922) and **44**, 546 (1922).

[4] Nishina, Phil. Mag. **49**, 521 (1925).

thanum and the curves show a bend at that point. This is exactly what would be expected, for the next element, cerium, marks the beginning of the rare earth group and Bohr has stated that electrons begin to be inserted here in 4_4 orbits. This produces a distinct shielding effect upon these outer orbits so that they increase in energy less rapidly with increasing atomic number than previously, as is made apparent by a change of direction of the graphs and a distinct bend at the element before which the 4_4 group begins to receive electrons.

Since free elements were used in the absorbing screens for antimony, tellurium, and iodine, and compounds for the higher elements, this would

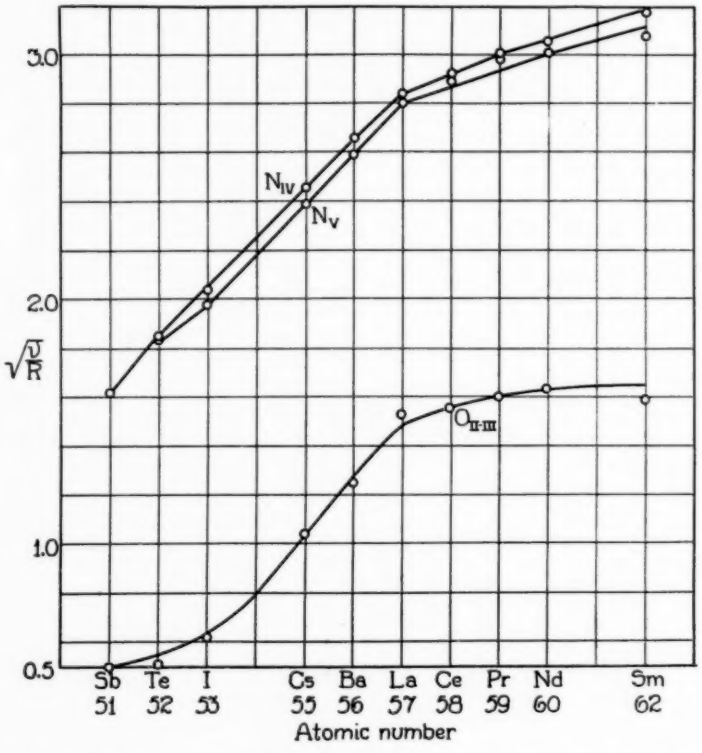

Fig. 1. Graph of the N_{IV}, N_V and O_{II-III} energy levels as functions of atomic number.

have a tendency to displace our energy level diagrams upward from caesium to samarium as the wave-length of the absorption edge with a compound is usually slightly less than with a free element. The only one of these elements whose absorption we have obtained in the free state is cerium and this shows little shift in the location of the absorption edges made with the free element as compared with those made with compounds, so it seems likely that the values of $(\nu/R)^{1/2}$ obtained here would be only slightly altered had it been practicable to use the free element in every case.

The O_{II-III} level is of particular interest because it represents the outermost occupied orbit in the case of antimony, tellurium and iodine and would

thus appear to offer direct experimental evidence of the precise meaning to be attached to absorption edge determinations such as these. Figure 2 is a diagram to represent the possible electron transitions that might be expected for these three elements. An electron ejected from the L_I orbit might go to infinity and a valency electron from O_{II-III} might drop back into the vacated place as is represented by A in the diagram. If this is the case, the energy difference in equivalent volts between the L_I edge and the γ_4 line should be equal to the ionizing potential. Another possibility is that the ejected electron from L_I can stop in the incompletely filled O_{II-III} level and an electron drop back from this same level to L_I giving rise to γ_4 radiation which would mean that the energy difference in equivalent volts between L_I and γ_4 would be zero. This is represented by B in Figure 2. The third possibility is that the electron ejected from L_I goes to a virtual orbit and one then drops back from O_{II-III} as is represented by C in the diagram.

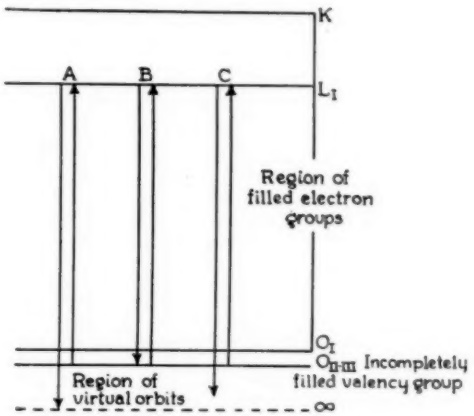

Fig. 2. Diagram to represent the possible electron transitions that might be expected in the case of antimony, tellurium and iodine.

In this case the energy difference in equivalent volts between the L_I edge and the γ_4 line would have a value somewhat less that the ionizing potential.

It will be noted that our values for O_{II-III} for antimony, tellurium and iodine are intermediate between zero and the ionizing potential. It will be realized that the actual separation of L_I and γ_4 in these cases is very small, smaller even than the correction applied for the half slit width. Moreover, these edges show a distinct gradient in blackening which raises a question regarding exactly which portion is to be considered the real beginning of the absorption. Our measurements were made by setting the microscope on the extreme limit of the blackest portion and then 0.05 mm was applied as a correction for the half slit width. Another difficulty is that γ_4 is an unresolved pair of lines and so not as narrow as could be desired.

For the reasons mentioned, it does not seem practicable to attempt to state too definitely the orbit to which transitions have occurred as indicated by the beginning of the absorption edge. It does seem possible, how-

ever, to state that the value of O_{II-III} obtained in this way cannot be as great as the ionizing potential, and to offer this as additional evidence that transition from inner orbits to virtual orbits do occur. Kossel,[5] Coster and van der Tuuk,[6] and Andrewes, Davies and Horton[7] have also offered evidence of such transitions. This would apparently imply that all energy level determinations obtained as was done here represent the energy required to take an electron from the inner orbit concerned to infinity diminished by an appreciable fraction of the ionizing potential.

It might be noted that antimony, tellurium and iodine represent a particularly favorable group of elements in which to investigate the outermost occupied orbit. In the case of heavier elements K or L emission lines repre-

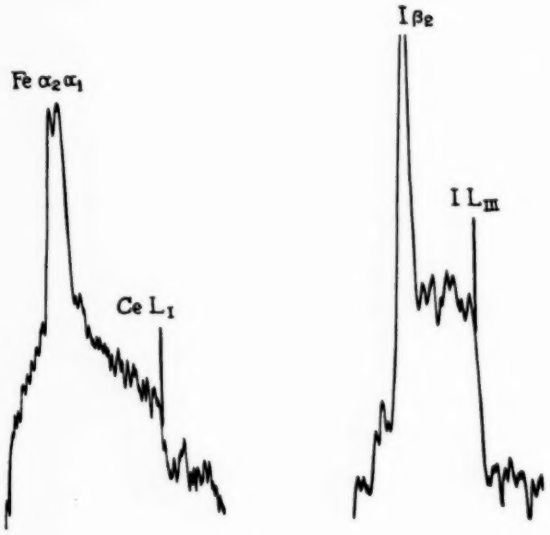

Fig. 3.

Fig. 4.

Fig. 3. Microphotometric records of absorption edges.
Fig. 4. Photograph of absorption edges.

senting the transition from the valency orbit are known for relatively few elements and similar investigations in the M series would represent much greater uncertainty and difficulty. In the case of lighter elements, experimental difficulties are increased by the necessity of dealing with longer wavelengths and by the increasing lack of sharpness of edges or lines representing transitions involving the valency ring.

Another interesting point is that the increase in ν/R from barium to lanthanum is as much as that from caesium to barium. The electron added at lanthanum is usually put back in a 5 quantum orbit while the two added just previously have gone into 6_1. If this last added electron does go into a

[5] Kossel, Zeits. f. Physik **1,** 119 (1920).
[6] Coster and van der Tuuk, Zeits. f. Physik **37,** 367 (1926).
[7] Andrewes, Davies and Horton, Proc. Roy. Soc. **A110,** 64 (1926).

5 quantum group, it might be expected to exert rather greater shielding than if it were added in a 6 quantum group and this would be made evident by a smaller increase in ν/R between barium and lanthanum than between caesium and barium. Beyond cerium, the O_{II-III} level runs horizontally within the limits of experimental error, as is to be expected in the case of elements representing the rare earth group.

Figures 3, 4 show photometric records and reproductions of certain absorption edges. As has usually been found with the free element on the absorbing screen, the iodine L_{III} edge shows a single discontinuity and no fine structure. The Ce L_I with cerium nitrate on the screen is of interest because it is unusually sharp for an L_I edge and gives evidence of the presence of a faint secondary edge on the short wave-length side of the main edge.

PHYSICS LABORATORY,
UNIVERSITY OF MICHIGAN,
June 20, 1927.

THE SECOND SPARK SPECTRUM OF ZINC, Zn III

By Otto Laporte and R. J. Lang

Abstract

New accurate wave-lengths of the spectrum of the high-potential spark between zinc electrodes made it possible to identify the most important line groups of Zn III, after their position and separations had been predicted closely by means of the screening and relativistic doublet laws respectively. The *ionization potential* of the shell of ten equivalent 3_3 electrons is found to be 40 volts.

I. Introduction

THE investigation and comparison of iso-electronic spectra, i.e., of spectra emitted by atoms and ions with the same number of electrons has become one of the main problems of modern ultra-violet spectroscopy. It was found by Millikan and Bowen[1] that for families of iso-electronic spectra (such as Na, Mg^{+}, Al^{2+}, Si^{3+} $\cdots$) the regular and irregular doublet laws of the x-ray region furnish a powerful tool for predicting location and separations of line groups. The spectra which have thus been investigated, have however been always of the type which Heisenberg[2] designated as "normal," i.e., spectra of first or higher rank but with small level-separations.

In the following we shall show that the above-mentioned methods can also be applied to spectra with a high number of electrons and with large separations between sub-levels which are comparable with the separations between different terms. The second spark spectrum of zinc seems most suitable for an investigation as the structure of its less-ionized analogues Ni I[3] and Cu II[4] is well known. Also these two spectra follow fairly well the irregular doublet law, as Table I shows, and one may thus expect to be able to predict the location of homologous groups for the Zn III. As explanation of Table I, it may suffice that in Ni I and Cu II two ^3D terms are known which

Table I

	$^3D(3d^9, 4s)$	$^3D - ^3D'$	$^3D'(3d^9, 4p)$	$\Delta\nu^{1/2}$
Ni I	62750	29464	33290	68.0
Cu II	144200	48915	95290	71.5

are due to the configuration $(3d)^9$ $(4s)$ and $(3d)^9$ $(5s)$ respectively. By means of a simple Rydberg formula one can determine the absolute term values for $^3D(3d^9, 4s)$ which are given in the first column. Another (primed) ^3D term arising from $(3d)^9$ $(4p)$ combines most conspicuously with $^3D(3d^9, 4s)$ in a

[1] Papers in the Physical Review.
[2] W. Heisenberg, Zeits. f. Physik **32,** 841 (1925).
[3] K. Bechert and L. A. Sommer, Ann. d. Physik **77,** 351 (1925).
[4] A. G. Shenstone, Phys. Rev. **29,** 380 (1927).

multiplet whose frequency is written in the second column. In the third column the term value of $^3D(3d^9, 4p)$ is given. The differences of the square roots of the term values are approximately the same in both spectra as it should be if the two terms form an irregular doublet.

Not only the location of the group $^3D(3d^9, 4s) - ^3D(3d^9, 4p)$ can thus be computed for Zn III but also the $\Delta\nu$ of the terms may be predicted with good accuracy by means of the relativistic doublet law and of certain data on the first spark spectrum of zinc as given by v. Salis.[5] We shall show in a later paragraph, how the classified line groups agree with theoretical and empirical laws.

In the earlier stage of the investigation the identification of the line groups of Zn III was based to a large extent on such theoretical considerations. The published wave-length material on the ultra-violet spectrum of zinc, as contained in papers of R. W. Wood[6] and of R. A. Sawyer[7] was not reliable and complete enough to establish the terms and levels merely by means of constant frequency differences. Only after new photographs of the high-potential spark spectrum of zinc had been taken at Edmonton, and thus wave-length material of much higher accuracy and completeness had become available, did the classification of the lines around 1600A become entirely unambiguous and the identification of the three lines at 700A which establish the fundamental level of Zn^{++} was made possible.

2. Experimental Procedure

The vacuum-spark between electrodes of pure metallic zinc was photographed by means of a two-meter grating having 30,000 lines per inch, which has been described previously.[8] The dispersion obtained is about 4.5A per mm resulting in an error of measurement which does not exceed 0.05A at least as far as 1000A. The grating was ruled by Professor Wood of Johns Hopkins University on speculum and gives excellent results in the region 2000–1000A. It shows Rowland ghosts conspicuously about the strong lines but these because of their symmetry of position do not cause much confusion.

The standards of wave-length used were carbon lines, together with the hydrogen line 1215.68, standardized by Smith and Lang.[9] In one case the carbon line 1931.03 given by Bowen and Ingram[10] was used.

Two samples of zinc were used, one of which was purchased from the Powers-Weightman-Rosengarten Co. and the other was very generously supplied by the New Jersey Zinc Co. of America. Both these samples were found to be of high purity. In the case of the latter no known lines of impurities were found in the spectrum except those of hydrogen and carbon, the latter being introduced purposely in order to obtain standards. Fig. 1 is a reproduction of one of the photographs taken at Edmonton, showing the

[5] G. v. Salis, Ann. d. Physik **76,** 145 (1925).
[6] R. W. Wood, Phil. Mag. **46,** 741 (1923).
[7] R. A. Sawyer, Astrophys. J. **52,** 286 (1920).
[8] R. J. Lang, Jour. Opt. Soc. Amer. **12,** 523 (1926).
[9] Stanley Smith and R. J. Lang, Phys. Rev. **28,** 36 (1926).
[10] J. S. Bowen and S. B. Ingram Phys. Rev. **28, 444 (1926).**

region from 1850 to 1400A. The classified lines are marked on the upper margin.

3. The Classification of the Lines

In Table II the frequency scheme of the classified lines of Zn III is given. At the left and at the top of the table the relative term values are given

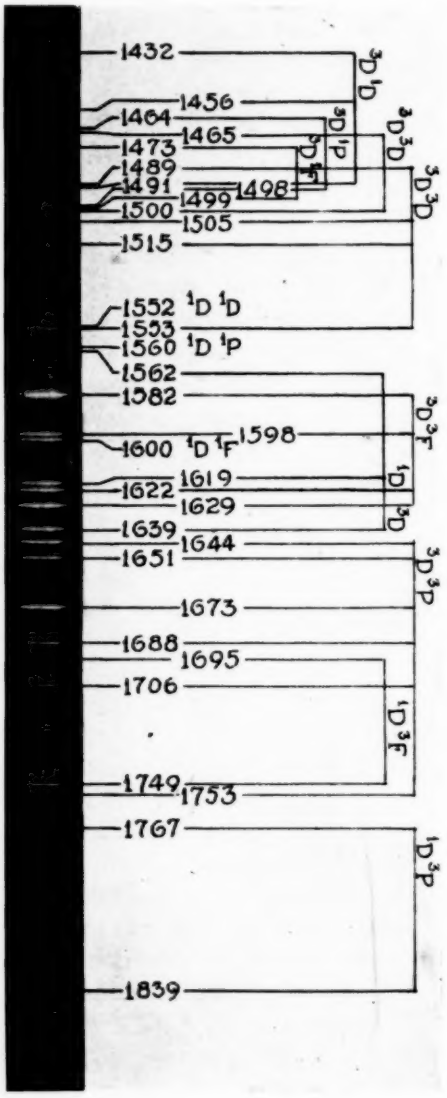

Fig. 1. Photograph of the zinc spectrum in the region from 1850 to 1400A.

taking the lowest term to be zero. The numbers in parentheses are the intensities. The satisfactory constantcy of the frequency differences (which are italicized in Table II) proves the accuracy of the wave-lengths. Except

for the $\Delta\nu$ which are linked to line ν 64391, an unresolved doublet, the differences show a fluctuation of only a few wave-number units.

TABLE II

Classification of the lines of Zn III.

		$^1S_0$ 0	$^3D_3$ 78105	*1178*	$^3D_2$ 79283	*1576*	$^3D_1$ 80859	*2650*	$^1D_2$ 83509
			(9)		(6)		(3)		(4)
$^3P_2$	137876		59771	*1178*	58593	*1577*	57016	*2650*	54366
					2204		*2205*		*2203*
		(3)			(10)		(7)		(7)
$^3P_1$	140080	140080			60797	*1576*	59221	*2652*	56569
							1321		
							(8)		
$^3P_0$	141401						60542		
			(15)						
$^3F_4$	141335		63230						
			−672						
			(8)		(10)				(9)
$^3F_3$	140664		62558	*1177*	61381				57154
			1833		*1827*				*1827*
			(x)		(10)		(10)		(3)
$^3F_2$	142491		64391	*1183*	63208	*1575*	61633	*2652*	58981
			2012						*2021*
			(8)						(10)
$^3D_3'$	144511		66403						61002
			741						*742*
			(2)		(8)		(7−x)		(8)
$^3D_2'$	145252		67144	*1175*	65969	*1578*	64391	*2647*	61744
					2253		*2255*		*2254*
		(5)			(4)		(6)		(9)
$^3D_1'$	147505	147519			68222	*1576*	66646	*2648*	63998
		72			*72*		*72*		*70*
		(5)			(5)		(5)		(7+c)
$^1P_1$	147577	147591			68294	*1576*	66718	*2650*	64068
					351		*350*		*351*
			(5)		(8)		(7)		(7)
$^1D_2'$	147928		69821	*1176*	68645	*1577*	67068	*2649*	64419
			−1952		*−1956*				*−1951*
			(8)		(6)				(9)
$^1F_3$	145974		67869	*1180*	66689				62468

There is only one possible combination in the table for which a line is not observed, namely the combination $^3D_2-{}^3D_3'$. Its theoretical intensity should be about 3. It is remarkable and certainly no accident, that the corresponding combination is also absent in the spectrum of Cu II.

The ^1S term which corresponds to the normal state of Zn^{++} lies 78100 cm^{-1} below the $^3D_2$ level; it is established by but three lines at 700A, which are the only possible combinations for a level with inner quantum number $j=0$. These three lines are, however, the only strong lines in this region of the spectrum. Additional evidence for the reality of the ^1S term will be given below.

4. DISCUSSION

a. A few words may suffice for the interpretation of these new terms, as a more complete discussion is given in Shenstone's paper on the analogous

Cu II. The whole term system of Zn III, as given in Table II, is built upon the normal state of the preceding ion Zn^{+++} which is a ^2D term arising from nine equivalent 3_3 electrons or in abreviated notation $^2D(d^9)$. The important

TABLE III

Wave-length list of doubly-ionized zinc

R. W. Wood R. A. Sawyer	this Investigation	Int.	ν	Classification
1839.21	1839.40	4	54,366	$^1D_2-^3P_2$
1767.79	1767.75	7	56,569	$^1D_2-^3P_1$
1754.04	1753.90	3	57,016	$^3D_1-^3P_2$
1749.87	1749.66	9	57,154	$^1D_2-^3F_3$
1707.18	1706.67	6	58,593	$^3D_2-^3P_2$
1659.49	1695.46	3	58,981	$^1D_2-^3F_2$
1688.72	1688.60	7	59,221	$^3D_1-^3P_1$
1673.21	1673.05	9	59,771	$^3D_3-^3P_2$
1651.94	1651.74	8	60,542	$^3D_1-^3P_0$
1645.05	1644.81	10	60,797	$^3D_2-^3P_1$
1639.54	1639.28	10	61,002	$^1D_2-^1D_2$
1629.43	1629.17	10	61,381	$^3D_2-^3F_3$
1622.87	1622.50	10	61,633	$^3D_1-^3F_2$
1620.01	1619.59	8	61,744	$^1D_2-^3D_2$
1601.15	1600.83	9	62,468	$^1D_2-^1F_3$
1598.1	1598.51	8	62,558	$^3D_3-^3F_3$
	1582.09	10	63,208	$^3D_2-^3F_2$
1581.4	1581.54	15	63,230	$^3D_3-^3F_4$
	1562.54	9	63,998	$^1D_2-^3D_1$
	1560.83	7+C	64,068	$^1D_2-^1P_1$
	1553.01	7	64,391	$^3D_3-^3F_2$
				$^3D_1-^3D_2$
1552.2	1552.34	7	64,419	$^1D_2-^1D_2$
1515.9	1515.84	8	65,969	$^3D_2-^3D_2$
1505.8	1505.95	8	66,403	$^3D_3-^3D_3$
	1500.47	6	66,646	$^3D_1-^3D_1$
1499.5	1499.49	6	66,689	$^3D_2-^1F_3$
	1498.84	5	66,718	$^3D_1-^1P_1$
	1491.02	7	67,068	$^3D_1-^1D_2$
	1489.33	2	67,144	$^3D_3-^3D_2$
1473.5	1473.43	8	67,869	$^3D_3-^1F_3$
	1465.80	4	68,222	$^3D_2-^3D_1$
1464.3	1464.26	5	68,294	$^3D_2-^1P_1$
1456.8	1456.77	8	68,645	$^3D_2-^1D_2$
	1432.23	5	69,821	$^3D_3-^1D_2$
	713.88	3	140,080	$^1S_0-^3P_1$
	677.88	5	147,519	$^1S_0-^3D_1$
	677.55	5	147,591	$^1S_0-^1P_1$

configurations of Zn^{++} are therefore $(3d)^9\ (3d)$ or $(3d)^{10}$, $(3d)^9\ (4s)$ and $(3d)^9\ (4p)$. They give the following terms:

(1)	$(3d)^{10}$	:	^1S
(2)	$(3d)^9\ (4s)$	:	^3D, ^1D
(3)	$(3d)^9\ (4p)$	:	$^3(P\ D'\ F)$, $^1(P\ D'\ F)$

Obviously only transitions from the term group (3) to (1) and (2) are possible, whereas (1) and (2) cannot combine with each other. As a comparison with Table 2 shows all the predicted terms have indeed been found. A search is being made for levels arising from configurations with higher total quantum numbers such as $(3d)^9\ (4d)$ or $(3d)^9\ (5s)$, although they will produce only rather weak lines in the hot spark spectrum.

b. For a combination of the higher term triads (d^9p) and the metastable terms ^3D and ^1D, corresponding to a transition from a 4_2 to a 4_1 configuration, the irregular doublet law must hold; i.e., the frequency of the lines in question must be a linear function of the nuclear charge as we go from Ni I to Zn III. We choose, as in Table I, the line $^3D(d^9s) - {}^3D'(d^9p)$.

TABLE IV

Irregular doublet law.

Ni I	29464	-19451
Cu II	48915	-17488
Zn III	66403	

We have an approximate agreement as we found it in Table I when we compared the $\Delta\nu^{1/2}$ in Ni and Cu. If we assume (which certainly is not true) that the irregular doublet law holds *exactly* at the transition from Cu II to Zn III, i.e.,

$$[(^3D(4s))^{1/2} - (^3D(4p))^{1/2}]_{Cu} = [(^3D(4s))^{1/2} - (^3D(4p))^{1/2}]_{Zn}$$

we are able to obtain an estimate of the absolute term value of $^3D(4s)$ in Zn III. As we see from Tables I and IV the result will probably be some thousand wave-number units too low. We obtain:

$$^3D(4s) = 235{,}000 \text{ cm}^{-1}$$

Another way of getting an estimate of the absolute value of this term is by means of the Moseley law, which was found by Bowen and Millikan to hold also fairly accurately for iso-electronic spectra. All the $(\text{Term})^{1/2}$ curves of these optical Moseley diagrams are, however, slightly concave downwards, so that our extrapolated value will be too high. By means of the values of $^3D(d^9,4s)$ in Ni I and Cu II as given in Table I we obtain

$$^3D(4s) = 260{,}000 \text{ cm}^{-1}$$

As an unweighted mean of these two values we have adopted 247,000 cm^{-1} for ^3D. We then get for the lowest term

$$^1S(d^{10}) \leqq 325{,}000 \text{ cm}^{-1}$$

which corresponds to an ionization potential of 40 volts. This value will not be in error by more than 1 volt. For comparison the other ionization potentials of Zn may be added; for the arc spectrum: 9.35 volts and for the first spark spectrum (according to von Salis' analysis) 17.90 volts.

The Moseley diagram drawn with the above adopted term scale for Zn III and with the term values for Cu II and Ni I as given in Table I, is shown in Fig. 2. The ordinates at the left-hand side of the diagram are $\text{cm}^{-1/2}$, those at the right $(\nu/R)^{1/2}$ values. The $(\text{Term})^{1/2}$ lines are—as was to be expected— slightly curved. As the ^1S term has not yet been discovered in the spark spectrum of Cu, the point was drawn according to Shenstone's p edictions from the arc spectrum. The fact that this theoretical point fits

so well into the curve may be regarded as a confirmation of Shenstone's prediction and of all his conclusions drawn from it, first of all, of the value for the ionization potential of Cu^+.

Of the four levels resulting from the configuration $(3d)^9\ (4s)$ and of the twelve levels resulting from $(3d)^9\ (4p)$ only the two $^3D_3$ levels were drawn for the sake of clearness. The corresponding Moseley curves run satisfactorily parallel.

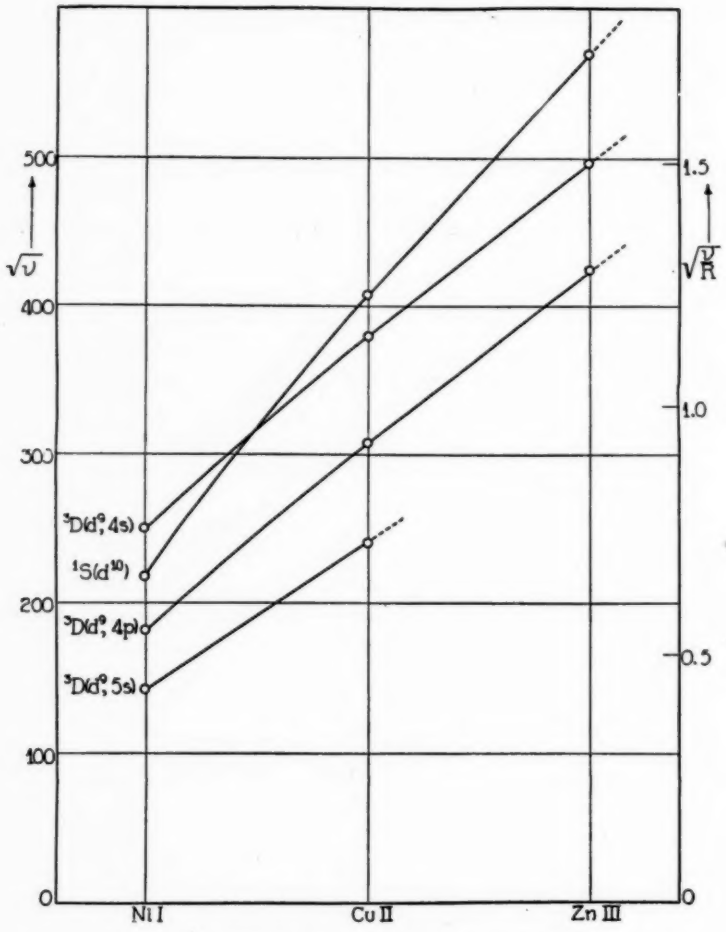

Fig. 2. Moseley diagram for Zn III.

The crossing of the $^1S(d^{10})$ and $^3D(d^9s)$ lines illustrates clearly the increase in stability of the 3_3 electrons as compared with that of the 4_1 electrons, with increasing core charge. The ten-electron configuration being at the end of the 3_3-shell ought to show a decided rare gas-energy diagram with $^1S(d^{10})$ as lowest term. In Ni I, however, the three configurations (d^8s^2), (d^9s) and (d^{10}) are about equally stable; in Cu II the configuration (d^8s^2) has become rather unstable, whereas (d^9s) and (d^{10}) have changed places; finally in Zn III (and also in the following ions) (d^{10}) is rapidly gaining in stability while (d^9s) remains a close companion of the configuration (d^9p).

c. The relativistic doublet law

$$\frac{\Delta\nu}{R}=\frac{\alpha^2(Z-s)^4}{n^3l(l+1)}$$

served as a means to predict the separation of the triplet term $^3D(d^9s)$. A further estimate of the $\Delta\nu$ of this term may be obtained from the doublet term $^2D(d^9s^2)$ which occurs in the next following ionization stage and which also

TABLE V

Separations and screening constants of D terms.

	Ni	Cu	Zn
$^2D(d^9s^2)$		arc $s=13.56$ 2043	1. spark $s=13.42$ 2719
$^3D(d^9s)$	arc $s=13.69$ 1508	1. spark $s=13.51$ 2070	2. spark $s=13.37$ 2754

follows the doublet law.[11] This term was discovered by Shenstone in the spectrum of Cu and by von Salis in that of Zn^+. In Table V the separations and screening constants of triplet or doublet D terms in the three iso-electronic

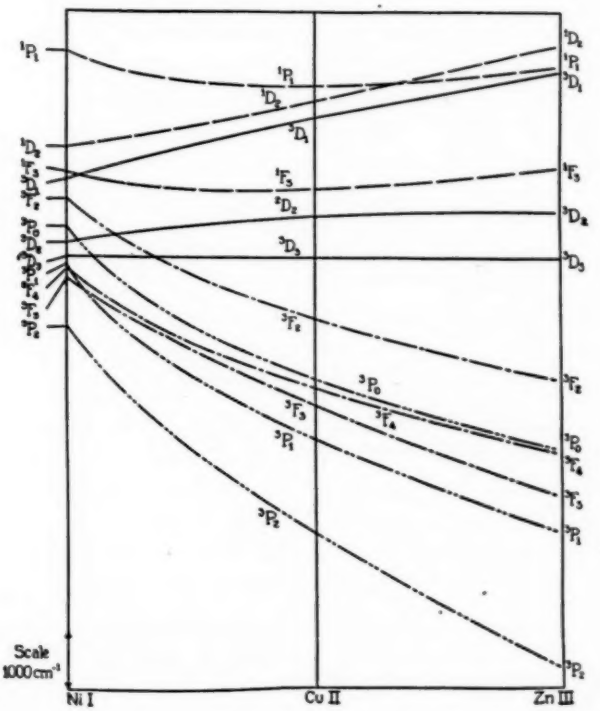

Fig. 3. Term values for Ni I, Cu II and Zn III.

[11] Compare O. Laporte, Phys. Rev. 29, 650 (1927).

spectra are given. One can imagine that the thus *predicted* separation $\Delta(^3D_{3,1})$ was a great help in finding the combinations of Table II.

The screening constants show the familiar slow decrease as the atomic number increases, the limit being the x-ray screening constant for the doublet $M_{32}M_{33}$: $s_\infty = 13.0$

The last point which needs further discussion is the identification of the twelve high levels as $^{1,3}(P, D', F)$. These levels are not at all grouped in two term-triads each with three easily recognizable terms. The apparently irregular grouping which one notices in Table 2 is a typical feature of the spectrum of higher rank. Of course the inner quantum numbers can readily be ascribed; but there seems to be no unambiguous way to assign the l- and s-values. The crucial argument in favor of our assignment is furnished by the extrapolation from the spectra Ni I and Cu II in which Zeeman effect patterns and combinations with other terms gave additional evidence. In Table VI the separations of the P, D, and F terms are given in the three iso-electronic spectra. For further illustration the relative term values of the twelve levels with respect to $^3D_3$ are drawn in Fig. 3, and corresponding levels are connected by curves.

TABLE VI

Separations of the triplet terms arising from (d^9p)

Spectrum	ΔP		ΔD		ΔF	
	0,1	1,2	1,2	2,3	2,3	3,4
Ni I	691	931	1024	220	1298	−160
Cu II	933	1498	1608	652	1420	−283
Zn III	1321	2204	2254	741	1827	−672

All these regularities, the Moseley law, the screening and relativistic doublet laws and the above discussed increase of the $\Delta\nu$ can easily be used for an extrapolation to higher iso-electronic spectra, e.g., Ga IV, Ge V, etc. In this way the authors intend to investigate these spectra.

Mr. Lang acknowledges gratefully a grant from the Research Council of Canada, which enabled him to carry on this work.

UNIVERSITY OF MICHIGAN, ANN ARBOR.
UNIVERSITY OF ALBERTA, EDMONTON.
July 11, 1927.

THE ROTATIONAL DISTORTION OF MULTIPLET ELECTRONIC STATES IN BAND SPECTRA[1]

By Edwin C. Kemble*

Abstract

Theory of rotational distortion in multiplet band spectra.—Hund's theoretical interpretation of the contracting multiplet type band spectra for diatomic molecules is thrown into quantitative form for the doublet case and also for the extreme components of higher multiplicities. The discussion is based on the conventional Bohr theory.

The ultra-violet OH bands.—The theory is applied to the ultra-violet doublet OH bands and is shown to be in approximate agreement with the data. Following suggestions of Mulliken these bands are interpreted as of the $^2S \rightarrow {}^2P$ type with the ^2P doublet inverted.

Introduction

HUND'S theory of the spectra of diatomic molecules[2] requires that the spacing of the energy levels forming an electronic multiplet shall decrease as the rotational quantum number increases, ultimately approaching zero as a limit. This variation in the energy difference between the electronic substates originates in a distortion of the molecule by rotation owing to the loose coupling of electron spin vector and nuclear axis. It accounts for the existence of bands such as those of OH type[3] in which each line is multiple and the spacing of the components decreases from a maximum at the origin toward zero as one passes out along any band branch.

In the general case Hund's theory is difficult to subject to a quantitative test. He supposes that the spin vector in a molecule, as in an atom, tends to precess about the effective axis of the magnetic field because of the orbital electronic motion. When the nuclear motion is slow this effective magnetic axis may be identified with the internuclear or molecular axis, but when the molecule is spinning rapidly the coupling is not strong enough to permit the spin angular momentum to follow the motion of the nuclear axis. Hence at very high rotational speeds the effective magnetic axis is to be identified with the axis of the mean magnetic field obtained by averaging the instantaneous field over a complete period of the nuclear rotation. This high speed effective magnetic axis is parallel to the resultant of the orbital electronic angular momentum and the nuclear angular momentum and is nearly

* Fellow of the John Simon Guggenheim Memorial Foundation.

[1] This paper is an elaboration of the theoretical part of a joint paper by Kemble and Jenkins presented to the American Physical Society, February 1927, cf. Phys. Rev. **29**, 607 (1927).

[2] F. Hund, Zeits. f. Physik. **36**, 657 (1926).

[3] Cf. R. T. Birge, Chapter IV, part 5d, of Bulletin 57 of the National Research Council, "Molecular Spectra in Gases."

perpendicular to the low speed effective magnetic axis. The interesting intermediate state between the two types of simple precession characteristic of very low and very high speeds respectively involves a complicated motion which is not easy to analyze.

In the case of doublet states and the extreme components of other multiplets, however, the precession of the spin angular momentum either for large or small values of the rotational quantum number j degenerates into a static orientation parallel or antiparallel to the corresponding effective magnetic axis and the transition from small to large values of j presents no difficulty. The following theoretical discussion is closely related to the discussion of a molecular model with an elastically mounted gyroscope previously given by the author.[4] In this previous discussion it was shown that if the electronic angular momentum of a molecule is thought of as equivalent to a gyroscope oriented with respect to the nuclear axis by means of quasi-elastic forces, there will be motions in which the gyroscopic axis lies constantly in the plane of j and the nuclear axis, making an angle with the latter which increases with the speed of rotation. The orientation of the gyroscopic axis relative to the line joining the nuclei is determined by the requirement that the torque of the elastic forces balance the torque reaction of the gyroscope due to the rotation of its axis with the molecule as a whole.

If we suppose with Hund that the orbital component of the electronic angular momentum is rigidly attached to the nuclear axis and that the spin angular momentum is oriented with respect to that axis by magnetic forces, the situation is not very different. There is a simple class of motions, call it Class A, in which the flexible component of the angular momentum lies constantly in the plane of the invariable axis (j) and the line joining the nuclei. The angle θ between the spin angular momentum s and the molecular axis (Cf Fig. 1) is fixed in a position of kinetic equilibrium determined by the speed of the nuclear rotation and by the magnetic interaction between s and the molecular axis. The motions of Class A are degenerate as s does not precess around the nuclear axis even at low speeds and the frequency of precession drops out. Hence there is only one frequency to be quantized, viz., the frequency of the nuclear rotation associated with the quantum number j. There are two states of Class A for each nuclear angular velocity and as the speed of nuclear rotation approaches zero, they normally degenerate into limiting cases in which the spin vector is parallel or antiparallel to the axial magnetic field of the orbital motion. These two limiting states are quantized according to the usual rule for the orientation of the spin in a stationary magnetic field and are to be identified with the extreme components of the multiplet for stationary nuclei. It therefore seems justifiable to identify the other states of Class A having quantized j values with the extreme components of the multiplet for the appropriate molecular rotational speeds. This procedure is supported by the adiabatic principle, for it is evident that a slow variation in the nuclear angular velocity will carry

[4] Chapter VII, Section 4 of Bulletin 57 of the National Research Council, "Molecular Spectra in Gases."

motions of Class A over into new motions of the same class. As the orientations of s along the nuclear axis for stationary nuclei satisfy the quantum conditions, the other orientations obtained adiabatically from them by gradually increasing the speed of rotation must also satisfy the quantum conditions. In the case of doublet electronic energy levels the theory of the stationary states of the degenerate Class A tells the whole story, but for higher multiplicities it gives only the extreme components.

The theory is here carried through on the basis of the conventional or classical Bohr theory and is subject to correction in the light of the wave mechanics, especially in the region of small j values. The initial comparison of the formulas with the experimental data for the NO β bands[1] and also the discussion of the ultra-violet OH bands in this paper give strong support, however, to the substantial validity of the theory.

Mathematical Theory for Normal Multiplets

Let σ_k denote the vector or scalar component of the electronic orbital angular momentum k along the nuclear axis. (All angular momenta are expressed in units $h/2\pi$.) Let θ be the angle between the vector σ_k and the spin angular momentum s. Denote the mutual magnetic energy of s and σ_k by $U(\theta)$. As in the atomic case, we may assume as a first approximation that U has the form

$$U(\theta) = A h \cos\theta. \tag{1}$$

For the present we assume that A is positive as in the case of normal atomic multiplets. Let Q denote the torque correlated with U and tending to increase θ. Then

$$Q = -dU/d\theta = A h \sin\theta. \tag{2}$$

Introducing the symbol ω for the frequency of molecular rotation and remembering that the spin angular momentum in absolute units is $sh/2\pi$ we may use the fundamental law of gyroscopic motion to derive the expression $2\pi\omega(sh/2\pi)\sin(j, s)$ for the torque reaction due to the rotation of s. Equating the torque Q to the torque reaction we obtain[5]

$$\omega s \sin(j, s) = A \sin\theta. \tag{3}$$

The direction of the torque reaction is that of the vector product of the spin s and the angular velocity of the nuclei. Two primary cases are to be considered as shown in Fig. 1. In case I, s is on the same side of the internuclear axis as j and if the angle between j and the axis is denoted by ϕ, it is necessary that $0 < \theta - \phi \leqq \pi$. At high speeds of nuclear rotation s tends to set itself parallel to j and at low speeds, if the torque constant A is relatively large, it orients itself along the molecular axis antiparallel to σ_k. In Case II, s is on the opposite side of the axis from j and $0 \leqq \theta + \phi < \pi$. At high speeds of nuclear rotation s sets itself antiparallel to j and if A is large, it becomes parallel to σ_k at low speeds. On the other hand, if the torque constant is small, s may set itself antiparallel to σ_k at low rotational speeds in Case II.

[5] Cf. Equation (21) Reference 4.

For the present, however, the discussion will be confined to the important and simple case where A is relatively large.*

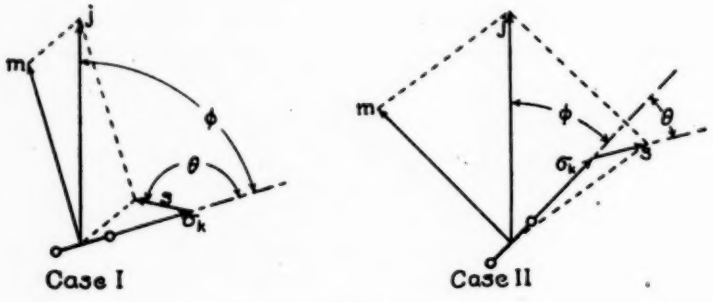

Fig. 1.

Let m denote the nuclear angular momentum and as usual let B stand for the constant $h/8\pi^2 I$. Then the frequency of rotation is given by[6]

$$\omega = 2mB/\sin\phi \tag{4}$$

and Eq. (3) becomes

$$\frac{2mBs}{\sin\phi}\sin(\theta \mp \phi) = A\sin\theta. \tag{5}$$

Here and in the succeeding equations the upper sign is to be associated with Case I. But from the geometry of the figures

$$m = j\sin\phi \mp s\sin\theta. \tag{6}$$

Hence Eq. (5) becomes

$$P\sin\theta = \sin(\theta \mp \phi)\left\{\frac{j}{s} \mp \frac{\sin\theta}{\sin\phi}\right\} \tag{7}$$

where P denotes the constant $A/2Bs^2$. ϕ may be eliminated by the geometrical relation

$$j\cos\phi = \sigma_k + s\cos\theta \tag{8}$$

which leads to

$$P = \sigma_k/s + 2\cos\theta \mp \frac{\sin\theta(\sigma_k/s + \cos\theta)}{[(j/s)^2 - (\sigma_k/s + \cos\theta)^2]^{1/2}} \mp \frac{\cos\theta}{\sin\phi}[(j/s)^2 - (\sigma_k/s + \cos\theta)^2]^{1/2}. \tag{9}$$

The above equation determines the relation between θ and j but unfortunately is not easily solved for the former quantity. In order to throw it into a form more convenient for use we introduce the symbols

$$\alpha \equiv \sigma_k/s\ ; \quad v \equiv [j^2/s^2 - (\sigma_k/s + \cos\theta)^2]^{1/2}/\sin\theta.$$

* *Footnote added at reading of proof:* The writer hopes to discuss small values of the magnetic interaction A in a later paper.

[6] Cf. Equation (19) Reference 4.

Eq. (9) becomes

$$v^2 \pm \left(\frac{P-\alpha-2\cos\theta}{\cos\theta}\right)v + \frac{\alpha+\cos\theta}{\cos\theta} = 0. \tag{10}$$

Solving for v we obtain

$$v = \mp\left(\frac{P-\alpha-2\cos\theta}{2\cos\theta}\right) \pm \left[\left(\frac{P-\alpha-2\cos\theta}{2\cos\theta}\right)^2 - \frac{\alpha+\cos\theta}{\cos\theta}\right]^{1/2}. \tag{11}$$

Here the double sign before the radical is independent of the case under consideration, but it is not difficult to show that the values of v of physical interest when the torque constant is large are those in which both terms of the right hand member of Eq. (11) have the same sign. Consequently Eq. (11) may be written in the form

$$v = \mp\left(\frac{P-\alpha-2\cos\theta}{\cos\theta}\right)\left\{1+\left(1-\frac{4(\alpha+\cos\theta)\cos\theta}{(P-\alpha-2\cos\theta)^2}\right)^{1/2}\right\} \tag{12}$$

or, if $P>>1$, approximately

$$v = \mp\left[\frac{P-\alpha-2\cos\theta}{\cos\theta} - \frac{\alpha+\cos\theta}{P-\alpha-2\cos\theta}\right]. \tag{13}$$

This equation permits the calculation of v and hence j from given values of θ. To get the corresponding term values we use the energy formula

$$F(j) = Bm^2 + Dm^4 + A\cos\theta. \tag{14}$$

With the aid of Eqs. (6) and (8) we may throw this into the form

$$F(j) = Bs^2(v\mp 1)^2\sin^2\theta + Ds^4(v\mp 1)^4\sin^4\theta + A\cos\theta. \tag{15}$$

In the important case where P is large and j and $\sin\theta$ are small, we may obtain an explicit expression for $F(j)$ in terms of j by approximations as follows. Developing v in a power series in $\sin\theta$, we find

$$v = v_0 + v_1\sin^2\theta + \cdots \tag{16}$$

where

$$v_0 = \frac{(P-\alpha\pm 2)}{2}\left[1+\left(1\pm\frac{4(\alpha\mp 1)}{(P-\alpha\pm 2)^2}\right)^{1/2}\right]; \tag{17a}$$

$$v_1 = \frac{P-\alpha}{2} + \frac{1}{2(P-\alpha\pm 2)} + \frac{(\alpha\mp 1)}{(P-\alpha\pm 2)^2} + \cdots \tag{17b}$$

Hence

$$(v\mp 1)^2 = (v_0\mp 1)^2 + 2(v_0\mp 1)v_1\sin^2\theta + v_1^2\sin^4\theta.$$

Neglecting the D term in (15) we may write $F(j)$ in the form

$$F(j) = \mp A + Bs^2\left\{[(v_0\mp 1)^2 \pm P]\sin^2\theta + [2(v_0\mp 1)v_1 \pm \tfrac{1}{4}P]\sin^4\theta + \cdots\right\}. \tag{18}$$

To get the relation between $\sin^2\theta$ and j we make use of the definition of v which gives

$$(j/s)^2=(\alpha+\cos\theta)^2+v^2\sin^2\theta$$
$$=(\alpha\mp 1)^2+(v_0^2-1\pm\alpha)\sin^2\theta+(2v_0v_1\pm\alpha/4)\sin^4\theta. \tag{19}$$

Let $\sigma_0=\sigma_k\mp s=$ value of σ for zero rotation,

$$\left.\begin{aligned} a&=v_0^2-1\pm\alpha,\\ b&=2v_0v_1\pm\alpha/4.\end{aligned}\right\} \tag{20}$$

Solving (19) for $\sin^2\theta$ we obtain

$$\sin^2\theta=\frac{j^2-\sigma_0^2}{as^2}-\frac{b}{a^3s^4}(j^2-\sigma_0^2)^2+\cdots \tag{21}$$

The elimination of $\sin^2\theta$ between (18) and (21) yields

$$F(j)=\mp A+B^*(j^2-\sigma_0^2)+D^*(j^2-\sigma_0^2)^2 \tag{22}$$

where B^* and D^* are defined by

$$B^*=B\left\{\frac{(v_0\mp 1)^2\pm P}{a}\right\}\cong B\left\{\frac{(P-\alpha\pm 1)^2\pm P}{(P-\alpha\pm 2)^2-1\pm\alpha}\right\}, \tag{23}$$[6]

$$D^*=\frac{B}{a^2s^2}\left\{2(v_0\mp 1)v_1\pm\frac{P}{4}-\frac{b}{a}[v_0\mp 1)^2\pm P]\right\}. \tag{24}$$

Eqs. (22), (23), (24) are useful in studying the lines near the origin in the case of a widely spaced multiplet. They show that the apparent values of B (i.e., B^*) differ from the true B, which is the same for both members of the doublet, by amounts which are calculable from the width of the multiplet for zero rotation (at the origin) and from the constant α.

Another type of approximation may be used for large values of

$$\frac{(j^2-\sigma_0^2)}{as^2}$$

and small values of $\cos\theta$ (Hund's case b). If $\cos\theta$ is small, Eq. (12) degenerates into

$$v=[(j/s)^2-\alpha^2]^{1/2}/\sin\theta\cong\mp[(P-\alpha)/\cos\theta-2]$$

Hence

$$\cos\theta\cong\mp(P-\alpha)s/[(j^2-\sigma_k^2)^{1/2}\mp 2s] \tag{25}$$

Neglecting higher powers of $\cos\theta$ and $1/j$ we may transform Eq. (15) with the aid of (25) into

$$F(j)=B[(j\mp s)^2-\sigma_k^2-D(j\mp s)^4/B\mp P(P-2\alpha)s^3/(j\mp s)] \tag{26}$$

This equation shows that a pair of levels so chosen from the two series for Case I and Case II that

$$j_1-s=j_2+s=T$$

[6] The last expression in Eq. (23) is an approximation good only for large values of $P-\alpha$ but more accurate than the formula given in reference 1. The error involved is not serious if $P-\alpha$ is as large as 10.

will form a natural doublet with a spacing approximately equal to $2P(P-2\alpha)s^3/T$. As the least value of j_2 (j_2 denotes the j for Case II) is greater by $2s$ than the least value of j_1, while the value of j_2 for any doublet should be *less* than the corresponding j_1 value by $2s$, it is clear that the lowest levels in the two series do not form a doublet. Fig. 2 shows the

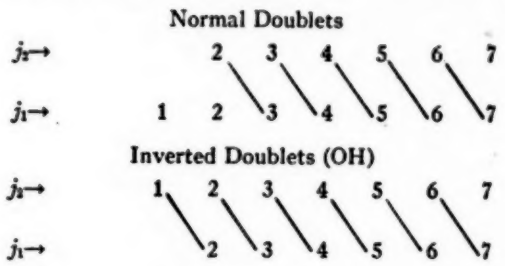

Fig. 2.

correlation of the lower energy levels in the two series when $s=\frac{1}{2}$, both for normal doublets and for the inverted doublets discussed below.

Formula (26) is in harmony with Hund's conclusion that in his case *b* the doublet interval should vary as $1/j$. The magnitude of the separation is much greater, however, than he predicted. The reason for the discrepancy lies in the fact that Hund assumed that in the case of the extreme components of a multiplet for large values of j (or of $(j^2-\sigma_0^2)/as^2$) the angles ϕ and θ could be assumed equal. In other words, he supposed that s would be parallel or antiparallel to j. This assumption is not verified by our computation which requires [Eqs. (7) and (8)] that for very large values of $(j^2-\sigma_0^2)/as^2$

$$\cos\theta=\mp(P/\alpha-1)\cos\phi. \tag{27}$$

Inverted Multiplets

In the case of a normal multiplet ($A>0$), to which the above equations apply, the parallel orientation of σ_k and s has the greater energy and with increasing rotational speed this upper electronic energy level is deformed in such a way that s tends to become antiparallel to j. On the other hand, in the case of an inverted multiplet the parallel orientation of σ_k and s has the least energy and with increasing rotational speed the deformation brings s into a position approximately *parallel* to j. Mulliken designates the term formulas for the cases where s is parallel and antiparallel to j at high rotational speeds by $F_1(j)$ and $F_2(j)$ respectively. In order to conform with this convention we designate as Case I for inverted multiplets the lower electronic energy level for which $\sigma_0=\sigma_k+s$. Then Eq. (15) holds as it stands, while Eq. (12) is replaced by

$$v=\pm\left(\frac{P+\alpha+2\cos\theta}{2\cos\theta}\right)\left[1+\left(1-\frac{4(\alpha+\cos\theta)\cos\theta}{(P+\alpha+2\cos\theta)^2}\right)^{1/2}\right]. \tag{28}$$

For small values of j we may again use Eqs. (19), (22), (23), and (24) if we redefine v_0, v_1, a, b by the equations

$$v_0=\frac{(P+\alpha\pm2)}{2}\left[1+\left(1\mp\frac{4(\alpha\pm1)}{(P+\alpha\pm2)^2}\right)^{1/2}\right]; \tag{29a}$$

$$v_1=\frac{P+\alpha}{2}+\frac{1}{2(P+\alpha\pm 2)}+\frac{(\alpha\pm 1)}{(P+\alpha\pm 2)^2}+\cdots; \tag{29b}$$

$$a=v_0^2-1\mp\alpha; \tag{30a}$$

$$b=2v_0v_1\mp\alpha/4. \tag{30b}$$

For large values of j we have

$$\cos\theta\cong\pm(P+\alpha)s/[(j^2+\sigma_k^2)^{1/2}\mp s] \tag{31}$$

instead of (25) and

$$F(j)=B[(j\mp s)^2-\sigma_k^2-D(j\mp s)^4/B\mp P(P+2\alpha)s^3/(j\mp s)+\cdots] \tag{32}$$

to replace Eq. (26).

The OH Bands

The theory given in this paper was originally developed in order to account for certain anomalies found by Dr. F. A. Jenkins in the empirical analysis of the NO β bands.[6a] The magnetic energy of orientation of the spin vector s is quite large for the NO β bands so that only the initial stages of the doublet contraction can be observed in them. On the other hand, the well known ultra-violet OH bands studied by Heurlinger,[7] Watson,[8] and others, have a much smaller relative magnetic energy and exhibit very well the transition from Hund's Case a, where Eq. (22) applies, to his Case b, where Eq. (26) or Eq. (32) is to be used. It therefore seems desirable to include in this paper a discussion of the application of the theory to the OH bands.

Their contracting doublet structure is one to which the Kramers and Pauli formula

$$F(j)=B[(j^2-\sigma^2)^{1/2}\pm\epsilon]^2 \tag{34}$$

is apparently adapted. A critical examination[3] shows, however, that though qualitatively plausible, Eq. (34) is not capable of adjustment to quantitative agreement with the experimental data.

Before entering on the detailed discussion of the OH bands it may be wise to call the attention of the reader to the obvious limitations in the theory. First among these may be mentioned the assumption of the cosine law for the variation of the magnetic energy with θ [Eq. (1)]. In the case of atomic multiplets this law is not rigorous and breaks down completely in some cases. Hence it can be only an approximation for molecules. Another obvious limitation of the theory is its failure to account for the so-called "σ-type doubling" which occurs in the OH bands and others, producing a small "quantum defect" when the usual P, Q, R combination relations are applied. A doubling associated with electronic states for which σ_k is not

[6a] F. A. Jenkins, H. A. Barton and R. S. Mulliken, Phys. Rev. The application of the theory as developed here to the *NO* β bands will probably be discussed in a later paper by Dr. Jenkins.

[7] T. Heurlinger, Dissertation, Lund (1918).

[8] W. Watson, Astrophys. J. **60**, 145 (1924).

zero has been predicted by Hund[2] on general formal grounds, but the phenomenon is still mysterious from the physical standpoint and is not taken into account in the present mathematical formulation of Hund's theory.

The theory is also incomplete because it does not take into account the magnetic field developed by the rotation of the molecule as a whole. This magnetic field, as previously pointed out by the writer[9] should be parallel and approximately proportional to j. It gives a natural explanation of the type of doubling observed in ^2S states and of the Zeeman effect in the visible I_2 absorption bands. In the case of ^2P states (among which the final states associated with the OH bands belong) it should produce a contribution to the doublet interval $F_1(T)-F_2(T)$ approximately proportional to j (or T) and superposed on the doublet interval predicted by equations given above. Whether this contribution to the doublet interval should be additive or subtractive is not yet clear to the writer.

Finally we must mention again the obvious deficiency in our theory due to the fact that it is worked out on the basis of the Bohr postulates instead of by the rigorous method of the quantum mechanics.

The OH bands are classified by Mulliken (private communication)[10] as of the $^2S\rightarrow{}^2P$ type. The upper electronic state is obviously of the ^2S type since the combination formulas show that to a close approximation

$$2\Delta F_1' = 2\Delta F_2' = 4B'T + 8D'T^3 \tag{35}$$

In the case of the $\lambda 2811$ band ($n'=1$, $n''=0$) to which alone our tests will be applied $B'=16.12(5)$ cm^{-1} and $D'=-0.0020$ cm^{-1}.*

The lower electronic state has the characteristic doubling of ^2P and ^2D states. Owing to the selection principle $\Delta\sigma_k=\pm 1, 0$ we may conclude that it belongs to the former class and set $\sigma_k=1$, $\alpha=2$. Mulliken has also suggested that this state is to be interpreted as an inverted doublet so that the larger value of σ_0 (i.e., $\sigma_0=1\frac{1}{2}$, s parallel to σ_k) is to be assigned to the lower level of the doublet. This proposal is in harmony with the fact that *all* the rotational sublevels of F_1'' and F_2'' combine to form doublets as in the lower diagram of Fig. 2.

We have to account for the empirical double P-form, Q-form, and R-form branches shown in the Fortrat diagram (Fig. 3) by means of transitions between four electronic energy levels with rotational term formulas which degenerate for large values of j into the approximate expressions

$$\left.\begin{aligned} F_1'(j) &= B'(j-\tfrac{1}{2})^2+\cdots \\ F_2'(j) &= B'(j+\tfrac{1}{2})^2+\cdots \end{aligned}\right\} \tag{36a}$$

$$\left.\begin{aligned} F_1''(j) &= B''(j-\tfrac{1}{2})^2+\cdots \\ F_2''(j) &= B''(j+\tfrac{1}{2})^2+\cdots \end{aligned}\right\} \tag{36b}$$

[9] "Molecular Spectra in Gases" (National Research Council Bulletin 57), Chapter VII, pp. 345–347.

[10] Cf. also Mulliken, Phys. Rev. **29**, 637 (1927).

* These numerical values were obtained by a semigraphical method and have not the accuracy of a least squares solution. As is customary, the numerical results are given in reciprocal centimeters though the definitions of B and D in the text require them to be expressed in reciprocal seconds.

The possible transitions available for the interpretation of the empirical data are listed in Table I. According to Mulliken[11] the six transitions of the type $F_1' \rightarrow F_1''$, $F_2' \rightarrow F_2''$ should give rise to strong branches (P_1, P_2, Q_1, Q_2, R_1, R_2) while the branches ${}^PQ_{12}$, ${}^QR_{12}$, ${}^QP_{21}$, ${}^RQ_{21}$ should have appreciable intensities only for very small values of j. The double-P-form and double-R-form branches violate the principle of selection $\Delta j_k = 0, \pm 1$ and should drop out entirely. The six theoretically intense transitions account for all six of the observed branches, but we cannot infer the absence of the predicted satellite branches since each of them coincides in position with one of the primary branches due to the sensible equality of $F_1'(j-\frac{1}{2})$ and $F_2'(j+\frac{1}{2})$ (for example, the satellite branch ${}^PQ_{12}$ falls on top of P_2).

TABLE I

Possible transitions available for the interpretation of the data.

Transition	Δj index	Apparent form	Mulliken symbol
$F'_1(j-1) \rightarrow F''_1(j)$	P	P	${}^PP_{11}$ or P_1
$F'_2(j-1) \rightarrow F''_2(j)$	P	P	${}^PP_{22}$ or P_2
$F'_1(j) \rightarrow F''_2(j)$	Q	P	${}^PQ_{12}$
$F'_1(j) \rightarrow F''_1(j)$	Q	Q	${}^QQ_{11}$ or Q_1
$F'_2(j) \rightarrow F''_2(j)$	Q	Q	${}^QQ_{22}$ or Q_2
$F'_1(j+1) \rightarrow F''_2(j)$	R	Q	${}^QR_{12}$
$F'_2(j-1) \rightarrow F''_1(j)$	P	Q	${}^QP_{21}$
$F'_1(j+1) \rightarrow F''_1(j)$	R	R	${}^RR_{11}$ or R_1
$F'_2(j+1) \rightarrow F''_2(j)$	R	R	${}^RR_{22}$ or R_2
$F'_2(j) \rightarrow F''_1(j)$	Q	R	${}^RQ_{21}$
$F'_1(j-1) \rightarrow F''_2(j)$	P	Double-P	?
$F'_2(j+1) \rightarrow F''_1(j)$	R	Double-R	?

We can now interpret Fig. 3. As the F'' doublet is inverted, the high frequency component of each branch is associated with F_1'' and the branches may be labeled as shown in the figure. The ordinates are the empirical ordinal numbers of the lines in their respective branches (M) and must be correlated with the values of j''. The first line of each of the three branches P_1, Q_1, R_1 is associated with the lowest energy level in the F_1'' series. Hence we may set $j'' = (\sigma_0)_1 + \frac{1}{2} = 2$ for each of these lines and thus establish the relation $M = j_1'' - 1$ for the three branches in question.* Similarly the value of j'' for the first lines of the Q_2 and R_2 branches should be unity and we may conclude that for these branches $M = j_2''$. The first line of the theoretical P_2 branch originates in the transition $F_2'(1) \rightarrow F_2''(2)$, from which it might appear that for this branch $M = j_2'' - 1$. The combination relations first tested by Dieke[12] show, however, that the relation between M and j'' is actually the same for the empirical P_2 branch as for the R_2 and Q_2 branches. The apparent discrepancy is accounted for when we observe that the first line of the satellite ${}^PQ_{12}$ branch should fall on an extrapolated point of the P_2 branch with $j'' = 1$. The existence of this satellite branch should therefore

[11] R. S. Mulliken, Phys. Rev. (in press).

* The j values of the new quantum mechanics would be a half unit smaller.

[12] G. H. Dieke, Nature **115**, 194 (1925); Proc. Acad. Sci. Amsterdam, **28**, 174 (1925). Cf. also R. T. Birge, Phys. Rev. **25**, 240 (1925).

raise all the M values for the empirical P_2 branch by unity and gives a satisfactory explanation of the fact that for the P_2 branch M is empirically equal to j_2''.[13]

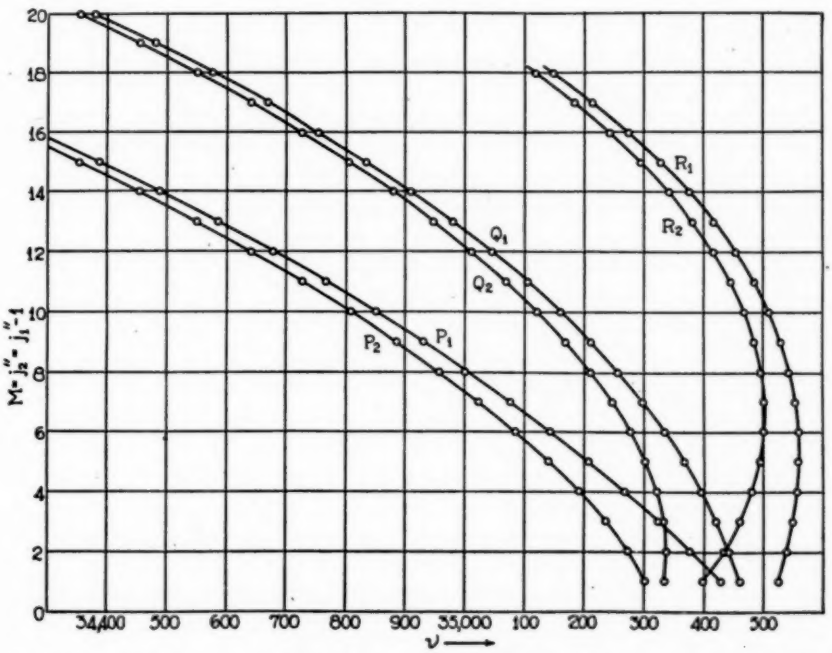

FIG. 3. Fortrat diagram of 2811 OH band. The circles show the empirical observations of Watson while the curves have been plotted from the theoretical frequency formulas.

In order to test the theory quantitatively the constants which enter into the formulas must be evaluated. Those which pertain to the initial states F' have been given above. The constants B'' and D'' can also be determined by means of the combination principle using the outer band lines only. This principle requires that

$$R_1(j-1)-P_1(j+1)=F_1''(j+1)-F_1''(j-1)=2\Delta F_1''(j), \tag{37}$$

$$R_2(j-1)-P_2(j+1)=F_2''(j+1)-F_2''(j-1)=2\Delta F_2''(j). \tag{38}$$

From Eq. (32) we have

$$2\Delta F_1''(j)=(4B''+8D'')T+8D''T^3+2P(P+2\alpha)s^2/(T^2-1) \tag{39}$$

where $T=j_1-\frac{1}{2}$. Also

$$2\Delta F_2''(j)=(4B''+8D'')T+8D''T^3-2P(P+2\alpha)s^2/(T^2-1) \tag{40}$$

where $T=j_2+\frac{1}{2}$. Hence we may conveniently introduce the mean of the values of $2\Delta F''$ which satisfies the relation

$$\overline{2\Delta F''}=(4B''+8D'')T+8D''T^3. \tag{41}$$

[13] Cf. Mulliken's theory of the CN bands—Phys. Rev. (in press).

Evaluating B'' and D'' from the above equation and the data for the lines from $j_1=16$ to $j_1=20$, we obtain $B''=18.47$ cm^{-1} and $D''=-0.00177$ cm^{-2}.

The origin of the band is also determinable from the observations for large values of j. For this purpose it is convenient to combine Eq. (32) with the corresponding rotational energy formula for F' and drop the term in $1/(j\mp s)$ to obtain the mean frequencies of the doublets. The resulting equation expressed in terms of the parameter T is

$$\bar{\nu}_{1,2}=\bar{\nu}_0+B'+B''+D'\pm(2B'+4D')T+(B'-B''+6D')T^2\pm 4D'T^3+(D'-D'')T^4. \quad (42)$$

Here the upper signs are for the R branch and the lower ones for the P branch The value of ν_0 obtained from the measurements of the outer lines with the aid of Eq. (42) is 35387.0 cm^{-1}.

We next turn our attention to the lines adjacent to the origin and the related lower F'' energy levels. With the aid of the combination principle and the formula

$$F'=B'T^2+D'T^4=B'(j\mp\tfrac{1}{2})^2+D'(j\mp\tfrac{1}{2})^4 \quad (43)$$

we can easily compute F_1'' and F_2'' to an additive constant. Formulas of the type (22) may then be fitted to the lower values so obtained. Table II shows the numerical magnitudes so deduced together with the theoretical values of B_1^*, B_2^*, D_1^*, D_2^* calculated from Eqs. (23) and (24). The agreement between the theory and the empirical data is particularly good for the difference $B_2^*-B_1^*$ which measures the initial rate of contraction of the doublets. While the empirical values of B_1^* and B_2^* are both somewhat lower than the theoretical ones, the agreement is sufficient to give strong support to the interpretation of the bands which we have given. There is also a discrepancy of 2.7 cm^{-1} between the value of ν_0 calculated from the outer band lines and the value given in Table II deduced from the lines adjacent to the origin.

TABLE II

(*All values except that of P are given in wave-numbers*).

	Expt.	Theory		Expt.	Theory
$2A$	140.25		P	7.595	
B_1^*	16.60	16.82	B_2^*	20.565	20.86
D_1^*	0.0129	0.0111	D_2^*	−0.0237	−0.050
$B_2^*-B_1^*$	3.965	4.04	ν_0	35384.21	

Fig. 4 shows the empirical and theoretical values of the doublet interval and also a plot of the difference between them.* While the agreement is excellent for small values of j, there is a large discrepancy for the outer lines. This is not surprising, however, as the theory does not take into account the contribution to the doublet interval from the magnetic field developed by the molecular rotation. This contribution, as previously mentioned, should be approximately proportional to j when j is large compared to σ. Curve d on the graph shows the discrepancy between the observed and calculated

* The doublet intervals for the Q branch differ from those of the R and P branches by a small linear function of j on account of the "σ-type doubling."

values of the double interval and indicates that this discrepancy varies roughly as required.

The curves on Fig. 3 show the theoretical forms of the six branches calculated from the data for B', B'', D', D'', and ν_0 given by the outer R and P lines together with the value of $2A$ given in Table II and computed from the inner lines. These curves are based on the accurate Eqs. (15) and (28). The scale of the reproduction is so small that the divergence between the curves and measured points is concealed, but the original large scale

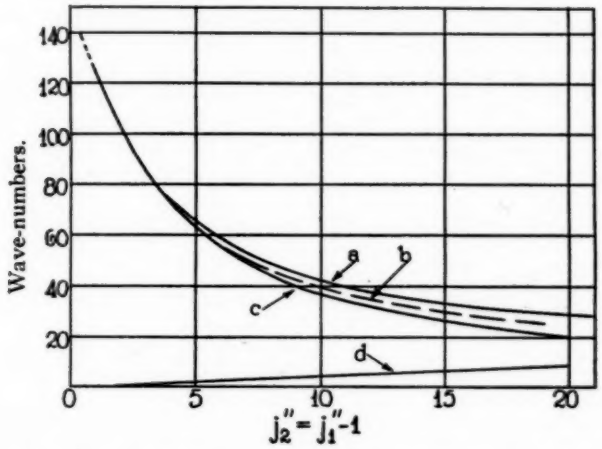

FIG. 4. Doublet intervals for 2811 OH band. Curve *a*, empirical intervals for *P* and *R* branches; curve *b*, empirical intervals for *Q* branch; curve *c*, theoretical intervals; curve *d*, discrepancy between *a* and *c*.

graphs indicate that aside from the discrepancies due to the "σ-type" doubling and the failure of the doublet contraction law for large values of j there remains only a small divergence between the theoretical curves and the empirical points in the immediate neighborhood of the origin. This divergence at the origin is responsible both for the discrepancy between the two values of ν_0 computed above and for the discrepancies in the values of B_1^* and B_2^* given in Table II. It is probably referable to the well-known inadequacy of the conventional Bohr theory for small quantum numbers. In view of the approximate nature of the cosine law [Eq. (1)], it is surprising that the theoretical formulas agree so well with the empirical data.

GÖTTINGEN,
May 26, 1927.

THE STRUCTURE OF THE ULTRA-VIOLET SPECTRUM OF THE HYDROGEN MOLECULE[1]

By G. H. Dieke and J. J. Hopfield

Abstract

The absorption spectrum of the hydrogen molecule has been photographed and also the emission spectrum under various discharge conditions. In the region between 1000A and 1650A the bands belong chiefly to two systems with a common final electronic state, which is the lowest state of the molecule. The correctness of the classification is proved by combination relations and the variation of the rotational energy with the vibrational quantum number. The *Lyman bands* are emitted when, by collisions of the second kind with excited metastable argon atoms, the hydrogen molecule is brought into the first excited electronic state with three vibrational quanta. From the energy diagram which is obtained from the analysis of the spectrum it follows that the *resonance potential of the hydrogen molecule* is 11.1 volts. The *heat of dissociation of the hydrogen molecule* is found by two independent methods to be 4.34 and 4.38 volts, respectively.

1. Introduction

THE existence of a spectrum very rich in lines below 1675A which must be attributed to hydrogen was first discovered by Schumann.[2] This spectrum was extended beyond the absorption limit of fluorite by Lyman[3] who investigated it more in detail and gave wave-length measurements of its lines. There could not be any doubt that the spectrum in question, as well as the many lined spectrum in the visible and near ultra-violet, is emitted by the hydrogen molecule. As all the lines belonging to the normal state of the hydrogen molecule must be expected in this region, one can hope to get some information about the structure of the molecule by the study of the spectrum. This seems especially important, because the hydrogen molecule must be the simplest of all molecules. Moreover, all the information which one can get from other sources is so meager and uncertain that results obtained from the spectrum are needed to check it. In the visible spectrum some regularities are known, but until very recently they have been practically useless for getting information about the structure of the molecule, because little connection between the different bands had been found. A knowledge of the ultra-violet bands is certain to aid in interpreting also the structure of the visible spectrum.

In the present paper an account is given first of experimental work in obtaining the emission and absorption spectrum and then of the interpretation of the experimental results.

[1] The main results of this article have been published in Zeits. f. Physik **40**, 299 (1926).
[2] V. Schumann, Wiener Anzeiger **29**, 230 (1892); Smith. Contrib. No. 1413 (1903).
[3] Th. Lyman, The spectroscopy of the extreme ultra-violet, (1914).

2. Experimental Arrangement

The photographs which form the basis of the present investigation were taken with the vacuum spectrograph described by one of us elsewhere.[4] The discharge tube with which most of the emission pictures were taken was essentially of the same type as that used by Wood[5] in his work on the hydrogen spectrum and the same phenomena could be observed. The electrodes were of aluminum. Wood observed that in the visible[6] the molecular spectrum is most strongly developed in the "white" stage of the discharge which occurs after the tube has run for several hours with pure, dry hydrogen. The same was found for the molecular spectrum in the extreme ultra-violet, and in the "white" stage the atomic lines had practically disappeared from the spectrum. Some of the emission pictures were taken with a tube of the same type as used in obtaining the absorption pictures.

The hydrogen was generated electrolytically, dried over phosphorous pentoxide, and admitted to the discharge tube by a capillary valve[7] which allowed one to regulate the flow of gas and to maintain any desired pressure by simply turning a pinch cock. The discharge tube and spectrograph were pumped out separately by two independent sets of oil and mercury diffusion pumps. The pressure in the spectrograph could be measured by a McLeod gauge and was usually less than 10^{-3} mm. In the discharge tube the pressure was estimated from the character of the discharge and was varied between wide limits. The current for the discharge tube was obtained from a 10 kilowatt transformer with a potential difference of 11500 volts. The spectrum was not appreciably changed when the current was rectified by a kenotron.

Commercial argon was used in the experiments with argon and no attempt was made to purify it. It was generally admitted directly from the reservoir, where it was stored over water, by a capillary and a capillary valve, as it was found that the small traces of water vapor did not appreciably change the spectrum. The argon contained air as impurity. If the pressure in the discharge tube was very low, the impurities practically did not show at all, neither in the pocket spectroscope nor in the ultra-violet spectrum. With increasing pressure (without changing the percentage of impurities) the nitrogen bands appeared very strongly in the visible, and no trace of the argon spectrum could be detected at pressures of a few millimeters. In the ultra-violet the nitrogen bands were also very strong as well as the line spectrum of nitrogen, although the argon resonance lines at 1048 and 1067A always remained intense.

Two gratings were used in this work, both with a radius of curvature of 50 cm. The one which was in use during the earlier part of the work has 15000 lines per inch. It had been used before with chlorine, selenium, and other corroding substances and had lost much of its reflecting power,

[4] J. J. Hopfield, Phys. Rev. **20**, 573 (1922).

[5] R. W. Wood, Proc. Roy. Soc. **A97**, 445 (1920); Phil. Mag. **42**, 729 (1921).

[6] Under the visible spectrum is understood in this paper always the secondary spectrum in the visible and near ultra-violet.

[7] J. J. Hopfield, Jour. Opt. Soc. **12**, 391 (1926).

especially in the higher orders. The other grating, ruled by Professor R. W. Wood, has 30000 lines per inch, thus giving twice the dispersion of the old one. The measurements have nearly all been made on photographs taken with this grating.

The special films were prepared by the method communicated previously by one of us.[4]

3. The Absorption Spectrum[8]

As hydrogen absorbs in a region, where even fluorite is no longer transparent, no windows of any kind could be used between the light source and the absorption chamber. Therefore the whole spectrograph was filled with hydrogen at pressures up to 70 mm, and was separated from the discharge tube, as usual, by the narrow slit. This arrangement allows one to maintain a fairly large difference of pressure between the spectrograph and the discharge tube. As the light path in the spectrograph is one meter, a relatively low density of the hydrogen was sufficient to produce strong absorption.

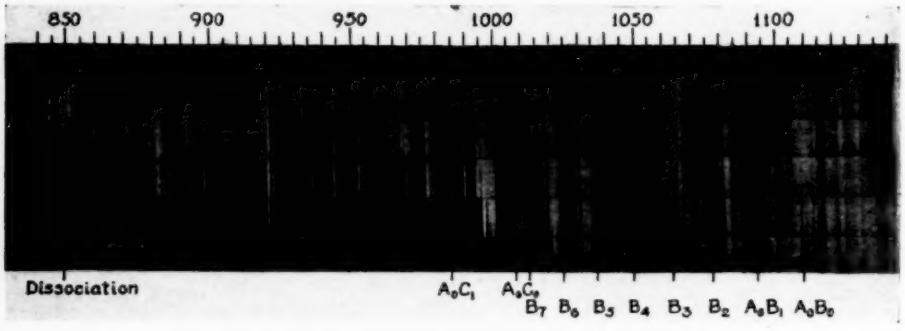

Fig. 1. Absorption spectrum of hydrogen at pressures of 2, 4, 8, 15, 36 and 50 mm, respectively.

Lyman[9] discovered that if a strong condensed discharge is passed through a narrow glass capillary, a continuous spectrum is emitted between 900 and 1900A which is practically independent of the nature of the gas in the tube. We used this spectrum as a continuous background for the absorption. Our tube, which was of Pyrex glass, was of the same type as that described by Lyman. The spectrum consisted of a continuous background with superimposed bright lines and extended towards the region of short wave-lengths to about 850A where it was cut off by the strong continuous absorption of hydrogen.

[8] J. J. Hopfield and G. H. Dieke; Nature, **118,** 592 (1926). Note. In this first communication of the absorption spectrum of H_2 it was stated, "This adds a new electronic level to the three already obtained." As a result of our more careful study of the absorption spectrum and its correlation with the emission spectrum it was found that an earlier note concerning the emission spectrum. (G. H. Dieke and J. J. Hopfield, Phys. Rev. **28,** 849, 1926) contained an error, so that there are but three electronic levels of H_2, *A*, *B*, *C*, known from the ultra-violet spectrum instead of the four implied in the "Nature" letter. Also the absorption bands of H_2 start at 1116A rather than at 1245A as mentioned there.

[9] Th. Lyman, Astrophys J. **60,** 1 (1924). Compare also Nature **118,** 156 (1926).

Fig. 1 shows the absorption spectrum of hydrogen obtained in this way with hydrogen pressures of about 2, 4, 8, 15, 36, and 50 mm of hydrogen in the spectrograph. The hydrogen molecule begins to absorb at about 1115A. There are on our plates a few absorption bands on the side of longer wave-lengths, but they must apparently be attributed to traces of impurities, as control experiments with other gases show. In particular, a strong band at 1245A, which appears very easily, seems to belong to oxygen or an oxygen compound. The line 1215A of the hydrogen atom appears as a sharp absorption line and forms a good standard for the measurement of the absorption plates.

TABLE I

Absorption lines of hydrogen in the extreme ultra-violet.

λ	Int.	ν	Designation	λ	Int.	ν	Designation
849.43		117726*		1036.56	4	96473	a, B_8-A_0
986.14	3*b*	101405	C_1-A_0	36.98	4	434	
87.73	1	242		38.13	4	327	*b*
89.45	0	066		38.52	4	291	
91.25	3	100883	a, B_9-A_0	40.21	0	134	*c*
91.86	3	821		41.04	0	058	
92.60	3	746	*b*	43.44	0	95837	*d*
92.47	3	758		49.45	2	288	a, B_4-A_0
95.84		418		49.90	2	248	
1001.65	2	99835	a, B_8-A_0	51.22	4	128	*b*
02.29	2	772		53.18	00	94950	*c*
03.21	2	680	*b*	53.95	0	881	
03.90	2	611		56.33	00	668	*d*
05.20	1	483	*c*	63.29	5*d*	048	a, B_3-A_0
06.29	1	375		64.74	5	93919	*b*
08.42	3	165	a, C_0-A_0	66.95	0	752	*c*
09.71	3	039	*b*	67.49	0	678	
10.78	1	98933	*c*	70.14	0	446	*d*
12.77	3	739	a, B_7-A_0	77.16	4	92837	a, B_2-A_0
13.40	3	677		77.80	4	782	
14.21	3	599	*b*	79.07	4	672	*b*
14.80	3	541		92.23	3	91556	a, B_1-A_0
16.32	1	395	*c*	92.70	3	517	
17.28	1	301		94.16	3	395	*b*
19.34	0	103	*d*	96.57	2	194	*c*
20.54	0	97987		99.84	2	90922	*d*
24.43	1	615	a, B_6-A_0	1108.17	0	239	a, B_0-A_0
24.91	2	570		08.68	2	197	
25.67	2	497	*b*	10.09	2	083	*b*
26.36	1	431		12.57	2	89882	*c*
27.89	1	287	*c*	14.00	0	767	
28.87	1	194		14.68	0	712	
				15.72	2 *br*	628	*d*

*Limit of continuous absorption.

The absorption spectrum of the hydrogen molecule shows a number of regularly grouped bands of the same structure as the bands of the emission spectrum. The first bands are clearly resolved and can be measured satisfactorily. Toward the short wave-lengths the bands overlap and at about 850A a strong continuous absorption begins. The measured absorption lines are tabulated in Table I.

4. Measurements

One great difficulty in obtaining accurate wave-lengths is that there are, in the region under investigation, no satisfactory standards which could be used. On the best hydrogen pictures no traces of lines belonging to impurities could be detected. The atomic lines, the wave-lengths of which are accurately known, are very weak on the photographs which show the secondary spectrum in its best development. Only the two first members of the Lyman series can be found on such plates. In addition λ1215 is usually very broad and very probably blended with secondary lines, and λ1025 is an unresolved doublet, the one component of which is a molecular line (*b* of C_2-A_3). Both lines are therefore, as a rule, useless as standards. On one photograph, which was taken after the tube had been operated with oxygen for some time, the secondary spectrum is strongly developed and at the same time at least five members of the Lyman series show up. The lines 972.54, 949.74, and 937.80 could here be used as standards for the part of the spectrum below 1000A, although also here the possibility remains that they are blended with molecular lines. On the films taken with the older grating some of the secondary lines could be measured in the third and fourth order between the Balmer lines $H\gamma$, $H\delta$, and $H\epsilon$ as standards. ($H\beta$ is superimposed on the fourth order of λ1215.67 which is very broad on these pictures and therefore unsuitable as a standard.) Other secondary lines were measured on plates which show lines of impurities, such as oxygen, nitrogen, and mercury lines which were used as standards. The values of the wave-lengths of molecular lines determined on these films were then used as standards on the other films.

Owing to this procedure the values of the wave-lengths may be in error by more than 0.1 of an Angstrom unit. The relative accuracy of clearly defined lines is however much greater, and the error does not exceed a few hundredths of an Angstrom unit, as can be seen from the coincidence of the wave-lengths of the same line obtained on different films and from the accuracy with which the combination relations hold. For very weak and diffuse lines and blends and lines which lie very close together and the absorption lines, the error may be considerably greater.

Because it is intended to re-photograph the spectrum with a larger grating, no attempt has been made to obtain the best possible values for the wave-lengths from our plates. Therefore corrections for the non-normality of the spectrum, etc., were not applied as the relative wave-lengths are sufficient to establish the regularities. Wave-lengths of lines obtained from different plates between different standards have, however, been reduced when necessary, in such a way that they are consistent with each other.

The lines below 1330A could be measured in the second order of the new grating the dispersion of which is 8.3A per millimeter. The remaining lines had to be measured in the first order of the new grating (dispersion 16.6A per mm) or in the third order of the old grating (dispersion 11.1A per mm).

5. Nomenclature

An electronic state is designated by a capital letter, and an added number shows the vibrational state of the molecule (e.g. A_5). A band is then, for instance, characterized by C_3-A_5, or some times by the wave-length of its first line. In this paper only the electronic and vibrational states will be dealt with and the rotational structure will be regarded only as far as can be used for proving the correctness of the vibrational scheme and as far as it is independent of any special assumption. In order not to anticipate anything about the rotational structure, a discussion of which is reserved for another paper, the successive lines in one band are designated by the letters $a, b, c, \cdots$.

6. Classification of the Lines

Figures 2 to 7 give the appearance of the spectrum under ordinary conditions (uncondensed discharge and low pressures in the discharge tube). As with the visible, the ultra-violet spectrum is very rich in sharp lines. The

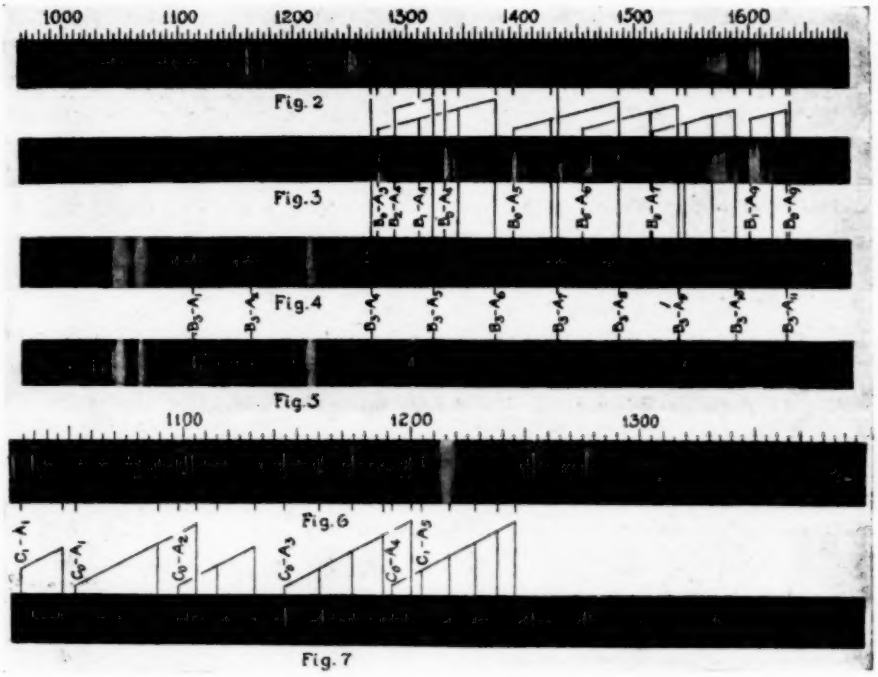

Figs. 2–7. Emission spectrum of hydrogen under various conditions of discharge.

most striking feature of the spectrum is the presence of several groups of lines of apparently the same structure between 1100 and 1200A. In the other parts of the spectrum the regularities are not so obvious. We have, however a much simpler form of the spectrum in either the absorption spectrum or in the emission spectrum, when it is produced in a discharge tube filled with a

mixture of argon and hydrogen, as first observed by Lyman.[10] These simplified spectra can be used as a first method of attack in the analysis.

In order to obtain the simplified emission spectrum, pictures with argon containing traces of hydrogen were taken. Usually it was not necessary to introduce hydrogen in the discharge tube, as the aluminum electrodes gave off enough hydrogen to bring out the hydrogen bands quite strongly. By varying the conditions in the discharge tube it was possible to obtain the hydrogen spectrum in all stages of transition from the most simplified form to its full development with no argon present. Fig. 5 shows the spectrum in the stage at which only the bands found by Lyman (the "Lyman bands") are present and Fig. 4 gives an intermediate stage. The bright background on Fig. 5 is due to the impurities in the argon and is not present on Lyman's plates.

While the present work was in progress, a paper by Witmer[11] appeared in which he analyzed the simplified spectrum, using recent photographs of Lyman. He derived critical potentials and the heat of dissociation from this spectrum. We shall discuss his results presently.

TABLE II

Wave-lengths and frequencies of the Lyman bands.

	λ	Int.	ν
	λ1112, B_3-A_1.		
a_1	1112.01	3	89 928
a_2	12.57	3	882
b	13.81	3	782
c	16.18	4	591
d	19.52	4	324
e	23.77	1	88 986
	λ1162, B_3-A_2.		
a_1	1162.79	2	86 000
a_2	63.32	2	85 961
b	64.75	3	856
c	67.16	3	678
d	70.56	3	429
e	74.90	0	114
	λ1268, B_3-A_4.		
a_1	1268.64	*6	78 825
a_2	68.91	*2	808
b	70.53	4	707
c	73.11	3	548
d	76.64	*3	331
e	81.06	1v	060
	λ1323, B_3-A_5.		
a	1323.31		75 568
b	25.09		467
c	27.63		322
d	31.14		123
e	35.61		74 872
	λ1378, B_3-A_6.		
a	1378.03	1	72 568
b	80.07	4	460
c	82.63	2	326
d	86.13	3	144
e	90.50	1	917
	λ1432, B_3-A_7.		
a	1432.90	10d	69 789
b	35.14	5	685
c	37.59	*4	561
d	40.95	*6	399
	λ1486, B_3-A_8.§		
a	1486.73	*6dr	67 262
b	89.21	*5	150
c	91.83	5	032
d	95.32	*4	875
	λ1539, B_3-A_9.		
a	1539.50	3	64 956
b	41.94	5	854
c	44.24	*2	757
d	47.16	*3	635
e	50.66	4	489
f	55.13	2	303
	λ1589, B_3-A_{10}.		
a	1589.10	10d	62 929
b	91.48	*6	836
c	93.57	*4	752
d	96.20	8	649
e	99.41	5	523
f	1503.02	3	382
	λ1633, B_3-A_{11}.		
a	1633.76	*6	61 208
b	36.44	5	108
c	38.30	5	039
d	40.40	5	60 961

§ This band practically coincides with the strong band B_1-A_7, and only very poor measurements were possible.

* These lines are probably blended with others.

[10] Th. Lyman, Astrophys J. **33**, 98 (1911). Spectroscopy of the extreme ultra-violet p. 79.

[11] E. E. Witmer, Proc. Nat. Acad. Sci. **12**, 238 (1926).

The wave-lengths and frequencies of the Lyman bands are given in Table II. The intensities in the tables are rough estimates on plates under fairly normal conditions. The relative intensities change considerably with changed conditions in the discharge tube. The successive bands can be represented by a Deslandres formula, and the sign of the quadratic term shows that they have a common initial level and are due to transitions from this level to a set of levels with the same electronic and successive vibrational quantum numbers. It is easy to obtain the absolute values for the vibrational quantum numbers, if we regard also the absorption spectrum the other simplified

TABLE III

Other hydrogen bands in the region from 1275A to 1632A.

	λ	Int.	ν		λ	Int.	ν		λ	Int.	ν
	λ1275, B_0-A_3				λ1310, B_1-A_4				λ1289, B_2-A_4		
a_1	1274.92	3	78 436	*a*	1310.87	3	76 285	*a*	1289.29	2	77 562
a_2	75.65	2	391	*b*	12.79	4	174	*b*	91.04	1	457
b	76.81	*3	320	*c*	15.42	2	022	*c*	93.62	1	302
c	79.48	2	157	*d*	19.04	4	813	*d*	97.19	3	090
d	83.10	5	77 937	*e*	23.63	0	550				
e	87.73	2	656								
	λ1333, B_0-A_4				λ1427, B_1-A_6				λ1345, B_2-A_5		
a	1333.85	6	74 971	*a*	1427.74	8	70 041	*a*	1345.46	4	74 324
b	35.93	6	854	*b*	30.01	7	69 930	*b*	47.37	6r	219
c	38.62	3	704	*c*	32.90	10d	787[2]	*c*	50.68	3	075
d	42.31	6	498	*d*	36.23	*8r	627	*d*	53.54	5	73 880
e	46.91	8d	244	*e*	40.95	*6	399	*e*	58.04	3	636
	λ1394, B_0-A_5				λ1486, B_1-A_7				λ1515, B_2-A_6		
a	1394.94	10	71 739	*a*	1486.73	*6dr	67 262[3]	*a*	1515.19	5	65 998
b	96.24	6	621	*b*	89.21	*5	150[4]	*b*	17.61	4	893
c	99.00	6	480	*c*	91.83	5	032[5]	*c*	20.08	3	786
d	1402.69	*8	292	*d*	95.37	*10r	66 873[6]	*d*	23.40	6	643
e	07.34	*4	056	*e*	99.71	5	680	*e*	27.44	2	469
f	12.89	8	70 777	*f*	1504.93	5	448				
	λ1455, B_0-A_6				λ1545, B_1-A_8				λ1569, B_2-A_9		
a	1455.05	*6	68 726	*a*	1544.90	*5v	64 729	*a*	1569.59	4	63 711
b	57.56	5	608	*b*	47.56	*3	618	*b*	72.16	4	607
c	60.20	*4	484	*c*	50.23	2	506	*c*	74.51	4	512
d	63.94	7d	309	*d*	53.62	*5	366	*d*	77.46	10bd	393
e	68.53	4	096	*e*	57.65	1	199				
f	73.96	3	67 845								
	λ1516, B_0-A_7				λ1602, B_1-A_9				λ1621, B_2-A_{10}		
a	1516.33	5	65 949	*a*	1601.67	*2	62 435	*a*	1621.03	6d	61 689
b	18.88	5	838	*b*	04.63	4	319	*b*	23.62	4	591
c	21.77	2	713	*c*	unmeasurable			*c*	25.79	3	509
d	25.34	4	559	*d*	09.92	2	115	*d*	28.48	5	407
e	29.53	2u	379					*e*	31.70	3	286
	λ1636, B_0-A_9				λ1655, B_1-A_{10}						
a	1636.44	5v	61 108[1]	*a*	1655.16	*1	60 417				
b	38.99	3	013	*b*	58.16	1	308				
c	41.58	4	60 917	*c*	60.36	0	228				
d	44.48	4	810	*d*	63.10	2	129				
e	48.63	0	656	*e*	66.32	0	013				

* These lines are probably blended with others.

[1] Coincides with *b*, B_3-A_{11}.

[2] Coincides with *a*, B_3-A_7.

[3] Coincides with *a*, B_3-A_8.

[4] Coincides with *b*, B_3-A_8.

[5] Coincides with *c*, B_3-A_8.

[6] Superimposed by heavy line.

form of the spectrum. The first Lyman band (in emission) which can be recognized on our plates lies at 1112A. It cannot be due to transitions to the normal state of the molecule, because it is not found in absorption. The next band on the short wave-length side would be obscured on the argon plates by one of the heavy argon resonance lines. But in the place where it is to be expected is the fourth absorption band λ1063, which must be due to transitions from the first excited state with three vibrational quanta (B_3)

TABLE IV

Hydrogen bands which dominate the spectrum below 1250A.

	λ	Int.	ν
	λ1052, C_0-A_1		
a	1052.58	2b	95 005
b	54.00	2	94 877
c	55.12	0	776
d	56.82	0	624
(*e*	58.81	2	445)
	λ1097, C_0-A_2.		
a	1097.90		91 083
b	99.41		90 986
c	1100.46		871
d	02.10		736
e	04.29		556
	λ1144, C_0-A_3.		
a	1144.20	5	87 397
b	45.85	8	272
c	46.87	5	194
d	48.44	7	074
e	50.78	6	86 898
f	53.03	1	728
	λ1191, C_0-A_4.		
a	1191.49	3d	83 928
b	93.20	5	809
c	94.17	8	740
d	95.62	5	639
e	97.87	2	482
	λ1027, C_1-A_1.		
a	1027.75	0	97 300
b	28.77	1	204
c	30.16	1d?	073
d	31.80	0	96 917
	λ1114, C_1-A_3.		
a	1114.92	5	89 693
b	16.34	*8	578
c	17.43	4	491
d	18.99	6	367
e	21.15	5	194

	λ	Int.	ν
	λ1159, C_1-A_4.		
a	1159.68	5	86 231
b	61.25	8	114
c	62.25	5r	040
d	63.75	6	85 929
e	66.04		761
	λ1204, C_1-A_5.		
a	1204.89		82 995
b	06.60		877
c	07.51		815
d	08.91		719
	λ1046, C_2-A_2.		
a	1046.56	5	95 551
b	47.79	5	438
c	48.94	2	333
d	50.64	3	180
e not resolved from *a*, C_0-A_1.			
	λ1088, C_2-A_3.		
a	1088.64	7d?	91 858
b	89.95	5	748
c	91.02	1	657
d	92.68	2	520
	λ1131, C_2-A_4.		
a	1131.34	2	88 391
b	32.68	3	286
c	33.69	0	208
d	35.27	4	085
e	37.00	2	
	λ1174, C_2-A_5.		
a	1174.28	3	85 159
b	75.79	6	049
c	76.74	2	84 980
d	78.21	7	875
e	80.42	5u	716
	λ1217, C_2-A_6.		
a_1	1217.28	3	82 151
a_2	17.64	3	
b	18.92	6	040
c	19.77	3	81 983
d	21.05	3	896

	λ	Int.	ν
	λ1024, C_3-A_2.		
a	1024.74	2	97 586
b not resolved from 2nd member of Lyman series			
c	26.98	0	374
d	28.77	1	204
not separated from *b*, C_1-A_1			
	λ1105, C_3-A_4.		
a_1	1105.71	1	90 439
a_2	06.03	1	414
b	07.08	5	328
c	08.17	1	239
d	09.79	2	107
	λ1187, C_3-A_6.		
a	1187.77	7	84 192
b	89.33	5	081
c	90.22	3	018
d	91.49	3d	83 928
not separated from *a*, C_0-A_4			
e	93.20	5	809
coincides with *b*, C_0-A_4			
	λ1228, C_3-A_7.		
a	1228.18	4	81 421
b	29.95	8bd?	304
c	30.72	4	254
d	31.90	3	176
	λ1199, C_1-A_7.		
a	1199.89	*4bd	83 338
b	1201.78	4d	210
c	02.57	3	156
d	03.86	2	066
	λ1237, C_4-A_8.		
a	1237.89	*4	80 782
b	39.48	5	679
c	40.16	3	635
d	41.24	2	565
	λ1245, C_5-A_9.		
a	1245.79	5	80 270
b	47.27	5	175
c	48.79	3	134
d	49.26	3	078

to the normal state A_0 of the molecule, and can be written in our notation B_3-A_0. The Lyman bands are then due to transitions from the same initial state B_3 to the successive vibrational levels of the lowest electronic state, and they must therefore be designated by B_3-A_n.

On photographs of the emission spectrum in pure hydrogen the Lyman bands can all be easily identified, though they are not as prominent as in the pictures with argon. There are a number of bands, some of them very strong, which are due to transitions from other B states to the same set of final A levels. They are given in Table III and their arrangement into the system can be seen from the upper part of Table V in which the bands are given by the wave-length of the head and the frequency of the b-line. The a-line is in many cases an unresolved doublet and is therefore not suitable for representing the regularities.

The bands which dominate the spectrum below 1250A if pure hydrogen is used, belong to another system which has the same final electronic state A but a different initial electronic state C. They are listed in Table IV, and the vibrational scheme is given in the lower part of Table V. These bands have

TABLE V

	A_0	A_1	A_2	A_3	A_4	A_5	A_6	A_7	A_8	A_9	A_{10}	A_{11}
B_0	1108 90 083			1275 78 320	1333 74 854	1394 71 621	1455 68 608	1516 65 838		1636 61 013		
B_1	1092 91 396				1310 76 174		1427 69 930	1486 67 150	1545 64 618	1602 62 319	1655 60 310	
B_2	1077 92 672				1289 77 457	1345 74 219			1515 65 893	1569 63 607	1621 61 591	
B_3	1063 93 919	1112 89 782	1162 85 856		1268 78 707	1323 75 467	1378 72 460	1432 69 685	1486 67 141	1539 64 848	1589 62 836	1633 61 108
B_4	1049 95 128						1355 73 661			1511 66 063		
C_0	1008 99 039	1052 94 887	1097 90 986	1144 87 272	1191 83 809							
C_1	985	1027 97 204		1114 89 578	1159 86 114	1204 82 877						
C_2			1046 95 438	1088 91 748	1131 88 286	1174 85 049	1217 82 040					
C_3			1024 (97 492)		1105 90 328		1187 84 081	1228 81 304				
C_4								1200 83 210	1237 80 679			
C_5										1245 80 175		

a structure analogous to that of the $B-A$ bands, and also in this system the absolute values of the vibrational quantum numbers can be determined from the absorption spectrum. The first two members of the absorption series C_n-A_0 can be measured and are found in the places where they must be expected. The presence of further members of the series can be recognized on the plates. They are, however too much confused with the $B-A$ bands to allow measurements.

The structure of most of the bands can immediately be recognized on the

plates, and these bands are, of course, the most important ones for establishing the regularities. In some parts of the spectrum the regularities are obscured, because several of the bands overlap, and the resolution of the grating is there insufficient. The wave-length measurements in such parts have therefore considerably less accuracy and such lines cannot be used to prove anything. Many gaps in Table V have their explanation in the fact that the corresponding bands must lie in places where other bands are strongly developed. Their existence is therefore still doubtful, and they have been omitted from the tables for that reason. That is, for instance, the case for the bands of the $B-A$ system which correspond to transitions between small numbers of the vibrational quantum numbers and which lie in the region where the most intense bands of the $C-A$ system occur.

7. Combinations

The correctness of the above classification can be tested by an application of the combination principle. A band line can always be written in the form:

$$\nu = B(n',m') - A(n'',m'')$$

in which A and B are two arbitrary electronic states, n the vibrational, and m the rotational quantum number. If we take two bands with the same initial state (vibrational and electronic) i.e. two bands of the same horizonta] row of Table V, and form the difference of corresponding lines, the result

$$\Delta\nu = A(n_1,m) - A(n_2,m) \qquad (2)$$

is entirely independent of the initial state. We can therefore form the corresponding differences for each row of Table V, and they must all have the same value. These differences are given in Table VI, as a rule for the

Table VI

Wave-number differences between the various A terms as calculated from the wave-number differences of various band lines.

		a	b	c	d	e			a	b	c	d	e
A_2-A_1	B_2	3921	3926	3913	3895	3872	A_6-A_4	B_0	6245	6246	6220	6189	6150
	C_0	3922	3919	3905	3891			B_1	6244	6244	6233	6186	6151
A_3-A_1	C_0	7607	7605	7582	7549			B_2	6240	6247	6222	6187	6144
A_3-A_2	C_0	3686	3686	3677	3661	3658		C_2	6247	6247	6221	6179	
	C_2	3693	3691	3676	3660		A_7-A_6	B_0	2777	2770	2771	2750	2716
A_4-A_2	B_2	7153	7148	7130	7089	7054		B_1	2780	2780	2756	2753	2719
	C_0	7157	7149	7131	7097			B_2	2779	2775	2765	2745	
	C_2	7146		7133				C_2	2771	2777	2765	2753	
A_4-A_3	B_2	3465	3466	3453	3438	3411	A_8-A_7	B_1	2533	2532	2525	2508	
	C_0	3471	3463	3454	3436	3416		B_2	2527	2535	2529	2524	2481
	C_1	3462	3464	3451	3437			C_2	2555	2531	2521	2501	
	C_2	3467	3462	3449	3435		A_9-A_8	B_1	2295	2299		2251	
A_5-A_4	B_0	3232	3233	3224	3206	3188		B_2	2287	2286	2274	2249	
	B_2	3238	3238	3227	3209	3187		B_3	2305	2296	2275	2241	
	B_3	3240	3241	3226	3208	3188	A_9-A_7	B_0	4840	4825	4796	4750	4723
	C_1	3236	3237	3225	3210			B_1	4827	4831		4760	
	C_2	3232	3237	3227	3210	3186		B_2	4832	4831	4804	4764	
A_6-A_5	B_0	3013	3013	2996	2983	2961	$A_{10}-A_9$	B_1	1996	2011		1986	
	B_2	3001	3007	2996	2980	2956		B_2	2022	2016	2003	1986	
	C_2	3008	3009	2997	2978	2365		B_3	2027	2028	2004	1985	

successive bands of the rows. The second column gives the common initial state. It is seen from the table that the relations derived from the combination principle hold well within the limits of the experimental errors. The agreement is very satisfactory, if one considers that an error of 0.1A in the wave-lengths would give an error of 7 wave numbers at 1200A. As mentioned before, the wave-lengths could generally be measured with a much greater precision, but the errors in the four wave-lengths concerned may work together in some cases. Also if the lines whose differences have been calculated lie in parts of the spectrum which have been measured between different standards, the error may be greater. In judging the coincidence for the line *a* it must not be forgotten that this line is often an unresolved doublet with varying separation of the components. Relations corresponding to those expressed by Eq. (2) hold, of course, for bands with the same final state.

8. Variation of the Rotational Energy with the Vibrational Quantum Number

Though the rotational structure of the bands is not discussed in this paper, we can use some general features of it which are entirely independent of any special assumption to obtain additional evidence for the correctness of the vibrational scheme as given in Table V. The rotational energy can always be written in the form Bhm^2, in which $B=h/8\pi^2 I$ (I is the "effective" moment of inertia) and m the rotational quantum number (not necessarily an integer or a half-integer). As a first approximation B depends linearly on the vibrational quantum number[12]

$$B=B_0-\alpha n. \tag{3}$$

A line of a band can then be written

$$\nu=\nu_0+B'm'^2-B''m''^2$$

and if we form in all bands of a horizontal row of Table V the differences of two corresponding lines

$$\Delta\nu=B'(m_1'^2-m_2'^2)-B''(m_1''^2-m_2''^2),$$

in this difference only B'' changes from band to band. Therefore, on account of (3), we must obtain approximately a straight line, if we represent $\Delta\nu$ as a function of n'', and all lines which belong to different initial states must be parallel to each other. Figs. 8 and 9 show the differences $b-c$ and $c-d$, and it is seen that within the limits of experimental errors the lines have exactly the properties which we must expect. The lines for the B_1-A_n and B_2-A_n bands for which fewer and less accurate data are available have been omitted in order not to crowd the figures.

[12] A. Kratzer, Zeits. f. Physik. **3**, 269, (1920); Ann. d. Physik. **67**, 127 (1922).

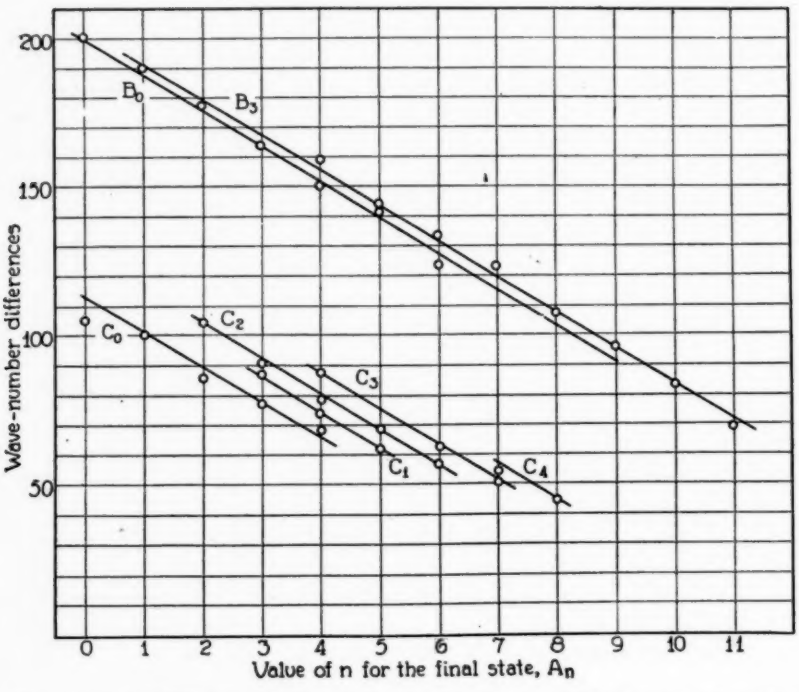

Fig. 8. Wave-number differences between the *b* and *c* members of the bands as functions of the vibrational quantum number of the final state.

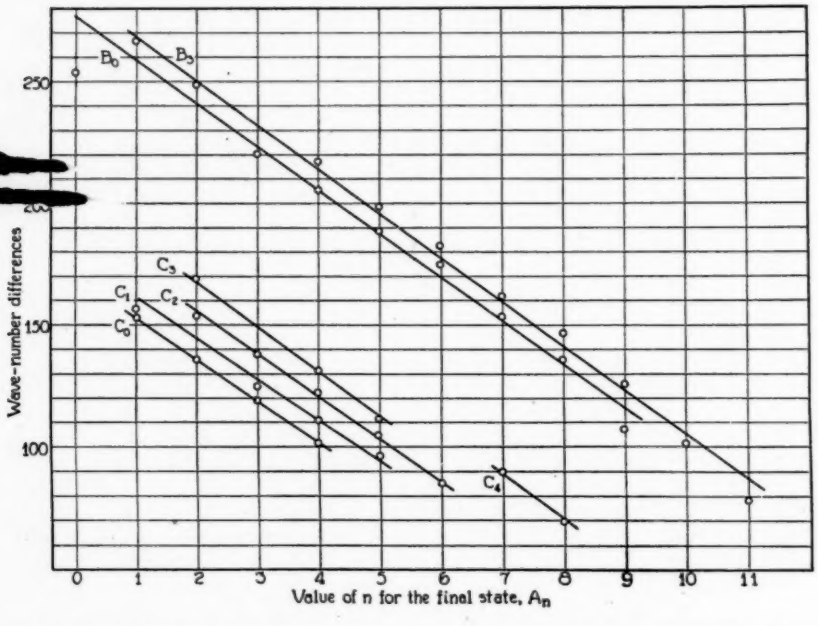

Fig. 9. Wave-number differences between the *c* and *d* members of the bands as functions of the vibrational quantum number of the final state.

9. Energy Levels

Fig. 10 gives a representation of the relative position of the levels as they have been determined from the preceding data. The absorption measurements show that A is the lowest electronic state so that A_0 can be called the normal state of the molecule. The two observed systems can be represented approximately by the usual formula.

$$\nu=\nu_e+(\omega_0'n'-x'n'^2+\cdots)-(\omega_0''n''-x''n''^2+\cdots) \qquad (4)$$

In this formula ν_e is the share of the electronic energy, ω_0 the vibrational frequency for infinitesimal amplitudes, and x a constant which is determined by the non-harmonic character of the law of force between the two nuclei.[12] According to the more recent investigations n has half-integer values.[13] The constants for the hydrogen molecules are given in Table VII. In order to enable a direct comparison with older data on other molecules the values for the constants, if integer vibrational quantum numbers are used in (4), are given in parentheses. The numbers which have been used to characterize the different vibrational states are always half a unit lower than the true vibrational quantum numbers.

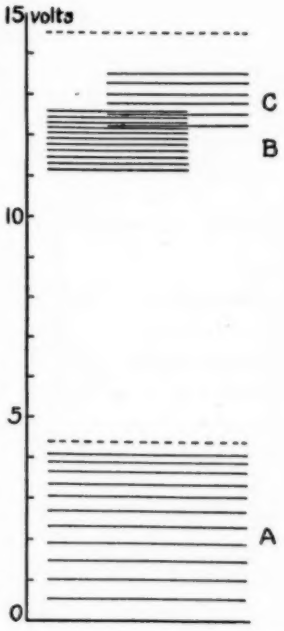

Fig. 10. Energy level diagram for the hydrogen molecule.

TABLE VII

Constants of the hydrogen molecule.

	$B-A$		$C-A$
ν_e	91 562		99 986
	(90 083)		(99 039)
	A	B	C
ω_0	4362	1355	2444
	(4247)	(1337)	(2377)
$2x$	229	36	134

Strictly speaking the constants have only the above meaning if formula (4) represents the zero lines of the bands. The deviations, if a real line is taken (in our case the b-line), are however only small. It is very remarkable how much ω_1 changes in a transition from the B to the A-state.

[12] R. S. Mulliken, Phys. Rev. **25**, 259 (1925); W. Heisenberg, Zeits. f. Physik **33**, 879 (1926).

10. Critical Potentials

It follows from the preceding scheme that the resonance potential of the hydrogen molecule is 11.1 volts, and electrons with 11.3, 11.4, 11.6 volts energy must be able to bring the molecule into the B_1, B_2, B_3, state respectively, while the C_0 state is excited at 12.2 volts. The agreement of these values with those determined by direct experiments is not very satsifactory. The discrepancy can however be understood, if we realize that a critical potential in a molecule is something different from a sharply defined critical potential of an atom. As the molecules are distributed over the different rotational states each of which has its own values for the critical potentials, the breaks in the curves cannot be expected to be sharp. As the bands are degraded towards the red, the lines corresponding to a high rotational quantum number require a lower excitation potential than those corresponding to the lower states. In hydrogen the excitation potential for the *a*-line is more than 0.1 volt higher than that of the *e*-line. Therefore it is difficult to decide, what we ought to call the critical potential for a band, and its value cannot be given with great accuracy and will be slightly variable with temperature. What is measured is always a value which is obtained by extrapolation of the curve representing the electronic current before and after the critical potential. It is apparent that this procedure will give only an average value. Furthermore the breaks corresponding to the successive critical potentials must be expected in a distance of about 0.15 volt and probably cannot be resolved by the experiments. The observations give therefore an average value which is dependent on the relative probabilities of the transitions. In our case the first members of the absorption series are very weak, which means also that the probability that an electron excites one of the first states must be expected to be small, and that would shift the observable average critical potential considerably to higher values.

The Lyman bands are due to transitions from the B_3 state to the different A states. This shows that in an argon-hydrogen mixture they must be excited almost exclusively by collisions of the second kind with excited argon atoms. For, if direct electron impacts would also play any considerable role, the B-levels with vibrational quantum numbers smaller than three would necessarily have to be excited as well. Bands which belong to transitions from these states are practically absent on the argon-hydrogen plates, though they are very strong in pure hydrogen. It is remarkable how strong in this case is the selection of the levels which are excited by the collisions of the second kind. In other cases it has been observed that those states are most strongly excited by collisions of the second kind, for which the least amount of energy is converted into translational energy, and we seem here to have a particularly good example of such a resonance effect. The matter is complicated somewhat by the fact that four excited argon levels $1s_5$ with 11.50, $1s_4$ with 11.57, $1s_3$ with 11.67, and $1s_2$ with 11.77 volts energy[14] must be taken into account.

[14] Compare K. W. Meissner, Zeits. f. Physik **37**, 238 (1926).

[15] K. W. Meissner, Ann. d. Physik **76**, 124 (1925); H. B. Dorgelo, Zeits. f. Physik **34**, 766 (1925).

For the corresponding states of neon it has been shown by absorption experiments in the excited gas[15] that most atoms are in the metastable states s_3 and s_5, and these will therefore probably be the most important ones for the excitation of the hydrogen molecules. From a purely energetic point of view, however, it remains unexplained, why the B_2 and B_4 states are not also excited to an appreciable extent.

From an analysis of the Lyman bands only, Witmer[10] concluded that in an argon hydrogen mixture the hydrogen molecule is brought by both electronic collisions and collisions of the second kind into the first excited electronic state with no vibrational energy. The critical potentials which result from this conception of the bands are considerably higher, but they cannot be brought into accordance with the absorption spectrum and the full analysis of the emission spectrum.

11. Dissociation

The maximum of vibrational energy which a molecule can have determines the heat of dissociation of the molecule and this has recently been determined spectroscopically with more or less precision for a number of molecules.[16] For hydrogen the heat of dissociation can be determined from the ultra-violet band spectrum according to two independent methods.

In the first method the mechanical vibrational frequency $\omega_n = (1/h)\partial E/\partial n$ is represented as a function of the vibrational quantum number n, and the curve obtained in this way is extrapolated to $\omega_n = 0$. The heat of dissociation is then $h\int \omega_n dn$ and can be found by graphical integration of the $\omega_n = F(n)$ curve. The accuracy of this method is the greater the longer the portion of the curve which has been determined by the observations. Witmer applied this method to the final state of the Lyman bands, which is, as we have seen, the lowest state of the molecule and found 4.34 volts for the heat of dissociation. We can take over his results. Though a large part of the ω_n-curve is empirically known, the uncertainty of the extrapolation must be estimated to be about 0.1 volt.

The second method for determining the heat of dissociation which can be applied in the case of hydrogen uses the limit of the continuous absorption. By the absorption of light of the right frequency the hydrogen molecule can be brought from the normal state A_0 to a series of excited states with increasing amounts of vibrational energy. For high values of the vibrational quantum number the corresponding bands lie closer and closer together until, in our case, they are no longer resolved. If the vibrational energy exceeds a certain limit which is the heat of dissociation the nuclei do not stay together any longer, i.e. dissociation takes place and a continuous spectrum is absorbed, because the two atoms can separate with any arbitrary amount of translational energy. The limit of this continuous absorption is particularly sharp for hydrogen. It lies at λ849.4 or 14.53 volts. The hydrogen molecule

[16] J. Franck, Trans. Faraday Soc. **21**, part 3 (1925). E. G. Dymond, Zeits. f. Physik **34**, 553 (1925); R. T. Birge and H. Sponer, Phys. Rev. **28**, 259 (1926).

must fall apart into one normal and one excited atom in the two quantum state which has 10.15 volts energy. We have therefore the energy equation

$$D+10.15=14.53 \text{ volts},$$

from which we obtain the value 4.38 volts for the heat of dissociation D which agrees better than could be expected with the value found by the first method. On the energy diagram (Fig. 10) the dissociation is marked by the dotted lines.

It seems probable that both the B-A and the C-A absorption series converge to the limit 14.53 volts. A rough extrapolation which cannot claim any accuracy gives 14.2 and 14.8 respectively for the two limits. Now the experimental facts have shown that, in dissociating, a molecule can fall apart only into atoms which are in definite quantum states. To dissociate a hydrogen molecule into one normal and one excited atom in the three quantum state 16.4 volts are required. The values found by extrapolation lie sufficiently close to 14.5 volts to justify the conclusion that this is the common limit of the B-A and C-A series. This means that if the nuclear distance of a hydrogen molecule in a B or C state is increased adiabatically the molecule, falls apart into one normal and one excited molecule with the electron in a two quantum orbit. The different character of the B and C state makes it probable that in the one case the electron moves in a 2_1 and in the other in a 2_2 orbit.

We must in some cases expect an emission analogue to the continuous absorption spectrum. For if a molecule makes a transition from an excited to a lower level, it is possible that it gains so much vibrational energy that it dissociates into two atoms. A continuous spectrum is then emitted extending towards the longer wave-lengths from a limit which is given by

$$h\nu=E'-D,$$

where E' is the energy before the transition and D the heat of dissociation. This continuous spectrum starting at the end of a series like the Lyman bands must be expected to be very intense, if the bands, which correspond to high values of the final vibrational quantum number are strong. That is the case in hydrogen for the B-A system, and it is very probable that the continuous spectrum which extends from the ultra-violet band spectrum towards the visible must be regarded as a dissociation spectrum in the above sense. The end-product is here two *normal* atoms and not one normal and one excited atom as in the case of the continuous absorption spectrum. This conception of the continuous hydrogen spectrum is identical with the modified Franck-Blackett interpretation.[17] All our observations in the ultra-violet can be brought into accord with it. It extends with great intensity to about 1650, the long wave-length limit of the Lyman bands. Farther to the ultra-violet its presence is obscured by the great number of ultra-violet lines. Of course, in our case, we must not expect the continuous spectrum to extend only to

[17] P. M. S. Blackett and J. Franck, Zeits. f. Physik **34**, 389 (1925); J. Franck and P. Jordan, Anregung von Quatensprüngen durch Stösse, p. 266 (1926).

the long wave-length limit of the Lyman bands, as other similar progressions may also be followed by a continuous spectrum. The intensity of the continuous spectrum seems quite independent of the intensity of the atomic lines. On some plates even the strong line λ1215 is scarcely visible while the continuous spectrum is very strong. Under the conditions under which our pictures were taken the secondary spectrum was always present with great intensity when the continuous spectrum was strong. This is in accord with what we must expect if we interpret the spectrum as a dissociation spectrum. The behavior of the intensity of the *visible* secondary spectrum with respect to that of the continuous spectrum, must, however, be quite different and it must be possible to get a strong continuous spectrum without any trace of the visible molecular spectrum. An experimental decision between the dissociation explanation and an interpretation of Schüler and Wolf[18] could probably be obtained in this way.

It is of course of great importance to find connections with the visible many lined spectrum of hydrogen. In the visible the Fulcher bands are the only known regularities of a sufficient extent to enable a direct comparison with the ultra-violet bands. It seems certain that the Fulcher bands do not belong to one of the levels A, B, C, of this paper. There are however a number of lines in the blue which belong probably to transitions to the B-levels. The results are however still too uncertain to comunicate them at this time.

The latter part of this work was done when one of the authors, Mr. Dieke, was a National Research Fellow, and we wish to express our thanks to the National Research Council and to the International Education Board.

NOTE. This paper has been in the present form for almost a year. Its publication, however, has unfortunately been delayed by the authors. Since this article was written two papers dealing with the ultra-violet spectrum of hydrogen appeared and it seems desirable to state briefly their relation to our work. The first article is the full paper of Witmer[19] giving a more detailed account of his work on the Lyman bands discussed above. He gives some additional bands which he interprets as belonging to the same system as the Lyman bands. They are, however, identical with the strongest $C-A$ bands according to our interpretation. The article by Werner[20] contains measurements of bands which are also identical with bands of the $C-A$ system.

UNIVERSITY OF CALIFORNIA,
July 1, 1927.

[18] H. Schüler and K. L. Wolf, Zeits. f. Physik **33**, 42 (1925); **35**, 477 (1926).
[19] E. E. Witmer, Phys. Rev. **28**, 1223 (1926).
[20] Werner, Proc. Roy. Soc. **A113**, 107 (1926).

THE INFRA-RED RADIATION OF HYDROGEN

By A. H. Poetker

Abstract

Measurement of higher members of Paschen series.—The atomic spectrum of H was investigated in the infra-red region by the photographic method. Neocyanin plates, hypersensitized by an ammonia bath, were used. A powerful discharge tube, maintained in the so-called black stage by careful adjustments, yielded under long exposures six higher members of the Paschen series, the third to the eighth inclusive. The measured wave-lengths agree with the values calculated from the Bohr theory to within the limits of experimental error.

Extension of infra-red secondary spectrum of hydrogen.—By changing the conditions of the discharge a strong molecular spectrum of H was produced. This was photographed in the region from 7500 to 10700A under a dispersion of 9A per mm. The wave-lengths of about 425 lines, mostly new, were measured and are given in tables. A number of these lines seem to be members of band groups analogous to the Paschen series of the elementary spectrum.

Introduction

IN VIEW of the fundamental and unique position held by hydrogen in the entire scheme of the elements, and of the important rôle it plays in every theory of atomic or molecular structure, there has always been a special interest in its spectrum. Despite this, the work done in the infra-red portion of this spectrum has been rather meagre. Paschen,[1] in 1908, discovered the first two lines of the third series of the elementary spectrum. Two members of a fourth series were discovered by Brackett[2] in 1922, and the initial member of a fifth series by Pfund[3] in 1924. Brackett also identified three further lines of the Paschen series,[1] but his apparatus—he worked with a thermocouple and prism—did not enable him to determine their wave-length to within less than 100A. At the same time a number of other maxima occurred in the same region of the hydrogen radiation curve, giving evidence of a fairly complicated spectrum. Of the secondary spectrum, some eighty lines between 6900 and 8029A have been published by Croze.[4] Since a good portion of the spectrum beyond this, including the region occupied by any members of the Paschen series that might be present, is accessible by the method of photography, it was thought worth while to investigate the region by this method. A similar investigation of the secondary spectrum was carried on by Allibone at the same time as the earlier work to be described, and a table of wave-lengths far more comprehensive and accurate than Croze's, and including

[1] Paschen, Ann. d. Physik **27**, 537 (1908).
[2] Brackett, Astrophys. J. **56**, 158 (1923).
[3] Pfund, Jour. Opt. Soc. Amer. **9**, 106 (1924).
[4] Croze, Ann. d. Physique **1**, 48 (1914).

about twenty of the strongest lines beyond 8000A, has recently been published by him.[5]

I. The Elementary Spectrum of Hydrogen

Apparatus. The hydrogen tube was of the shape of an inverted and angular U, somewhat over two meters in length, of 14 mm bore, but widening out at the ends to about 4 cm in order to accommodate rather large cylindrical electrodes 15 cm long and 2 cm in diameter. Usually a smaller tube of about 10 mm bore was inserted in the central cross-piece of the tube to concentrate the discharge still more.

Hydrogen was fed into the tube by a fine capillary near one electrode, and the exhaustion was carried on continuously by a Hyvac pump. By careful adjustment of the capillary and the rate of exhaustion, the precise balance could be maintained to give a maximum of radiation of the type desired.

Excitation of the tube was effected by alternating current from a 6900 volt, 5 kilowatt transformer operating on a 110 volt, 60 cycle primary circuit, and the voltage regulation was by means of a rheostat in the primary.

The dispersion was produced by means of a 3.5 by 3 inch plane grating having 15,000 lines to the inch. It provided, together with the mirror to be described, a dispersion of approximately 18Å to the mm. Since higher dispersion must be at the expense of intensity, it appeared best, with a source as weak as our discharge tube and the low sensitivity of the infra-red plates, to sacrifice higher dispersion and resolution that the intensity might be kept sufficient.

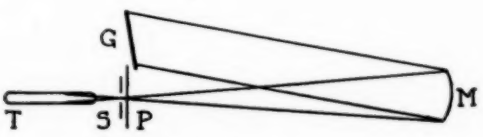

Fig. 1. Plan of apparatus.

The arrangement of the apparatus is clear from Fig. 1. Light was taken end-on from the central portion of the discharge tube. First filtered through a piece of Jena red glass to prevent the overlapping of a second order spectrum, it passed through the slit *S* to the concave mirror *M*, and was reflected as a parallel beam to the grating *G*. The diffracted beam was returned by the mirror to the plate *P* set directly beneath the slit. The mirror was of 90 cm focal length and 10 cm aperture. Slit, grating, mirror and plate were all solidly attached to a single *I*-beam and the whole was enclosed in a light-tight box. Since long exposures were necessary, a thermostat and heating coils were introduced to maintain the temperature constant to within about 0.1°C.

Method. To excite the elementary spectrum, and therefore the Paschen series, the tube was brought by the adjustment of pressure and current density to the so-called "black" stage.[6] The dark space about the electrodes

[5] Allibone, Proc. Roy. Soc. **A112,** 196 (1926).
[6] Wood, Phil. Mag. **42,** 729 (1921).

was about 5 mm, and striations disappeared entirely except for two or three in the wide part of the tube immediately above the electrodes. The secondary spectrum was in evidence only in the same region near the electrodes. The spectrum of the rest of the tube, as seen through a direct vision spectroscope, consisted almost entirely of the pure Balmer lines. For this condition the current through the tube was usually maintained at close to half an ampere. The presence of water vapor seems to be absolutely essential for the elimination of secondary spectrum; other impurities seem rather to enhance it.

The plates used for the photographs were the recently developed neocyanin sensitized plates prepared by the Eastman Company. These were hypersensitized immediately before use by bathing them for about a minute in an ammonia solution at about 10°C and drying rapidly in a blast of warm air. A solution of about 8 to 10 cc ammonia (28 percent) to 100 cc of water seemed to give greatest sensitivity without causing noticeable fog. Rapid drying, however, is the most essential requisite for the sensitizing action. These plates have recorded the 11288 mercury line,[7] and dicyanin, too, has repeatedly brought out lines up to 11,000A under long exposure,[8] but in all these cases far more powerful sources of light like the mercury lamp and various metallic arcs were used.

While the performance of the plates, in general, was good, and quite regularly reliable up to the region of about 9000A, it was found that some of the plates were certainly more sensitive than others of the same batch. Such plates under proper treatment could be made to register lines over 10,000A if moderately strong—with a small prism spectrograph we have brought out the nitrogen bands at 1.04μ in 8-minute exposures—whereas repeated attempts with other plates treated by the same process and used under even more favorable conditions failed to reproduce similar results. It is probable that differences in the rate of drying after the original staining process may account for such differences.

For the comparison spectrum an iron arc was used whose light was focussed on the slit from the side by means of a lens and a right angled prism. In addition to this the second order lines of the secondary spectrum were sometimes introduced by the removal of the filter and the introduction of the proper diaphragm before the slit. As a check on the constancy of temperature during the exposure, a comparison spectrum was made before and after the hydrogen exposure.

The plates were measured on the large and excellent dividing engine of the University. The pitch of the screw is 1 mm and the head has a diameter of about 25 cm and its circumference is divided into 1000 parts, so that one division of the head moves the carriage one micron along the axis of the screw. This corresponds in the present case to about 0.018A. Second order standard iron lines were chosen at intervals of about 5 to 10 mm, the plate scale was determined for these intervals, and the wave-lengths were calculated on the basis of this scale from the engine readings.

[7] Dundon, Schoen and Briggs, Jour. Opt. Soc. Amer. **12**, 397 (1926).
[8] See, for example, Bull. Bur. Stds. **17**, 637 (1922).

Results. The effort to record some of the higher members of the Paschen series resulted in finding the third to the eighth inclusive. The lines are exceedingly faint, even despite the unusual length of exposure and the widening of the slit to about 0.2 mm. This precludes the satisfactory representation of them in a half-tone, but they are unmistakable. The first three of these, the third to the fifth of the series, are quite removed from the stronger portion of the molecular spectrum. Beyond the eighth member the secondary spectrum is already so complex that it would be hard to recognize lines as weak as these higher members of the series would naturally be.

A number of photographs were taken with a small Hilger constant deviation spectroscope receiving its light from the other end of the central section of the discharge tube. Since the instrument was not intended for photographic work only a small portion of the spectrum could conveniently be brought into focus. Fig. 2 (magnification, 3×) shows $P\gamma$ unmistakably. The heavy lines are oxygen 7774, 8446, and 9265. This exposure lasted 60 hours, though $P\gamma$ registered in as low as 15 hours with sharper focus.

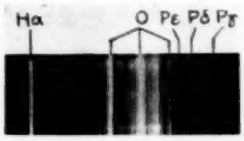

Fig. 2.

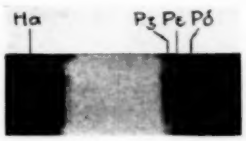

Fig. 3.

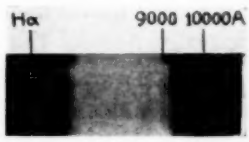

Fig. 4.

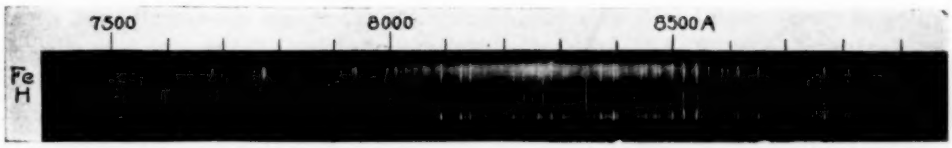

Figs. 2 and 3. Hydrogen, Paschen lines (magnification, 3x).
Fig. 4. Hydrogen secondary spectrum.
Fig. 5. Infra-red secondary spectrum of hydrogen.

Fig. 3 is the result of a 21 hour exposure. The more pronounced secondary and less strong oxygen lines are simply due to the fact that the plate was taken under a completely different set of conditions. The detail in the negative of the central portion of the spectrum was sacrificed in printing to bring out the fainter lines. The region of the visible was absorbed by a deep red filter. Removal of this filter for a few seconds showed the Hα line, quite out of focus but much stronger than the Paschen lines. Now the neocyanin plates are particularly *insensitive* in the region of Hα; still the time of exposure for Hα on this plate was of the order of 1/10,000 of that used to obtain the Paschen lines. One questions the propriety of speaking of such plates as being *sensitive* out to the region of 10,000A.

The Paschen lines, of course, are produced according to the Bohr theory by the falling of an electron into the third stable orbit from higher orbits. Hence their wave-lengths are predicted by the theory from the formula:

$1/\lambda = 109{,}677.7(1/3^2 - 1/n^2)$. For the lines recorded on the plates, $n = 6$, 7, 8, 9, 10, 11. Errors of measurement in this region might easily be as large as 1A due to the faintness of the lines and the width of the slit used. As may be seen from Table I, the observed values agree to within this limit with the

TABLE I

Observed and calculated values of the Paschen lines of hydrogen.

Line	λ Observed in Air (I. A.)	Calculated Value
$P\alpha$	18751.3 (Paschen)	18751.4
$P\beta$	12817.6 (")	12818.3
$P\gamma$	not measured (Brackett 1.09μ)	10938.2
$P\delta$	10049.8	10049.5
$P\epsilon$	9546.2	9546.0
$P\zeta$	9229.7	9229.1
$P\eta$	9015.3	9014.9
$P\theta$	8863.4	8862.9

calculated. The lines are averaged from a half-dozen plates. The lines originally discovered by Paschen are included in the table for the sake of the completeness of the series.

II. The Secondary Spectrum of Hydrogen

It was evident from the work described in Part I that there was a strong secondary hydrogen spectrum in the region from 7000 to 9000A on which practically nothing had been published. Accordingly this spectrum was also photographed with the apparatus already described. It was found that with exposures of from 12 to 15 hours with a slit as narrow as 0.1 mm or less, about 350 lines could be measured between 7250 and 9300A.[9] This suggested that the investigation be made under higher dispersion so that higher accuracy might be obtained, since errors in this preliminary work might have amounted to 0.5A.

Apparatus and Method. An entirely new spectrograph was built up, very similar to that already described in Part I. For greater convenience the slit was mounted to the side and the entering beam was reflected by a silvered interferometer plate to the concave mirror at the other end of the *I*-beam. This was of 6 ft focal length and of 5 inch aperture. The 7 inch plane grating used was ruled with 15,000 lines to the inch and had a strong second order for the visible. The combination supplied a dispersion of about 9A per mm. The whole spectrograph was made perfectly light-tight and well insulated, and a thermostat and heating coils maintained the temperature constant to within 0.1°C.

The discharge tube was made of Pyrex; this eliminated the minute punctures which had caused frequent trouble in the previous work. For part of the work, in order to enhance the secondary spectrum, a second Pyrex tube, 40 cm long and 13 mm bore, lined with small aluminum cylinders was inserted in the central section of the tube and the radiation taken end-on through its

[9] Poetker, Nature **119**, 123 (1927).

center. The most important factor for producing a strong secondary is the thorough elimination of water vapor. Hence the hydrogen was passed through tubes of phosphorous pentoxide as it was fed continuously from a H_2SO_4 electrolytic generator. The pressure was kept considerably higher than for the atomic spectrum. Applied potentials were somewhat over 2000 volts and the currents through the tube ranged from 1/3 to 2/3 amperes. Striated discharge would occupy the entire tube and the elementary spectrum would shade into insignificance.

A comparison spectrum was provided by the second order lines of a Pfund[10] iron arc. It was registered above and below the hydrogen by means of the usual occulting shutter. The arc with the lens used to focus it on the slit was, after alignment, kept permanently in its position. By means of a screw arrangement the tube with its mounting and appurtenances could be lowered and returned to position without any change of orientation, the leads to pump, hydrogen supply, etc., being made flexible. This enabled the initial alignment of the system to be maintained indefinitely. The iron comparison spectrum was taken before and after, but no shifts due to change of temperature or alignment could be detected between them.

Exposures averaged 20 hours for the range below 8900A and 40 hours for the range beyond. The slit widths used were about 0.04 and 0.1 mm respectively. One exposure of 3.5 days was tried with a slit of 0.25 mm but the whole plate became rather fogged. Success depends far more on optimum sensitizing than on mere length of exposure. Deep red filters which had been tested previously were used for the elimination of the second order spectrum.

Results. The plates revealed some 425 lines between 7500 and 10700A. Over 350 of these are below 8900A. These are reproduced from a typical plate in Fig. 5. It is roughly at 8900A that the sensitivity of the neocyanin plates drops off very rapidly. Still it is evident from comparison with work in other spectra that the secondary hydrogen radiation becomes noticeably weaker in the same vicinity. Under low dispersion with the small Hilger spectroscope traces of lines could be followed as far as 1.15μ (Fig. 4). Though no attempt was made to measure wave-lengths by these small spectrograms because of the low dispersion, they provided a convenient preliminary exploration of the remoter field. Besides, they afford about the only possibility of registering the higher lines with sufficient intensity to have them brought out in a reproduction. Using the Paschen lines for reference, the correspondence between these plates and those of higher dispersion was perfectly evident—additional proof that the absorbing filters were trustworthy.

For comparison standards the international secondary iron standards were supplemented by many of the interferometer measurements of Burns, Meggers and Merrill.[11] These standards were selected at intervals of 20 to 40A and were measured with the hydrogen lines on the comparator. From an initial and final standard the average dispersion or the plate constant was

[10] Pfund, Astrophys. J. **27**, 296 (1908).

[11] Burns, Meggers and Merrill, Bull. Bur. Stds. **13**, 245 (1916).

calculated for the whole plate. Since the spectrum is not entirely normal a large-scale correction curve was then drawn from the known values of the frequent standards on coordinate paper, from which the necessary correction for the hydrogen lines could easily be read off.

The values given in Table II up to 8900 are calculated from the measurements of three plates, each of which was measured twice. Above 8900A about six plates were used varying somewhat in range, slit-width, and success of registration. The general rule was followed not to include lines in the table which could not be measured at least on two plates. This meant the dropping of some fifty lines and quite a few more which were doubtful. Several of the strongest lines were examined for ghosts, but since none was detected we think the lines included in the table are real.

One of the somewhat inferior plates showed some additional lines the origin of which is unknown. Their wave-lengths were measured as: 8694.57, 8693.80, 8680.27, 8679.50, 8668.36, (wave-numbers, 11498.28, 11499.30, 11517.22, 11518.24, 11533.04). It is suspected that they are due to impurities, that the exposure was begun before the tube had been sufficiently washed out by the stream of hydrogen, since the oxygen 8446 and the sodium doublet 8194, 8183 were also visible. We know of no impurity lines on the other plates.

The wave-lengths up to 8900A are thought to be accurate, in general, to within 0.03 or 0.04A. While the agreement between different plates for many of the lines was closer than this, it also was not always attained, especially in the case of very faint or diffuse lines which were rather difficult to measure with the high power eye-piece in the comparator telescope. In such cases the error might amount to 0.1A. A number of lines where the disagreement was most noticeable have been marked with an asterisk. Even assuming no defects in the plates themselves due to unequal drying or the like, the several sources of error in the measurement itself hardly justify higher expectations.[12]

Beyond the limit of the lower range plates the possible error increases even more. Hence above 9000A the wave-lengths are given only to tenths of an angstrom, and the error may approach 1A. This error was unavoidable and due to a variety of causes, the widening of the slit (in some cases to 0.2mm) and consequent fusion of standards with neighboring lines, the extreme faintness of most of the lines, occasionally bad fogging or streaks. For the measurement of these plates a low power eye-piece was usually put on the comparator telescope, which of itself likewise lowered the accuracy of measurement though necessary to find the fainter lines with certainty. But even this reduced accuracy is certainly much higher than could be obtained by a prism instrument or by the ordinary radiometric methods.

The wave-lengths in air and the wave-numbers in vacuo are given in Table II for the region measured. The wave-numbers were calculated by means of Kayser's tables which at the same time reduce to vacuum values. For the wave-lengths beyond 10,000A the correction for the refraction of air was

[12] See Kayser, Hauptlinien der Linienspektra, Preface, p. IV.

TABLE II

Wave-lengths and wave-numbers of the infra-red lines of the hydrogen spectrum. In the second column the numbers are a visual estimate of the intensities, while the letters denote the character of the line; h, hazy, diffuse; d, perhaps double; b, broad; v, shades toward violet; r, shades toward red.

λ(air) I. A.	Int.	ν (vacuo)	λ(air) I. A.	Int.	ν (vacuo)	λ(air) I. A.	Int.	ν (vacuo)	λ(air) I. A.	Int.	ν (vacuo)
10654.5		9383.2	8884.12	2	11252.95	8440.72	1	11844.05	8187.47	1	12210.43
10650.0		9387.1	81.82	1	55.86	21.86	1v	70.60	84.84	1	14.36
10510.0		9512.1	77.40	1	61.47	17.46	1	76.81	81.74	1	18.99
10460.5		9557.1	75.78	4	63.53	16.06	1	78.78	79.92	1*	21.71
10429.8		9585.2	46.11	0	11301.30	14.18	2v	81.44	70.02	0*	36.51
10426.3		9588.5	8840.87	2	11308.00	09.35	2	88.26	65.88	0	42.72
10330.3	h	9677.6	07.39	3	50.99	8406.43	1	11892.39	64.41	5	44.92
10284.6		9720.6	8796.17	1	65.47	8399.54	0	11902.15	55.88	1	53.22
10265.9		9738.3	94.64	5	67.45	98.04	7	04.27	41.46	1	79.44
10115.2		9883.4	89.80	3	73.71	89.60	0	16.25	38.98	2	83.18
10085.3		9912.7	76.93	0*	90.38	8386.93	2	11920.04	38.24	0	84.30
10074.3		9923.5	67.18	1	11403.05	80.88	1	28.65	30.38	3	96.20
10057.4		9940.2	64.77	1	06.18	78.85	2	31.54	28.82	2	12298.53
10045.0		9952.5	50.31	1	25.03	75.33	0	36.55	25.85	1	12303.03
10010.5	b	9986.8	48.21	0*	27.77	73.97	0	38.49	24.42	1	05.19
9910.4		10087.6	46.71	2	29.73	71.60	2h	41.87	8123.27	1	12306.93
9881.9		10116.7	39.00	1	39.82	69.85	1	44.36	19.11	0	13.24
9868.4	h	10130.6	32.57	1*h	48.24	68.03	0	46.96	17.81	1*	15.21
9830.6		10169.5	23.88	3	59.65	66.63	4	48.96	17.08	0*	16.32
9743.1	1	10260.9	14.82	0*	71.56	63.75	0	53.08	16.19	1	17.67
9715.2	0	10290.3	08.57	1	79.79	60.87	0*	57.20	14.77	3	19.82
9642.3	1	10368.1	01.81	1*h	88.71	59.59	1	59.03	08.24	1	29.75
9581.0	0	10434.5	8693.69	0	99.43	57.00	1	62.73	07.47	1	30.92
9578.3	0	10437.4	88.68	0	11506.07	50.84	2	71.56	8103.96	2	36.26
9573.2	0	10443.0	70.52	6	30.17	49.35	10	73.69	8099.88	3	42.48
9567.4	1h	10449.3	63.57	5	39.42	45.49	0	79.23	94.41	2	50.81
9561.2	1h	10456.1	56.95	1	48.25	43.82	1	81.63	92.57	0	53.62
9553.1	1h	10464.9	40.90	0	69.69	37.78	1	90.31	91.02	2b,d	56.00
9524.5	0h	10496.4	33.09	0	80.16	35.91	0*	93.00	86.13	2	63.46
9444.1	0	10585.7	28.89	1	85.80	34.38	1	11995.20	75.94	0h	79.00
9429.6	0h	10602.0	8623.62	0	11592.87	30.10	4	12001.36	70.98	2	86.66
9410.6	1	10623.4	8599.92	1	11624.83	23.91	0*	10.29	65.73	0	12394.73
9403.3	0	10631.7	94.44	1	32.24	19.30	1	16.94	59.60	1	12404.16
9389.5	1h	10647.3	90.77	2	37.20	17.21	4	19.96	58.59	2h	05.71
9338.5	1b,d	10705.5	85.03	1	44.99	8303.39	1	39.97	55.97	1*	09.75
9318.6	0	10728.3	83.66	3	46.84	8298.47	0	12047.11	54.25	3	12.55
9314.1	0	10733.5	74.59	3	59.17	96.40	1b,d	50.11	50.16	2	18.70
9299.7	0h	10750.1	67.11	0	69.35	91.74	0*	56.89	48.33	0*	21.53
9292.1	0	10758.9	61.50	1	76.99	86.69	0b,d	64.23	47.08	1	23.46
9288.4	1	10763.2	60.20	1b,d	78.77	84.59	1	67.29	41.82	2	31.58
9276.0	0	10777.6	58.20	1b,h	81.49	83.74	1	68.53	8039.66	0	12434.92
9266.1	0	10789.1	55.68	0*	84.93	80.75	1h	72.89	36.29	2	40.14
9252.0	0	10805.5	53.88	0*h	87.39	74.06	1	82.65	31.80	1	47.09
9242.7	0	10816.4	51.90	0	90.10	73.07	8	84.09	27.60	1	53.60
9237.2	0	10822.8	47.75	0	95.77	69.28	1	89.63	24.08	0	59.07
9218.8	1b,d	10844.4	46.00	8	11698.17	64.94	2	12095.98	22.74	2	61.15
9212.4	0h	10852.0	41.42	1h	11704.44	55.62	2	12109.63	19.31	0	66.48
9184.7	0	10884.7	35.42	5	12.67	53.79	4	12.32	18.47	5	67.78
9178.8	1h,d	10891.7	33.47	0	15.35	51.51	1	15.67	13.04	3	76.23
9172.4	0	10899.3	27.78	5	23.17	46.64	3	22.82	07.91	1	84.22
9162.9	0	10910.6	22.62	3	30.26	42.66	1	28.68	06.72	2	86.08
9160.0	0	10914.0	20.11	8	33.72	40.49	4	31.87	8000.24	1b,d	96.19
9158.1	2h	10916.3	16.62	1	38.52	38.42	3	34.92	7998.15	0	12499.46
9129.7	0	10950.3	11.98	1	44.93	37.46	2	36.33	97.03	4	12501.21
9084.6	1h	11004.6	08.90	0	49.18	35.50	2	39.22	94.88	0*	04.57
9075.8	0	11015.3	8504.82	0	11755.92	33.51	1	42.15	93.34	1	06.98
9068.1	1	11024.6	8495.81	1	67.28	22.68	7	58.15	91.38	2	10.05
9022.0	2h	11081.0	85.78	6	81.19	19.94	1	62.20	87.21	0	16.58
9017.5	1h	11086.5	78.34	1	91.53	17.92	0*	65.19	85.61	2	19.08
9016.0	1h	11088.4	74.59	0*	11796.74	14.51	1h	70.24	83.97	1	21.66
8978.86	0	11134.22	71.72	0*	11800.74	8209.53	1	12177.62	81.91	0*h	24.89
8972.07	0	42.65	69.79	1	03.43	08.23	1	79.55	81.06	1	26.22
66.84	3	49.15	66.78	0	07.62	06.57	1	82.02	69.91	3	43.75
47.82	1	72.84	63.26	1	12.54	03.13	1	87.12	68.57	1	45.86
30.70	1	94.27	56.77	2h	21.60	8201.48	1	89.57	67.21	3	48.00
08.19	0	11222.55	51.46	0h,d	29.03	8199.89	0	91.94	7963.26	1	12554.22
01.64	2	30.81	48.64	0	32.98	98.80	0*	93.56	62.35	1	55.66
8898.44	3	34.85	47.69	0*	34.31	95.82	0	12197.99	60.35	0	58.81
96.54	2h	37.25	44.35	2	38.99	93.74	0	12201.09	58.38	0	61.92
85.81	0*	50.81	43.38	2	40.35	90.75	1	05.54	56.93	1	64.21

TABLE II (continued)

λ(air) I. A.	Int.	ν (vacuo)	λ(air) I. A.	Int.	ν (vacuo)	λ(air) I. A.	Int.	ν (vacuo)	λ(air) I. A.	Int.	ν (vacuo)
7954.67	0	12567.78	7824.86	0	12776.27	7716.47	0	12955.73	7609.75	1	13137.42
53.26	2	69.98	22.36	0	80.36				06.06	3	43.80
50.22	1	74.81	15.95	0d, h	90.83	14.04	0b, d	59.81	03.17	4	48.79
47.22	0	79.56				09.08	1*	68.15	7602.39	1	50.14
42.46	2	87.10	13.24	2	95.27	07.41	0	70.31	7597.76	3	58.16
			12.23	3	12797.03	06.02	3	73.30			
40.74	2	89.82	09.12	1h, r	12802.02	04.75	2	75.44	96.83	4	59.77
37.07	3	95.65	07.07	1	05.38				95.58	1	61.94
35.74	0	12597.76	05.56	1	07.86	7702.98	2	78.42	93.43	1	65.66
32.96	5	12602.17				7698.05	2h	86.73	84.20	4r	81.68
26.54	1*	12.38	7804.15	3	12810.18	94.48	0*	92.76	79.16	2	90.45
			02.60	1	12.72	92.53	2	96.05			
23.22	2	17.67	7800.39	0*	16.35	91.84	3	12997.22	7576.06	2	13195.85
22.54	1	18.75	7798.76	1	19.03				71.37	3	13204.02
12.91	1	34.10	96.41	1	22.89	90.17	1	13000.04	68.63	0	08.80
08.58	0h	41.02				85.26	3	08.35	66.83	1	11.94
06.31	0v, d	44.65	89.54	5	34.20	83.41	0	11.48	64.97	1	15.19
			87.26	0	37.96	79.52	1	18.07			
03.45	2	49.23	83.98	0	43.37	73.39	1	28.47	61.01	2	22.11
02.52	2	50.72	79.55	1h	50.68				58.52	2	26.47
7900.09	3	54.61	77.21	1	54.55	72.19	2	30.51	55.85	0	31.14
7897.95	0*	58.04				69.63	1	34.86	48.32	1	44.34
95.76		61.55	73.95	2	59.94	68.83	1	36.22	44.74	2	50.62
			68.78	0*	68.50	67.25	0	38.90			
7886.70	1	12676.09	61.87	0	79.95	65.03	1	42.68	41.71	2	55.95
85.29	0*	78.36	59.97	0	83.11				38.07	2	62.35
75.14	2	12694.70	56.69	1	88.56	7663.23	0	13045.74	36.85	2	64.50
63.80	0*	12713.00				62.37	0	47.21	34.57	1	68.51
62.56	1	15.01	54.84	2	91.63	61.25	2	49.11	31.42	1	74.06
			51.81	0	12896.67	60.36	3b	50.63			
60.27	0	18.72	45.30	1	12907.51	54.17	3	61.18	28.18	0	79.77
59.15	0*	20.53	39.71	2	16.83				27.11	0	81.66
56.39	3	25.00	37.23	1	20.97	51.77	0	65.28	25.77	1	84.02
53.37	0	29.89				50.50	3	67.45	24.39	4	86.46
47.70	1	39.09	34.23	0	25.98	47.45	3	72.66	22.02	1	90.65
			32.58	3	28.74	44.76	1	77.26			
45.67	1	42.39	30.42	0	32.36	43.14	1	80.03	21.15	1	92.18
43.03	0*	46.67	28.80	1	35.07				20.20	1	13293.86
40.49	0	50.80	24.16	1	42.83	41.47	1	13082.89	12.03	2	13308.32
37.91	1	55.00				31.21	2	13100.48	07.63	2	16.12
36.77	1	56.85	7723.05	1	12944.69	22.35	2	15.71	06.71	2	17.70
			21.51	2	47.27	20.48	2	18.93	7504.51	2	13321.66
33.94	1	61.46	18.83	2	51.77	13.61	1	30.76			
29.57	1h	68.59	17.73	0*	53.62						

obtained by simple extrapolation of the Meggers and Peters values below 10,000. The intensities adjoined are only visual estimates and hence make no pretence at accurate quantitative value, but are intended rather for purposes of identification. The value 0 indicates a line that is barely measurable. The change of sensitivity of the plates at about 8700 to 8900A should be allowed for in judging actual relative energy intensities between the sections above and below this. Above 9800A no intensities are given since obviously only the strongest lines can be detected.

A comparison of the wave-lengths in Table II with the corresponding measurements of Allibone shows that within the region of greatest sensibility of dicyanin he has listed all the moderately strong lines. It will be noticed that for most of the overlapping region of the two investigations there is a difference of about 0.3A which must be due to some general shift between the Fe and H spectra in one of the researches. In view of the good agreement between our different plates, the care we took to establish and maintain perfect alignment, and the perfect functioning of our temperature control, we are loath to believe the existence of such shifts in our work. The residual differences in the values obtained and the failure of Allibone to resolve some of the doublets can be easily accounted for by the lower dispersion (25A per mm) used in his work.

A rather cursory examination was made to find new band relations among these lines. Richardson[13] has recently arranged the various known bands in the visible into groups which he calls the Hα, Hβ, etc., bands because of the electron levels involved. Applying simple combination principles, band groups analogous to the Paschen series, $P\alpha$, $P\beta$, etc., can be calculated from

TABLE III

Band groups analogous to the Paschen series.

Group	$n'\rightarrow n''$	m	λ(IA) air	Wave-number (vac) Obs.	Calc.	Defect	Combination Method
$P\beta$	3→1	1	8184.84	12214.36	12213.19	−1.17	$({}_1\gamma_1-{}_1\alpha_1)$
		2	8193.74	12201.09	12200.27	− .82	+(5, 3−5, 1)
$P\beta$	4→2	1	8378.85	11931.54	11931.13	− .41	$({}_2\gamma_2-{}_2\alpha_2)$
		2	8389.60	11916.25	11917.54	−1.19	+(5, 4−5, 2)
$P\gamma$	1→0	1			11787.72		$({}_0\delta_0-{}_0\alpha_0)$
		2	8485.78	11781.19	11781.04	− .15	+(6, 1−6, 0)
		3	8495.81	11767.28	11768.86	+1.58	
		4	8508.90	11749.18	11750.21	+1.03	
		5	8522.62	11730.26	11731.39	+1.13	
$P\gamma$	2→1	3	8623.62	11592.87	11593.27	+ .40	$({}_1\delta_1-{}_1\alpha_1)$ +(6, 2−6, 1)
*$P\gamma$	2→0	1	7218.35	13849.76	13850.45	+ .69	$({}_0\delta_0-{}_0\alpha_0)$
		2	7225.33	13836.39	13837.88	+1.49	+(6, 2−6, 0)
*$P\gamma$	3→1	1	7460.29	13582.67	13583.08	+ .41	$({}_1\delta_1-{}_1\alpha_1)$
		2	7467.01	13570.29	13570.84	+ .55	+(6, 3−6, 1)
*$P\gamma$	4→2	1	7514.77	13303.46	13303.00	− .46	$({}_2\delta_2-{}_2\alpha_2)$
		2	7524.39	13286.46	13285.60	− .86	+(6, 4−6, 2)
$P\delta$	0→0	1	9573.2	10443.0	10443.02	.0	$({}_0\epsilon_0-{}_0\alpha_0)$
		2	9578.3	10437.4	10438.22	+ .8	
**$P\delta$	1→0	1	7947.22	12579.56	12582.30	+2.74	$({}_1\epsilon_1-{}_0\alpha_0)$
		2	7950.22	12574.81	12575.94	+1.13	+(2, 1−2, 0)
		3	7956.93	12564.21	12565.31	+1.10	
		4	7963.26	12554.22	12554.34	+ .12	
$P\delta$	2→1	1	8054.25	12412.55	12411.67	− .88	$({}_2\epsilon_2-{}_1\alpha_1)$
		2	8055.97	12409.75	12409.71	− .04	+(2, 2−2, 1)
		3			12400.01		
		4	8075.94	12379.00	12378.26	− .74	
		5	8094.41	12350.81	12350.75	− .06	
$P\delta$	3→2	1	8130.38	12296.20	12295.38	− .82	$({}_3\epsilon_3-{}_2\alpha_2)$
		2			12290.17		+(2, 3−2, 2)
		3	8138.24	12284.30	12285.24	+ .94	
$P\delta$	4→3	1	8235.50	12139.22	12139.89	+ .67	$({}_4\epsilon_4-{}_3\alpha_3)$
		2	8237.46	12136.33	12135.65	− .68	+(2, 4−2, 3)
		3			12125.81		
		4	8255.62	12109.63	12108.13	−1.50	
		5	8273.07	12084.09	12084.43	+ .34	

* Values taken from Allibone's table.
** Richardson called attention to this probable band. (Loc. cit.)

[13] Richardson, Proc. Roy. Soc. **A113,** 368 (1926).

the known vibration intervals of the upper levels of these so-called Balmer term groups. Since a number of these bands would fall in the region investigated, the values of the lines composing them were computed. The fact that the higher band groups given by Richardson are fragmentary and undeveloped makes the data for the application of the combination principle somewhat meagre and unsatisfactory. Still, using the data provided by his tables, a number of our lines were found to fit in well as members of bands of some of the Paschen term groups, so that they hardly seem mere coincidences. A number of such lines are listed in Table III. They would give considerable irregularities in first and second differences, but this was the case also with the band groups from which they were calculated. Their presentation will at least confirm the reality of the higher Balmer term groups. In the second-last column the difference between calculated and observed wave number is given; because of the uncertainty of the data defects as large as 1.5 were admitted. In the last column the method of applying the combination principle is indicated. For convenience Richardson's notation is retained, the $\alpha, \beta, \cdots$, indicating that the electronic levels involved correspond to those for Hα, Hβ, etc., and the subscripts giving the initial and final vibration levels.

There are traces also of a sequence of the Hα bands farther in the infra-red than the sequence given by Richardson. A few of the lines correspond quite well; on the other hand, some of the calculated wave-lengths lie so close together that they would not be resolved by our plates.

Whether these fragmentary bands be authentic or not, the greater number of the new lines and the most intense are not involved in them. Since it now appears[14] that the secondary hydrogen spectrum is rather analogous to that of the helium atom, new sets of relations between its lines are suggested, and it is hoped this new material may reveal such relations and thus bring us closer to the solution of this complex spectrum.

This work was carried on at the suggestion of Dr. Pfund to whom I am indebted for numerous helpful suggestions. I wish to express my appreciation to him, to Professor Wood for his kindly interest, and to Professors Ames and Herzfeld for their encouragement and support.

JOHNS HOPKINS UNIVERSITY,
May 31, 1927.

[14] Richardson, ref. 13, see Additional Notes, p. 400.

THE SODIUM AND POTASSIUM ABSORPTION BANDS

By W. R. Fredrickson and William W. Watson

Abstract

Vibrational relations.—Formulas for the heads of the bands are:

Green Na_2: $\nu = 20301.62 + (123.84n' - 0.79n'^2) - (157.57n'' - 0.57n''^2)$

Red Na_2: $\nu = 15006.68 + (115.69n' - 0.427n'^2) - (157.81n'' - 0.538n''^2)$

Near red K_2: $\nu = 15368.63 + (74.58n' - 0.30n'^2) - (92.01n'' - 0.34n''^2)$

Since the coefficients of the n'' terms for the green and red Na_2 bands are the same, the two systems must have the same initial state (^1S) in absorption. The similarity of the green Na_2 and the near red K_2 band systems is pointed out. The n' progressions are very large for small n'' values, especially in the red Na_2 system.

New potassium bands.—A new K_2 band system has been discovered on the long wave-length side of the λ7699, 7665 K doublet. This system bears a marked resemblance to the red Na_2 bands, and is no doubt due to the same electronic transition.

Fine-structure analysis.—The lines in the (1, 0), (1, 1), (0, 1) and (0, 2) green sodium bands have been assigned into branches by correlation with the fluorescence and magnetic rotation data of R. W. Wood. There are apparently two Q branches but only single P and R branches. An explanation of this is offered, together with the details of the agreements between Wood's data and the present analysis. The usual combination relations hold, except for a small P, Q, R "defect" which is to be expected. The K_2 bands show exactly the same structure, but no resonance series have been located with which to check our analysis. It is concluded that the green Na_2 and the near red K_2 bands are both $^1S - {}^1P$ transitions. For the initial absorption state, *the moment of inertia* is 7.20×10^{-39} gm cm^2 for Na_2 and 8.72×10^{-39} gm cm^2 for K_2.

Introduction

ALTHOUGH some of the green sodium and near red potassium absorption bands have been arranged into branches by Smith,[1] no really satisfactory analysis of these bands with combination relations to verify the assignments has been available. Also it seemed necessary to have higher dispersion plates than those used previously since the band lines have such a close spacing. Judging by the character of the fluorescent spectra found in sodium vapor by Wood,[2,3] Mulliken[4] has recently concluded that these bands are due to a $^1S - {}^1P$ transition in the Na_2 molecule, and that therefore the bands should consist of simple P, Q, R branches like the AlH bands. The presentation of the direct evidence as to the validity of this conclusion together with the report of the constants of the Na_2 and K_2 molecules are the objects of the present paper.

The vibrational relations in these band systems are first presented, and then the discussion of the fine-structure, using as a basis for the analysis

[1] H. G. Smith, Proc. Roy. Soc. **106**, 400 (1924).
[2] R. W. Wood, Phil. Mag. (6), **15**, 581 (1908).
[3] Wood and Hackett, Astrophys. J. **30**, 339 (1909).
[4] R. S. Mulliken, Phys. Rev. **28**, 1216 (1926).

Wood's fluorescence and magnetic rotation data. We also include the vibrational data of the red system of sodium, but as yet the fine-structure of these bands has not been completely determined. The photographs were taken in the first and second orders of a Rowland concave grating giving a dispersion of 2.6 and 1.3A per mm respectively. The source was a 150-watt lamp and the vapor was kept in glass tubes 40 to 60 cm long, heated electrically.

Vibrational Data

The band heads of the green and red systems of sodium and the near red system of potassium can be expressed by the following formulas:

Green Na_2 $\nu = 20301.62 + (123.84n' - 0.79n'^2) - (157.57n'' - 0.57n''^2)$

Red Na_2 $\nu = 15006.68 + (115.69n' - 0.427n'^2) - (157.81n'' - 0.538n''^2)$

Red K_2 $\nu = 15368.63 + (74.58n' - 0.30n'^2) - (92.01n'' - 0.34n''^2)$

An inspection of Tables I and II discloses the fact that the intensity distribution among the green Na_2 and the K_2 bands is practically identical. An

TABLE I

Green Na_2 band system.

n'	$n''=0$	1	2	3	4	5	6	7	8
0	20301.62 (2)	20144.40 (5)	19988.77 (5)	19834.18 (5)	19678.63 (4)	19527.92 (2)			
1	20425.40 (9)	20267.56 (6)			19803.44 (4)	19652.08 (3)	19502.47 (1)		
2	20546.98 (8)			20078.47 (3)			19624.02 (2)	19474.40 (1)	
3	20667.12 (6)		20352.48 (3)	20200.61 (2)		19893.29 (3)		19593.74 (1)	19447.77 (1)
4	20785.53 (5)	20627.23 (2)	20471.95 (3)						
5	20901.76 (2)	20743.38 (5)							
6	21016.00 (1)	20858.53 (4)							
7		20972.71 (2)							
8		21084.04 (2)	20926.19 (1)						
9	21351.17 (1)	21196.74 (2)							
10		21303.70 (1)	21147.10 (2)						
11		21409.32	21253.91						

TABLE II

Near red K_2 band system.

n'	$n''=0$	1	2	3	4	5	6	7	8	9	10
0	15368.63 (3)	15277.08 (8)	15186.32 (9)	15095.92 (6)	15005.86 (3)	14916.55 (1)					
1	15442.88 (10)	15351.28 (5)			15079.75 (5)	14991.85 (3)	14902.94 (2)	14814.97 (0)			
2	15516.71 (8)		15337.75 (2)	15242.33 (3)			14975.84 (1)	14887.92 (2)	14800.92 (1)		
3	15590.15 (7)		15407.36 (3)						14874.97 (1)	14787.39 (2)	14702.68 (0)
4	15661.14 (5)	15569.61 (3)								14859.34	14773.93
5	15733.35 (3)	15641.12 (4)		15461.35 (2)							
6	15805.38 (2)	15712.19 (4)									
7	15875.58 (2)	15782.47 (3)	15691.43 (3)								
8		15851.29 (2)	15760.72 (3)								
9			15829.18								

TABLE III

Red Na_2 band system.

n'	$n''=0$	1	2	3	4	5	6	7	8	9
0	15006.68 (3)	14850.60 (4)	14691.34 (4)							
1	15122.33 (4)	14966.61 (5)	14807.95 (5)	14655.14 (4)				14045.21 (1)	14893.89 (1)	13744.23 (1)
2	15236.35 (5)	15078.50 (5)	14921.66 (4)	14767.18 (4)	14614.15 (3)	14465.41 (2)	14308.27 (2)	14156.88 (1)		
3	15349.23 (5)	15191.97 x(3)				14573.25 (2)	14422.45 (2)			13972.20 (1)
4	15461.83 (5)									
5	15575.87 (5)	15421.36 (4)								
6	15683.82 (5)									
7	15796.92 (3)									
8	15904.00 x(4)									
	16011.67 (3)	15851.80 (4)								
10	16120.44 (2)	15962.95 x(3)								
11	16232.60 x(2)	16070.39 (2)								
12	16333.59 (3)	16177.04 (3)								
13	16440.45 (2)	16286.53 (2)								
14	16542.61 x(1)	16389.13 (2)								
15	16647.32 (1)	16494.00 (2)								
16		16590.25 (1)								

Bands indicated by x are difficult to measure accurately.

eye estimate of the intensity of each band is given by the number below the frequency of the head. The (0,0) band in each system is weak, but is definitely there. In each system the (2, 1), (3, 1), (1, 2), and (1, 3) bands are missing, and if a line were drawn through the squares of the most intense bands, we would have a parabola which is rather wide.[5] The similarity of these two systems is very marked, and, as will be shown later, is even more evident when the fine-structure is considered.

At our instigation, C. H. Hsü has very recently looked for and found a new potassium absorption band system in the region around 8000A. This system is situated with respect to the first doublet in the principal series of K(λ7699.3 and 7665.6) as is the red sodium band system with respect to the *D* lines of Na. No doubt an investigation of the structure of these two systems will reveal their likeness, since they are undoubtedly produced by the same electronic transition.

Particularly in the red sodium bands, the n' progressions are very large for small n''(i.e., $n''=0$, 1). This is perhaps solely a temperature effect showing that at the temperature of the absorbing gas most molecules are in a low vibrational quantum state, and thus on the basis of probability should give the distribution observed.

An interesting fact is that the coefficients of the n'' terms in the red and green bands of sodium have practically the same values:

[5] See R. T. Birge's discussion in Bulletin No. 57 of the National Research Council.

$$\text{Green } Na_2 \quad (157.57n'' - 0.57n''^2)$$
$$\text{Red } Na_2 \quad (157.81n'' - 0.538n''^2)$$

This shows that the final states in emission (the initial states in absorption) are the same in both systems, in agreement with Mulliken's prediction that the two band systems arise from the same electronic state. However from the data we find that we have too few bands with high quantum numbers to be able accurately to determine the energies of dissociation and thus the exact energy and state of each atom. We observe, though, that the bands appear only when the D lines are very broad which suggests that the sodium molecule may be due to the joining of a normal atom with an excited one in a P state. This combination, as well as the union of two normal atoms, will give a ^1S molecular state.

Fine-Structure Analysis

Green sodium bands. Four bands—(1, 0), (1, 1), (0, 1), (0, 2)—have been analyzed. At high dispersion the bands display a great number of lines, and therefore due to the closeness of the lines at the head and the possible overlapping of another band, it was found that we could not with any degree of accuracy carry the branches within six or eight wave-numbers of the head. However, in each case studied the following band in the same sequence was missing or so weak that we could measure a sufficient number of lines in the band and make the assignments by correlation of our data with the fluorescence and magnetic rotation data.

Wood and Hackett[2,3] have obtained fluorescent spectra of sodium using various lines as the exciting source. Two of the lines, silver λ5209 and cadmium λ4800 give rise to singlet fluorescent series, while the two lines cadmium λ5086 and lead λ5006.1 excite doublet series. A number of other lines were also used as sources; barium λ4934 (or λ4900), lithium λ4972, 4603—, magnesium green triplet, copper triplet, but their fluorescent lines show no such regularity as that mentioned above. For example, in the bands analyzed the fluorescent lines due to one of the mentioned sources may be single, double, or triple, and they do not appear at corresponding distances from the heads. Therefore, the doublets of cadmium and lead were used as the only safe clue for making the assignments.

We find that these doublets appear only in the bands with zero initial vibrational state. It seems, then, that the molecules excited by cadmium λ5086 and lead λ5006.1 pass to an excited zero vibrational state and emit the doublet lines in returning to the various vibrational levels in the unexcited state. According to the theory as developed by Kemble and Witmer,[6] and Loomis,[7] we should expect one component of the doublet to lie on the R branch and the other on the P branch with the Δj between the lines equal to 2. Also, we should expect the $R(j)$ and $P(j)$ to be the same for all the doublets due to the same source.

[6] E. C. Kemble and E. E. Witmer, Phys. Rev. **28**, 633 (1926).
[7] F. W. Loomis, Phys. Rev. **29**, 112 (1927).

With the above as a guide, we find that each band is composed of four branches, on two of which the lines of the singlet resonance series lie. These two branches are apparently, then, Q, type. A possible explanation of this will be given later. The magnetic rotation data of Wood and Hackett also serve as a guide since the lines which are rotated negatively should appear on R branches, while those positively rotated should lie on P branches. The wave-numbers of the lines of the branches in each of the four bands are given in Table IV.

TABLE IV

Sodium bands.

The magnetic rotation lines are designated by "x" and the fluorescent lines are marked by the symbol of the source.

j	R	Q_R	Q_P	P	R	Q_R	Q_P	P
	(1, 0) band				(1, 1) band			
6½	20421.30		20417.70CuLi	20414.80	20262.70			20255.87
7½	19.78		15.40Ba	11.99x	61.07Ba			53.59
8½	17.90	20413.70	12.70	08.99	59.27			51.00
9½	15.60	10.80	09.34	05.50	57.08		20252.00	48.09Ba
10½	12.90	07.69	06.19	02.32	54.80		49.20	44.87
11½	10.08	04.55	02.90	398.70x	52.30		46.30	41.15
12½	07.01	01.50	399.54Ba	94.47	49.80		42.81	37.47
13½	03.75x	397.54	95.37	90.08	46.67x	20241.95	39.40	33.80
14½	00.56Ba	93.40	91.73	85.90	43.22	38.47	35.75	29.77x
15½	396.86	89.37	87.32Cu	81.34	40.08	34.60	31.89	25.20
16½	92.90	84.47	82.75	76.40	36.46	30.57	27.50	21.05
17½	88.51	79.32	77.63	70.86	32.73	26.29	23.18	16.23Cd
18½	83.82				28.60	22.11	18.57	11.00
19½	78.92				24.10	17.47Cd	13.27	06.00
20½	73.70				19.83	12.42	08.67Mg	00.00
21½	68.20				14.80	07.01Ag	03.21	
22½	62.34				10.06	01.90Cu		
	(0, 1) band				(0, 2) band			
5½	20139.15			20133.50	19982.45x			
6½	37.60Pb			31.00x	80.67Pb			19974.20
7½	36.10		20132.00	28.45	79.20			71.60
8½	34.50		29.80CuMg	25.70Pb	77.47			68.86xPb
9½	32.50		27.25	22.70	75.40		19970.40	65.70x
10½	30.30	20126.30	24.50	19.60	73.20		67.40Li	62.50
11½	27.70	23.44	21.70	16.10	70.66	19965.70Ba	64.15	59.16
12½	25.00	20.46	18.11	12.45	68.12	62.80	61.00	55.59
13½	22.10	17.02	14.63	08.50x	65.20	60.02	57.60	51.40
14½	19.00Cd	13.72	10.80	04.40Ba	62.20xCd	56.35	54.40BaCu	47.70Ba
15½	15.40	09.78	06.82Li	00.21	58.20	52.32Cu	50.00	43.20
16½	11.50	05.68	02.60	95.40Cd	55.10	49.00Li	45.80	39.30Cd
17½	07.50	01.30	098.25	90.80	50.80Li	45.00	41.40	34.55
18½	03.30Ba	96.74	93.30	85.60	46.60	40.60	37.00	29.37Cu
19½					42.40	36.10	31.95	24.80
20½					37.80	31.20	27.00	19.30
21½					32.75	26.25	21.75	13.70
22½					27.70	20.89	15.44Cd	

Summary of the Magnetic Rotation and Fluorescent Data.

(1, 0) *Band.* There are no cadmium, lead, or silver lines. There are four magnetic rotation lines:[8] 20424.57 (−) is in the head of the band,[9] 20422.23 (+) falls on $P(7\frac{1}{2})$ or $Q_R(9\frac{1}{2})$, 20403.32 (+) on $R(13\frac{1}{2})$, and 20399.15 (+) on $P(11\frac{1}{2})$. The magnetic rotation line 20388.75 is undoubtedly in the head of the weak (2, 1) band. Barium has two lines in the band: 20415.82 on $R(9\frac{1}{2})$ or $Q_R(7\frac{1}{2})$, and 20400.40 on $R(14\frac{1}{2})$ or $Q_P(12\frac{1}{2})$. Lithium has a line 20417.07 on $Q_P(6\frac{1}{2})$ or $P(5\frac{1}{2})$. Copper has a line 20417.48 on $Q_P(7\frac{1}{2})$, and magnesium has a line 20387.92 on $Q_P(15\frac{1}{2})$.

[8] The ν values given in this summary are obtained directly from Wood's data. The (+) sign signifies positive rotation, the (−) sign signifies negative rotation.

[9] From Loomis' abstract (Phys. Rev. **29**, 607, 1927), we find that there is a magnetic rotation line in the head of each band.

(1, 1) *Band.* Cadmium (λ4800) and silver each have a line far out in the band. These lines may be a part of the (2, 2) band which is apparently unnoticeable, but if we consider them as belonging to the (1, 1) band, the cadmium line 20216.41 falls on $Q_R(19\frac{1}{2})$ or $P(17\frac{1}{2})$, and the silver line 20206.60 on $Q_R(21\frac{1}{2})$. There are four magnetic rotation lines: 20267.64 (−) and 20262.71 are in the head of the band, 20245.89 falls on $R(13\frac{1}{2})$ and 20230.73 on $P(14\frac{1}{2})$ or $Q_R(16\frac{1}{2})$. Barium has three lines: 20261.07 on $R(7\frac{1}{2})$, 20247.94 on $P(9\frac{1}{2})$, and 20254.91 on a Q line. Copper has two lines: 20266.82 in the head and 20202.93 on $Q_R(21\frac{1}{2})$. Lithium has a line 20259.84 on a Q_P line and magnesium has a line 20208.65 on $Q_R(20\frac{1}{2})$.

(0, 1) *Band.* There are two doublets in this band. Lead (λ5006.1) doublet has one component 20137.82 on $R(6\frac{1}{2})$ and the other 20125.25 on $P(8\frac{1}{2})$. The cadmium (λ5086) doublet has one component 20119.76 on $R(14\frac{1}{2})$ and the other 20094.91 on $P(16\frac{1}{2})$. There are four magnetic rotation lines: 20145.53 and 20139.44 are in the head, 20108.25 falls on $P(13\frac{1}{2})$ and 20131.33 $P(6\frac{1}{2})$. The magnetic rotation line 20108.25 undoubtedly belongs to the (1, 2) band. Barium has a line 20103.80 which falls on $R(18\frac{1}{2})$ or $P(14\frac{1}{2})$, or it may possibly belong to the (1, 2) band. Lithium has two lines: 20106.63 on $Q_P(15\frac{1}{2})$, and 20081.19. This last line was not included in the measurements. Copper and magnesium have the same line 20129.71 which falls on $Q_R(8\frac{1}{2})$ and copper alone has a line 20143.50 which is in the head.

(0, 2) *Band.* Here we also have the doublets of cadmium and lead. The lead doublet has one component 19980.85 on $R(6\frac{1}{2})$ and the other 19968.48 on $P(8\frac{1}{2})$. The cadmium doublet has one component 19962.90 on $(R14\frac{1}{2})$ and the other 19940.20 on $P(16\frac{1}{2})$. Silver has a line 19905.66 which falls on $Q_R(25\frac{1}{2})$, or it may possibly belong to the (2, 4) band, although this band appears to be missing. Cadmium (λ4800) has a line 19915.97 which falls on $Q_P(22\frac{1}{2})$. There are five magnetic rotation lines: 19988.04 (−) is in the head, 19982.45 on $R(5\frac{1}{2})$, 19969.28 on $P(8\frac{1}{2})$, 19965.69 on $P(9\frac{1}{2})$, and 19961.70 on $R(14\frac{1}{2})$. Barium has three lines: 19966.09 on $Q_R(11\frac{1}{2})$, 19954.93 on $Q_P(14\frac{1}{2})$, and 19947.3 on $P(14\frac{1}{2})$, although this last line may belong to the weak (1, 3) band. Lithium has three lines: 19967.28 on $Q_P(10\frac{1}{2})$, 19950.95 on $R(17\frac{1}{2})$, and 19949.35 on $Q_R(16\frac{1}{2})$. The last two lines may belong to the (1, 3) band. Copper has three lines: 19978.05 on either $P(4\frac{1}{2})$ or on a Q line, 19953.73 on either $Q_R(14\frac{1}{2})$ or $Q_P(15\frac{1}{2})$, and 19929.87 either on $P(18\frac{1}{2})$ or in the (1, 3) band. The magnesium lines are too far out in the band to be accounted for.

As mentioned before, no confidence can be placed in the fluorescent lines due to the barium, magnesium, lithium and copper excitations as far as their being an aid in the location of the branches is concerned. Apparently, in the assignments made, these lines predominate on Q branches. Of the four bands measured, the singlets due to silver and cadmium λ4800 appear only in two bands (1, 1) and (0, 2) and far out in each band. Therefore it is to be concluded that these singlets form in two series with initial vibrational levels 0 and 1.

The $P-R$ initial and final state combinations between bands together with the typical P, Q, R combinations for one of the bands, are shown in Table V. The expected combination defect such as Eriksson and Hulthén[10] found in the AlH bands (also a $^1S-{}^1P$ transition) is seen to be present. Since one of the Q branches lies close to the R branch, while the other lies close to the P branch we have designated them Q_R and Q_p respectively. Fig. 1 is a plot of the branches in one of the bands, showing the way in which the resonance lines and the magnetic rotation lines fit into this assignment.

Mulliken[11] has explained the combination defect in AlH on the basis of a σ-type doubling, and has suggested that the cause of the doubling may be

[10] Eriksson and Hulthèn, Zeits. f. Physik **34,** 775 (1925).

[11] Mulliken, Phys. Rev. **28,** 1202 (1926).

TABLE V

Combinations in sodium bands. P and R-branch combinations.

j	(0, 1) Band Δ_2F'	(0, 2) Band Δ_2F'	(1, 1) Band Δ_2F'	(1, 0) Band Δ_2F'	(0, 1) Band Δ_2F''	(1, 1) Band Δ_2F''
6½	6.60	6.47			11.90	11.70
7½	7.65	7.60			13.40	12.98
8½	8.80	8.61	8.27	7.79	14.90	14.40
9½	9.80	9.70	8.99	9.00	16.40	15.93
10½	10.70	10.70	9.93	10.10	17.85	17.33
11½	11.60	11.50	11.15	10.58	19.20	18.50
12½	12.55	12.53	12.33	11.34	20.60	20.03
13½	13.60	13.81	12.87	12.64	21.90	21.47
14½	14.60	14.50	13.45	13.67	23.60	22.17
15½	15.22	15.00	14.88	14.66	24.60	23.85
16½	16.08	15.80	15.41	15.52	25.90	25.46
17½	16.72	16.24	16.48	16.50		
18½	17.74	17.23	17.57	17.65		

Typical P, Q, R combination. (0, 2) *Band*

j	$R(j)-Q_R(j)$	$Q_R(j+1)-P(j+1)$	Diff	$R(j)-Q_P(j)$	$Q_P(j+1)-P(j+1)$	Diff.
9½				5.00	4.90	.10
10½				5.80	5.01	.79
11½				6.51	5.41	1.10
12½				7.12	6.20	.92
13½	5.18	8.62	3.44	7.60	6.70	.90
14½	5.85	8.65	2.80	7.82	6.81	1.01
15½	5.88	9.12	3.24	8.20	6.54	1.66
16½	6.10	9.70	3.60	9.29	6.85	2.44
17½	5.80	10.45	4.65	9.40	7.63	1.77
18½	6.01	11.23	5.23	9.62	8.17	1.45
19½	6.30	11.29	5.01	10.45	7.70	2.75
20½	6.58	11.90	5.32	10.80	8.05	2.75
21½	6.50					

the presence of "secondary ρ's." Should this be the case, it seems plausible that if the F_B and F_A states have different ρ's, the ρ_A appears with both + and − signs, and thus the cross-over transitions from $F_A\pm$ to F_B should give rise to two Q branches.

It is impossible to verify with any certainty this analysis by consideration of the intensity distribution in the various branches, since estimates of the intensities of absorption lines such as these are much more unreliable than those of emission lines. Roughly, however, the relative intensities are as expected for a $^1S-{}^1P$ transition; the Q branches are the strongest, while the R branch is stronger than the P branch.

Potassium bands. As mentioned above, the analysis of the fine-structure of the K_2 bands verifies the prediction based on the general similarity of the two systems that the blue-green Na_2 and the K_2 bands are identical in every respect. No fluorescence data being available, the assignment of the lines of the K_2 bands into branches is a more difficult problem than that presented by the Na_2 bands. When the (0, 1), (0, 2), (1, 0), and (2, 0) bands (the only bands free from the overlapping of neighboring bands of the same groups) are measured and plotted to a large scale, however, it becomes apparent that

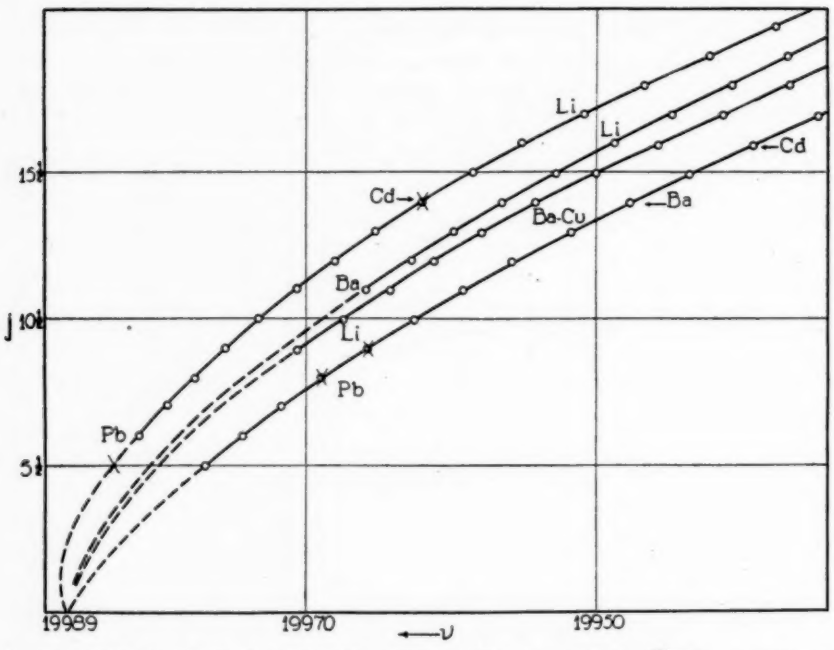

Fig. 1. Na_2, λ5001 band, $(0, 2) = (n', n'')$. Curves of the j, ν variation. The magnetic rotation lines are designated by × and the fluorescent lines are marked by the symbol of the source.

TABLE VI

Potassium bands.

j	R	Q_R	Q_P	P	R	Q_R	Q_P	P
	(0, 1) Band				(0, 2) Band			
10½					15177.26	15173.91	15173.14	15169.16
11½					74.96	71.28	70.50	66.32
12½	15263.55	15259.10	15258.60	15253.48	72.46	68.53	67.74	63.10
13½	60.39	56.05	55.22	49.92	69.92	65.46	64.74	59.69
14½	57.59	52.68	51.74	46.38	66.97	62.26	61.35	56.15
15½	54.40	49.19	48.10	42.48	63.90	58.90	57.93	52.16
16½	50.92	45.41	44.43	38.13	60.63	55.13	54.15	47.99
17½	47.32	41.39	40.53	33.54	57.03	51.39	50.18	43.69
18½	43.41	37.05	35.99	29.11	53.18	47.02	45.82	39.21
19½	39.24	32.47	31.33	24.02	49.15	42.74	41.47	34.32
20½	34.90	27.77	26.55	18.84	44.81	37.96	36.82	29.19
21½	30.28	22.70	21.36	13.33	40.27	33.05	31.86	23.94
22½	25.32	17.36	16.20	07.56	35.59	27.96	26.60	18.43
23½	20.17	11.88	10.57	01.77	30.54	22.64	21.17	12.76
24½	14.92	06.28	04.61		25.34	16.87	15.60	06.56
25½	09.14	00.28	98.60		19.84	11.12	09.78	00.39
26½	03.23				14.16	05.21	03.55	
27½	197.13				08.15	98.84	97.21	
28½					02.21			
	(1, 0) Band				(2, 0) Band			
10½	15432.20	15429.05	15428.38	15424.68				
11½	29.58	26.05	25.56	21.48		15500.68	15499.99	15495.85
12½	(27.00)	23.13	22.39	18.06	15501.26	497.56	96.74	92.52
13½	23.87	19.81	18.98	14.29	498.35	94.29	93.48	88.75
14½	20.68	16.19	15.34	10.38	95.13	90.80	89.78	84.79
15½	17.19	12.44	11.40	06.25	91.70	86.83	85.92	80.62
16½	13.33	08.26	07.25	01.67	87.88	82.68	81.65	76.04
17½	09.29	03.96	02.80	397.00	83.81	78.46	77.29	71.20
18½	(05.15)	399.50	398.14		79.52	73.60	72.57	66.25
19½	00.55	94.46	93.20		74.89	68.62	67.47	60.77
20½					70.00	63.52	62.30	55.13
21½					64.84	58.07	56.71	49.52
22½					59.45	52.36	50.95	43.50
23½					53.84	46.41	45.01	37.30
24½					48.27	40.52	38.88	30.70
25½					42.10	34.50	32.50	

every fourth line is a member of the same series. The usual combination relations are sought among the lines of these four series, and their designation as R, Q_R, Q_P, and P branches thus made. Table VI gives the assignments for the four bands, the j values having been obtained by extrapolation of the ΔF's to zero value. Since the lines become so fused together near the head of a band, it is impossible to follow any of the branches accurately to the zero-point. However, it is evident that the zero-points are very close (within 1 cm^{-1}) to the head in every case.

The $P-R$ combinations between the bands are given in Table VII, together with a typical set of data showing the extent to which the $R(j)-Q(j) = Q(j+1)-P(j+1)$ relation holds for one of the bands. A slight combination

TABLE VII

Combinations in potassium bands.

j	(0, 1) band Δ_2F'	(0, 2) band Δ_2F'	(0, 1) band $R(j)-Q_P(j)$	(0, 1) band $Q_P(j+1)-P(j+1)$	(0, 1) band Diff.	(0,1) band $R(j)-Q_R(j)$	(0, 1) band $Q_R(j+1)-P(j+1)$	(0, 1) band Diff.	(1, 0) band Δ_2F''	(2, 0) band Δ_2F''
12½			4.95	5.30	−.35	4.45	6.13	−1.68	16.62	16.47
13½	10.47	10.23	5.17	5.36	−.19	4.34	6.30	−1.96	17.62	17.73
14½	11.21	10.82	5.85	5.62	+.23	4.91	6.71	−1.80	19.01	19.04
15½	11.92	11.74	6.30	6.30	+.00	5.21	7.28	−2.07	20.19	20.50
16½	12.79	12.64	6.49	6.99	−.50	5.53	7.85	−2.34		
17½	13.78	13.34	6.79	6.88	−.09	5.93	7.94	−2.01		
18½	14.30	13.97	7.42	7.31	+.11	6.36	8.45	−2.09		
19½	15.22	14.83	7.91	7.71	+.21	6.77	8.93	−2.16		
20½	16.06	15.62	8.35	8.03	+.32	7.13	9.37	−2.24		
21½	16.95	16.33	8.92	8.64	+.28	7.58	9.80	−2.22		
22½	17.76	17.16	9.12	8.81	+.31	7.96	10.11	−2.15		
23½	18.40	17.78	9.59			8.29				

defect of the order of magnitude to be expected is apparent when the Q_P branch is used. The defect for the Q_R branch is larger and seems to have an approximately constant value of about 2 cm^{-1}. Except for the extra Q branch, we are dealing here apparently with a typical $^1S-{}^1P$ transition. A possible explanation of this doubling of the Q branch is that given above for the sodium bands.

TABLE VIII

Summary of the constants of the Na_2 and K_2 molecules.

	B_0'	B_1'	α'	B_0-B_1	$I_0'\times 10^{39}$	B_0''	B_1''	B_2''	α''	$I_0\times 10^{39}$	ω_0'	ω_0''
Na_2	0.264	0.245	———	0.019	1.05	0.384	0.375	0.367	0.0087	7.20	123.84	157.57
K_2	0.1985	0.1807	0.165	0.018	1.39	0.317	0.308	0.299	0.009	8.72	74.58	92.01

Table VIII summarizes the constants for the Na_2 and K_2 molecules in the two states represented by these bands. One notes that a change of over 60 percent occurs in the moment of inertia. The ratio $B'(B''-B')$ is 1.65, showing that the R branch turns at a very low number and the zero-point is just about at the head. It is thus clear why a magnetic rotation line is found exactly at the head of every band.

The writers wish to thank Mr. Jacob Rinker for taking the spectrograms of the potassium bands and for the measurement of one of the bands.

RYERSON PHYSICAL LABORATORY,
UNIVERSITY OF CHICAGO,
June, 1927.

THE ZEEMAN EFFECT IN THE ANGSTROM CO BANDS

By E. C. Kemble,* R. S. Mulliken, and F. H. Crawford

Abstract

Theory of the Zeeman effect in the band lines of rigid diatomic molecules.—The qualitative features of the Zeeman effect in the band lines of rigid diatomic molecules as given by the conventional quantum theory and the new quantum mechanics are the same. Both predict that the Zeeman pattern for electronic transitions of the type $^1S \rightarrow {}^1P$ will be greatest for the first line in each branch (for which M, the empirical serial number of a line in a branch, is 1) and will increase in complexity (N = number of component lines in a pattern $= 2M+1$) and decrease in scale as M increases. The size of the pattern is $2/(M+1+1/4M) \cdot \Delta\nu_n$ on the old and $2/(M+1) \cdot \Delta\nu_n$ on the new quantum theory. For $M>2$ the size of the pattern is almost exactly the same for both theories.

Measurement of the Zeeman effect in the λλ5610, 5198 and 4835 bands of CO.—Results on the λλ5610, 5198 and 4835 bands of CO are in agreement with the theoretical predictions. The effect is proportional to the field strength and the patterns are symmetrical about the positions of the lines with no field. Eight of the possible twelve patterns observable for the first two lines of the P and Q branches have been resolved, the rest together with all of the patterns for $R(1)$ and $R(2)$ being too faint for observation. With both polarizations superposed $P(1)$ and $Q(1)$ give symmetrical triplets of total width of 95 percent of $\Delta\nu_n$, thus falling almost exactly midway between the predictions of the two theories. The lines with $M>2$ are only partially resolved but give patterns which are characteristic and are in agreement with intensity predictions based both on the summation rule and the correspondence principle and on the quantum mechanics. The higher Q lines appear as doublets in the parallel polarization, and broad singlets in the perpendicular polarization. The P and R branches in the two polarization show a similar, but reversed and less pronounced difference in character. A fact not accounted for by theory is the slightly greater intensity of the low-frequency components of the Q doublets (parallel polarization) and of the high-frequency components of the P doublets (perpendicular polarization). The results completely confirm the assignment by R. S. Mulliken of the CO Angstrom bands to electronic transitions of the type $^1S \rightarrow {}^1P$ with $\sigma' = 0$ and $\sigma'' = 1$, where σ is the electronic angular momentum parallel to the nuclear axis and single and double primes refer respectively to the initial and final states.

Introduction

UNTIL quite recently there has been no satisfactory interpretation of the magnetic behavior of band spectra and the study of the Zeeman effect has played no part in the analysis of molecular spectra comparable with that which it has taken in connection with the study of atomic spectra. The primary reason for the backward condition of this phase of molecular spectroscopy is experimental, for the difficulties involved in the accumulation of empirical data are very great. The confusing nature of most of the observations made to date and the tardy growth of a satisfactory theory of the other characteristics of band spectra have also had much to do with

* Fellow of the John Simon Guggenheim Memorial Foundation, 1927.

the slow development of an understanding of the Zeeman effect for bands. Recent theoretical advances, however, throw much light on the scattered empirical information gathered up to the present time and should be of great assistance to experimental workers in this field.

The experimental work described in this paper, which had its inception in the theoretical investigations of one of the authors,[1,2] leads to a much closer correlation of theory and experimental data than any published hitherto in this field. Hence we precede the description of our experimental technique and results by a brief review of the theoretical background of the problem.

Summary of Theory[2a]

The first important theoretical contribution to the understanding of the magnetic behavior of band spectra was a brief discussion by Kramers and Pauli[3] of the application of the conventional Bohr theory to the problem of the Zeeman effect for a diatomic molecular model with an electronic angular momentum fixed in magnitude and rigidly oriented with respect to the nuclear axis. The same problem has been discussed somewhat more fully by Kemble[1,2] who independently reached essentially the same result. The formula given by Kramers and Pauli (in a somewhat altered notation) is

$$\Delta F = -(rH\mu/j^2)\left[(j^2-\sigma^2)^{1/2}\sin\beta+\sigma\cos\beta\right] \qquad (1)$$

Here ΔF is the displacement of the "term" value F by the magnetic field H, r is the magnetic quantum number, and j is the rotational quantum number which measures the total angular momentum of the molecule. μ is the magnetic moment and β is the angle which it makes with the internuclear axis. σ is the component of the electronic angular momentum parallel to the nuclear axis in units of $h/2\pi$.

Hund,[4] in a notable paper on the theory of band spectra and its relation to the spinning electron hypothesis, has given theoretical reasons for supposing that normally the mean electronic angular momentum and the magnetic moment are parallel to the nuclear axis when the nuclear angular velocity is not too great, except in S states (where the mean orbital electronic angular momentum is zero). This conclusion is in harmony with Mulliken's scheme for the systematic interpretation of band spectra.[5,6] Aside from the S states, we may therefore set β equal to zero in equation (1). In view of the anomalous ratio of magnetic moment to angular momentum for the electron spin, the expression for μ in terms of the corresponding quantum numbers is

$$\mu = (\sigma_k+2\sigma_s)\mu_1 = (\sigma+\sigma_s)\mu_1 \qquad (2)$$

[1] E. C. Kemble, Phys. Rev. **27**, 799A (1926).

[2] E. C. Kemble, Chapter VII, Section 6, of Bulletin 57 of the National Research Council, "Molecular Spectra in Gases."

[2a] For a more detailed account of the general theory, together with a review of the experimental literature, see reference (2).

[3] H. A. Kramers and W. Pauli, Jr., Zeits. f. Physik **13**, 351 (1923).

[4] F. Hund, Zeits. f. Physik **36**, 657 (1926).

[5] R. S. Mulliken, Proc. Nat. Acad. Sci. **12**, 151 (1926); ZnH, CdH, HgH bands.

[6] R. S. Mulliken, Phys. Rev. **28**, 481, 1202 (1926).

where μ_1 is the magnetic moment of the Bohr magneton and σ_k and σ_s are quantum numbers giving the respective contributions of the orbital motion and the spin to σ. Eq. (1) then takes the form

$$\Delta F = -[r(\sigma+\sigma_s)\sigma\mu_1 H]/j^2 \tag{3}$$

given by Hund. Eq. (3) is based on the assumption that the angular momentum of the electron spin s with respect to the nuclear axis is not appreciably disturbed by the nuclear rotation. Its applicability is therefore limited to singlet states for which s vanishes or, in the case of multiple electronic energy levels, to rotational states in which the product Bj ($B=h/8\pi^2 I$) which measures the frequency of rotation is small compared with the spacing of the levels which form the multiplet. Hund also gives another Zeeman effect formula for use with large values of the ratio of Bj to the spacing of the levels in the multiplet, but this second case is not the one to which our data apply.

Van Vleck[7] has recently called attention to the fact that a possible modification of (3) in conformity with the new quantum mechanics is implicitly contained in a paper by Dennison[8] on the application of the quantum mechanics to the symmetric rigid rotator. Van Vleck gives the explicit formula

$$\Delta F = -\frac{r\mu\sigma H}{j^2-\frac{1}{4}} = -\frac{r(\sigma+\sigma_s)\sigma\mu_1 H}{j^2-\frac{1}{4}} \tag{4}$$

which differs from (3) only in the substitution of $j^2-1/4$ for j^2. The formula assumes that the conventional empirical values of $j(j=\sigma+1/2, \sigma+3/2, \cdots)$ are to be used. If these values are all reduced by $1/2$ in accordance with the usual notation of the quantum mechanics, the denominator in Eq. (4) becomes $j(j+1)$. We shall adhere to the usual band spectrum convention regarding j in this paper, however,—thereby fixing the maximum and minimum values of the magnetic quantum number r consistent with any given j as $j-1/2$ and $-(j-1/2)$ respectively. Hence in this notation the number of magnetic sub-levels associated with any given rotational state, i.e., its a priori probability, is $2j$.

These theories all agree qualitatively. For example, all of them require that the scale of the Zeeman pattern shall be greatest for the faint lines adjacent to the origin and shall diminish rapidly as the rotational quantum number j increases, so that the outer lines of a band should be magnetically insensitive. They also require that each parent energy level shall be resolved by a magnetic field into equally spaced sublevels, the number of which is exactly or approximately equal to $2j$. Hence the complexity of the Zeeman pattern should increase as its scale decreases. Since the theories are all based on the assumption that the molecule executes a uniform precession in the magnetic field, the principle of selection $r'-r''=0, \pm 1$ is equally applicable in all three cases.

[7] J. H. Van Vleck, Phys. Rev. **28**, 980 (1926).
[8] D. M. Dennison, Phys. Rev. **28**, 318 (1926).

In the light of the above theories and of the systematic interpretation of band spectra made possible by the recent work of Mulliken[5,6,9,10] and Hund,[4] the complete absence of a first order Zeeman effect (i.e. of a magnetic resolution of the lines into components having displacements of the same order of magnitude as for line spectra) is to be expected in the case of certain band types. Thus electronic states of the ^1S type have no normal magnetic moment[10a] and bands of the $^1S \rightarrow {}^1S$ type should accordingly show no first order Zeeman effect. Moreover, in the case of ^2S and ^3S states the normal magnetic moment is associated solely with the electron spin and is coupled to the molecular axis by very weak forces which vanish with the nuclear rotation. Hence even a small magnetic field should effectively break this loose coupling and create a Paschen-Back effect in which the molecule behaves as if the spin magnetic moment did not exist. Thus we may generalize the above statement regarding bands of the $^1S \rightarrow {}^1S$ type and say that no first order Zeeman effect is to be expected from any $S \rightarrow S$ transitions.

Hitherto the experimental work on the Zeeman effect for bands has been fragmentary in character and not well adapted to testing even the fundamental qualitative requirements of the theory. A general review of the experimental literature is given in reference 2. The experimental situation may be summarized briefly as follows: (a) most bands are much less sensitive to magnetic influence than line spectra; (b) the lines near the origin are as a rule more sensitive than the lines farther from the origin, and frequently show first order Zeeman patterns comparable in scale with the patterns of typical atomic lines; (c) no first order Zeeman effect has been observed in the case of $S \rightarrow S$ bands; (d) the bands most studied, such as the λ3900 CH band,[11,12] show a variety of anomalous effects indicating that the molecule is distorted by the field so that the rigid molecule theories are not applicable. Thus the existing data are on the whole in qualitative agreement with the requirements of theory, but fail to confirm it with any degree of completeness. With respect to the important predicted increase in the complexity of the Zeeman pattern with increasing rotational quantum number, no conclusive evidence has been found, and it was primarily in the

[9] R. S. Mulliken, Phys. Rev. **29**, 391 (1927); intensity relations.

[10] R. S. Mulliken, Phys. Rev. **29**, May (1927); Hund's theory, etc.

[10a] By a "normal magnetic moment" we mean a magnetic moment characteristic of a non-rotating molecule. Evidence has been given by Knauer and Stern [Zeits. f. Phys. 39, 780 (1926)] and by one of the present writers (reference 2, page 345) indicating that a small magnetic moment in the direction of the j axis is produced either directly or indirectly by the rotation of the nuclei. The rotational magnetization may produce a second order Zeeman effect for the outer lines in a band even when the "normal magnetic moment" is zero for both of the associated electronic states. This second order effect will not be taken into consideration in this paper, however.

[11] E. Hulthén, Thesis, Lund, (1923).

[12] R. Fortrat, Ann. de Physique **19**, 81 (1923). This paper purports to be a study of the Zeeman effect in the λ3872 Swan band, but R. T. Birge has kindly called our attention to the fact that the wave-lengths given by Fortrat prove that the band which he studied was really the λ3900 CH band.

hope of securing definite confirmation of this theoretical prediction that the present investigation was undertaken.

In order to test theories based on the assumption that the magnetic moment is rigidly oriented with respect to the nuclear axis one must, of course, pick out bands for which this assumption is approximately fulfilled. Now, as Hund has pointed out, there is reason to believe that the angular momentum and magnetic moment originating in the orbital motion of the electrons is quite rigidly bound to the nuclear axis, while the angular momentum due to electron spin is loosely attached. Hence the most rigid molecular states should be those in which the spin vector vanishes, i.e., those of the singlet system. We have therefore chosen the Angstrom CO, bands which are of the $^1S \rightarrow {}^1P$ type[6] and lie in a favorable part of the spectrum. These bands have a very simple structure with singlet P, Q, and R branches. The rotational term formula

$$F(j) = B(j^2 - \sigma^2) \qquad j = -1/2, 3/2, 5/2, \qquad (5)$$

fits the data very well if σ is given the values 0 and 1 for the upper and lower electronic levels respectively. This fact affords direct evidence of the rigid character of the initial and final states.

Since σ vanishes for the upper energy level and the angular momentum of spin is also zero, the upper level can have no magnetic moment and should contribute nothing to the Zeeman pattern. Denoting the lower energy level by a double prime and setting $\sigma'' = 1$, $\sigma_s'' = 0$, we may write out the following special forms of equations (3) and (4) applicable to the Angstrom CO bands:

$$\Delta F = r''\mu_1 H/j''^2 \qquad (3A)\ ; \qquad \Delta F = r''\mu_1 H/j''^2 - \tfrac{1}{4} \qquad (4A)$$

These formulas become definite only when the values to be assumed by r'' are specified. The new quantum mechanics on which Eq. (4A) is based requires that r'' shall take on the values $\pm(j''-1/2)$, $\pm(j''-3/2)$, etc. Independently of the new mechanics we arrive at the same result by observing that in the case of atoms the priori probability of any parent state is $2r_{max}+1$ whether the number of electrons be odd or even. Moreover, in the case of diatomic molecules the a priori probability is always $2j$ as required by the summation rule and confirmed by the quantitative intensity measurements of Bourgin and Kemble[13] for HCl, as well as by other work on even[9] and odd[14] molecules. Hence $2r_{max}+1$ is equal to $2j$ or $r_{max} = (j-1/2)$.

We can now predict the exact character of the magnetic structure of each of the rotational levels associated with the lower electronic state. The minimum value of j'' is 3/2 (equal to $\sigma''+1/2$). Hence the lowest rotational state should split into three magnetic sub-states corresponding to values 0, +1, −1 of the magnetic quantum number r''. The spacing

[13] E. C. Kemble and D. Bourgin, Nature, June 5, (1926). D. Bourgin, Phys. Rev. **29**, 794 (1927).

[14] R. S. Mulliken, F. A. Jenkins, and H. A. Barton, Nature **119**, 118 (1927); Phys. Rev. **29**, 211A (1927) and later articles: NO bands.

of the components of this triplet should be 4/9 of the "normal" spacing, $\mu_1 H$, according to Eq. (3A) and 1/2 "normal" according to Eq. (4A). The second rotational level should yield five components with a spacing 4/25 normal or 1/6 normal according to Eqs. (3A) and (4A) respectively. The magnetic structures of these two rotational energy levels should be reproduced in the Zeeman patterns of the first and second lines, respectively, of each of the three branches.

If we denote the ordinal number of any line in the corresponding branch by M[14a] and set Me qual to unity for the first observed line of each branch, we have $M=j''-1/2$ and the general rule for the number of Zeeman components N in the pattern of any given line is

$$N=2j''=2M+1$$

The over-all width of the Zeeman pattern for the Mth line is

$$\Delta\nu=\frac{\mu_1 H(2j''-1)}{j''^2}=\frac{2M\mu_1 H}{(M+\frac{1}{2})^2}=\frac{2\mu_1 H}{M+1+\frac{1}{4}M}=\frac{2\Delta\nu_n}{M+1+\frac{1}{4}M} \tag{6}$$

according to Eq. (3A), and

$$\Delta\nu=\frac{2\mu_1 H}{M+1}=\frac{2\Delta\nu_n}{M+1} \tag{7}$$

according to Eq. (4A).

In order to predict the appearance of the Zeeman patterns as observed with a spectroscope with insufficient power to resolve completely the fine structure, it is necessary to compute the intensities of the components. For this purpose we may use the intensity formulas deduced for line spectra by Kronig and by Hönl from the summation rule.[15] The applicability of these formulas to bands has the same justification as for line spectra. In order to show the relative intensities of components belonging to different parent lines, the Zeeman intensity formulas may be combined with the Hönl and London formulas for the intensities of the unperturbed band lines.[16] The combination formulas are in harmony with those deduced from the matrix mechanics by Dennison[8] for the Zeeman components of the spectrum lines of a rigid symmetrical rotator. When σ' and σ'' are given the values 0 and 1 respectively the equations take the form:

$$P \text{ branch} \begin{cases} I_0=\dfrac{3(M^2-\tau''^2)(M+1)}{(2M-1)(2M+1)M} \\ I_{\pm 1}=\dfrac{3(M\pm\tau'')(M\pm\tau''-1)(M+1)}{4M(2M-1)(2M+1)} \end{cases} \tag{8A}$$

[14a] i. e. M is equal to the value of j'' as used in the new quantum mechanics.

[15] R. de L. Kronig, Zeits. f. Physik **31**, 885 (1925); H. Hönl, Zeits. f. Physik **31**, 340 (1925).

[16] H. Hönl and F. London, Naturwiss. **13**, 756 (1925); Zeits. f. Physik **33**, 803 (1925).

$$Q \text{ branch} \begin{cases} I_0 = \dfrac{3r''^2}{M(M+1)} & (9A) \\ I_{\pm 1} = \dfrac{3(M \pm r'')(M \pm r''+1)}{4M(M+1)} & (9B) \end{cases}$$

$$R \text{ branch} \begin{cases} I_0 = \dfrac{3[(M+1)^2 - r''^2]M}{(M+1)(2M+1)(2M+3)} & (10A) \\ I_{\pm 1} = \dfrac{3(M \mp r''+1)(M \mp r''+2)M}{4(M+1)(2M+1)(2M+3)} & (10B) \end{cases}$$

Here I_0, I_{+1}, and I_{-1} are the intensities of the components associated with the transitions $r''=r'+0$, $r''=r'+1$, $r''=r'-1$, respectively, for transverse observation. As the components I_{+1} and I_{-1} for any given value of r'' are superimposed, in the present case, because of the lack of Zeeman splitting

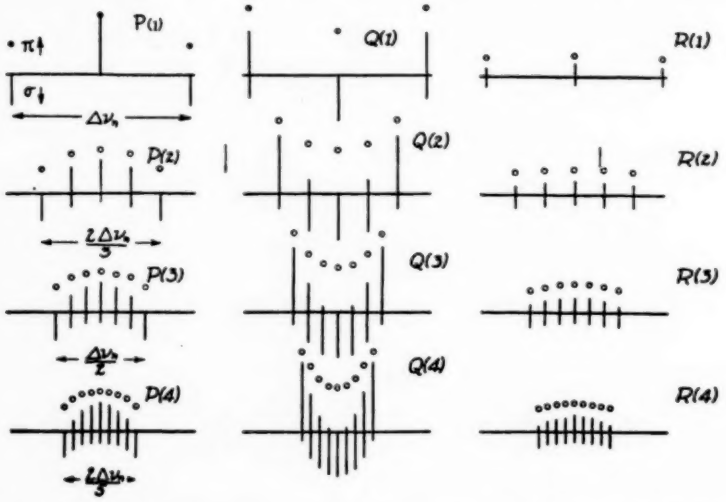

Fig. 1. Theoretical Zeeman patterns for P, Q, R lines of $^1S \rightarrow {}^1P$ bands. The magnitudes of the patterns are calculated from Eq. (4A) and the intensities from Eqs. (8A) to (10B) inclusive. (These equations take account of the relative intensity of the lines in a band.) Intensities calculated for the case of polarization (π) parallel to the field are plotted upward from the horizontal lines, while those plotted downward are for polarization perpendicular (σ) to the field. The intensities with both polarizations superposed are represented by the small circles. The distance between outermost components for a given value of M is the same in each branch

in the initial electronic state, their intensities must be added to get the total intensity of the corresponding line with polarization perpendicular to the lines of force.

Figure 1 shows the positions and relative intensities of the Zeeman components of the first four lines of each branch as computed from Eqs. (4A), (8A), (8B), (9A), (9B), (10A), (10B) for transverse observation with both polarizations. The parallel or π-components (I_0) are plotted above the zero

line and the perpendicular or σ-components (I_{+1}, I_{-1}) below the zero line. It will be apparent at once that the early lines in the Q branch as observed in a spectroscope with moderate resolving power (insufficient to give the full structural detail) should appear to be doublets in the parallel polarization and (with the exception of $Q(1)$) broad singlets in the perpendicular polarization. The two polarizations of the P and R branch lines should show a similar, but reversed and less pronounced difference in character.

Apparatus and Experimental Details

The light source was an uncondensed high-potential alternating discharge passing between copper electrodes in an atmosphere of CO_2. The gas was contained in a Back-box[17] enclosing the magnet poles of a large Weiss-electromagnet. The pole-tips of this magnet were about 7 mm in diameter and when kept about 5 mm apart gave a maximum field of around 35,000 gauss. The discharge passed parallel to the field between disc or wire-ring electrodes, the light from the discharge being sent through a quartz window and lens and focussed on the slit of a 21-foot concave grating. This was arranged in the Paschen mounting,[18] so that the entire spectrum could be photographed at once.

The CO_2 was generated by the action of pure HCl on marble, being then passed in succession through $NaHCO_3$ solution and granulated $CaCl_2$ to remove HCl and moisture. During the runs, a slow stream of CO_2 was pumped through the Back-box, in order to minimize the effect of impurities due to possible leakage and to the liberation of gases by the action of the discharge. Best results were obtained when the CO_2 pressure was maintained at 8 mm or less.

The magnet is one of the standard Weiss types with water-cooled copper coils and can be operated on a current between 60 and 70 amperes indefinitely without serious heating. Since with currents of this magnitude the iron was nearly saturated, satisfactory constancy of field was obtained by regulating the field current to an ampere or less. The necessary current was supplied at about 60 volts by a 5-kw motor-generator set operating on a 550-volt line. Preliminary to a run, the field current was allowed to flow until approximately constant temperature conditions were established in the magnet.

Design of Back-box. The Back-box was built in the Laboratory shop essentially according to Back's description, but with certain modifications. In Back's design (l.c., p. 124) the ends of the box are separated from the pole pieces by means of rubber gaskets, and troublesome adjustments were necessary to keep the faces of the pole pieces parallel and thus to insure a uniform field despite the distortion of the magnet yoke at the higher fields. In order to avoid these adjustments and to keep the pole faces automatically parallel, the following changes were made. (See Fig. 2) Both pole pieces

[17] Cf. E. Back and A. Lande, Zeemaneffekt und Multiplett Struktur der Spectrallinien. Pp. 122–31, Julius Springer, Berlin (1925).

[18] Cf E. Back and A. Landé, l.c., p. 150.

were cut off squarely from their stems and the back of one was given a convex-spherical shape (see Fig. 2 at *B*) in a lathe. The corresponding magnet-stem was then turned to fit the back of the pole piece. The two pole pieces (with shoulders cut to fit snugly) were finally inserted in the cylindrical box, the joints being made air-tight by rings of soft wax. To allow for varying gap lengths a series of bronze gaskets were provided which could be inserted between the shoulders of the pole pieces and the ends of the box. The rigid unit of pole pieces and box was then inserted in the magnet so as to complete the magnetic circuit. The spherical end enabled centering to take place almost automatically. By increasing the pressure on the box and pole pieces by means of the main adjusting screws of the magnet, (not shown in figure) most of the wax was extruded, the thin films remaining showing no discernible tendency to allow even slight buckling of the magnet frame. The box was provided with four windows, and with an inlet and an outlet tube at opposite sides. In addition to the electrodes for gas excitation, two electrodes were provided for obtaining an interrupted metal arc,[17] to provide standard lines for the determination of field strengths.

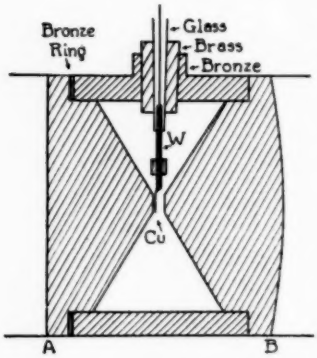

Fig. 2. Modified Back box.

Electrodes. The discharge electrodes had tungsten leads in tapered pyrex plugs. The latter were ground to fit into brass plugs which were themselves conical and ground to fit into openings in the box. The ground joints were kept tight with stop-cock grease. By means of a small brass sleeve with set screws, the actual electrodes were fastened to the leads. The chief difficulties are the elimination of stray discharge between the electrode leads and to the pole pieces, and the keeping of the electrodes properly centered and at the optimum separation. Stray discharge is especially noticeable at low pressures. If the pressure is raised to lessen this stray discharge (or if a condensed discharge is used), undesired band spectra appear, as well as the line spectrum of the electrodes, while the CO Angstrom bands are weakened. (The total luminous intensity may at the same time be much increased.) The second negative carbon bands of Deslandres and D'Azambuja are regularly present, especially at higher pressures, but cause no serious trouble, since they are in the ultra-violet. The discharge has a greenish-blue color when the CO Angstrom bands are strong.

Various forms of electrodes were tried. A simple and good one can be made from a piece of No. 16 copper wire, by bending one end into a ring 5 mm in diameter, flattening slightly, and sheathing the stem with a piece of capillary pyrex or silica tubing. The pole pieces must also be insulated, e.g. by fitting glass caps over them (fastened with de Khotinsky cement) or using thin pieces of mica attached to the electrodes themselves. In operation such electrodes become red hot even with the minimum current

in the primary of the transformer, and consequently eventually burn away and must be replaced.

Exposures. Most of the exposures were made with a field of about 35,000 gauss. One exposure (no polarization) was made with about 24,000 gauss (for this a magnet current of 14 amperes was needed). In another (no polarization) a comparison was made of the spectrum with a field of 35,000 gauss and that with the residual field of the magnet, which served as "zero field." (Actually there was even here a very slight broadening of the lines of widest Zeeman pattern.) Most of the exposures were made with a Nicol prism interposed in front of the slit so as to give light polarized either parallel, or perpendicular, to the direction of the field.

Exposures up to forty-two hours were made, during which the electrodes had to be replaced occasionally. With the co-operation of Mr. R. A. Loring, a continuous plate-holder was arranged to keep the plates at the position of best focus, the latter having been carefully redetermined throughout the spectrum. Photographs were taken in the first and second orders, using Eastman Speedway plates (or in some cases Eastman 33) below 4900A, and Eastman Astronomical Green Sensitive plates up to about 5900A. After each exposure, the plates, and the gas electrodes, were removed without interrupting the magnet current; a photograph was then taken with the other electrodes so as to obtain the Zn triplet λλ4660, 4722, 4811 for use as a field standard.[19] Or in some cases this was omitted and the Cu lines λλ3247, 3274, which were always present on the band plates (because of the use of Cu electrodes) were used as field standards. Photographically the most intense bands in the first order were the green bands λ5610 (0, 3) and λ5198 (0, 2), followed by λ4835 (0, 1), λ4511 (0, 0), λ4123 (1, 0), and λ4394 (1, 1); the numbers in parentheses are the vibrational quantum numbers.[20]

Six sets of plates, with exposures varying between 5 and 42 hours, gave the first four of these bands in sufficient intensity in the first order so that some of the lines in each of the above bands could be studied. The plates of the last two bands were rendered completely useless by the presence of an intense background of impurity lines. The band λ4511, not having been thus far analyzed,[21] is reserved for future discussion, the present paper being confined therefore to the bands λλ5610, 5198 and 4835.

The chief difficulty, of course, lies in the fact that the lines which can be resolved into Zeeman patterns are those which correspond to the lowest values of j and which at ordinary temperatures, due to the fairly large moment of inertia of the CO molecule, are of *very* low intensity. The second order of the grating being considerably weaker (over the range of wave lengths

[19] The Zeeman separations for these lines have been shown to be accurately proportional to field strengths. See Cotton and Weiss, Journal de physique **6,** 429 (1907). The magnetic field was calculated from the expression $H=\Delta\nu_n/4.698\times10^5$ where $\Delta\nu_n$ is the normal Lorentz separation in wave-numbers as obtained from the zinc lines.

[20] For assignment of vibrational quantum numbers see: R. T. Birge, Phys. Rev. **28,** 1157 (1926).

[21] O. Jasse, Comptes rendus **182,** 692 (1926).

used) than the first, the second order plates were of use only for certain strong Q lines somewhat removed from the band origins.

Plate measurements were made on a Max Wolz comparator on which 0.0001 cm could be estimated. The quantities to be measured varied in magnitude from 0.02 cm to about 0.005 cm, the extreme faintness of the earlier patterns and the lack of definition of the higher rendering the accuracy of a given reading in all cases much less than the graduations of the comparator would suggest. It was consequently necessary to average a great number of settings (as high as 20 or 30) made at various points along a given line. The dispersion at any point was obtained from measurements on unaffected lines using the frequency differences given by Hulthén.[22]

Temperature control in grating room. The natural variations in the temperature of the grating (which is in a basement room) were found to be too great to give the desired line-sharpness. Hence, during the exposures the temperature of the grating room was maintained constant to less than 0.1°C (probably to $\pm 0.03°$ or 0.04°C) by thermostatic control. Heating

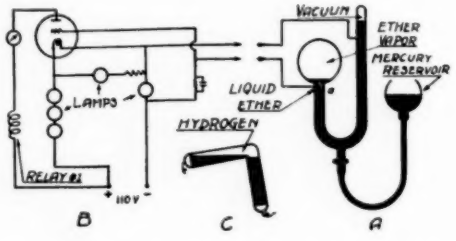

Fig. 3. When the ether vapor contracts sufficiently, an electrical contact is made at a which short-circuits the grid to the filament, thus changing the plate current and operating relay number 1. This actuates a second heavier relay which tips the mercury circuit breaker shown at C and turns on the current in the heating coils.

was accomplished by means of forty foot lengths of number 22 nichrome wire, connected in parallel and strung along one wall and so adjusted that each took a current of 5 amperes from a 110-volt line. Air circulation was provided by an electric fan on the other side of the room.

The details of the thermostatic control are given schematically in Fig. 3. A represents a temperature control device constructed with the co-operation of Dr. F. A. Jenkins. It may be set for any desired temperature by varying the height of the mercury reservoir, its operation being clear from the diagram. The advantages of this device are its reliability and its responsiveness. By using only very minute currents and having a layer of (liquid) ether over the mercury at a (the bulb is filled with air-free ether vapor) fouling of the mercury surface on make and break is almost completely prevented. Since, furthermore, ether has a large vapor pressure at room temperatures, small temperature differences cause a considerable displacement of the mercury levels with resultant high sensitivity. The avoidance, moreover, of sparking on break of circuit, by preventing the consequent heating, reduces the time lag in operation.

[22] E. Hulthén, Thesis, Lund (1923).

This control device was used to operate the vacuum tube relay shown in Fig. 2B. The latter is an adaptation of an idea described by H. S. Roberts[23] and is used to actuate a very small telephone relay (Relay 1). This then operates a larger telegraphic relay which in turn works the L-circuit-breaker shown at C. This circuit-breaker contains hydrogen under a pressure of several atmospheres over the mercury and is capable of breaking a current of 15 amperes or more without danger.

In practice the control device was adjusted for an amount (usually 0.5° to 1.0°) sufficiently above the slowly changing room temperature to provide a safe operating margin. In the case of very long exposures where a greater margin of safety was necessary, an additional continuous heater, capable of producing an elevation of from 0.5° to 1.0°, was employed, its use being confined to the beginning or end according as the natural room temperature was slowly rising or falling

Results

The effects produced by the magnetic field on the bands studied here are in general of two sorts, (1) those effects noticeable near the origin and covered by the theory given in this paper, and (2) certain perturbations found only in the higher lines (i.e. $M = 26$ to 29) and apparently confined chiefly to one line in each branch These latter effects manifest themselves as more or less symmetrical patterns of total width several times the normal effect, $\Delta\nu_n$, together with a light continuous (or presumably unresolved) background. Due to uncertainty caused by the possible presence of impurity lines superposed on these patterns, their discussion is reserved until further data have been obtained.[24]

In comparing the experimental data with the theoretical predictions, it is well to remark at the outset that the displacements observed seemed always to be symmetrical around the undisplaced positions of the lines.[25] Furthermore, the data for the widths of the $Q(1)$ pattern with fields of 24,400 and 34,900 gauss respectively showed that the size of the pattern was a linear function of the field (to within ± 2 per cent). In addition there remain three general heads under which theory and experiment can be compared, viz. occurrence or nonoccurrence of (1) predicted types of pattern in a given state of polarization, (2) proper relative intensity of components in individual patterns and in nieghboring ones, and finally (3) correct quantitative scale of patterns. Since no microphotometric measurements have thus far been made, the first two tests are essentially qualitative. (See footnote 33).

[23] H. S. Roberts, Jour. Opt. Soc. Am. **11**, Aug. 1925.

[24] Because of the length of time required for exposures, an exposure with field was taken alongside one without on only one set of plates. This, however, served for the location of the faint impurity lines which might be expected to cause ambiguity in measuring the weaker Zeeman patterns. In the case of only one or two of the band lines discussed in the present paper did such impurities cause difficulty.

[25] Future plates taken with zero field comparison exposures may serve to reveal slight bodily shifting of patterns, although such effects must be very small if they exist.

Because of the varying arrangement of the lines in the three bands used, only rarely can the same line be studied in each band. Frequently a pattern partially obscured by another line or rendered ambiguous by an impurity for one field can be measured for a larger or smaller field. To render clear the cases in which difficulties of this sort occur, the earlier lines of the bands under consideration are given schematically in Fig. 4, the relative intensities

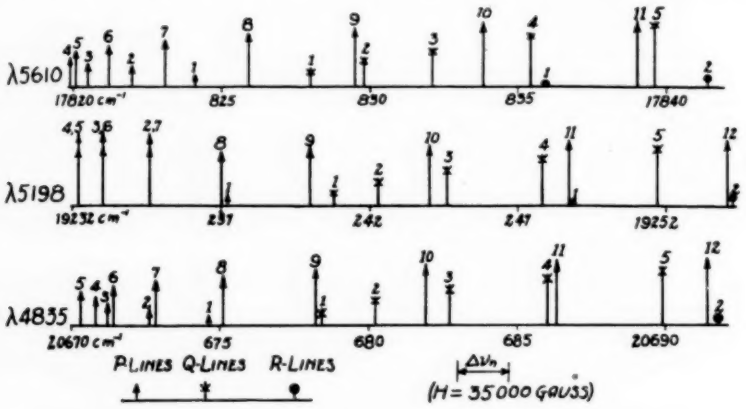

Fig. 4. Schematic diagrams showing the arrangement of the lines in the P, Q and R branches near the head of the three Angstrom CO bands considered in this paper. Ordinates represent relative intensities. Double arrowheads indicate superposition of two lines. To aid in following the text $\Delta\nu_n$ for $H=35{,}000$ gauss is plotted to scale.

of the lines in the same band being indicated by the height of the corresponding ordinates.[26] For comparison the scale of the Zeeman pattern for $H=35{,}000$ gauss is represented by a line equal in length to $\Delta\nu_n$. When it is considered that only the first two lines of the P and Q branches were definitely resolved into their fine line patterns and that the pattern for either $P(2)$ or $Q(2)$ consists normally of four or five separate components, the difficulties regarding intensity are thrown sharply into relief.

Notation. The lines whose fine-structure could be studied will be considered singly and in some detail, the higher lines requiring little individual attention. In order to be able to refer to the individual components of a given line, we shall adopt a convenient notation, writing for example $\pi-P(2)_{-2}$ to designate that component, in parallel polarization, of the P line for which $j''=5/2$ (i.e. for which $M=2$) and $r''=-2$; $\pi-\sigma-P(2)_{-2}$ to designate the same with both polarizations superposed, etc.[27]

Structure of $P(1)$. Beginning with the P lines we find that in parallel polarization in both λ5610 and λ4835 $P(1)$ occurs in the presence of the

[26] R. S. Mulliken, Phys. Rev. **29**, 411 (1927).

[27] Since there is no experimental means of determining the orientation of a given molecule in the magnetic field, the above notation regarding r'' values is purely arbitrary. If it be assumed that components having a higher frequency than the undisplaced line result from transitions in which r'' is negative, then those having a lower frequency result from transitions in which r'' is positive.

field as a sharp singlet in the original position of the line (not favorably situated for observation in λ5198, (of Fig. 4). Its intensity is about the same as that of $\pi - Q(1)_{-1}$, but distinctly greater than that of $\pi - Q(1)_{+1}$. (According to Fig. 1, of course, these two Q components should be of equal intensity; cf. below.) In the perpendicular polarization it occurs in λ5198 as a symmetrical doublet, whose components are displaced by equal and opposite amounts on either side of the zero-field position. Were an undisplaced component also present, it would of course be obscured by $P(8)$. That such is not present is shown by the fact that in λ4835 no line occurs at the undisplaced position (the displaced components are here not favorably situated for observation). When both polarizations are superposed we have a triplet (λ5610) with the central component much the more intense. It is about the intensity of $\pi - \sigma - Q(1)_{+1}$. Although this is the only plate showing the outer components of the $P(1)$ pattern with sufficient intensity for comparison,[28] it is significant that the $P(1)_{-1}$ component is much more intense than the $P(1)_{+1}$. This, if confirmed on future plates, is a fact not accounted for by the theory. It is to be correlated with the dissymmetry in the corresponding Q patterns in parallel polarization, the difference being that in the first case the component of *higher* frequency is the more intense, while in the latter the reverse is true.[29]

It is to be noted that in making the enlargements from which the reproductions in Fig. 5 were made the weak lines near the head had to be exposed about twice as long as the higher-numbered lines in order that they should be visible at all on the reproduction. Consequently, although the relative intensities of say the $P(1)$ and $Q(1)$ patterns are preserved, these patterns appear much more intense (when compared with the stronger P lines) in the figure than on the original plates.

For the numerical width of the $P(1)$ triplet, Eq. (3A) predicts 88.9% and Eq. (4A) 100% of $\Delta\nu_n$. The observed widths are given in Table III, the value from λ5610 being much the more reliable. The observed values lie near the arithmetical average of the predictions of the two theories (cf also results for $Q(1)$ lines).

[28] As Fig. 1 shows the outer lines of the $P(1)$ pattern with both polarizations superposed should be of the same intensity as with perpendicular polarization alone. This follows from the fact that for parallel polarization where $\Delta\nu = 0$, Eq. (8A) gives $I_0 = 0$. Consequently the outer components in this polarization have zero intensity. Hence when both polarizations are superposed, whatever intensity these outer components have is due to transitions for which $\Delta r = \pm 1$, i.e. is due solely to light polarized perpendicularly to the field.

[29] It should be pointed out that in all probability the final states for the P and R lines of these bands are not identical with those for the Q lines (σ-type doubling). The separation of these two final states (which we may refer to as A and B rotational substates; see R. S. Mulliken Phys. Rev. **28,** 1202 (1926), Fig. 1, also Phys. Rev. **29,** 637 (1927)) for the Angstrom bands is practically zero for low M values, but becomes large enough to be noticed for large M values. (See E. Hulthén, Thesis, where the resulting combination defect was first noted.) It is likely then that the difference in the intensity dissymmetry in the P and Q patterns is correlated with the difference in the final states of these lines (the initial states being magnetically insensitive). The dissymmetry itself is probably a function of the field strength disappearing for very low fields. This question will be considered in another paper.

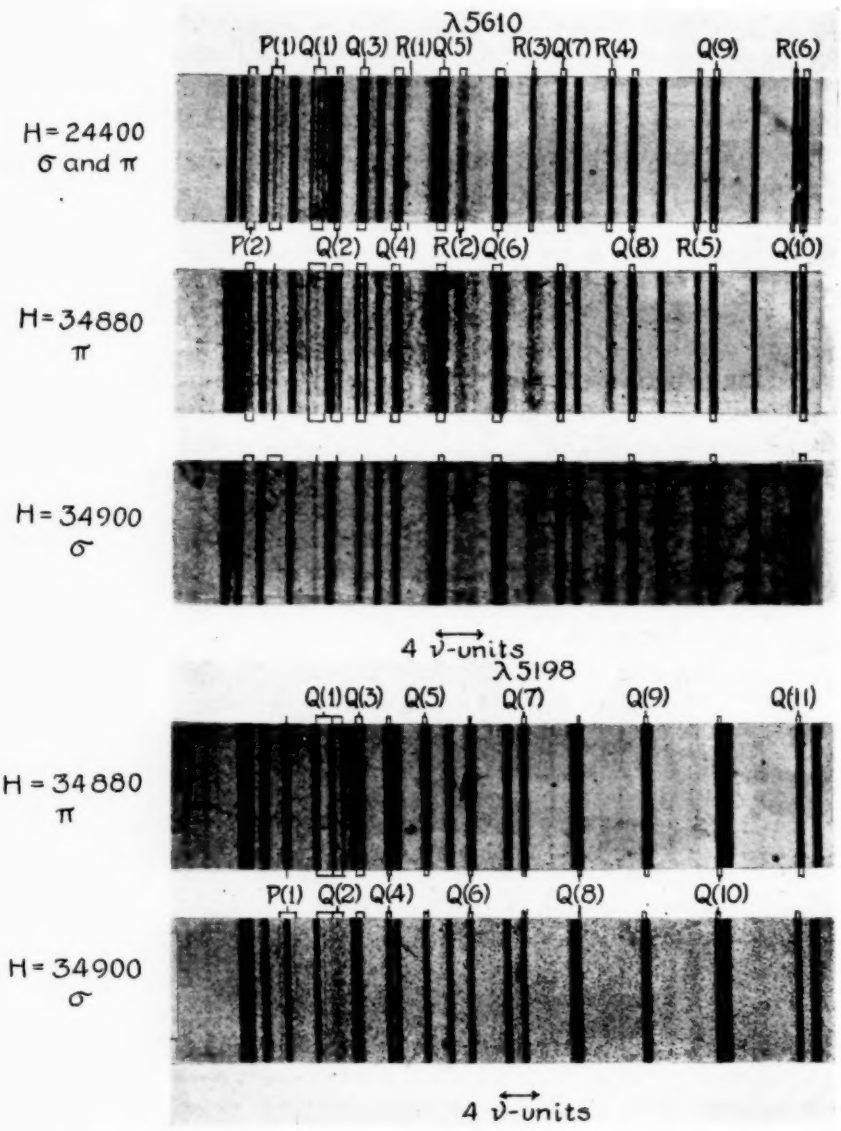

Fig. 5. These reproductions represent enlargements (about 15 times) of regions near the heads of the λλ5610 and 5198 bands. In order to insure the reproduction of at least some of the fainter patterns the left ends of the bands (as explained in the text) were exposed longer in printing than the rest. Consequently the patterns of the $P(1)$, $P(2)$, $Q(1)$, and $Q(2)$ lines have a much greater relative intensity than on the original plates. Faint lines not marked are impurities (including the faint line almost midway between the $Q(1)$ doublet of λ5610. π polarization.) In λ5610, parallel (π) and perpendicular (σ) polarizations superposed, the triplets given by $Q(1)$ and $P(1)$ are to be noted. The $Q(1)$ triplet is quite symmetrical in intensity with the central component, as shown by photometric curves just obtained, slightly stronger than the other components. The left component of the $P(1)$ triplet, however, is so faint as to be scarcely recognizable on the reproduction (see Fig. 1). In the parallel polarization $P(1)$ appears as a sharp singlet and $P(2)$ as a triplet (with only two lines showing in the reproduction). The Q lines appear as doublets, $Q(1)$ being a real doublet, the higher ones appearing as such due to the resolving power being much too low to reveal the fine structure. In second order plates this doublet appearance of the Q lines could be observed as far as $Q(14)$. $\Delta\nu_n$ for $H = 24{,}000$ gauss is of the order of 1.1 wave number units.

Other P lines. The $P(2)$ patterns were resolved in only two cases. In parallel polarization (λ5610) a very narrow and faint triplet was found of width 95 percent of that from Eq. (4A). In λ5198 in perpendicular polarization two very faint lines occur, one on either side of the strong line $P(7)$. They are of about equal intensity and perceptibly weaker than $\sigma - Q(1)_0$. The qualitative data on these P lines are summarized briefly in Table I. Under the caption "plates used" is given the number of plates from which the nature of a given pattern was determined. Cases rendered doubtful by reason of extreme faintness are marked with a question mark.

TABLE I

P line patterns.

Bracketed patterns indicate that part of pattern is obscured by some other line but that the part visible has proper position and magnitude. (See Fig. 4) Question marks indicate doubt due to great faintness or possible presence of impurities.

Polarization	Line	λ5610			λ5198			λ5835		
		Nature	Remarks on intensity	Plates used	Nature	Remarks on intensity	Plates used	Nature	Remarks on intensity	Plates used
π	$P(1)$	sharp singlet	same as $\pi - Q(1)_{+1}$	2				sharp singlet	$> \pi - Q(1)_{-1}$	1
σ	$P(1)$				Doublet	$< \pi - Q(1)_0$	1	[Doublet]	?	1
π, σ	$P(1)$	triplet	Center component strongest and of intensity $> Q(1)_{\pm}$	2				[triplet]	central component most intense	1
π	$P(2)$	very narrow triplet	?*	1						
σ	$P(2)$				[quartet]	$\sigma - P(2)_{+2}$ $< \sigma - Q(1)_0$	1			

* $\pi - P(2)_{-1}$ seems to be anomalously faint and does not show in the reproduction in Fig. 5.

The patterns of the higher P lines, which are observable, are in parallel polarization all narrower than in perpendicular. In parallel polarization the intensity in a given pattern (unresolved in detail) is greatest in the center, while in the perpendicular polarization a distinct doublet effect is noticeable (less marked than for Q doublets). In the only case where the width of a P doublet could be measured with any precision a value agreeing closely with that for the corresponding Q doublet was obtained (see below).

Q lines. In the case of the Q lines the data are more complete as well as more certain. In parallel polarization $Q(1)$ shows itself a doublet in all three bands. In the perpendicular polarization in λ5610 only $\pi - Q(1)_0$ is visible and it is very faint (this doubtless accounts for the absence of the other components whose intensity from Fig. 1 should be only half as great). In λ5198 likewise only $\pi - Q(1)_0$ is visible, the others here being obscured by $\pi - Q(2)_{+2}$ and P_{10}.

On only two plates (see Table II) were $Q(2)$ patterns resolved. The first, in λ5610, due to the presence of $P(9)$ shows only the right half of the pattern, and the second (due to nearness of $\pi - Q(1)_{-1}$) gives only three of the four lines. In both cases, however, the outer components are three or four times as intense as the inner. While very difficult to measure with any

precision, the magnitudes of the separations average within 10 percent of the calculated ones.

TABLE II

Q line patterns.

Polarization	Line	λ5610 Nature	λ5610 Remarks on intensity	λ5610 Plates used	λ5198 Nature	λ5198 Remarks on intensity	λ5198 Plates used	λ4835 Nature	λ4835 Remarks on intensity	λ4835 Plates used
π	$Q(1)$	doublet	$\pi-Q(1)_{+1}$ more intense than $\pi-Q(1)_{-1}$	1	[doublet]		2	[doublet]	very faint	1
σ	$Q(1)$	single†	very faint	1	[triplet]	Central component only visible*	1			
π,σ	$Q(1)$	triplet	$Q(1)_0$ fainter than $Q(1)_{\pm 1}$	2	[triplet]		1	[triplet]	very faint	1
π	$Q(2)$	quartet	$\pi-Q(2)_{-1}$ very faint	1	[quartet]	$\pi-Q(2)_{\pm}$ much fainter than $\pi-Q(2)_{-2}$				

* This component is more intense than $\pi-P(1)_{+1}$ or $\pi-P(1)_{-1}$ (See Table I).
† Should be triplet. (Outer components probably too faint to show. See Fig. 1).

The patterns for the higher Q lines are in rather striking harmony with the theory. In perpendicular polarization they are simply broadened to approximately the same width as corresponding R lines. With both polarizations superposed a distinct lightness in the center is observable (in all three bands) up to $Q(4)$ or $Q(5)$, beyond which the pattern is too narrow for observation of the effect. In the parallel polarization the Q lines appear as distinct doublets, the centers being very much lighter and the doublet components much sharper than in the case of the corresponding P and R doublets. (see Fig. 5) It was found possible to measure these doublet widths (by use of both first and second-order plates) up to $Q(14)$ for λ5610, to $Q(8)$ for λ5198 and to $Q(7)$ for λ4835. These results expressed as percentages of $\Delta\nu_n$ and averaged for the two available plates of each band are represented in Fig. 6.[30] (Since the fields differed on the two plates by only 150 gauss, this averaging is quite justified even though the rigid proportionality of the separation to field strength has been only approximately established.

The observed doublets, at least those with $M>2$, evidently represent two unresolved groups of lines corresponding to the outer and more intense parts of the theoretical patterns. Fig. 1 in fact shows that in measuring the doublets, since settings are made on the apparent centers of gravity of the two doublet members, the observed widths will of necessity be less than the theoretical maximum pattern widths. This is amply borne out by the data given in Table III and plotted in Fig. 6. The two smooth curves are calculated from Eqs. (6) and (7), the ordinates representing percentages of $\Delta\nu_n$. The two curves for all values of M greater than unity are so nearly coincident that the present data could not be expected to favor one more than the other.

[30] The difficulty in measurement of the doublets is due to the low intensity of the patterns for small M values and the lack of definition of those for large M values. Each value represents the average of from 20–30 measurements.

The most trustworthy value for total pattern width of lines with $M=1$ is 94.8 percent of $\Delta\nu_n$, the five other values obtained agreeing with this to within less than 2 percent. Consequently all the observed points lie midway between the two theoretical curves. The best results for $M=2$ are not of comparable accuracy, but give for the pattern width 63 percent of $\Delta\nu_n$ (i.e. 99 and 94 percent of the values predicted, respectively, by Eqs. (3A) and (4A)). The results for the patterns of higher M values being taken from the Q doublets (parallel polarization) must, as explained above, fall a certain amount below the theoretical predictions. As a matter of fact for λλ5610 and 5198 between $Q(3)$ and $Q(14)$ the observed doublet widths average

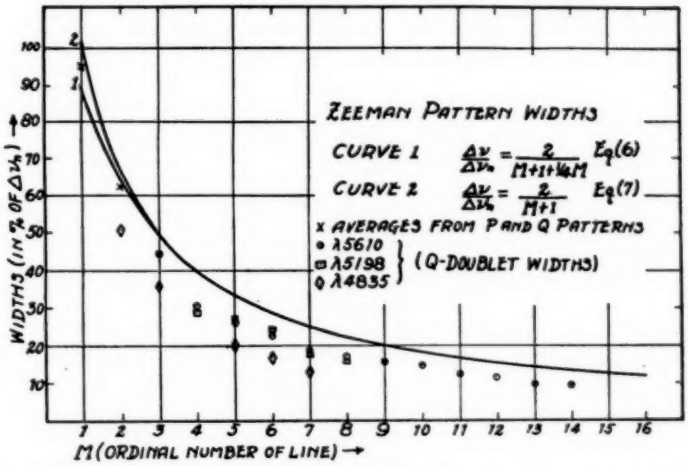

FIG. 6. The widths of resolved patterns having M-values 1 and 2, i.e. those of $P(1)$, $Q(1)$, $P(2)$, $Q(2)$, are averaged and plotted as x. The other points represent widths of Q doublets and fall regularly below the theoretical extreme widths for reasons given under Table III. The M-values used as abscissas are the empirical ordinal numbers of the lines in their respective bands. They are numerically equal to the final j-values of the new, and $\frac{1}{2}$ unit smaller than the final j-values of the old quantum theory.

77 percent of the theoretical total widths. Why the values from λ4835 should fall below the rest as they do is not clear.[31]

R lines. The R lines were so weak on all of the plates that no R pattern was definitely resolved. The higher R lines behave quite similarly to the P lines except that they have the same widths in both polarizations and the lightness in the center (perpendicular polarization) is much less marked than for P lines of the same M value. This doublet-character was visible for $R(3)$, $R(4)$ and $R(5)$ in λ5610 and $R(4)$ in λ4835 (not observable in λ5198; see Fig. 4). With both polarizations superposed the results were qualitatively the same as for parallel polarization except that $R(2)$ here seemed to have a

[31] For a further check the over-all widths (measured from edge to edge) of the Q patterns taken with both polarizations superposed were measured. These magnitudes although not very precisely defined, all fall regularly *above* the theoretical curves of Fig. 6.

light streak in the center. This shows on only one plate of one band[32] and if confirmed represents a distinct disagreement with the theoretical expectations.

TABLE III

P and Q doublet separations. The values given in this table are expressed as percentages of $\Delta\nu_n$ the normal Lorentz separation. Those for $P(1)$, $P(2)$, $Q(1)$, and $Q(2)$ of λλ5610 and 5198 are total widths of resolved patterns, that for $Q(1)$ in λ5610 being the most reliable. The other values represent Q doublet separations in parallel polarization. Since we are for these measuring not the distance between sharp lines, but the distance between the centers of gravity of unresolved patterns, Fig. 1 predicts that such measurements must give values which are less than the theoretical separations of the outermost components. These latter theoretical separations as calculated from Eqs. (6) and (7) are given at the bottom of the table

Band	Line	$P(1)$	$P(2)$	$P(6)$	$Q(1)$	$Q(2)$	$Q(3)$	$Q(4)$	$Q(5)$	$Q(6)$	$Q(7)$	$Q(8)$	$Q(9)$	$Q(10)$	$Q(11)$	$Q(12)$	$Q(13)$	$Q(14)$
λ5619	width	96.1		21	94.8	60*	44.5	30.4	26.1	22.8	18.9	17.0	15.3	14.8	12.3	11.8	9.7	9.5
	No. of plates	1		1	1	1	2	2	2	2	2	2	1	1	1	1	1	1
λ5198	width	93	62		94.2	65		28.7	27.4	24.3	18.0	16.0						
	plates	1	1		2	1		2	2	3	3	1						
λ4835	widt					51	35.7		20	16.8	13							
	plates					2	2		1	1	1							
Eq. (6)	width	100.0	66.7	28.6	100.0	66.7	50.0	40.0	33.3	28.6	25.0	22.2	20.0	18.2	16.7	15.4	14.3	13.3
Eq. (7)	width	88.9	64.0	28.4	88.9	64.0	49.0	39.5	33.0	28.4	24.9	22.1	20.0	18.2	16.7	15.4	14.3	13.3

* Calculated from displaced position of line.

Conclusions. Summing up, then, we find that eight of the twelve patterns given in Fig. 1 as characteristic for the first two lines of the P and Q branches have been resolved. The corresponding R lines were too faint for observation. The unresolved patterns of the higher lines of all three branches in the various polarizations behave in the definite and characteristic way predicted by theory. The results definitely confirm the classification of the Angstrom CO bands as $^1S \rightarrow {}^1P$ with $\sigma' = 0$, $\sigma'' = 1$[6].

The intensity relations among the components of the resolved patterns have in the main supported the summation rule predictions, at least as far as correct order of intensities is concerned (visual estimates.)[33] Departures from the theoretical intensity relations are of three sorts, of which the first two, occurring on one plate only, are doubtful, while the last, being found in the case of about fifteen lines in four different bands is definitely established. The doubtful conflicts with theory are: the somewhat greater intensity of $\sigma - \pi - P(1)_{-1}$ as compared with $\sigma - \pi - P(1)_{+1}$ (i.e. the greater intensity of the high-frequency component); and the occurrence in the case of the $R(2)$ pattern (on the same plate) of a slight but distinct lightness in the center (see Fig. 1). The definite and well-supported departure from theory is the occurrence of distinctly greater intensity in the low frequency than in the high-frequency members of Q doublets as observed in parallel polarization, the dissymmetry gradually decreasing for higher M values ceasing to be observable beyond $M = 6$. Since in the case of the $Q(1)$ pattern with

[32] This is the *only* plate on which $R(2)$ shows distinctly enough for observation.

[33] Dr. O. Sandvik of the Eastman Kodak Research Laboratories has kindly made microphotometric curves of some of our better plates. The results which it is hoped to give in another paper are in accord with the above, particularly as to the predicted fact that $\pi - \sigma - Q(1)_0$ should be slightly less intense than $\pi - \sigma - Q(1)_{+1}$ or $\pi - \sigma - Q(1)_{-1}$.

both polarizations superposed this dissymmetry has disappeared, it must follow that the reverse order of intensity must hold for the outer components in the perpendicular polarization alone.[34]

The magnitudes of the patterns are directly proportional to the field strengths. The widths of the $P(1)$ and $Q(1)$ patterns average 95 percent of $\Delta\nu_n$ and thus fall midway between the 88.9 and 100 percent of $\Delta\nu_n$ predicted respectively by Eqs. (6) and (7) for $M=1$. The patterns of the other lines are of the expected magnitude, the Q doublets in particular falling regularly (as anticipated for reasons already given) somewhat below the theoretical curves for maximum pattern widths.

Since, according to theory, the nature of the Zeeman effect varies with the type of electronic transitions involved, it should give valuable information as to what sort of transitions give rise to a given set of bands, the characteristic behavior of the various branches further enabling the quantum analysis of a given band to be carried through more readily than otherwise.

We are under great obligation to the Milton Fund of Harvard University for a generous grant which made our experimental work possible.

JEFFERSON PHYSICAL LABORATORY,
HARVARD UNIVERSITY,
July, 1927.

[34] This could not be determined directly from the plates thus far obtained.

ON THE ZEEMAN EFFECT IN THE CERIUM SPECTRUM BETWEEN 3000 and 5000A

By Henry Margenau

Abstract

Measurement and classification of the Zeeman effects of about 300 lines of the Ce spectrum between 3000 and 5000A.—The spectrum was photographed along the focal range of a Rowland concave grating, radius of curvature 21.5 ft., ruled surface 6 inches wide, 14,326 lines to the inch. A spark in air first served as a light source: later, to increase the sharpness of the lines, a vacuum arc was used. A qualitative interpretation of the patterns on the basis of the Landé-Sommerfeld theory is presented. A great number of lines having the appearance of sharp triplets in the field have been found. It is shown that the strongest combinations of regular terms in Ce would give such patterns. (Each component consists of a number of lines having separations of the order of 1/40 normal, which, at present, cannot be resolved.) Most of the *s* components which are noticeably broadened display one of two characteristic intensity distributions. To explain these types it is necessary to use (1) displaced (anomalous) terms, (2) in some cases, displaced terms and cross-system combinations ($^3G - \overline{G}^5$, etc.). Higher azimuthal quantum numbers (3, 4, 5, $\cdots$) are to be associated throughout with the energy levels concerned in the stronger lines of the Ce spectrum. Several of them have separations which might be interpreted as belonging to combinations of the ^3H term. This is in favor of F. Hund's prediction that the fundamental term of Ce is a ^3H term. A number of lines which probably belong to the ionized atom are tabulated.

1. Experimental Procedure

THE spectral photographs of cerium were taken at various times during the year 1925 in the Brace Laboratory of Physics, at the suggestion of the late Professor B. E. Moore. With the spark discharge in air at atmospheric pressure, the first method described below, the lines yielded some interesting and varied patterns, but the resolution was incomplete, and the publication of the results has been deferred until the Zeeman effects of at least the stronger lines had been obtained with more adequate experimental means. To this end, the light source was placed in a vacuum. The result was distinctly better resolution, but the details of the patterns did not appear. Many lines were remeasured, and errors in the measurement of some of the *p*-components were corrected. The subsequent considerations make it seem probable that a great number of cerium lines have Zeeman effects of such narrow separations that most of them could not be expected to be resolved.

In the first arrangement the light source was a condensed spark between carbon electrodes. The direction of the discharge was along the lines of magnetic force. The carbons were impregnated, and their surface coated, with cerium salt. A potential of 6600 volts, obtained from a 3 kilowatt transformer, produced the spark. For the purpose of reducing the intensity of the air lines and improving the steadiness and brilliancy of the discharge

a coil of large self-inductance was placed in series with the spark gap. This system was shunted by a capacity of about 3 microfarads. During the exposure the electrodes were slowly fed into the gap.

The Brace electromagnet[1] served to produce the magnetic field. The gap between the cone-shaped pole-terminals, in which the electrodes and an insulating quartz slab were inserted, was 5 mm wide. With an exciting current of 6.5 amperes this arrangement was capable of giving constant fields of about 30,000 gauss.

The light was focussed on the slit by a quartz lens. A calcite rhomb was interposed between light source and lens. Its rotation about a vertical axis caused the ordinary or the extraordinary beam to fall upon the slit, thus allowing a convenient adjustment for obtaining the parallel and the perpendicular components.

The light passing through the slit was resolved by a concave Rowland grating. Its radius of curvature is 21.5 feet, the ruled space on its surface is 6 in. wide, and it has 14,326 lines per inch. An iron plate holder is rigidly mounted along its focal range. It is constructed to receive 18 feet of film, and permits of taking photographs in the first, second, and third order. The most favorable conditions for obtaining satisfactory spectrograms prevail in the second order (greatest intensity, optimum relative resolution). Although the actual resolving power as calculated from the observed resolution of the lines did not even approach the theoretical resolving power of the grating, it was as high as could be expected considering the lack of homogeneity of the light source. The resolution in the second order was sufficiently great to measure separations of about 1/5 normal magnitude with fair accuracy in the region around 4000A.

Shutters on the plate holder were so arranged as to permit the exposure of the upper or the lower half of the films. Thus it was found convenient to photograph the unseparated lines and one type of the Zeeman components on the same film.

Of the numerous spectrograms obtained,—all of which were inspected and compared—five, two with parallel and three with perpendicular components, were selected for measuring separations. A Gaertner micro-comparator served for this purpose.

The vacuum arc arrangement, used afterwards to replace the spark, was constructed in a manner similar to the one outlined by Back.[2] The cylinder was inserted between the pole pieces of the magnet already described. The electrode holder carrying the cerium preparation was carefully insulated from the outer parts of the cylinder and mounted in a glass tube in such fashion that it could be moved in toward the pole gap by turning the tube about a greased glass joint. The other electrode was a brass rod with a tungsten tip, capable of vibrating about a transverse axis. Extending through a rubber stopper in the upper orifice of the cylinder it was held in position and its tip was free to oscillate between the pole pieces. A small iron plate, soldered to

[1] For its detailed description see D. B. Brace, Phil. Mag., Series 5, **44**, 342 (1896).

[2] Back und Lande, Zeemaneffekt und Multiplettstruktur, p. 123.

the outer end of the rod, formed the armature of two solenoids, the cores of which were facing each other. A timing device permitting easy regulation closed alternately the circuits of the solenoids and caused the rod to vibrate with the proper amplitude. The distance between the solenoids could be adjusted so that the tungsten tip would touch the other electrode and then recede until it hit the insulation of the opposite pole face. Care had to be taken to remove the solenoids sufficiently far from the magnet to avoid all interference with the homogeneity of the field.

An alloy of aluminium and cerium was first chosen for the electrode material. On account of the warping of the metal as it became hot, and of unsatisfactory intensity, various other possibilities were tried. After some experimenting the following method of preparing the electrode was found most advantageous with regard to intensity and ease of manipulation. Carbons of rectangular cross-section were placed in an electric furnace for several hours and heated until the surface was burned away and their structure became thoroughly porous. Afterwards they were allowed to soak for a few days in a solution of cerium salt, and then put in the holder. Such carbons may be used from 15 to 30 minutes with currents of about 5 amperes. They frequently outlast the tungsten tips.

The insulation of the pole terminals caused considerable difficulty. The scheme finally adopted was to place circular quartz plates of thickness 3/4 mm and large enough to cover twice the area of the pole face into copper clamps surrounding the pole terminals. These clamps were fastened to copper strips sealed on to the rim of the back window. By taking off the window and breaking the sealing wax the clamps could be removed and the insulation replaced.

Exposures were taken at pressures varying from a fraction of a mm to 4 cm. The vibrator made and broke the current 8 times per second. The other parts of the arrangement were left unchanged. The pictures thus obtained were distinctly sharper than the previous ones, except for the complex Zeeman patterns.

The Ca-lines (λ3968.5 and λ3933.7A), whose presence was due to impurities in the electrodes, were used as standards for field-strength determinations. On the two best spark spectrograms (second and third order) the field-strength was computed to be $(1.322 \pm .001)$ times normal, corresponding to 28130 gauss. On the vacuum arc films the field was about 3 percent weaker on account of the greater width of the pole gap.

2. Results

In discussing the results it is appropriate to call attention at once to the peculiar fact that in no case could more than two perpendicular components be measured. Although many of the components show clearly a complex appearance, they are not sufficiently resolved to reveal their detailed constitution. It is not difficult to account for the frequent occurrence of such types in the cerium spectrum, but it is somewhat disappointing to find that none of them is resolved. Variation in the time of exposure did not bring out the desired detailed features of the complex types.

The multi-component *s*-patterns of the described character, though not resolved, show two characteristic intensity distributions. For simplicity we shall refer to them as intensity types *A* and *B*. Their appearance is

Fig. 1. Typical intensity distributions in the multi-component *s* patterns.

indicated in Fig. 1. Type *A* suggests the presence of weaker inner components, while evidently several strong components form the intensity maximum in type *B*.

The lines are arranged in tables according to the general appearance of the Zeeman patterns. $\Delta\nu$ represents in all cases the fraction or multiple of normal separation and is equivalent to $(\Delta\lambda/\lambda^2)(H_n/H)$. Most of the tabulated separations represent averages of observations in the second and third order. The weaker lines have not been remeasured on the vacuum arc films.

Lines whose appearance was simple and whose *s*-separation did not differ from 1 (normal) by more than 1 percent have been tabulated in Table I. In Table II are found lines which have precisely the same general character as those in the first but have *s*-separations greater or smaller than normal.

TABLE I

Triplets with nearly normal separation.

λ	$\Delta\nu$	λ	$\Delta\nu$	λ	$\Delta\nu$
3539.07	0.994	4003.77	0.997	4300.33	1.002
3555.00	1.000	4120.84	1.011	4403.30	0.997
3895.12	1.010	4150.91	0.995	4427.92	0.998
3980.89	1.000	4234.21	0.99	4509.18	1.02
3993.82	1.017	4270.19	0.992	4899.88	1.00

No significance is attached to this classification, the distinction has merely been made for statistical reasons. The presence of a large number of symmetrical "triplets" is exactly what might have been expected. From the position of cerium in the periodic table, from analogy with similar elements, and from the evident lack of simple relations in its spectrum it may be concluded that terms of high azimuthal quantum number are involved in the generation of the cerium lines. Combinations of the type $^3G_5\ ^3H_6$, $^3H_6\ ^3I_7$ etc., which would be strong lines, give a separation pattern having the appearance of an approximately normal triplet, the strongest components of both the *s* and the *p*-separation on each side lying so close together that their resolution is impossible. It would require a resolving power of almost one million (and a perfectly homogeneous light source).[3]

The patterns compiled in Table III have as their common peculiarity intensity distribution *A*. Probably all of them contain inner components.

[3] If the number of lines having a certain *s*-separation is plotted against the numerical amount of this separation one obtains a distribution curve whose center of gravity lies somewhat above one. This is consistent with the explanation given, for the presence of weaker external components would probably cause an apparent outward displacement of the two measured lines.

TABLE II

Lines whose s-separation shows two distinct components. The *p*-component appears in all cases unseparated and at the zero position.

λ	Δν	λ	Δν	λ	Δν	λ	Δν	λ	Δν
3201.71	1.26	3769.05	1.14	4075.71	1.18	4245.88	1.45	4460.21	0.720
3272.25	0.85	3782.52	0.960	4078.33	1.27	4246.72	0.590	4464.70	0.919
3274.86	1.17	3792.33	1.181	4085.25	1.208	4248.67	1.178	4467.54	1.133
3377.13	1.035	3808.12	1.14	4092.72	1.21	4253.37	0.94	4471.24	0.929
3385.06	1.62	3838.54	0.862	4093.96	1.16	4264.37	0.913	4472.72	1.078
3417.45	1.22	3889.99	1.177	4105.00	1.36	4270.72	1.06	4474.70	1.09
3422.71	0.865	3907.29	1.095	4107.43	0.94	4273.45	1.17	4479.36	0.963
3426.21	0.783	3908.42	1.17	4111.40	1.063	4278.87	1.14	4485.52	1.07
3441.21	1.064	3918.28	0.840	4113.73	0.845	4280.14	0.855	4494.23	0.908
3458.87	1.36	3923.11	0.745	4117.01	1.062	4285.37	1.079	4500.34	1.19
3459.83	1.34	3924.65	0.67	4118.15	0.93	4288.67	0.909	4508.08	0.990
3476.84	1.20	3940.34	0.94	4123.88	1.24	4296.68	0.941	4511.7	1.15
3485.06	0.766	3942.16	0.84	4127.37	1.185	4306.73	1.150	4515.86	0.715
3517.38	1.052	3942.75	1.145	4130.71	0.98	4311.59	1.235	4519.60	1.435
3521.88	0.89	3943.89	1.138	4131.10	1.04	4324.79	0.787	4532.49	0.922
3534.04	1.060	3952.57	1.206	4132.32	1.235	4331.76	0.645	4536.89	1.10
3560.80	1.080	3956.28	1.160	4133.80	1.164	4332.71	0.67	4537.88	1.24
3577.45	1.064	3975.07	0.859	4135.43	0.77	4342.48	1.18	4551.31	0.922
3607.63	0.831	3978.65	0.788	4137.64	1.35	4345.96	0.965	4555.42	0.94
3609.69	1.22	3984.68	0.93	4142.39	1.27	4349.79	1.047	4560.28	1.117
3623.84	1.06	3989.44	1.16	4149.94	1.11	4352.70	0.874	4569.72	0.834
3631.19	1.13	3992.39	1.34	4151.98	1.325	4357.91	0.675	4576.47	0.77
3646.96	0.990	3999.23	1.102	4159.04	0.923	4359.07	1.19	4582.51	0.936
3653.67	1.19	4012.38	1.175	4166.88	1.07	4364.66	0.860	4597.19	1.16
3655.85	0.662	4019.05	1.27	4167.81	1.25	4373.82	1.252	4606.38	1.26
3660.64	1.06	4019.89	1.27	4176.71	1.11	4375.93	1.098	4624.88	1.264
3667.98	1.119	4022.27	1.30	4181.08	1.27	4380.06	1.24	4644.19	0.84
3694.91	1.02	4024.49	1.30	4185.33	1.05	4390.28	1.091	4663.23	1.122
3709.29	1.190	4030.16	0.933	4186.60	1.099	4393.19	0.835	4684.60	1.155
3709.93	0.940	4031.34	1.161	4194.91	0.92	4394.78	1.087	4686.75	1.15
3716.37	0.811	4042.58	1.010	4196.34	1.074	4410.64	1.342	4712.02	1.15
3718.38	1.09	4045.23	1.28	4202.95	0.703	4427.08	0.867	4737.24	0.991
3725.67	0.916	4046.34	1.12	4209.41	1.132	4428.44	0.980	4744.92	0.95
3728.02	1.125	4053.51	1.225	4214.04	1.16	4429.27	1.35	4757.84	0.97
3728.42	1.148	4056.90	1.49	4222.60	0.925	4437.61	1.115	4773.94	0.750
3730.34	1.169	4060.47	1.135	4223.88	0.985	4439.25	1.04	4783.95	1.26
3733.53	0.868	4062.95	1.063	4231.75	1.263	4440.89	0.959	4873.96	1.04
3762.98	1.04	4068.84	1.227	4236.02	0.965	4443.75	0.948	4882.45	0.903
3764.12	1.110	4073.49	0.809	4242.73	1.263	4444.70	1.29	4943.43	0.77
								4971.46	0.992

TABLE III

Complex types with inner components. (Intensity distribution *A*). The *p*-components of lines marked with an asterisk appear broadened, those with a double asterisk, very broad. Otherwise the *p*-component is unseparated and at the center. Lines for which no separation is given were recognized as belonging to this type, but not measurable because of overlapping or insufficient intensities.

λ	Δν	λ	Δν	λ	Δν	λ	Δν
3590.60	1.01	**4098.99		4263.43	1.50	**4450.74	1.80
3801.43	1.09	4110.38	1.37	4278.25		*4463.41	1.33
*3896.81	1.74	4146.23	1.36	4302.66	1.575	**4483.90	1.70
3898.28	1.42	*4163.53	1.462	4305.14	1.48	4484.82	1.52
*3919.81	1.57	**4227.75	1.72	4315.41		4496.24	1.94
*3983.28	1.60	**4239.91	1.75	*4336.25	1.47	**4523.08	1.60
*4014.89	1.50	4259.75		*4337.78	1.25	**4560.98	
4077.48	1.57	4261.17		**4388.01	2.25	**4562.35	1.09
				4407.28	1.79	*4593.94	1.22

The figures under $\Delta\nu$ refer to the distance between points of deepest blackening of the *s*-pattern. Another interesting common feature of these lines is their wide separation. To account for them it seems necessary to give attention to anomalous terms. Combination of two "adjacent" ^3G, or ^3H-terms, loosely speaking, gives components of the desired type, as may be shown by computing according to Landé's scheme the patterns $^3G_3\ ^3\overline{G}_4$, $^3G_4\ ^3\overline{G}_5$, $^3H_4\ ^3\overline{H}_5$, and others. The same is true for quintet "displaced" terms ($^5H_3\ ^5\overline{H}_4$, $^5H_5\ ^5\overline{H}_6$ etc.), and for combinations of the character $^5F_5\ ^5\overline{G}_4$ with the *L*-value of $^5\overline{G}_4$ equal to 5/2 (instead of $K=9/2$). From the knowledge of term relations in Ca, Ba, Sr[4] such assumptions seem to lie within reason.

It may be observed that many of the lines in Table III have a broad *O*-line as *p*-component, which is in no case measurably separated or of a double appearance. All of the hypothetical combinations referred to above have the maximum intensity of the *p*-pattern at the center, so that with complete resolution this would be occupied by a broadened line. That not all the *p*-types in question appear broadened may be due to small intensity of the outside components, or to unusual narrowness of the separations.

It appears more difficult to produce the moderate separations ranging from 1 to 1.5, with the characteristic intensity distribution mentioned above (strongest components outside), if the *g*-values are computed in the ordinary manner by Landé's formula. But by forming cross-system combinations between triplets and quintets, i.e., by permitting transitions between these two systems, separations are found which are in qualitative and rough quantitative agreement with the types under consideration. Here again it is necessary to assume anomalous "displaced" terms, e.g., $^5F_2\ ^3\overline{F}_3$, $^5G_4\ ^3\overline{G}_5$, $^5H_5\ ^3\overline{H}_6$.

TABLE IV

Complex types. (Intensity distribution *B*). Lines for which no separation is given were recognized as belonging to this type, but not measurable because of overlapping or insufficient intensities. The *p* component is double in all cases.

λ	Δν s	Δν p	λ	Δν s	Δν p	λ	Δν s	Δν p
3344.76	0.98	0.59	4124.80	1.112	0.443	4399.21	0.80	0.419
3622.15	1.04	0.64	4144.99	1.06	0.617	4416.91	0.888	
3912.43	0.988		4148.90	1.02	0.462	4418.78	1.23	0.325
3921.74	1.05		4198.72	1.23	0.490	4423.68	1.08	0.734
3931.09	0.87	0.39	4217.59	1.165		4449.34	1.102	0.178
3938.09	1.053		4255.79	1.320	0.43	4461.14	1.083	0.304
3960.91	0.72	0.452	4289.93	0.878	0.320	4486.91	0.99	0.42
4028.41	1.021	0.392	4299.36	0.908		4497.85		1.04
4040.76	0.95	0.347	4309.74	0.99	0.76	4527.35	1.010	0.339
4062.23	1.084		4310.70			4528.48	1.18	0.508
4067.29	1.085	0.414	4317.33	1.35		4544.96	0.875	
4081.22		0.704	4367.00	1.240		4565.84	1.18	0.59
4101.78	1.19	0.648	4382.17	1.101	0.400	4572.28	1.07	0.597
						4628.14	0.92	0.587

Table IV contains lines which display a Zeeman pattern described as intensity distribution *B*. Each of the two *s*-components is doubtless com-

[4] Russel and Saunders, Astrophys. J. **61**, 38 (1925).

plex, for its width considerably exceeds that of the line in zero field. It appears probable that the broadness is due to the presence of several strong components with weaker companions whose intensity decreases on both sides. Almost all the lines in this table have measurable p-separations, a somewhat interesting fact since this feature was not considered as a criterion of classification. Comparison with Exner and Haschek's intensity data shows that many lines in this table are stronger in the spark than in the arc exposure. P-separations which are symmetrical about the unoccupied O-center usually indicate that the terms involved belong to the group of even multiplets, i.e., in cerium to the spark spectrum. If this is true the respective lines would be due to combinations of terms for which $j_x=j_y$ and $k_x=k_y-1$, for instance ${}^4G_6\ {}^4H_6$, or ${}^2G_5\ {}^2H_5$. If, on the other hand, they were lines of the neutral atom, they would also be caused by transitions characterized by $j_x=j_y$ and $k_x=k_y-1$. (Back's Grundtypus 3, e.g., ${}^5F_4\ {}^5G_4$, or ${}^3G_5\ {}^3H_5$.) However the latter combinations would violate Burger and Dorgelo's intensity rule, since Table IV contains some of the strongest lines of the cerium spectrum. Hence it is fairly safe to assign the lines in this table to the ionized spectrum.

In a paper on the neutral and ionized spectra of cerium presented by King at the recent meeting (June 23) of the American Physical Society there is evidence that the major part of the conspicuous lines of the arc

TABLE V

Complex types. The *s* pattern is double and shades off distinctly toward the outside.

λ	Δν
4201.24	0.703
4320.73	0.672
4330.45	0.585

TABLE VI

Miscellaneous patterns.

λ	Δν *s*	Δν *p*
3878.37	0.40 components broad	0
3882.45	0.547	0 broad and diffuse without field sharp field components
3967.05	0 1.100	0
4054.99	1.60 components broad	0 broad and foggy
4083.24	1.10	0.208
4115.38	unresolved broad band of width about 0.4 A	0.621
4187.32	0 broad and foggy	0 broad and foggy
4339.32	1.173	0 slightly broadened
4386.70	1.23	0 broad
4391.67	1.075	0 very broad
4412.02	0	0
4413.81	0.924 stronger with field	0
4444.40	0.860 character not recognized because of overlapping	0 broadened
4654.28	0.571	0 diffuse

forms the singly ionized spectrum, and that the neutral spectrum has been to a large extent unrecognized in the photographic region. It would be interesting to know if, according to King's observations, the lines in Tables I, II, III, are recognized as belonging to the spark spectrum. If their Zeeman effects are interpretable on the basis of the displacement law they should be lines of the neutral or perhaps doubly ionized atom.

In Table V are found three lines with the following characteristics: The *s*-separation is unusually narrow, and the intensity of the pattern decreases outward. The innermost *s*-components of the completely resolved picture would be strongest. On the *p*-film there appears only one line at the *o*-position, which is possibly slightly broadened.

Table VI contains lines whose irregular features—irregular only in so far as they differ from the ones commonly observed and already described—required separate classification.

It is a pleasure for the writer to express his appreciation of the interest which the department maintained in his work, and his sincere gratitude to Professor J. E. Almy and Mr. M. J. Brevoort for their assistance in connection with the construction and adjustment of the vacuum arc.

BRACE LABORATORY OF PHYSICS,
UNIVERSITY OF NEBRASKA,
June 24, 1927.

ABSORPTION OF RESONANCE RADIATION IN MERCURY VAPOR

A. Ll. Hughes and A. R. Thomas

Abstract

The absorption of the resonance radiation (2536A) of mercury was studied by dividing the radiation from a resonance lamp into two parts, each part going into a separate photo-electric cell. An absorption cell containing mercury vapor whose pressure could be controlled by cooling a side tube was placed in the path of one beam. The ratio of the amount of light passing into each beam could be varied by a mechanical device. From the setting of the mechanical device, giving a balance between the two photo-electric currents, the absorption of the mercury vapor could be inferred. The absorption per atom was calculated and found to decrease rapidly as the total amount of absorbing vapor was increased, thus showing that the resonance radiation is not homogeneous. The maximum atomic absorption coefficient was 11×10^{-14}, which indicates that an atom can stop the radiation which falls upon an area one hundred times larger than its cross sectional area.

THE first attempt to determine the magnitude of the absorbing power of mercury vapor for its own resonance radiation (2536A) was made by R. W. Wood,[1] who found that its intensity diminished to half-value on passing through 5 mm of mercury vapor at a temperature of 22°C. Quite recently Goos and Meyer[2] investigated the absorption quantitatively. They passed the radiation from a water cooled mercury arc through a monochromatic illuminator to isolate a beam of wave-length 2536A, which then passed into a quartz tube containing mercury vapor. The resonance radiation emitted at right angles to the main beam was photographed and from the diminution in its intensity in the direction of the primary beam, the absorption coefficient was calculated. The absorption coefficient became less and less, the further the primary beam penetrated, indicating a strong filtering effect, whereby the more easily absorbed parts of the beam are taken out first.

The present investigation, which was begun before the work of Goos and Meyer appeared, is a study of the absorbability of mercury resonance radiation in mercury vapor, by an entirely different method. A knowledge of the nature and magnitude of the absorbability is important in any thorough discussion of the physics of resonance radiation. In the method to be described we divided the radiation from a resonance lamp into two parts, one part passing through the absorption cell containing mercury vapor to one photo-electric cell while the other part passed directly to a second cell. By a suitable balance method it was possible to determine the absorption coefficient of the resonance radiation with various amounts of mercury vapor in the cell.

[1] R. W. Wood, Phil. Mag. **23**, 696 (1912).
[2] F. Goos and H. Meyer, Zeits. f. Physik **35**, 803 (1926).

Apparatus and Method

The primary source of radiation was a water-cooled, magnetically deflected, mercury arc, *A*, (Fig. 1). By means of quartz lenses, radiation from this lamp was concentrated on a resonance lamp of special design, *R*. The

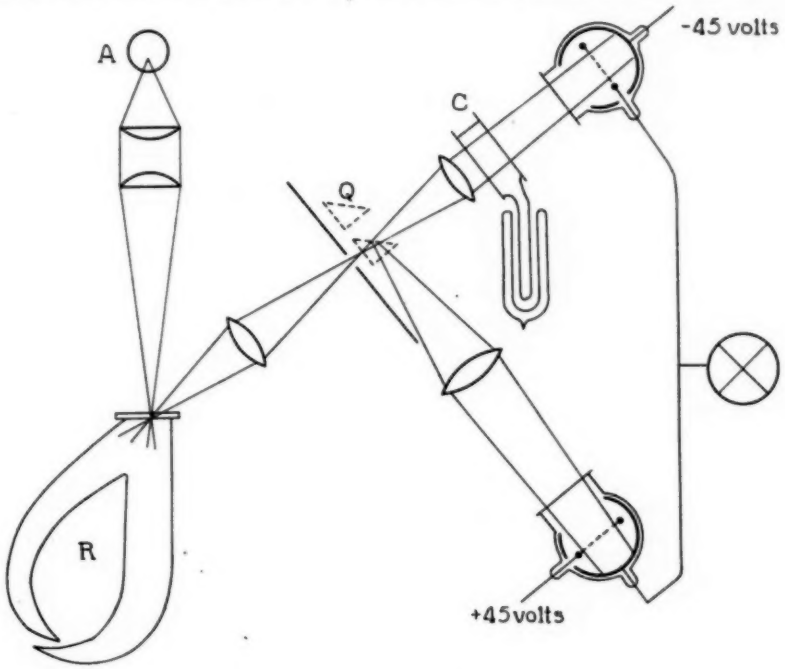

Fig. 1. Arrangement of apparatus.

curved and tapered horn-shaped glass tubes prevented any reflection of the radiation from the primary source into the direction selected for resonance radiation. When the side tube containing a drop of mercury was at room temperature, a photograph of the resonance line (2536A) could be obtained in 5 seconds, while an exposure of 320 seconds, hopelessly overexposing the resonance line, failed to show any other lines whatsoever. This type of mercury resonance lamp gave approximately fifteen times as much radiation as the more usual type in which primary radiation from the mercury arc is passed into the lamp through one window and resonance radiation is taken out at right angles through a side window. The resonance radiation was focussed on a small right angled prism of quartz *Q* which was rocked in and out of position (about once per second) by a mechanical device. This device could be set to alter precisely, the ratio of the time during which the light is reflected to one photo-electric cell to the time during which it is allowed to pass to the other photo-electric cell. The absorption cell, *C*, consists of a glass tube, 1.622 cm long to which quartz windows are cemented. A side tube contains a drop of mercury. The pressure was controlled by cooling the side tube to different temperatures. The active material in the photo-electric cell (high vacuum type) was zinc, which allowed us to work in day light. The

cells were both connected to the same Compton electrometer in such a way that the current from one opposed that from the other.

The experimental procedure was as follows. The side tube of the absorption cell was immersed in a Dewar flask containing gasoline cooled by liquid air. Its temperature was measured by a platinum resistance thermometer. The temperature was held constant for twenty or thirty minutes before making any observations, to insure that the equilibrium pressure had been established. Then the setting of the mechanical device for moving the quartz reflecting prism in and out of the beam was altered until the photo-electric current in the first cell balanced that in the second cell. (In actual practice, however, it was found speedier to measure the net photo-electric current for equally spaced settings of the mechanical device in the neighborhood of the balance point, and to infer its exact position from the intercept of the straight line obtained when one plotted the reciprocals of the photo-electric currents against the position of the settings.) A "zero" reading for the absorption cell was frequently checked by surrounding the side tube with liquid air. Calling the amount of resonance radiation passing through the cell under these conditions I_0, and the amount passing through at a temperature high enough to give measurable absorption, I, it is clear that we can compute I_0/I from the setting of the mechanical device which gives us a balance between the photo-electric cells.

Results

The experimental values for the radiation transmitted, viz. I/I_0 for different temperatures of the mercury on the side tube, are plotted in Fig. 2.

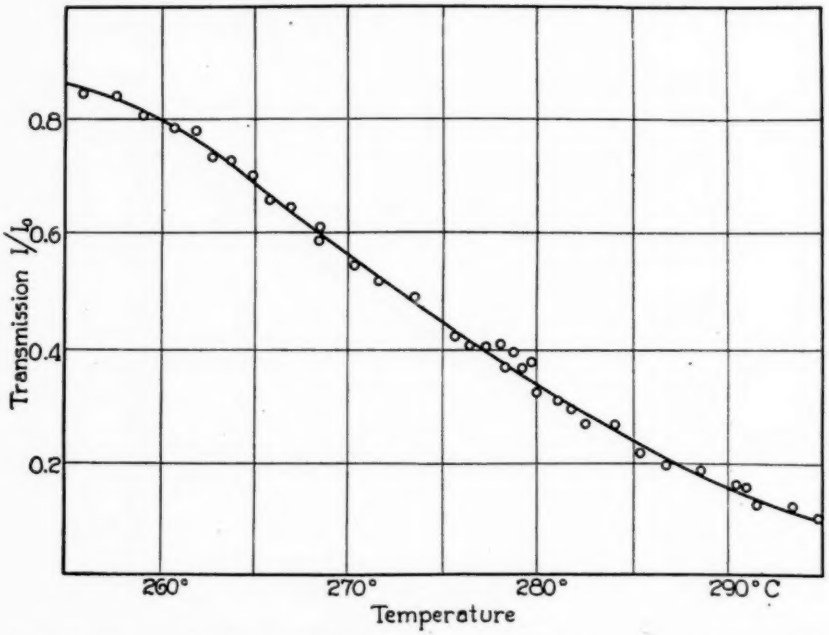

Fig. 2. Ratio of transmitted to incident radiation for various temperatures of mercury vapor.

To get the most likely value of the ratio I/I_0 at different temperatures, a smooth curve is drawn, as shown, through the somewhat irregularly distributed points. To determine the atomic absorption coefficient of the mercury vapor in the absorption chamber, we proceed to construct Table I, as follows. In the second column, we put the values of the ratio I/I_0 taken from the smooth curve of Fig. 2 for the temperature of the mercury in the side tube recorded in the first column. The next column gives the values of the natural logarithm of I_0/I. To determine the atomic absorption coefficient, we have to calculate the number of atoms involved in the absorption in each case. This has to be calculated from the pressure. The fourth column gives the pressures of the mercury vapor in the side tube for the corresponding temperatures recorded in the first column. Poindexter's determination[3] of the vapor pressure of mercury at different temperatures was used in this computation. However, the vapor pressure which is significant for the calculation of the absorption coefficient is that in the absorption cell and this is not identical with the pressure in the side tube when there is a difference of temperature. Let p and p_m be the pressures in the absorption cell, and in the side tube respectively, and T and T_m the corresponding temperatures These are connected according to the kinetic theory of gases at low pressures by the relation

$$p/p_m=(T/T_m)^{1/2}$$

We are now in a position to calculate the number, n_a, of the atoms in a column 1 sq. cm in area and 1.622 cm long (the length of the absorption cell). According to the kinetic theory of gases, we have

$$p'=nkT$$

where p' is the pressure (dynes/sq. cm.), n the number of molecules per cc, k the gas constant referred to a single molecule, and T the absolute temperature. Since the cell is 1.622 cm long, $n_a=1.622n$. It is usual to measure the pressure in mm and not in dynes/sq. cm. Let

$$p=\epsilon p'=\epsilon nkT$$

$$\therefore\ \epsilon=p/nkT$$

Since $n=2.705\times10^{19}$ molecules per cc at standard pressure and temperature, we have

$$\epsilon=\frac{760}{(2.705\times10^{19})(1.372\times10^{-16})273}=7.50\times10^{-4}$$

The number of atoms, n_a, in the absorption cell, per unit area of cross section, when the vapor is at room temperature ($T=293°$K) is given by

$$n_a=1.622n=1.622p/\epsilon kT$$

$$=(5.38\times10^{16})p$$

[3] F. E. Poindexter, Phys. Rev. **26**, 859 (1925).

The values of n_a calculated by the formula are given in the sixth column. The atomic absorption coefficient, γ is defined by the equivalent equations

$$I = I_0 e^{-\gamma n_a} \text{ or } \gamma = (1/n_a) \log (I_0/I)$$

TABLE I

Temperature (side tube)	$\frac{I}{I_0}$	$\log \frac{I_0}{I}$	Pressure side tube p_m (mm)	Pressure abs. cell p (mm)	No. of absorbing atoms n_a	γ
255°K	.859	.1518	2.35×10^{-5}	2.53×10^{-5}	1.35×10^{12}	11.2×10^{-14}
260	.798	.2255	4.29	4.57	2.44	9.22
265	.691	.3694	7.66	8.09	4.33	8.52
270	.560	.5799	13.4	14.0	7.49	7.73
275	.446	.8077	22.9	23.8	12.8	6.33
280	.340	1.079	38.4	39.4	21.1	5.10
285	.245	1.407	63.2	64.4	34.5	4.08
290	.166	1.796	102.6	103.5	55.5	3.23
295	.109	2.216	163.7	163.7	87.6	2.53

To get γ we proceed to divide the values in the third column by those in the sixth column and the results are tabulated in the seventh column. The results are shown graphically in Fig. 3. Now it is very evident that

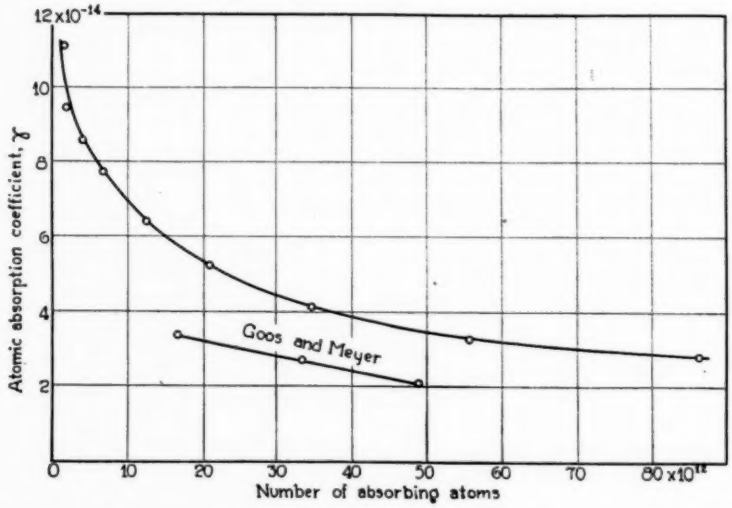

Fig. 3. Variation of the atomic absorption coefficient with the number of absorbing atoms.

γ is far from being constant as it would be if the radiation were homogeneous. Consequently the values of γ are to be regarded only as *average* values for the number of molecules involved. From the way in which γ decreases as the number of absorbing atoms is increased, it is clear that there is a strong filtering effect as a result of which the radiation becomes relatively more penetrating the greater the number of atoms which have taken part in the absorption.

It is interesting to compare our results with those of Goos and Meyer. According to these authors, the linear absorption coefficient (given by α in $I = I_0 e^{-\alpha x}$ where x is the distance traversed) takes the values 1.8, 1.5 and 1.2 cm^{-1} after the radiation has traversed 0.3, 0.6 and 0.9 cm respectively. These values are in satisfactory agreement with R. W. Wood's early results from which we may compute an absorption coefficient of 1.4 over a path 0.5 cm at 22°C. These results cannot be compared with ours until we have calculated the atomic absorption coefficient from the linear absorption coefficient. As these results were obtained with the cell at 20°C, the number of atoms per sq. cm for the various lengths mentioned are 16.2×10^{12}, 32.4×10^{12}, and 48.6×10^{12}.

The atomic absorption coefficient calculated from these values are respectively 3.34×10^{-14}, 2.78×10^{-14} and 2.13×10^{-14}. These results of Goos and Meyer are indicated in Fig. 3. It will be observed that they are well below our values, but, like ours, they show that the radiation is not homogeneous, but becomes more penetrating the more it is absorbed.

Discussion

In view of the success of treating radiation as a collection of negligibly small discrete quanta in certain fields of physics, it was thought worth while to estimate the order of magnitude of the atomic absorption coefficient, on the assumption that a mercury atom stops every quantum which hits it. The atomic absorption coefficient on this view would simply be the cross-sectional area of the atom. The radius of the mercury atom is about 1.8×10^{-8} cm (L. Loeb, Kinetic Theory of Gases, p. 527) which yields $\pi(1.8\times10^{-8})^2 = 9.6\times10^{-16}$ for the atomic absorption coefficient. This is approximately 110 times smaller than the largest experimental values given in Table I. In other words, the diameter of the effective stopping area of a mercury atom at least ten times greater than the actual diameter of the molecule.

A change in the effective absorption coefficient such as we have observed in the present investigation with the amount of absorbing matter, is to be interpreted as indicating non-homogeneity in the radiation, or a finite width to the resonance line. Narrow as this line is, the absorption coefficient for different parts of it changes from a maximum value for the very center to smaller and smaller values as we consider parts further and further away from the center. The value of the absorption coefficient which should have the most useful theoretical significance is that for the center of the line. As this must have a finite (though possibly very high) value, the obvious way of approximating to it from experiment would be to extrapolate the curve for absorption coefficients (Fig. 3) to zero absorbing material. Unfortunately, owing to the increasing concave upward character of the curve for the smallest amounts of absorbing material used, this cannot be done with any hope of obtaining a reliable value. It is to be anticipated that, if the experiment could be carried out with smaller and smaller amounts of absorbing material, then ultimately the curve for the absorption coefficients would flatten out and cut the vertical axis through the origin with little or no inclination.

At present we can say that the atomic absorption coefficient for the resonance line of mercury vapor in mercury is greater than 11×10^{-14} possibly considerably greater.

A possible way of looking at the absorption of mercury resonance radiation by mercury vapor is suggested by the corpuscular theory of light. One might suppose that a quantum of radiation of wave-length λ_0 (the center of 2536A) is absorbed only by those atoms, which at the instant of impact have practically no component velocity in the line of motion of the corpuscle, and that a quantum or radiation $\lambda=\lambda_0(1\pm\Delta\lambda)$ is absorbed only by atoms with component velocities close to $\pm u$, where u is related to λ by the Doppler Effect. This viewpoint offers a natural explanation for the filtering out process, for the number of atoms having component velocities between u and $u+du$ is a rapidly diminishing function of u, and the parts of the line furthest out from the center experience the least absorption. It will be noticed that in the statement of the proposed viewpoint, we have avoided saying that there must be an exact correspondence between the wave length of the corpuscle and the component velocity of the atom absorbing it. This is because if we suppose that only those atoms with velocities between u and $u+du$ can absorb corpuscles of corresponding wave-length λ, then the number of atoms capable of absorbing λ becomes zero as we make du infinitely small.

WASHINGTON UNIVERSITY,
ST. LOUIS, MISSOURI,
July 28, 1927.

SECONDARY EMISSION FROM Mo DUE TO BOMBARDMENT BY HIGH SPEED POSITIVE IONS OF THE ALKALI METALS

By W. J. Jackson

Abstract

Work has been extended to measurements on secondary emission from Mo due to the bombardment of positive ions of Na^+, Rb^+ and Cs^+ following the method used for K^+ and described in detail in a previous paper. Confirmatory evidence is obtained that heat treatment in general reduced the secondary emission. With degassed targets the following results were obtained: Na^+ ions showed a positive ion reflection of 3 percent or 4 percent independent of the speed of the impacting ion and electron emission of about 2 percent at 1000 volts. Experiments with Rb^+ indicated a reflection of positive ions of less than 2 percent and no electron emission within the experimental error. Cs^+ gave a secondary emission of about 9 percent at 1000 volts. It is suggested that the relatively large secondary emission from an untreated target as compared with a well degassed metal is possibly due to the minimum distance of the electron from the metal surface being greater in the former than in the latter case; also if secondary emission is due to local high temperatures arising from positive ion bombardment there would be more rapid dissipation of energy by the target surface than by the gas molecules.

Introduction

In a previous paper[1] the writer described a method for measuring secondary emission from metals due to the bombardment of K^+ ions. The method was designed to separate the phenomenon of positive ion reflection from electron emission. A special feature of the apparatus was the arrangement whereby the target could be drawn back in the tube and heated by induced currents from a high frequency a.c. coil wound around the tube. The results of the above mentioned work showed that the secondary emission depended upon the metal used as a target and also very considerably on the condition of its surface. Since steady sources[2] of positive ions of different kinds were available it was decided to extend this work to the ions of the other alkali earth metals, Na^+, Rb^+ and Cs^+ ions, in an endeavor to find how the emission depends on the nature of the ions used.

Work by Cheney[3] showed that the electron emission from a metallic surface was a function of the bombarding ion. In the case of aluminum and platinum targets the emission due to potassium ions of a given energy lay between that due to rubidium and lithium ions of the same energy, the latter giving the greatest emission of the three kinds of ions used. The writer obtained smaller values for emission from aluminum using potassium ions and a degassed target than were found by the above investigator.

It was pointed out in the previous paper that in order to decide between present theories of sparking potential of a gas and also to construct theories

[1] Jackson, Phys. Rev. **28**, 524 (1926).
[2] Kunsman, J. of Phys. Chem. **30**, 525–534 (April, 1926).
[3] Cheney, Phys. Rev. **10**, 335 (1917).

of other phenomena of discharge in gases, such as normal cathode fall of potential and abnormal fall of potential, reliable data along the line of the present work should be obtained. The theory of sparking potential of a gas by Holst and Osterhuis[4] requires the sparking potential to depend not only on the cathode material but also on the nature of the positive ions striking the cathode. If this theory be correct, one might expect to find a secondary emission from a given metallic surface characteristic of the bombarding ion.

Apparatus and Method

The apparatus, Fig. 1, and the experimental procedure in the work of this paper were exactly similar to those described in the original paper.

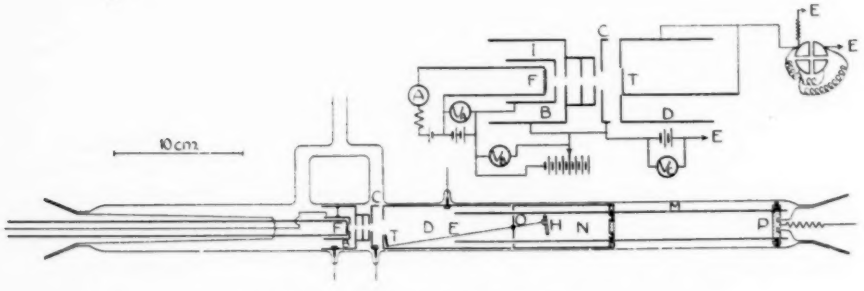

Fig. 1. Diagram of apparatus.

One thing should be mentioned which was not previously noted. It was necessary to carry out experiments on secondary emission and positive ion reflection separately owing to the fact that observations of secondary emission differed according to whether the magnet used for bending the emitted electrons was placed on or was removed from the experimental apparatus. The secondary emission was less in the former case.

Apparently there was sufficient residual magnetism in the pole pieces of the magnet appreciably to bend the paths of the lowest speed electrons. To eliminate all magnetic effects an iron shield was placed around the tube when experiments on secondary emission were made and removed when the magnet was set up for experiments on positive ion reflection.

The positive ions used in the experiments were obtained from the iron catalyst source discovered by Kunsman.[2] The ions emitted from the separate catalysts containing respectively Na, K, Rb and Cs were shown by Barton, Harnwell and Kunsman[5] to be only the corresponding singly charged positive ions, except for a trace of K as an impurity in relatively small amount. A Mo target was used throughout the experiments.

Sodium. The result of the original experiments, namely, that the emission was greatly reduced by baking the target in the experimental tube was confirmed by the experiments using Na^+ ions and also Rb^+ and Cs^+ ions. It should be noted in the case of a Mo target bombarded by K^+ ions that there

[4] Holst and Osterhuis, Comptes Rendus **175**, 577 (1922); Phil. Mag. **46**, 1117 (1923).
[5] Barton, Harnwell and Kunsman, Phys. Rev. **27**, 739 (1926).

was a secondary emission of about 3.8% due to 1000 volt ions and a reflection of positive ions of less than 2%. This would make the electron emission less than 5.8% at 1000 volts. Using Na^+ ions and a well degassed target values for positive ion reflection were obtained which amounted to about 3% or 4% and did not depend on the velocity of the impacting ion. The experiments with these (Na^+) positive ions were repeated twice at intervals of a month and the results checked well within the experimental error. The experiments on secondary emission indicated small values of electron emission, nothing appreciable below 600 volts, and even up to 1000 volts the electron emission amounted in some cases to less than 2% and the greatest value obtained in this region was about 2.7%. The experimental error is great in the case of the measurements taken where the emission is small for the results come from the difference of two experimental readings. It should also be noted that when observations on positive ion reflection were taken with an unbaked target a reflection of less than 2% was obtained.

Rubidium. Table I shows a typical set of data for secondary emission from an unbaked Mo target due to Rb^+ ion bombardment. V is the energy in volts of the positive ions.

TABLE I

Secondary emission from an unbaked Mo target due to Rb^+ ion bombardment.

V	Percentage Secondary Emission	V	Percentage Secondary Emission
137	0.0	692	3.9
342	0.4	792	7.8
492	1.5	892	7.8
592	2.5	1072	13.1

On baking the target the emission dropped to an unmeasurably small value and there was less than 2% positive ion reflection, or possibly no reflection, for the experimental error was such that the measurements cannot be relied upon for these small percentage differences.

It is important in measurements on secondary emission not to have large fields near the target which may distort the primary beam giving effects which may wrongly be interpreted as positive ion reflection or electron emission. A case of this kind was cited in the first paper.[6] Curve II of Fig. 2 below shows a typical curve for emission due to Rb^+ ions and an unbaked Mo target using the usual electrical connection as shown in Fig. 1. Curve I shows the measurements of secondary emission when the iron cylinder and B were kept at the same potential and the accelerating field for positive ions was applied between B and C; as before C was kept 2 volts positive with respect to earth.

As a possible explanation of this phenomenon it is suggested that this increased secondary emission may be due to the effect of the irregular field on the positive ions causing them to hit the target at angles other than perpendicular incidence. In the experimental arrangement used throughout

[6] Jackson, Phys. Rev. **28**, 529 (1926).

the work as shown in Fig. 1, it is more probable that the positive ion beam hits the target at right angles to the surface than in the latter arrangement. Preliminary experiments indicate that emission depends on the orientation of the target with respect to the primary beam, but the results are not definite enough to give decided support to the above suggestion.

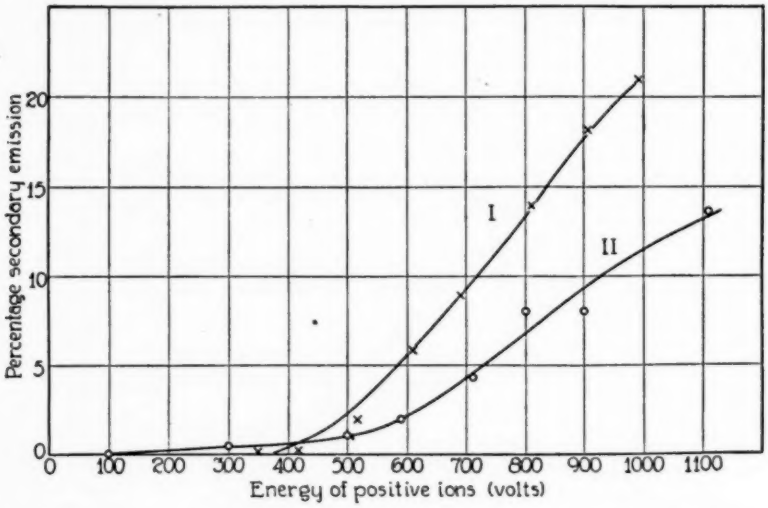

Fig. 2. Percentage of secondary emission as a function of velocity of positive ions.

It was found that the electrons emitted are of low speed.[7] Table II shows the velocity distribution among the secondary electrons for the case of Rb^+ ions bombarding a Mo target.

TABLE II

V	(f) 0.1 v	(f) 0.2 v	(f) 0.3 v	(f) 0.5 v	(f) 1.0 v	(f) 2.0 v
500	0.38	0.62	0.81	1.0	1.0	1.0
600	.42	.55	.66	.66	.79	1.0
700	.51	.58	.66	.71	1.0	1.0
950	.43	.53	.58	.68	.68	.93

f (v) means the fraction having speeds less than v volts.

The table indicates that the average velocity distribution among the secondary electrons increases with the speed of the impinging ion.

Caesium. In Fig. 3, curve A shows the secondary emission (electron emission plus positive ion reflection) from a baked Mo target when bombarded by Cs^+ ions, as compared with similar emission due to K^+ ions shown in curve B.

The writer found it a little difficult to interpret the results on caesium as regards separating positive ion reflection and electron emission. The readings obtained when the magnetic field was applied direct and reversed

[7] Baerwald, Ann. d. Physik. **60**, 26 (1919).

were different in the case of readings taken when the target was bombarded. No such difference in readings occurred when the target was withdrawn. However, the evidence indicates that there is little reflection and, if any, that this occurs when the ions have low speeds. Experiments were carried out to see if this effect of the magnetic field was due to the direct and reverse

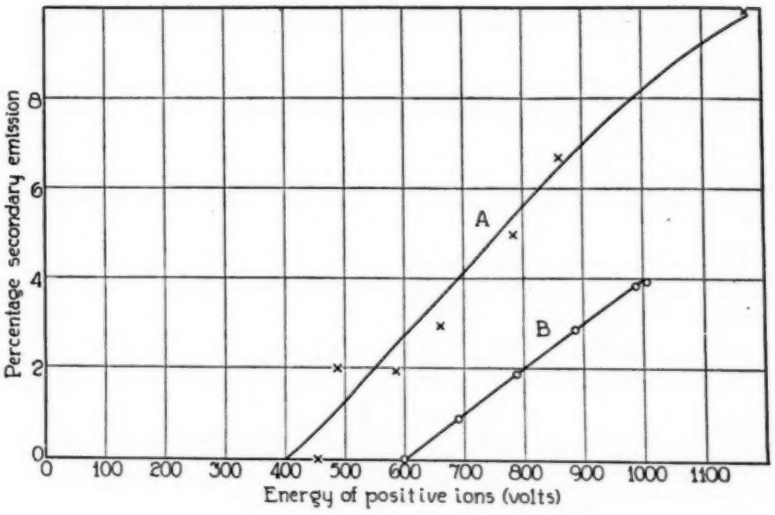

Fig. 3. Percentage of secondary emission as a function of velocity of positive ions.

field affecting the reflected positives of low speed. No evidence was obtained to support this hypothesis. The differences occur where electron emission sets in and it may be that due to non-symmetry of the apparatus all the electrons were not bent by the field in one direction.

Discussion of Results

The phenomena presented in this and the former paper have shown conclusively that when the surface of a target is in a condition to emit electrons due to positive ion bombardment the percentage secondary emission is a function of the speed of the impacting ion.

In a paper criticising the theory of sparking based on secondary emission as set forth by Holst and Osterhuis,[4] Townsend[8] rejects all modes of generating ions as contributing to the effect required to explain the disruptive discharge save the method which assumes the extra ionization as due to collisions of the positive ions with the gas molecules. Townsend rejects the notion that the extra ionization is produced by electron emission from the cathode by positive ion impact on the ground that such a process, in order to lead to the right relationships, requires that the number of electrons set free at the cathode should be independent of the velocity with which the positive ions impinge on the cathode. The writer would like to point out that this is not a requirement of the Holst and Osterhuis[4] theory. The theory

[8] Townsend, Phil. Mag. **45**, 444 (1923).

merely states that there exists a certain probability w, which is a function of the work-function of the metal, that the positive ion moving to the cathode surface before neutralization causes a second electron to escape from the cathode. The condition for the initiation of the spark is that $(2^{\sigma}-1)w>1$. Below the minimum sparking potential the probability w is such that $(2^{\sigma}-1)w<1$, and thus no discharge takes place. This would indicate that the positive ions must have a certain minimum velocity before w becomes large enough to produce the discharge.

Taylor,[9] from recent work on sparking potentials in neon-helium gas mixtures using treated cathodes, has suggested that the secondary electrons are given off from the cathode surface by the photo-electric effect of the radiation accompanying the neutralization of the positive ions at the cathode surface. Experiments showing an increase in sparking potential on passing a heavy discharge were explained by assuming the formation of a charged double-layer which inhibited the emission of electrons.

The question arises as to why electrons are more readily liberated from a gas covered surface than from a degassed metal. The explanation for our experiments cannot be as suggested by Taylor to account for his observations. The following is suggested as a possible explanation.

Consider a metal as an infinite plane. When the electron is at a distance r from the surface it may be considered as attracted by an equal mirror image positive charge. The force of attraction[10] is given by $F=e^2/4r^2$. Assuming that the only force on the escaping electron is its mirror image force then the work done in escaping is $e^2/4x_0$ where x_0 is the minimum distance or its equivalent. Perhaps this distance x_0 is less in the case of a gas free surface than when a gas layer is present.

Also if secondary emission is due to local high temperatures arising from positive ion bombardment certainly there would be more rapid dissipation of the energy by the conducting target surface than by the gas molecules which would favor emission from a gas covered surface.

The results of the earlier investigations regarding secondary emission as depending on surface conditions have been confirmed by the experiments described in this paper. It has not been possible to correlate results of emission due to Na^+ K^+ Rb^+ and Cs^+ ions using an untreated target with the atomic weight, or to obtain a correlation in the case of a degassed metal; surface condition in the former case played a decisive rôle.

My thanks are due to Professor K. T. Compton, who suggested this investigation, and has shown continued interest and has given much helpful advice throughout the course of the research.

PALMER PHYSICAL LABORATORY,
PRINCETON, NEW JERSEY,
June 17, 1927.

[9] Taylor, Phil. Mag. **3**, 753 (1927).
[10] Schottky, Phys. Zeits. **15**, 872 (1914).

THE VELOCITY AND NUMBER OF THE PHOTO-ELECTRONS EJECTED BY X-RAYS AS A FUNCTION OF THE ANGLE OF EMISSION

By E. C. Watson

Abstract

Magnetic spectra of the electrons ejected by x-rays from thin metallic films at angles ranging from 0° to 180° with the direction of the x-ray beam have been obtained by the method of Robinson, de Broglie, and Whiddington. To the degree of accuracy of the measurements (one-half of one percent) the maximum velocity of ejection is exactly the same in all directions. With thin foils of the heavier elements the number of electrons leaving the foil with this maximum velocity in the various directions (determined by the intensity of the edges) is approximately the same. With radiators of small density, or with sputtered films so thin that Wentzel's criterion for "single" scattering holds, the number of electrons leaving the foil is greatest in a direction a little forward of perpendicular to the direction of the x-ray beam. Rutherford's theory of nuclear scattering applied to electrons gives an explanation of these results if the assumption is made that all the electrons start out from the atom in the same direction.

1. Introduction

WHILE the work of Seitz[1] has shown that the greater ionization on the emergence side of a thin plate traversed by x-rays than on the incidence side observed by Beatty,[2] Cooksey,[3] Seitz,[4] and others is caused by more *high-speed photo-electrons* leaving the emergence side of the plate than leave the incidence side, nevertheless the question whether the velocity of ejection is *exactly* the same in the two directions has not been answered at all conclusively. Beatty's[5] discovery that the absorption coefficients in air are the same whether the electrons come from the emergence or incidence side of the plate shows that the velocities are at least approximately equal in the forward and backward directions, and the expansion-chamber photographs of C. T. R. Wilson,[6] Bubb,[7] Loughridge,[8] and others show that the forward and backward electron tracks have very nearly the same average range, but neither of these methods is sufficiently accurate to detect small velocity differences.

That the velocity of ejection of the photo-electrons is exactly the same in all directions has been tacitly assumed in all the experimental tests which

[1] W. Seitz. Ann. d. Physik **73**, 182 (1924); Phys. Zeits. **25**, 546 (1924), and **26**, 610 (1925).
[2] R. T. Beatty, Proc. Camb. Phil. Soc. **15**, 492 (1910).
[3] C. D. Cooksey, Nature **77**, 509 (1908), and Phil. Mag. **24**, 37 (1912).
[4] W. Seitz, Ann. d. Physik **73**, 182 (1924).
[5] R. T. Beatty, Phil. Mag. **20**, 329 (1910).
[6] C. T. R. Wilson, Proc. Roy. Soc. **104**, 1 and 192 (1923).
[7] F. W. Bubb, Phys. Rev. **23**, 137 (1924).
[8] D. H. Loughridge, Phys. Rev. **26**, 697 (1925).

have been made of the Einstein photo-electric equation. In fact, the best evidence that the velocities of ejection are the same in all directions is the fact that this equation has been shown by de Broglie,[9] Whiddington,[10] and Robinson[11] to hold so exactly. Actually, however, in the case of x-rays the equation has been tested only for electrons ejected approximately at right angles to the x-ray beam (de Broglie and Robinson) and for those leaving in the forward direction of the x-ray beam (Whiddington).

But even if the electron does always leave the *individual atom* with the velocity given by the Einstein equation, the work of Bothe,[12] Auger,[13] and Loughridge,[14] which shows that the vast majority of the photo-electrons are ejected at an angle a little forward (10 to 20 degrees) of the perpendicular to the x-ray beam, would lead one to expect that the velocities of the electrons which are scattered sufficiently to leave a thin plate in the forward or backward direction would be diminished because of that scattering and moreover that those which leave the plate in the backward direction, having been scattered through a larger angle, would be slower than those which leave in the forward direction. In view of these considerations it seemed desirable to determine as accurately as possible the velocity of the photo-electrons leaving a thin plate at a number of different angles.

II. Apparatus and Method

The apparatus used is shown in Fig. 1. It enables the method of Robinson, de Broglie, and Whiddington to be applied to the determination of the maximum velocity of ejection *in any given direction*.

A parallel beam of x-rays from a tube with water-cooled molybdenum target driven at approximately 25 milliamperes and 30,000 volts, a potential high enough to excite the K lines strongly, enters the vacuum chamber through the slit S which is covered by a thin sheet of mica and after traversing the radiator R leaves through the plate glass window W. The radiator R from which the electrons are ejected consists of thin metal foil supported on an aluminum frame at the exact center of the apparatus and capable of being set so as to make any given angle with the x-ray beam.

The whole apparatus is placed at the center of a solenoid 10 inches in internal diameter and 4 feet long, which produces a uniform magnetic field of 25.56 gauss per ampere of current. The electrons ejected by the x-rays are bent in circles by the magnetic field and recorded on the photographic plates, *pp*, as shown. The width of the x-ray beam where it strikes the metal foil is approximately 4 mm and all the electrons of a given velocity ejected from the foil through an angle of approximately 10° pass through the narrow slits (0.04 cm wide) in the quadrants 1 and 2 and are focused in a line on the

[9] M. de Broglie, Jour. de phys. et rad. **2**, 265 (1921).
[10] R. Whiddington, Phil. Mag. **43**, 1116 (1922).
[11] H. R. Robinson, Proc. Roy. Soc. **104**, 455 (1923).
[12] W. Bothe, Zeits. f. Physik **26**, 59 (1924).
[13] P. Auger, Comptes rendus, **178**, 929 (1924).
[14] D. H. Loughridge, Loc. cit.

photographic plates. The nature of the "spectra" thus obtained and the method of calculating the velocity of the electrons from measurements of the radius of curvature and magnetic field strength are too well known to

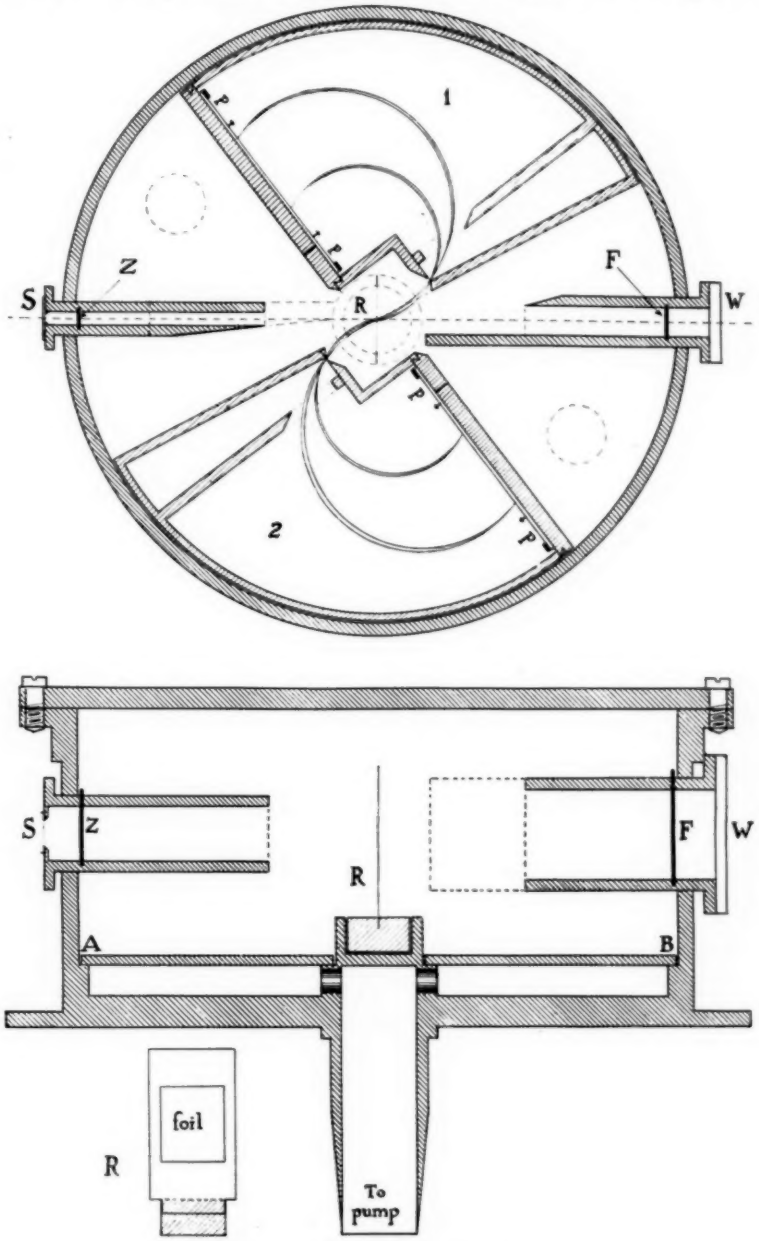

Fig. 1. Diagram of apparatus.

need further description here. Quadrants 1 and 2 are carried on the plate *AB* and may be rotated so that by a suitable adjustment of magnetic field and position of the quadrants, the velocities of electrons ejected in any

direction from 0° to 360° may be studied. Quadrant 1 records the emergence electrons and quadrant 2 simultaneously the incidence electrons. The whole inside of the vacuum chamber is lined with black paper to cut down any stray emission from the walls.

Z is a removable zirconium oxide filter to isolate the $K\alpha$ lines of molybdenum. It was not used in the experiments described in this paper, but instead was replaced by a strip of black paper to prevent light from entering the apparatus. F is a removable fluorescent screen to facilitate the alinement of the x-ray beam and radiator. The vacuum chamber is connected through a liquid-air trap to a two-stage mercury diffusion pump which is kept running continuously during an exposure. Exposures of from 50 to 100 hours are necessary to bring out the weak edges. Both Eastman x-ray plates and Hilger Schumann plates sensitized for cathode rays were used. For values of $H\rho$ greater than 300 both types of plate are satisfactory. For small electron velocities the Schumann plates are much superior. This is well shown in Fig. 2, the lower reproduction being from an Eastman x-ray plate, the four upper ones from Schumann plates.

III. Results

In Fig. 2 are reproduced two 100-hour exposures made on Schumann plates using ordinary gold foil as radiator. The magnetic field was held constant to better than 0.5% during the two runs and the quadrants were set so as to receive on the center of the photographic plates electrons emitted at approximately the angles indicated (namely 45°, 135°, 0°, and 180° with the forward direction of the x-ray beam). Because the radius of curvature is different for electrons of different velocities, the angles of emission of the electrons recorded at the two ends of the plate will differ by as much as 10° from these values and for electrons of intermediate velocities by corresponding amounts. The origin of the electrons responsible for the various edges is given in the subscript. The lower reproduction is a similar exposure taken on an Eastman x-ray plate in order to compare the relative sensitiveness of the two kinds of plates to electrons of different velocities. The spot at the left end of each spectrum is a fiducial mark for use in measuring up the plates.

These spectra and many others taken at different angles and with different materials as radiator have been measured with a comparator and the positions of the corresponding edges on various plates found to be exactly the same to the degree of accuracy with which the measurements can be made and duplicated, namely one-half of one percent. *We conclude therefore that the maximum velocity of ejection is the same in all directions.* This conclusion was to have been expected, but it is satisfactory to have this much abused question settled in so decisive a manner.

The surprising feature of the spectra obtained with gold foil is that the intensities of corresponding edges are nearly the same in the various directions. Some variations do appear in the reproductions, but they are due to irregularities in the emulsions of the Schumann plates and are not reproducible.

This result can be reconciled with the expansion-chamber results of Lough-ridge and Auger, who found a great preponderance of photo-electrons at from 70 to 80 degrees, only if a large fraction of the electrons have their directions changed in getting out of the foil without a corresponding loss in

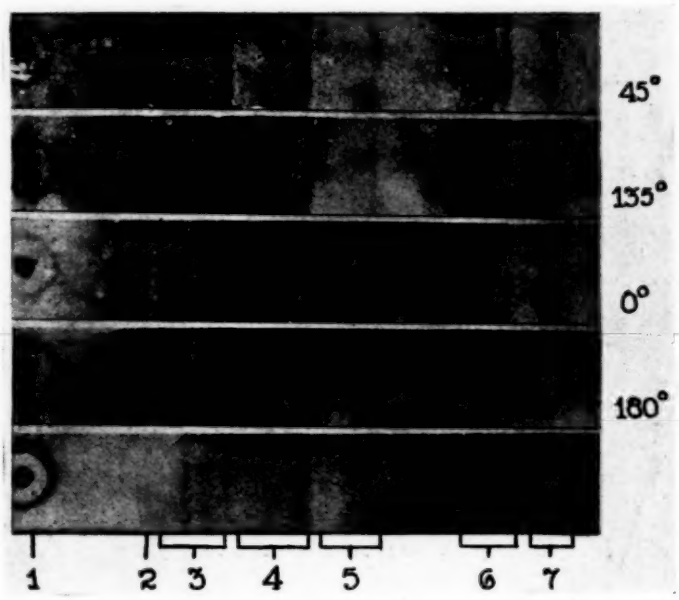

Fig. 2. Magnetic spectra of electrons emerging at various angles from gold leaf traversed by primary x-rays from molybdenum. 1. L_{II} electrons ejected by Mo $K\alpha$; 2. L_{III} electrons ejected by Mo $K\alpha$; 3. M electrons ejected by Au $L\alpha_1$; 4. M electrons ejected by Au $L\beta_1$; 5, M electrons ejected by Au $L\gamma_1$; 6, M electrons ejected by Mo $K\alpha$; 7, N and O electrons ejected by Mo $K\alpha$.

velocity, i.e. only if the nuclear scattering is large. To test whether this is the case similar experiments were made using still thinner films of gold obtained by cathodic sputtering on celluloid and also foils of the light elements such as aluminum. In these cases the nuclear scattering should be

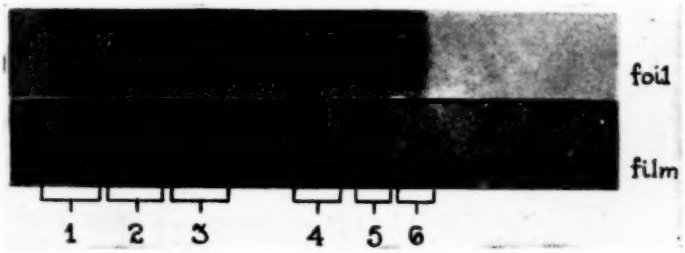

Fig. 3. Comparison of magnetic spectra of electrons from gold foil and sputtered gold film. 1, M electrons ejected by Au $L\alpha_1$; 2, M electrons ejected by Au $L\beta_1$; 3, M electrons ejected by Au $L\gamma_1$; 4, M electrons ejected by Mo $K\alpha$; 5, N and O electrons ejected by Mo $K\alpha$; 6, N and O electrons ejected by Mo $K\beta$.

less and directional effects are to be expected if the electrons are really emitted more copiously in one direction than in another.

With a sputtered film of gold so thin that it transmitted more than half the light which fell upon it, fairly sharp lines were obtained upon the photographic plate instead of edges which are sharp on the high velocity side and trail off on the low velocity side. This is well shown in Fig. 3 in which the

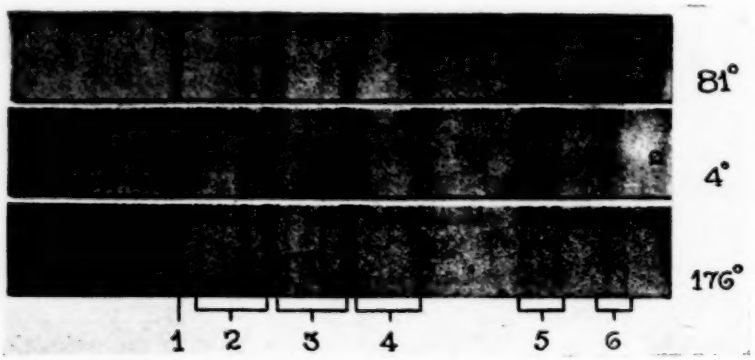

Fig. 4. Magnetic spectra of electrons emerging at various angles from a thin sputtered film of gold traversed by primary x-rays from molybdenum. 1, L_{III} electrons ejected by Mo $K\alpha$; 2, M electrons ejected by Au $L\alpha_1$; 3, M electrons ejected by Au $L\beta_1$; 4, M electrons ejected by Au $L\gamma_1$; 5, M electrons ejected by Mo $K\alpha$; 6, N and O electrons ejected by Mo $K\alpha$.

spectra obtained with the gold foil and the sputtered gold films are compared. Eastman x-ray plates were used in these experiments and in those which follow because they are far more uniform and dependable for intensity measurements.

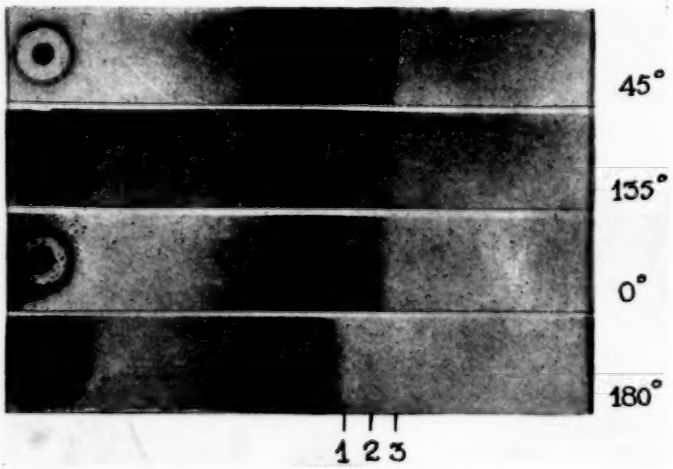

Fig. 5. Magnetic spectra of electrons emerging at various angles from aluminum foil traversed by primary x-rays from molybdenum. 1, K electrons ejected by Mo $K\alpha$; 2, L electrons ejected by Mo $K\alpha$; 3, K electrons ejected by Mo $K\beta$.

As was anticipated the intensity of the lines obtained with the sputtered film varied with the angle at which the electrons were emitted. Thus in Fig. 4, which shows results obtained at three different angles, the lines are all relatively strong in the spectrum taken at 81°, i.e. a little forward of perpendicular to the x-ray beam. At 4° all the lines (except those due to the fluorescent radiation of the gold itself which should be the same in all directions) are much weaker and at 176° they have practically disappeared.

The results with aluminum foil are also of interest. They are shown in Fig. 5. Here again edges are obtained instead of lines. These edges are strong and sharp when the electrons leave the foil at 45° with the direction of the x-ray beam. In the forward and backward directions they become weak and fuzzy and they are always less sharp in spectra taken in the backward direction than they are in spectra taken at corresponding angles in the forward direction. If the angles are measured from the 80° position instead of from the forward direction of the x-ray beam, the edges become systematically less sharp as the angle becomes greater. Also the position of the edges as measured on the comparator seems to shift systematically towards the left (i.e. towards smaller velocities) as the angle increases, so that the velocity seems measurably greater in the forward direction than it is in the backward direction. Photometer curves of the original plates show, however, that all the corresponding edges really start at the same distance from the fiducial mark and that it is the intensity maximum which shifts towards smaller velocities as the angle departs from the 80° position.

IV. Discussions of Results

The fact that with the thin sputtered film or the aluminum foil the lines or edges are always weaker or less sharp in the backward direction than they are for corresponding angles in the forward direction shows that the most probable direction of emission of the photo-electrons is forward of perpendicular to the direction of the x-ray beam in agreement with the results obtained by the expansion-chamber method. The measurements are not yet accurate enough, however, to determine precisely what this most probable direction is.

The theory of nuclear scattering developed by Rutherford for α-particles and applied by Crowther and Schonland,[15] Chadwick and Mercier,[16] and Schonland[17] to the case of beta-rays enables the relative intensities at various angles of corresponding lines in the spectra obtained with sputtered gold film to be calculated provided the assumption is made that all the electrons start out from the atom at approximately 80° with the direction of the x-ray beam. Intensity measurements have not yet been made with sufficient accuracy, however, to decide whether such nuclear scattering is sufficient to account for the whole of the angular distribution or not. but the fact that

[15] J. A. Crowther and B. F. J. Schonland, Proc. Roy. Soc. **100,** 526 (1922).
[16] J. Chadwick and P. H. Mercier, Phil. Mag. **50,** 208 (1925).
[17] B. F. J. Schonland, Proc. Roy. Soc. **113,** 87 (1926).

the intensity of the lines in spectra taken at angles other than 80° diminishes as the thickness of the radiator is decreased gives a strong presumption that this is the case.

The theory of nuclear scattering also explains very simply the results obtained with aluminum foil and the differences between these results and those obtained with the gold foil and film. The theory applies directly to the case of the sputtered gold film because its thickness is so small that the electrons experience only single collisions with atomic nuclei in getting out. Now Wentzel[18] has given a criterion for "single" scattering which enables the critical thickness which must not be exceeded if there is to be no more than one nuclear collision to be calculated and the change in velocity which electrons experience in passing through this critical thickness of foil can be computed by means of Whiddington's[19] fourth-power law. For the gold foil this change in velocity is less than 0.3% even for electrons emitted at 180°; i.e. it is less than the accuracy with which the edges can be measured. There is therefore no variation in the structure of the edges as the angle is changed. In the case of aluminum, however, the loss in velocity is 0.2% for electrons leaving at 45 and 0.6%, 1.1%, and 1.8% for those leaving at 135°, 0°, and 180° respectively, which agrees very satisfactorily with the apparent shift of the edges as measured with the comparator. This means that the electrons which are recorded on the plate close to the high velocity edges are electrons which have suffered at most one nuclear collision and therefore the intensity of this portion of the edge varies with the angle as does the intensity of the lines in the spectra obtained with thin sputtered films. Electrons coming from deeper layers in the foil will experience more than one such collision and so will be scattered to such an extent that there will be no change in intensity with angle of the part of the edge to which they contribute. All this is of course on the assumption that all the electrons start out at 80° with the direction of the x-ray beam and the success of this assumption is further argument for its correctness.

V. Conclusions

The conclusions which may then be drawn from these experiments are: (1) that most (probably all) of the photo-electrons ejected by x-rays from thin metallic radiators start out from the individual atoms in a direction a little forward of perpendicular to the direction of the x-ray beam with the velocity given by the Einstein equation; (2) that due to collisions with atomic nuclei some (many, if the radiator is thick and heavy) have their direction changed without a corresponding loss in velocity and so electrons leave the radiator in all directions with the same velocity; (3) that if precise results are to be obtained by the method of Robinson, de Broglie, and Whiddington on the velocity of ejection of x-ray electrons from radiators of small density, the apparatus must be so arranged as to focus upon the photographic plate

[18] G. Wentzel, Ann. d. Physik, 69, 335 (1923). See also Chadwick and Mercier, Loc. cit., and Schonland, Loc. cit.

[19] R. Whiddington, Proc. Roy. Soc. 86, 360 (1912).

electrons which leave the radiator in a direction a little forward of perpendicular to the direction of the x-ray beam. The velocities of electrons leaving in other directions may appear to be as much as one or more percent too small because the majority of them come from considerable depths in the radiator.

This work further emphasizes the importance of nuclear scattering in all experiments on the angular distribution of electrons ejected by radiation of any sort. It shows that essential features may be entirely obscured and wrong conclusions arrived at unless care is taken to work under conditions such that Wentzel's criterion for "single" scattering holds and allowance can be made for the effect of scattering.

Finally the writer desires to express his thanks to Dr. I. S. Bowen for his kind assistance many times in maintaining constant conditions during the long and tedious exposures necessary in this work; to Dr. R. M. Badger for sputtering the gold films used; to Mr. J. A. Van den Akker for his care in making the reproductions which accompany this article; and to Professor R. A. Millikan for his enthusiastic interest and constant encouragement during the course of the work. The investigation has been carried out with the aid of funds provided by the Carnegie Corporation of New York.

NORMAN BRIDGE LABORATORY OF PHYSICS,
CALIFORNIA INSTITUTE OF TECHNOLOGY,
June 14, 1927.

DIRECTION OF PHOTO-ELECTRON EMISSION

By Donald H. Loughridge

Abstract

Direction of emission of photoelectrons from hydrogen, air and argon irradiated by Mo Kα x-rays.—Photographs of the photo-electron tracks in a Wilson expansion chamber through which a narrow beam of monochromatic Mo Kα x-rays were passed were taken with a stereoscopic camera. The direction of the paths with respect to the x-ray beam was determined from measurements made with a *specially designed stereoscopic comparator*. 445 tracks were studied of which 231 were in argon, 123 in air and 91 in hydrogen. Curves showing the frequency of occurrence of different angles of ejection have a fairly sharp maximum for angles of about 70° with the forward direction of the x-ray beam. The curves are similar for the three gases studied except that the maximum in the case of hydrogen is somewhat sharper than for the other two gases.

NUMEROUS workers have observed an asymmetry in the photo-electric current arising from a radiator placed in the path of ultra-violet light, x-rays, or gamma rays. The ratio of the current in the forward direction to that in the backward direction has been found to vary from 1.17 in the case of ultra-violet light[1] using platinum films as radiators, to 20 for carbon plates and gamma rays.[2] De Foe[3] has recently obtained a ratio of 2.89 for the asymmetry of photo-electron paths in air, photographed by the cloud method, using the $K\alpha$ radiation of molybdenum. More specifically, the most probable direction of photo-electrons in gases, produced by means of x-radiation has been investigated by Bothe[4] and the author.[5] Using a method involving the counting of electrons by a Geiger counter set at various angles with respect to the x-ray beam, Bothe found a slight variaiton with the hardness of the radiation and also with the gases used. His values vary from 73° to 81° for the most probable direction of emission, depending upon the above factors and upon the gas pressure. The present author found, by photographing the tracks in air, and measuring their directions by means of a stereo-comparator (to be described in this paper) using $K\alpha$ radiations from a Mo-target Coolidge tube, the most probable angle of ejection was about 70°.

Since this work was published an entirely new expansion chamber has been constructed and much new data on the direction of ejection of photo-electrons in hydrogen, air, and argon, by the $K\alpha$ radiation of molybdenum has been obtained. The details of the expansion chamber and a discussion of the technic involved in obtaining distinct photographs is published

[1] Stuhlman, Phil. Mag. **22,** 854 (1911).
[2] Mackensie, Phil. Mag. **14,** 176 (1907).
[3] DeFoe, Phil. Mag. **49,** 817 (1925).
[4] Bothe, Zeits. f. Physik **26,** 59 (1924).
[5] Loughridge, Phys. Rev. **26,** 697 (1925).

elsewhere.[6] It will be sufficient to state here that the chamber is 10 inches (25.5 cm) in diameter by 1 5/8 inches (4.2 cm) deep. The timing of all necessary processes is done by a heavy pendulum rigidly swung from a cross rod: the latter carries the necessary commutators to provide electrical contacts for the removal of the field across the chamber, the production of the expansion, the x-ray beam, and the exposure with the camera. The photographs are taken with a box-type stereoscopic camera mounted 16 inches (40.5 cm) above the top of the chamber. The two separate plates are exposed simultaneously by a large Graflex focal plane shutter, released by an electromagnet. In all the present work the whole chamber is photographed on the $2\frac{1}{4}\times 3\frac{1}{4}$ inch plates, thus giving a reduction in size of 3.52 fold. The lenses used are Tessar f 4.5 specially matched by Bausch and Lomb Company. Eastman Speedway plates were found to be quite satisfactory when used in connection with a Sperry arc as a source of illumination.

Measurement of the Plates

Measurement of the plates was carried out on the original negatives. The stereocomparator is shown in Fig. 1. It was machined from brass cast-

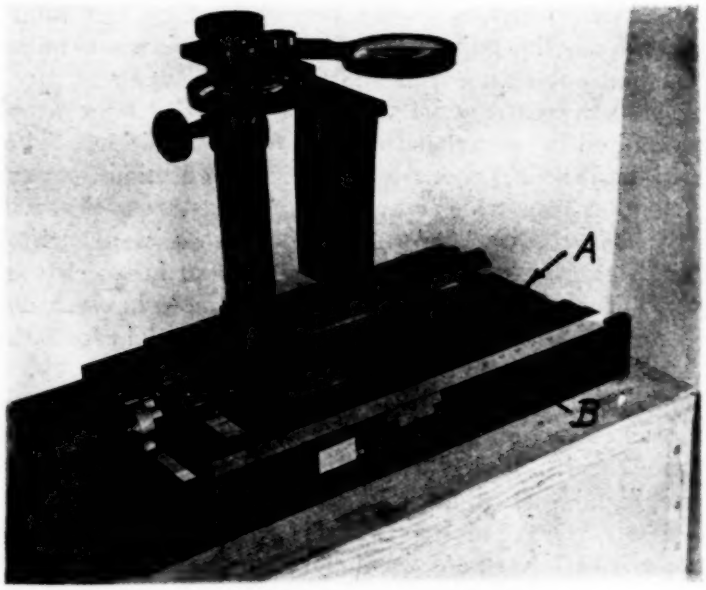

Fig. 1. Photograph of the stereoscopic comparator.

ings and consists of a heavy bed plate upon which the first carriage slides; the latter in turn carries the second carriage, and the two are moved relative to one another by the micrometer screw. Each carriage supports a cross hair which is stretched across horizontally, at such a height as to just clear the plates, which lie in a suitable support on the bed plate. It was found

[6] Simon and Loughridge, J. Opt. Soc. Amer. **13**, 679 (1926).

practicable to have the cross hair clear the plates by about 0.5 mm, although this would fluctuate some because of the differences in the thickness of the plates. The purpose in having the cross hairs as close to the plates as possible was to eliminate parallax.

The arrangement of the apparatus is such that the direction of the x-ray beam is in the vertical plane containing the center of the two camera lenses. Consequently components of tracks at right angles to this plane will be of the same length in each plate of the pair; this dimension is measured by the slider *A* which runs over a cross bar graduated in mm, with vernier reading to 0.1 mm, and this measurement, called the height is made upon the right hand plate. Components parallel to the incident beam, called the width components, are measured by the scale *B* which is engraved upon the bottom carriage and is provided with a vernier on the bed plate reading to 0.1 mm, components perpendicular to the plane of the photographic plate, called depth components, are measured by the drum *C*, mounted on the micrometer screw. Turning of this screw alters the distance between the two cross hairs but, in stereoscopic relief, appears to move the single cross hair, seen in the image space, perpendicular to the plane of the plates.

In the actual measurement of a track, the plates were placed in the bed plate, touching each other, and scale *B* read when the left hand cross hair was just over the junction point of the two plates. This was to allow the plates to be put back at any future time and the measurements on any particular part of the plate repeated at will. Thus no marking or scratching of the plates was required to reset them at their original positions. The arc light, used for the illumination, produced a caustic by reflection from the opposite side of the chamber from which it entered and this automatically insured the placing of the right side up. Only those tracks which were entirely separate from all others throughout their entire length and in which there was no doubt as to what was their head (or origin) were used in the measurements. There was two general means of distinguishing the origin from the end of a track, and usually they could both be used on a given track. The first, and more obvious method was to locate the geometric path of the x-ray beam by the large concentration of tracks which started on this line and then the end of the track which lay in this path was the origin.[7] In nearly all of the 174 stereoscopic pairs taken, the lead slits limited the x-ray beam to a cross section of about 1.5 by 0.5 mm, so that this gave a very sharp line containing most of the origins. Further, although most photo-electron paths show a small sphere, or dot, at both ends, of practically the same appearance, the section of track adjacent to the dot at the origin is nearly always less dense (showing less ionization) than the corresponding section near the end. This fact often aided in distinguishing the origins. After locating the origin of a given track the carriages were slid over the bed plate, and with respect to one another by the screw, until the cross-hair appeared to cut through the

[7] In a number of cases two photo-electron tracks started at the same point, as near as could be told, and if they were otherwise free from other tracks, both were used for measurement.

origin. This setting, as all others, could be checked for accuracy by alternately closing each eye and ascertaining if the respective cross-hair under the open eye was set above the corresponding point on each plate. However, it was found that after some practice and adjustment of one's eyes, the setting could be made as accurately with the stereoscopic vision as the slower "eye by eye" method. Scales *A* and *B* and drum *C* were read for the origin, and similar readings for a second point chosen on the path at the first bend. Obviously the difference between the corresponding readings were proportional to the three components of the path at right angles to each other. In order to obtain the actual components the instrument was calibrated by photographing two foot rulers, with sharpened metallic edges, clamped one in back of the other so that the edges, as measured by a traveling microscope, were separated 0.542 cm. These were placed at a distance in front of the camera equal to the distance of the x-ray beam. By measuring, on scale *B*, the distance between each inch mark on the rulers, the demagnification of the photographs was obtained directly and was found to be 3.52 and furthermore was constant in value across the entire 10 inches of the chamber's diameter. Likewise by setting, by stereoscopic vision, on corresponding division points on each ruler the divisions on the drum were evaluated at each inch point across the diameter of the chamber. Each drum division was equivalent to 0.226 mm in depth and was constant across the diameter of the chamber; after practice, the settings could always be repeated to within 1.5 divisions. Thus the depth readings were made to 0.34 mm, and the width and height to 0.1 mm. Having now obtained the components of the initial part of the track it is a perfectly straightforward calculation to obtain the angle with respect to the x-ray beam.

Before experiments were begun the lead collimating slits on the box enclosing the x-ray tube, were carefully lined up with a diameter of the chamber. The line connecting the two camera lenses was in the same vertical line as this diameter. This caused the x-ray beam to pass parallel to the plates and perpendicular to their long side so that the direction of the incident x-ray beam was parallel to the motion of the carriages in the stereocomparator.

The best photographs to measure were those containing about eight to ten tracks. More than this number overlapped so much that the photograph was almost useless, as far as accurate measurements were concerned. On the 174 pairs of photographs there were measured 434 separate photo-electron tracks. Of this total 231 were in argon, 123 in air, and 91 in hydrogen. The initial pressure in the chamber varied slightly from day to day, but was always between 60 and 65 mm of mercury. The expansion ratio was not determined exactly, as it was chosen so as to give the most distinct tracks, but was about 1.3.

Results

The results of measurements of tracks produced in hydrogen, air, and argon under similar conditions, by the $K\alpha$ line of Mo are shown in Fig. 2. The homogenity of the radiation was obtained by filtering that produced by

a Mo-target Coolidge tube through a zirconium oxide filter especially prepared for this purpose by the General Electric Company. The cross section of the beam was about 0.25 sq. mm.

The abscissa of these curves is the angle between the initial portion of the x-ray track and the forward direction of the x-ray beam. The ordinate gives the number of tracks found to start out within the chosen angular interval. (i.e. from Fig. 2 it is seen that 24 tracks in hydrogen started out making angles of between 60 and 72° with the forward direction of the x-ray beam.)

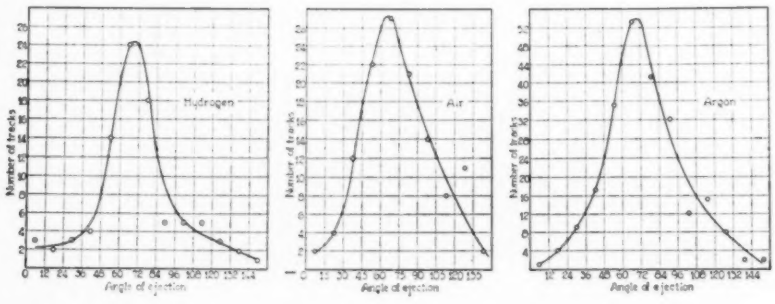

Fig. 2. Numbers of tracks of photo-electrons ejected at various angles by Mo $K\alpha$ x-rays from hydrogen, air and argon.

Practically the same maximum is obtained if the angular intervals chosen are 10°, 12°, 15°, 30°, or 45°, but the smaller intervals give points whose values are too much affected by the statistical fluctuations and the larger intervals give too few points to insure a clear curve. The 12° and the 15° intervals chosen show the effect fairly and clearly.

The curves show clearly that the most probable direction of emission is in a direction at about 70° with respect to the x-ray beam for all three of the gases studied. However, it is to be remembered that since the absorption coefficient is proportional to the fourth power of the atomic number, very probably all of the tracks dealt with in the case of hydrogen actually arise from heavier gases which are present as impurities.

These results yield a value for the most probable direction of emission somewhat smaller than that found by Bothe and Auger. This difference is larger than the probable experimental errors in the various pieces of work. Since the present work is the only one of the three in which monochromatic x-rays were used, this difference in angle may be due to the presence in previous work of soft radiation. The asymmetry of each curve is significant, being steeper on the side of the maximum toward smaller angles than on the other.

From the present work, in which the measurements on a given track can be re-checked to within about 4°, the work of using a Geiger counter by Bothe,[4] and the recent careful work of Auger,[8] there is no doubt but that there is a very appreciable forward component in the majority of the tracks.

[8] P. Auger, Jour. d. physique et le radium **8**, 85 (1927).

Discussion

The tendency toward ejection at right angles to the direction of the incident radiation is in accord with the classical theory which would demand that all of the tracks start initially in the plane of the electric vector for unpolarized rays, and in the direction of the electric vector for polarized rays. Since this last phenomenon has been observed by Bubb the classical theory would seem to be satisfactory were it not for the presence of the forward component. By allowing the momentum of the incident radiation in the forward direction to be passed on to the electron absorbing the energy, a shift of the peak forward to about 82° becomes theoretically possible. This, however, does not appear to be quite enough. Further the distribution of directions on either side of the most probable direction is not accounted for by these conceptions.

This distribution may be qualitatively accounted for by vectorially adding the random momentum of the electron in its orbit, as has been shown by Bothe, but a more satisfactory explanation would appear to be that recently put forward by Watson[9] which accounts for the spread of directions upon the basis of scattering and leads to a distribution function which fits the facts better than do any of the more elaborate theories. The asymmetry noted above is also beautifully explained by Watson's theory.

In conclusion I desire to express my warm appreciation for the inspiration and guidance given me during the progress of this work by Professor R. A. Millikan, and Dr. A. W. Simon for the help he has given in the design of the expansion chamber.

Norman Bridge Laboratory of Physics,
California Institute of Technology,
July 1, 1927.

[9] Watson, Phys. Rev. **29**, 752 (1927).

REFLECTED AND SECONDARY ELECTRONS FROM AN ALUMINUM TARGET

By J. B. Brinsmade

Abstract

Velocity distributions of secondary electrons from an aluminum target, bombarded with homogeneous streams of primary electrons, were examined with a magnetic analyser. The secondaries examined were those coming off approximately at right angles with the primary beam. The range of primary velocities used was from 5 volts to 175 volts. Sharply defined peaks, consisting of electrons reflected without loss of energy, constitute 2 percent of the whole distribution at 175 volts, 10 percent at 35 volts, 90 percent at 12 volts, and 95 percent at 7 volts. The coefficient of reflection at right angles is of the order of 10^{-3} to 10^{-2} per unit solid angle, increasing over twenty fold between 100 volts and 8 volts, attaining a maximum at 7 or 8 volts and decreasing sharply below that.

J. A. BECKER[1] and E. L. Rose,[2] using a magnetic velocity analyser, found evidence for the existence of a very sharply defined, true reflection of electrons without energy loss when a metal target is bombarded with a primary electron stream. Since the present work was started, C. F. Sharman[3] and D. Brown and R. Whiddington[4] have reported the same phenomenon. Other observers, notably A. Becker[5] and H. E. Farnsworth,[6] using total current and retarding potential methods, had shown the existence of a considerable fraction of the secondary electrons having a velocity at least very close to that of the primary stream. C. Davisson and C. H. Kunsman,[7] had investigated the angular distribution about the target, of the secondaries having velocities 90–100 percent of that of the primaries and had assumed, in interpreting their results, that they were dealing with electrons reflected by single atoms. The present work was undertaken with a view to securing quantitative data on the intensity of such reflection.

The apparatus used had been set up by Mr. O. Ritzmann and was originally intended to study soft x-rays by magnetic analysis of the photoelectrons ejected from an aluminum target. It consisted essentially, see Fig. 1, of an analyser, A, with the aluminum target, T_a, before the first slit, and a Faraday collector, C, behind the last slit; together with a straight tungsten filament, F, and copper target, T_c, enclosed in a cylindrical shield, G, having a window and wire grid between the two targets.

[1] J. A. Becker, Phys. Rev. **24,** 478–85 (1924).
[2] Rose, Phys. Rev. **25,** 883(A) (1925).
[3] Sharman, Proc. Cambr. Phil. Soc. **23,** 523–30 (1927).
[4] Brown and Whiddington, Nature **119,** 427 (1927).
[5] A. Becker, Ann. d. Physik. **78,** 209 (1925).
[6] Farnsworth, Phys. Rev. **25,** 41–57 (1925).
[7] Davisson and Kunsman, Phys. Rev. **22,** 242–58 (1923).

The whole was enclosed in Pyrex and could be evacuated by means of a two-stage mercury condensation pump backed by a Cenco Hyvac. Besides the usual vapor trap between pump and apparatus, there was a large charcoal trap near the aluminum target. The whole could be enclosed in a furnace and baked out at a temperature of 450°C before using. It was thus possible to get a vacuum of 1.5 to 2.0×10^{-6} mm of mercury as measured on an ionization gauge.

A large solenoid, with its axis vertical, could be lowered over the whole apparatus to supply the magnetic field for the analyser. A small earth inductor, mounted as indicated in the figure, gave a ready means of determining the correction to be applied for the vertical component of the earth's

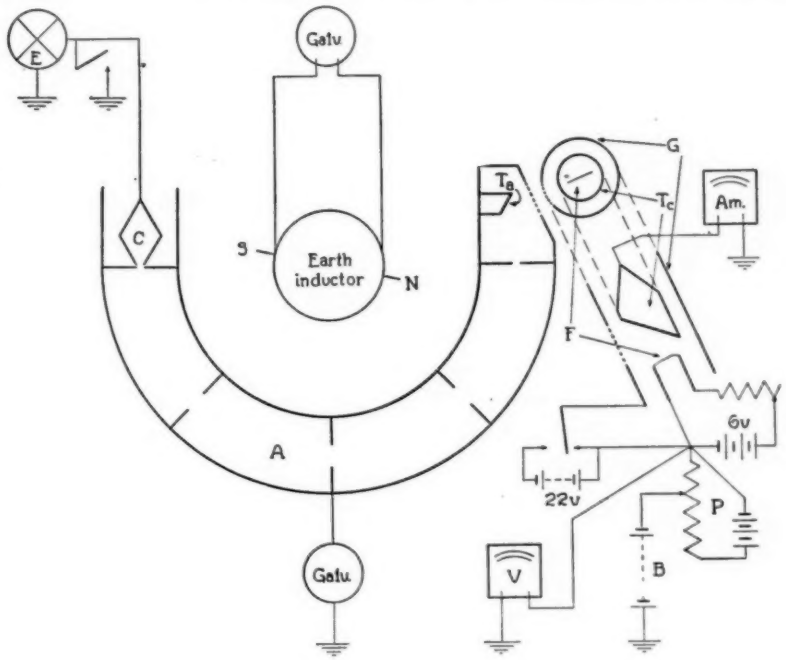

Fig. 1. Diagram of apparatus.

field by merely observing the reverse current through the solenoid needed to reduce the galvanometer throw to zero when the coil was flipped over.

The important dimensions of the apparatus were as follows: width of entrance and exit slits, 0.065 cm; mean radius of path between slits, 6.313 cm; width of middle slit (limiting angular width of beam), 1.4 cm; length of all slits, 1.4 cm; solenoid length, 126.95 cm; solenoid circumference, 87.9 cm; solenoid total turns, 1346.

The negative end of the filament was maintained accurately at a fixed negative potential relative to ground by a main battery, B, and an auxiliary potentiometer device, P, as indicated in Fig. 1, this potential being read on a voltmeter, V. The potential drop across the filament varied between 1.6 and 1.9 volts with heating currents of 6 to 8 amperes as read on a voltmeter and an ammeter not shown in figure.

The copper target was connected to ground through a microammeter and the whole metal body constituting the analyser and containing the aluminum target was connected to ground through a galvanometer.

The cylindrical shield, G, was usually connected to the negative end of the filament. Electrons from the filament were thus accelerated to the copper target; some of them, after suffering full velocity reflections at this target, passed against a retarding potential to the window in the shield, reaching this window with very little velocity; they were there again accelerated to the analyser and those passing through the second window and grid struck the aluminum target. A narrow beam of the resulting electrons from this target could pass through the first analyser slit and their velocity distribution be determined by observing the rates of drift of the electrometer for various solenoid currents.

The Dolezalek electrometer E, together with the leads had a capacity of 110 cm. It was generally used at a sensitivity of about 2000 mm per volt at a scale distance of 2 meters. There was usually a slight but fairly steady electrometer drift of unknown cause which was corrected for by frequent readings with the shield, G, put at 22 volts more negative than the negative end of the filament, thus preventing any electrons from reaching the analyser. This zero drift was subtracted from the observed drifts to get the true electrometer current for each setting. For consistent results, it was found highly important to maintain the filament temperature as nearly constant as possible; hence the use of the above method for getting the zero drift. In spite of the use of a very large capacity storage battery for the filament heating current, there was always a slow deterioration in the filament emission, so the procedure followed was to set the filament rheostat for a convenient upper limit value of the analyser current and allow this current to decrease during a series of drift readings, observing its value for each reading.

As is well known, the mere ratio of electrometer current to analyser current will not give the true velocity distribution, since the effective width of the slits in this type of apparatus varies directly with the velocity of the electrons passing through. These ratios must therefore be reduced to their values per unit effective slit width. Fig. 2 shows several of the velocity distribution curves obtained with various accelerating potentials on the primary electrons. They are plotted on a velocity scale, expressed for convenience in terms of amperes of solenoid current corrected for the earth's field. The unit slit width chosen is 10^{-2} amperes on this scale. The auxiliary voltage scale below is computed from the apparatus constants.

Each distribution shows two main features: a full velocity peak whose position and intensity vary with the primary potential; and a broad distribution of lower velocity electrons having a maximum whose position varies little but whose intensity varies greatly with the primary potential. This accords with Sharman's[3] results. Also the almost complete separation of the two features at the higher primary potentials agrees with Brown and Whiddington's[4] brief report. Observations on the lower velocity distributions were much less accurately reproducible than those on the full velocity peaks,

owing probably to varying surface contamination of the target. The position of the maximum varied erratically over a range of 10 volts or so but usually appeared at 5 or 6 volts. As A. Becker and Sharman both suggest, the position and magnitude of this maximum must be influenced by image forces in the surface and hence also be a function of the angle of emission, so that it should be studied at varying angles, which was not possible with the present apparatus.

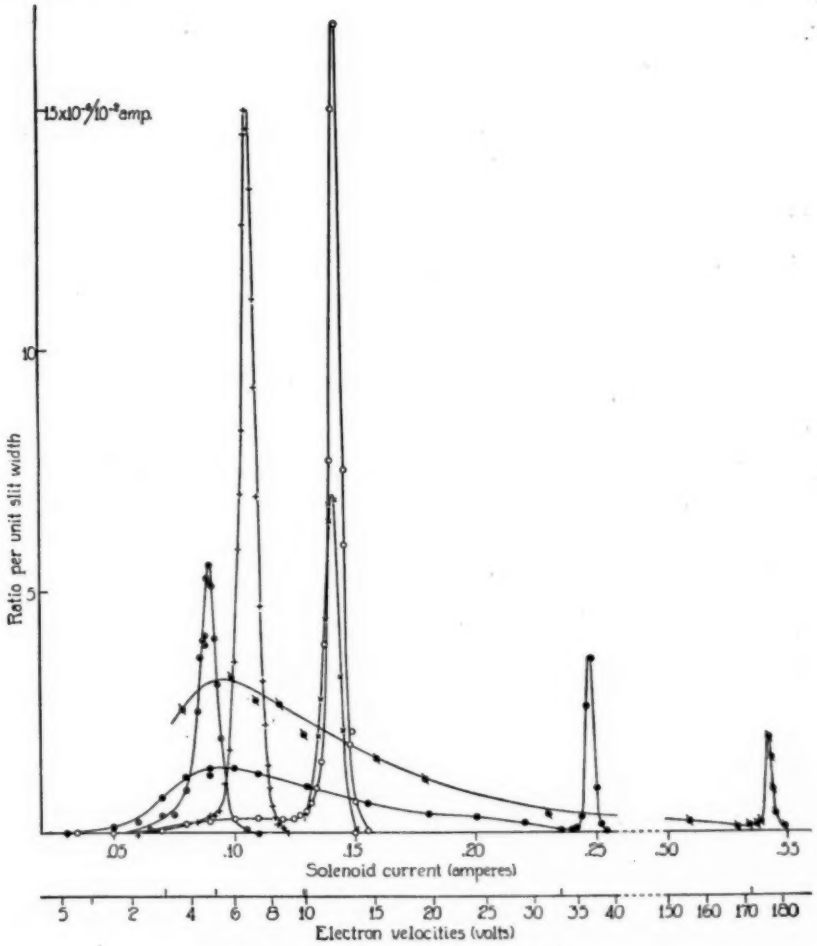

Fig. 2. Velocity distributions of secondary electrons.

That the full velocity peaks consist of electrons truly reflected without appreciable energy loss is clearly shown by their extreme sharpness, the whole observed width down to about 10 percent of the total height being fully accounted for by the effective slit width and the potential drop in the filament. The toeing off at the bottoms is presumably due to scattering in the analyser rather than to appreciable energy losses, since this toeing off is as marked on the high velocity as on the low velocity sides of the peaks.

It will be noticed that each peak comes at a voltage somewhat higher than the primary potential at the center of the filament, the latter being indicated by short lines above the voltage scale. This is undoubtedly due largely to the emission of the primary electrons from the hot filament with a finite velocity which is added to the velocity produced by the accelerating potential. The observed discrepancy averaged 1.95 volts for all observations below 30 volts primary energy with lowest and highest values of 1.36 and 2.52 volts respectively. Above 30 volts it averaged 3.9 with lowest and highest values of 1.5 and 6.8 respectively. The filament was run at bright white heat so that the initial finite velocity of emission is enough to account for the discrepancy in the lower range. In the upper range, any slight errors in calibration, in the setting of the solenoid or in the value of the earth's field

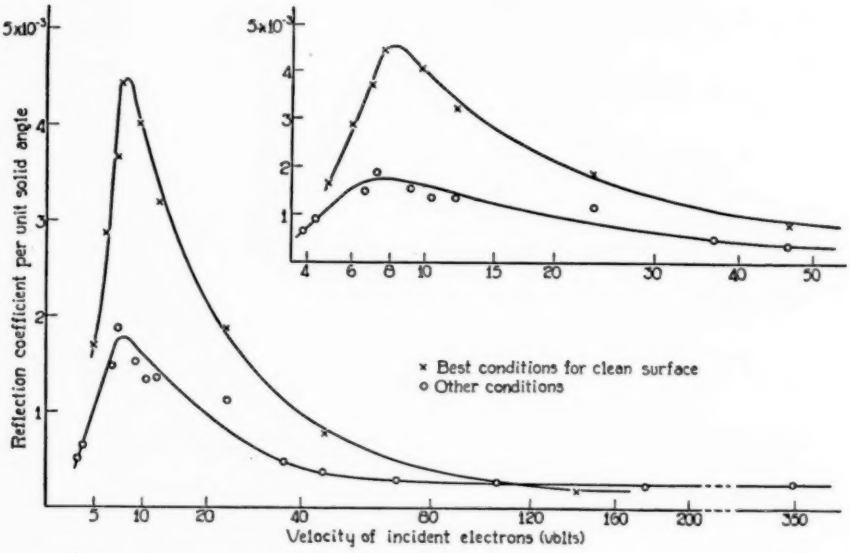

Fig. 3. Fraction of analyser current reflected per unit solid angle as function of primary velocity.

correction would produce more discrepancy on the voltage scale than would the same errors on the lower range.

Measurements of the areas under the full velocity peaks and under the rest of the distribution curves give the percentages stated in the abstract at the beginning of this article. Fig. 3 shows the collected results of all observations on the magnitude of the reflected peak alone for the range of primary velocities examined. The abscissas are observed positions of the peaks on the velocity scale of Fig. 2. The ordinates are the areas under these peaks each divided by the solid angle of the electron beam in the analyser. To get the true coefficient of reflection, one would need to know what fraction of the analyser current struck the target proper within the area effective for passage of secondary electrons through the analyser. From the construction and dimensions of the apparatus, a value somewhere between $\frac{1}{4}$ and $\frac{1}{2}$ seems

to be a reasonable estimate for this fraction. To eliminate the scattering effect, the areas were taken to be those of triangles; of heights equal to the observed heights of the peaks and bases equal to the combined slit-width and filament drop. The plotted points are each averages of from one to three sets of observations taken at the same accelerating potential.

The points on the upper curve were obtained on three separate occasions after the whole apparatus had been filled with hydrogen and baked at atmospheric pressure at 400 to 450°C for 12 hours, the pumps then started and baking continued for 7 hours, the furnace then removed, liquid air put on the charcoal trap and pumping continued for 24 hours or more with liquid air on the charcoal trap continuously. The lower points were obtained at numerous other times, some after no baking except of the charcoal trap, some after merely rinsing with dry air and baking, some after baking in hydrogen but with chance of contamination by vapor from shellac used to stop a slight leak. The difference between the two curves is therefore ascribable to differences in cleanness of the target surface.

Both curves show clearly that the coefficient of reflection at right angles increases markedly at low primary energies over its value at higher energies, attaining a sharp maximum at 7 or 8 volts. (See upper graph with voltage scale enlarged.) No other magnetic analysis of full velocity reflection at these low voltages seems to have been made previous to this; but the existence of the sharp maximum here shown explains the shapes in this region of the curves obtained by Farnsworth[6] for the total secondary current in all directions. The rapid rise of his curve for aluminum from zero to six volts is due to the initial rapid increase in the coefficient of reflection; the flat portion is due to a decrease in the reflection balancing an increase in the true secondary emission; and the rise beyond is due to rapidly increasing secondary emission. The fact that the maximum of reflection is found in this work at 7 or 8 volts while Farnsworth's curve has become nearly flat at 6 volts may be due to any or all of several causes: (a) differences in the initial velocity of emission of electrons from the sources in the two experiments, since he found a voltage discrepancy similar to the one above mentioned but of opposite sign; (b) differences in the amount or kind of adsorbed gas on the targets; (c) possible variation in the position of the reflected maximum for different angles of deflection, since his work includes all angles.

Another experimental fact which is related to the present results is the observation by H. E. Hartig[8] that the secondary current from the far side of a thin aluminum foil, bombarded with primary electrons, reaches a maximum at about 8 volts primary potential. This is perhaps all the more significant here because of Kurchatov and Sinelnikov's[9] observation that the effect appears only when there are slight perforations in the foil.

The writer has, as yet, no satisfactory theoretical explanation for this maximum in the coefficient of reflection. Davisson's[10] spherical condenser

[8] Hartig, Phys. Rev. **26**, 221–31 (1925).

[9] Kurchatov and Sinelnikov, Phys. Rev. **28**, 367–71 (1926).

[10] Davisson, Phys. Rev. **21**, 637–49 (1923).

theory of reflection by a single atom would predict curves of the general type here observed, the maximum occurring for electrons of such velocity as to execute a certain trajectory inside the outer electron shell. To account for the relative heights of the various points on the observed curve, the theory would call for an effective outer shell radius over twice that of the aluminum atom, while to account for the absolute height of the maximum it would call for a shell of radius less than half that of the atom. Thus the quantitative fit is far from satisfactory but perhaps as close as could be expected considering the very approximate character of the theory.

It is possible that the phenomenon may be connected with Davisson and Germer's[11] recent observations of a diffraction pattern in the reflection of electrons from a single crystal of nickel. Assuming a random orientation of crystals in the target and diffraction of De Broglie associated waves similar to Hull's powder patterns of x-rays, one can readily compute from Hull's[12] data the electron velocities at which diffraction at right angles would occur from the various crystal planes in aluminum. It appears that there would be a series of such velocities and if the relative intensities corresponded to Hull's observed intensities for x-rays, the distribution would be roughly similar to the present observed distribution but with its peak at 13.8 volts instead of at 7 or 8 volts. So that to make this theory fit the observations, it would be necessary to assume a virtual expansion of the aluminum lattice of about 40 percent instead of Davisson and Germer's virtual contraction of 30 percent in the case of nickel.

To decide between the two suggested types of explanation (or against both), further experimental evidence is needed at other angles of deviation, with other target materials and with improved resolving power; the last because the diffraction pattern explanation would call for a fine structure in and near the reflection maximum. Farnsworth's curves for very clean crystalline copper show slight peaks which he attributes to increased secondary emission accompanying inelastic collisions but which may possibly be evidence of such fine structure.

The writer is indebted to the Trustees of the California Institute of Technology for the excellent facilities provided and to the Trustees of Williams College for the sabbatical leave during which this work was performed. He also wishes to express his appreciation of the kindly and helpful interest shown by Professor Millikan, Professor Watson and other members of the Institute staff.

VISITING RESEARCH FELLOW,
CALIFORNIA INSTITUTE OF TECHNOLOGY,
PASADENA, CALIFORNIA,
July 9, 1927.

[11] Davisson and Germer, Nature **119**, 558–60 (1927).
[12] Hull, Phys. Rev. **10**, 661–96 (1917).

SPACE CHARGE AS A CAUSE OF NEGATIVE RESISTANCE IN A TRIODE AND ITS BEARING ON SHORT WAVE GENERATION

By Lewi Tonks

Abstract

The mathematical theory of negative resistance in both plate and grid circuit of a triode has been worked out. Negative resistance is found when a virtual cathode is formed between grid and plate. In general this requires a plate voltage low compared to the grid voltage, a minimum electron current density depending upon the voltages used, and proper electrode spacing. For plane parallel construction the plate-grid distance must exceed the grid-cathode distance and for cylindrical construction the ratio of plate to grid diameter must exceed 2.15. Typical theoretical plate and grid characteristics are plotted. Failure of the experimental verification of these static characteristics through the occurrence of oscillations is not unexpected in view of the short relaxation time of the triode. *Applied to the short wave oscillations discovered by Barkhausen and Kurz* this theory in combination with that proposed by Gill and Morrell is able to explain their main features.

GILL[1] has reported oscillations in a triode which he has ascribed to unstable space charge, and he has given just sufficient mathematical treatment to substantiate the theory. Having been led to the same theory as a possible basis for explaining the type of high frequency oscillation first described by Barkhausen and Kurz,[2] I have developed it rather more completely.

Gill applied 40 v. to the grid and 8 v. to the anode of a triode in which the anode diameter was about five times the grid diameter, and then he gradually increased the electron current by increasing the filament temperature. At first anode and grid current increased in proportion. But soon a point was reached at which the anode current dropped and the grid current rose discontinuously. Further investigation showed that this phenomenon could be used to generate oscillations and these oscillations were observed. In triodes in which the ratio of anode diameter to grid diameter was less than five, neither current discontinuity nor oscillations of this type were found.

Before beginning the mathematical theory it will be well to obtain a qualitative idea of the space charge conditions which may exist between grid and anode. For simplicity consider a triode of plane parallel electrodes—cathode F at a distance α from grid G, and anode P at a distance c from G. The grid is supposed to be a continuous equipotential surface so that all electrons pass through it with the same speed (their thermal energy being neglected) along undeviated paths. Let P be maintained initially at cathode

[1] Gill, Phil. Mag. **49**, 993 (1925).

[2] Barkhausen and Kurz, Phys. Zeits. **21**, 1 (1920).

potential, i.e., zero, and let G be maintained at $+V_G$ volts. For small electron currents all electrons leaving F are accelerated until they pass through G. Then they enter a retarding field which reduces their velocity to zero at the surface of P. There they may be either reflected or collected. In either case the space charge in the GP space simply depends on the total electron current, that is, the sum of outward and return currents, since at any point an outbound and a return electron have the same speed and thus make equal contributions to the space charge.[1] Accordingly, the potential distribution between G and P is the same as that arising from an electron emission current originating at P and equal in intensity to the actual total current in the GP space.

This equivalence enables us to see what happens as the outbound current density i_1 is increased. The total current density I_1 increases at the same

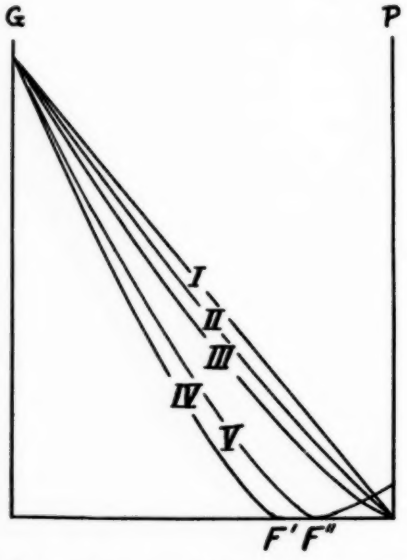

Fig. 1. Potential distribution between grid and plate for various current densities.

time and the potential distribution in the GP space passes successively through the states represented by Curves I and II, in Fig. 1, finally reaching Curve III representing the space charge saturated condition. Curve III is the graph of the space charge equation

$$V^{3/2} = I_1(\text{sat.})\, x^2/2.33\times10^{-6} \tag{1}$$

where

$$I_1(\text{sat.}) = 2.33\times10^{-6}V_G^{3/2}/c^2 \tag{2}$$

so that

$$V/V_G = (x/c)^{4/3} \tag{3}$$

It is clear that if I_1 be now increased above the value I_1 (*sat.*) we have a condition for which there is no corresponding simple emission state with P

as emitter. The equivalent state is space charge saturated emission from a fictitious plane electrode F' as shown by Curve IV. Such a fictitious electrode is called a *virtual cathode*[3] since it behaves theoretically and experimentally like a thermionic source of electrons. It is readily seen that the distance a_0 from G to F' is given by the ordinary space charge equation

$$I_1 = 2.33 \times 10^{-6} V_G^{3/2}/a_0^2, \qquad I_1 < I_1(\text{sat.}) \tag{4}$$

If, when the virtual cathode is at F', the potential V_P of P be made slightly positive, a small electron current reaches P and the virtual cathode shifts a small distance to the right into a new position F''. Denoting the current density i_P to P[4] by θi_1 and the separation of G and F'' by a, the space charge equations give

$$a = V_G^{3/4}/Bi_1^{1/2}(2-\theta)^{1/2} \tag{5}$$

$$c-a = V_P^{3/4}/Bi_1^{1/2}\theta^{1/2} \tag{6}$$

where $B = 656$ for practical units and $B = 3\pi^{1/2}(m/2e)^{1/4}$ for e.s.u. Adding, we find that

$$Bci_1^{1/2} = V_P^{3/4}/\theta^{1/2} + V_G^{3/4}/(2-\theta)^{1/2} \tag{7}$$

This equation relates θ, which is proportional to i_P, to both V_G and V_P. It shows that when V_P is small compared to V_G, θ, and, therefore, i_P vary as $V_P^{3/2}$, just as in the case of emission from a real cathode.

Eq. (7) may be transformed into another simpler form. Noting that $a = a_0$ when $\theta = 0$, Eq. (5) becomes

$$Bi_1^{1/2} = V_P^{3/4}/2^{1/2}a_0$$

When this is used to eliminate $Bi_1^{1/2}$ from Eq. (7) and we put V for V_P/V_G and η for a_0/c we obtain the reduced dimensionless equation,

$$V^{3/4} = \theta^{1/2}[1/2^{1/2}\eta - 1/(2-\theta)^{1/2}] \tag{8}$$

for the volt-ampere characteristic of P.

Instability is very apt to arise when an electrode possesses "negative resistance." In the present case the resistance of P is proportional to $\partial V/\partial\theta$. From Eq. (8)

$$\frac{\partial V}{\partial \theta} = \frac{4V^{1/4}}{3\theta^{1/2}}\left(\frac{1}{2^{3/2}\eta} - \frac{1}{(2-\theta)^{3/2}}\right) \tag{9}$$

[3] The first reference to the existence of a virtual cathode was made, so far as the author is aware, by Mr. D. C. Prince of this laboratory in an unpublished laboratory report dated June 8, 1922. There he calculated the position of the virtual cathode in the case of a grid with an axial filament.

[4] The hypothesis that all the electrons enter the GP space with the same velocity leaves no mechanism to select the electrons which are to pass on to P, but for mathematical handling it is simply sufficient to observe that some do pass on. Actually, of course, the electron beam is slightly non-homogeneous and the selection is accomplished by very small changes in the minimum voltage at the virtual cathode accompanying changes in the voltage of P.

and

$$\partial V/\partial\theta \leqq 0 \quad \text{when} \quad \theta \geqq 2(1-\eta^{2/3}) \tag{10}$$

Since θ is at most equal to unity it is necessary that

$$\eta \geq 1/2^{3/2} = 0.354 \tag{11}$$

That is, whenever with V_P zero a virtual cathode is formed more than 0.354 of the way from G to P, then, theoretically, P will possess negative resistance for some value of V_P.

Eq. (8) makes it possible to plot a single family of curves which will apply to any plane electrode P. Such a family is plotted in Fig. 2 with the θ-axis as axis of ordinates and V-axis as axis of abscissae. The characteristics

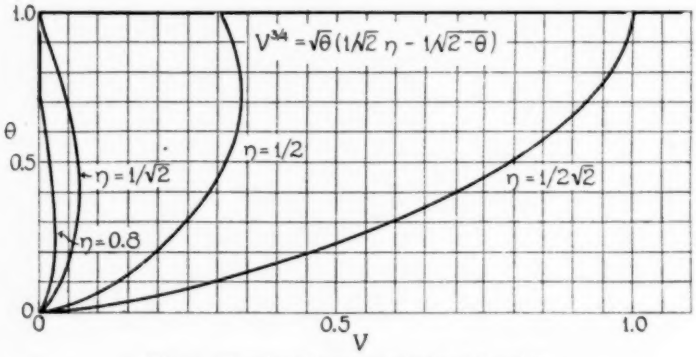

Fig. 2. Family of curves relating V and Θ.

for the smaller values of η (F' nearest G) follow the line $\theta = 1$ after striking it, those for the larger values of η strike the θ-axis first, following it to $\theta = 1$ and thereafter following the latter.

These curves show, as in every case of arc-type negative resistance, that for one applied voltage there may be three different currents, of which only two are stable. Qualitatively, how are these two possible? The answer is not difficult. When θ is small the GP space is carrying a total current of almost $2i_1$, and a virtual cathode is formed some distance from P on account of the large space charge. The large distance between F'' and P in turn, prevents more current from reaching P. But if, by any means, θ be increased sufficiently, even for a moment, then the space current falls to i_1 which, in some cases, will not be sufficient for the formation of a virtual cathode. Then the whole current i_1 will reach P and another stable state is attained. Between these two lies the unstable state in which the total space current exceeds i_1 only slightly, so that F'' is comparatively close to P and θ is comparatively large.

Thus far the whole argument has been based on the supposition that during the current and voltage changes which have been discussed, the electron current has remained constant, and the discussion has neglected the possibility of negative resistance in the grid circuit. The theory may be extended, however, so as to yield grid characteristics and to cover variations

of i_1 by making some reasonable assumptions concerning the collection of electrons by G and the behavior of the electrons which have returned to the FG space through the grid. We shall assume that of the current i_0 leaving the cathode, the fraction ϕ is intercepted by G and the fraction ϕ' (equal to $1-\phi$) is passed by G. Thus

$$i_1=\phi' i_0 \tag{12}$$

Of the current i_1 a fraction θ reaches P so that $(1-\theta)i_1$ returns toward G. Of this we shall again suppose the fraction ϕ to be intercepted by G leaving the current i_2 to pass into the FG space. The double passage through G has by now given the electrons of i_2 some transverse velocity so that they do not approach F closely before returning toward the grid. Accordingly they do not make a full contribution to the space charge. We estimate their contribution at one-half normal. The space charge in the FG space corresponds, therefore, to a current

$$I_0=i_0+i_2/2+i_2/2=i_0+i_2 \tag{13}$$

Finally, we assume that the electrons of i_2 are all collected on their return to G, which is equivalent to neglecting their contribution to space charge after their third grid passage.

Before proceeding, it will be well to establish complete analytical relations between the currents i_0, i_1, i_2, i_G, i_P and I_0. Eqs. (12) and (13) give two of the necessary five equations. The three additional ones are readily seen to be

$$i_0=i_G+i_P$$
$$i_2=\phi'(1-\theta)i_1$$
$$i_P=\theta i_1$$

From the five the following useful equations can be derived by suitable eliminations:

$$i_G=(1-\phi'\theta)i_0 \quad =I_0(1-\phi'\theta)f(\theta) \tag{14A,B}$$
$$i_P=\phi'\theta i_0 \quad =I_0\phi'\theta f(\theta) \tag{15A,B}$$
$$i_1=\phi' i_0 \quad =I_0\phi' f(\theta) \tag{16A,B}$$

Where

$$f(\theta)=1/[1+\phi'^2(1-\theta)]$$

Examining the physics of the situation it is seen that when V_G is small and of the same order as V_P, c/α being not too great, then P will take the full current i_1 because any potential minimum between G and P lies above zero potential. This condition of the tube may be called State A. In this state i_G, and hence $J_G=B^2 i_G$ which is plotted instead in Fig. 3, is proportional to $V_G^{3/2}$ as shown by the line Oz. Here $\theta=1$ and I_0 is fixed by space charge according to the space charge equation

$$B^2 I_0=Z_G/\alpha^2 \tag{17}$$

where Z_G is put for $V_G^{3/2}$ for convenience. As V_G is increased State A persists until the potential minimum strikes zero potential, forming a virtual cathode. Referring to Fig. 3, for $V_P = 9.7$ v. this occurs at w. At this point the virtual cathode begins to limit the current to P, θ begins to decrease and i_G begins to increase more rapidly. The tube is now in State B. I_0 is still fixed by Eq. (17). Increasing V_G further, the end of the space-charge-limited condition is reached at x where i_0 becomes equal to the cathode emission i_e. State C begins here. From this point on i_0 is constant and the virtual cathode

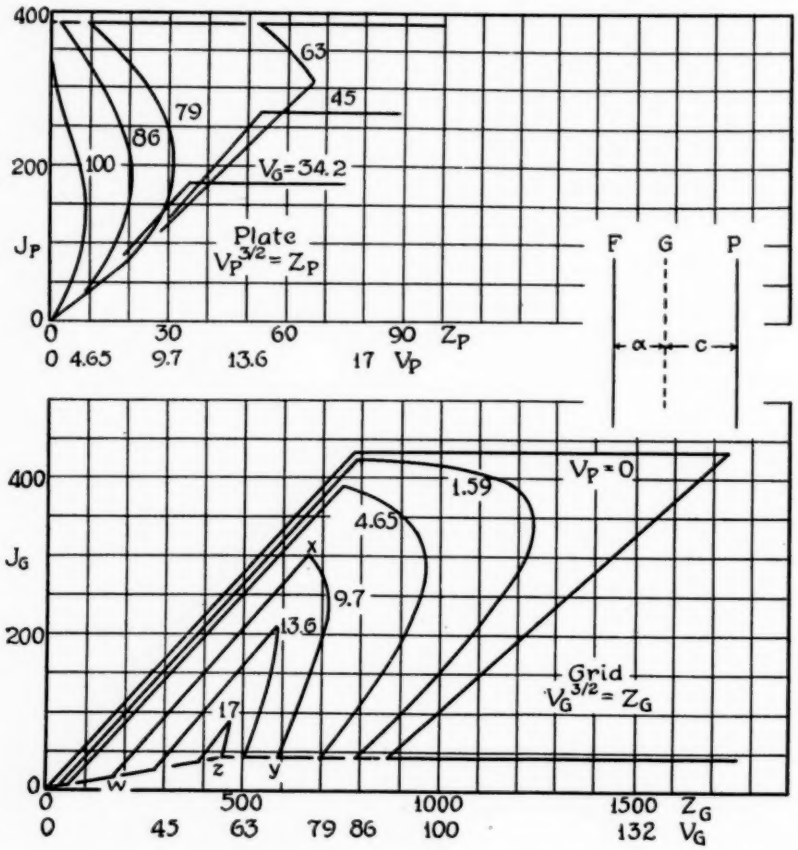

Fig. 3. Theoretical volt-ampere characteristics of triode for $\alpha = 1$ and $c = 1.5$ cm.

approaches P causing i_P to increase and i_G to decrease. The curves of Fig. (3) show that in State C V_G cannot be indefinitely increased if the tube conditions are to vary continuously. The reasons are those that have been discussed already in the simple case involving grid and plate only. Finally at y the virtual cathode again disappears through rising of the potential minimum, θ becomes equal to 1, and the tube is in State D. In this state i_G appears as the horizontal straight line at $J_G = 43$ in the figure.

With this description in mind it is a simple matter to write the volt-ampere equations for each state.

State A. Substitution of Eq. (17) in Eqs. (14B) and (15B), noting that $\theta=1$ gives

$$J_G=(1-\phi')Z_G/\alpha^2 \tag{18}$$

$$J_P=\phi' Z_G/\alpha^2 \tag{19}$$

Where

$$J_G = B^2 i_G, \qquad J_P = B^2 i_P.$$

State B. Substituting Eq. (16B) in Eq. (7) to introduce I_0 in place of i_1, and then noting that I_0 is fixed by Eq. (17), we easily find

$$Z_P/Z_G=\theta[c/\alpha(\phi'(2-\theta)f(\theta))^{1/2}-1]^2/(2-\theta) \tag{20}$$

Again, from Eqs. (17), (14B) and (15B)

$$J_G=(1-\phi'\theta)f(\theta)Z_G/\alpha^2 \tag{21}$$

$$J_P=\phi'\theta f(\theta)Z_G/\alpha^2, \tag{22}$$

parametric equations in θ which allow J_G and J_P to be plotted as functions of Z_G when Z_P is fixed, or vice versa.

State C. Under emission limitation i_0 is constant and equal to i_e. Using Eq. (16A) to replace i_1 by i_0 in Eq. (7) we then have

$$c(\phi' J_e)^{1/2}=(Z_P/\theta)^{1/2}+(Z_G/(2-\theta))^{1/2} \tag{23}$$

where $J_e=B^2 i_e$. From Eqs. (14A) and (15A) we have for the currents,

$$J_G=(1-\phi'\theta)J_e, \qquad J_P=\phi'\theta J_e, \tag{24} \quad (25)$$

another set of parametric equations.

State D. From Eqs. (24) and (25) for $\theta=1$

$$J_G=(1-\phi')J_e, \qquad J_P=\phi' J_e \tag{26} \quad (27)$$

independent of Z_G and Z_P.

Characteristics calculated from these equations show the existence of negative resistance in both grid and plate circuits. Fig. (3) shows J_G plotted against V_G (Z_G) for various plate voltages for the following set of constants:

Cathode-grid separation $=\alpha=1$ cm.
Grid-plate separation $=c=1.5$ cm.
Electron emission $=i_e=10^{-3}$ amp. cm^{-2}
Grid capture fraction $=\phi=0.1$

The plate current against plate voltage curves for the same constants also appear in Fig. (3). The effect of increasing i_e is to change the J_G, J_P, Z_G, and Z_P scales in the same proportion, so that not only would the marginal scale numbers have to be increased but the individual voltages applying to each curve would also have to be increased.

Figure (4) is a plot similar to Fig. (3) and for the same constants, except α, which in this case is taken to be 1.363 cm. It is noted that for V_P greater than about 1.35 v. the characteristic is composed of two unconnected branches, the

two straight lines Oz and zs forming one, and a closed loop the other. If α be increased until $\alpha^2/c^2=\phi'$ it is found that point z moves to point v and all characteristics for $V_P>0$ consist of two branches; and if α be further increased until $\alpha^2/c^2=2\phi'/(1+\phi'^2)$ the point t coincides with point u, and the loop system vanishes. It is doubtful whether any significance can be attached to these mathematical peculiarities. They are mentioned simply to give a more complete picture of the degeneration of the curve systems.

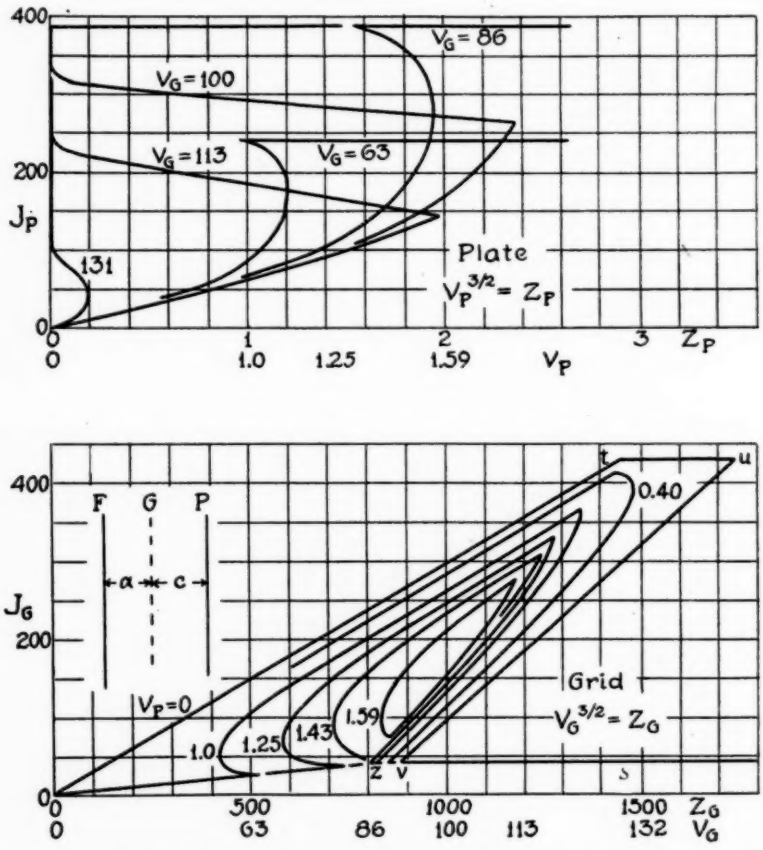

Fig. 4. Theoretical volt-ampere characteristics of triode for $\alpha=1.36$ and $c=1.5$ cm.

There are two factors which may affect the shapes of these characteristics, electron reflection (or secondary emission) from the plate and the transverse velocities imparted to the electrons by the grid. As long as there is a virtual cathode between G and P, or even a potential minimum at which the potential is not more than $\frac{1}{2}V_P$, perhaps, few electrons are able to leave P. Therefore this factor does not affect the xy portion of the $V_P=9.7$ v. grid characteristic in Fig. 3, for example, but may well result in a turning upward of the characteristic somewhat to the right of y. This is probably enhanced by the second factor which, in the first place, makes the whole virtual cathode phenomenon less distinct, and secondly allows less electrons to reach P

the higher V_G on account of the greater transverse velocities imparted. The effect of the two factors on the plate characteristics is possibly a downward slant in their $J_P = 387$ portions. The essential features of the curves are, however, unaffected.

The present theory has been developed for a triode of plane parallel structure for mathematical reasons. But any tests must almost of necessity be made with cylindrical tubes because of the difficulty of obtaining a plane electron emitter. It becomes necessary, then, to adapt the present theory to the cylindrical case.

The condition for the existence of a virtual cathode is of primary importance. A virtual cathode is possible when in any cross-section of the triode (and except for a small correction due to grid captures) the space charge limited current, j_0, from the cathode to the grid exceeds the space charge limited current, j_1, which the grid could draw from the plate as emitter, that is, when

$$j_0 > j_1$$

Now, in the cylindrical case[3]

$$\left.\begin{aligned} j_0 &= V_G^{3/2}/A_c r_G \beta_{FG}^2 \\ j_1 &= V_G^{3/2}/A_c r_G \beta_{PG}^2 \end{aligned}\right\} A_c = (9/2^{3/2})(m/e)^{1/2}$$

where β^2 denotes the function of the ratio of collector to emitter radius which has been tabulated by Langmuir and Blodgett.[5] For a virtual cathode, then, we must have $\beta_{PG}^2 > \beta_{FG}^2$. In the usual single wire filament tube the grid is about 100 times the filament diameter and β_{FG}^2 is not very different from 1.08. Accordingly $\beta_{PG}^2 > 1.08$, and from the table, $r_P/r_G > 2.15$. This is the condition analogous to $c > \alpha$ in the case of the plane tube.

Beyond this single quantitative feature, the qualitative results for the plane case can be bodily transferred to the cylindrical one.

It is of utmost importance to reproduce the theoretical volt-ampere characteristics experimentally, if possible. In determining the volt-ampere characteristic of a device possessing negative resistance oscillations are usually prevented by loading the oscillating circuit with an excess of ohmic resistance. The possibility still remains, however, that the circuit may oscillate in some higher frequency mode. In most cases this can be prevented by making the possible parasitic frequency high compared to the relaxation time of the device, so that were the device to oscillate, it could no longer follow its static characteristic and the effective negative resistance would be very much reduced or obliterated.

In the present case there is the peculiar difficulty that the relaxation time of the triode is extremely short. The time required for an electron to pass from grid to virtual cathode and back to grid gives its order of magnitude. For a 0.5 cm diameter grid at 40 v. operating under space charge limited conditions, this is about 5.4×10^{-9} sec. The tube leads themselves form possible oscillating circuits having natural periods comparable with this.

[5] Langmuir and Blodgett, Phys. Rev. **22**, 353 (1923).

For example an oscillating circuit consisting of two concentric cylinders of 0.5 and 1.0 cm diameter, respectively, and 2.5 cm long joined by a 4 cm loop of 0.05 cm wire has a natural period of 3.1×10^{-9} sec. Accordingly no matter how heavily the external circuits of the triode are loaded with resistance, parasitic oscillations confined practically to the tube itself may arise. Thus it may well be extremely difficult if not impossible to prevent the triode from oscillating in the range where it shows negative resistance. As a matter of fact, I have not been able to stop the very high frequency oscillations by any system of loading the circuit which I have tried.

Turning now to a possible relation between the present theory and short wave oscillations of the type discovered by Barkhausen and Kurz, we find that several important features of those oscillations can be accounted for.

(1) According to the theory, negative resistance is only to be found when a virtual cathode exists in the tube. In a cylindrical triode this can occur only if $r_P/r_G > 2.15$. Experimentally it has been found that no high vacuum triode oscillates if $r_P/r_G \leqq 2.0$.[6]

(2) The theory calls for an intimate dependence of oscillations on space charge conditions. Several of the tubes tested in the course of an experimental investigation showed this dependence clearly in that the three-halves power law relating current to voltage was brought out in the oscillation behavior.

(3) The characteristics of Fig. 3 lead one to expect oscillations at the point where emission limitation of current sets in. This was found to be the case in many instances. According to Fig. (4), on the other hand, when corresponding to c but slightly greater than α, r_P is but slightly greater than $2r_G$, then oscillations may be expected even when the tube is in the space-charge-limited condition. This also, has been verified. But not all the experimental results can be handled so easily.

Many tubes fail to exhibit the space charge dependence of the oscillations through the three-halves power law. Another difficulty lies in the fact that the strongest oscillations occur with the plate at a negative voltage and only weak oscillations occur when the plate is positive as required by the theory. Once oscillations have begun one can understand how current can reach a negative plate and oscillations continue, but one would expect this voltage arrangement to be somewhat unfavorable. However, the outstanding phenomenon which is inexplicable on this theory is the frequency behavior of the oscillations.

In general, experimenters have found that tuning of the triode circuits affects the frequency but little, if at all. The frequency depends apparently on the time an electron remains in the grid-cylinder space. Thus the period of the oscillation is seldom very different from this time as calculated and the variation of this time with grid and cylinder voltages gives the approximate variation of the oscillation period.[7] To explain this behavior Gill and

[6] The experiments of Kapzov, Zeits. f. Physik **35** (2), 129 (1925) are of particular interest in this connection. Several tubes having $r_P/r_G \leqq 2.0$ oscillated with mercury vapor present but stopped oscillating as the pressure was reduced. The vapor may well cause a redistribution of potential that makes a virtual cathode possible.

[7] A. Scheibe, Ann. d. Physik **73**, 54 (1924).

Morrell[8] have advanced a dynamic theory. They considered a plane triode with plate at filament potential and, supposing electron currents to be so small that space charge played no part, they studied the energy interchanges between each electron in the grid-plate space and a small alternating electric field superposed on the static field between grid and plate. They found that as the impressed frequency is increased continuously, the a.c. resistance between grid and plate decreases to a maximum negative value at a period 1.33 times the time taken by an electron to travel from grid to plate and back to grid. Thereafter the resistance oscillates indefinitely as higher and higher frequencies are attained.[9]

Blurring effects probably prevent negative resistance in the overtones, leaving the fundamental as the only possible self-sustaining oscillation. This theory is thus able to explain the frequency behavior. Incidentally it requires zero voltage on the plate, which agrees with experiment better than does the static theory.

We have, then, two independent theories, each of which is capable of explaining those characteristics of the oscillations which the other cannot, and each supplements the other in its weakest feature. For, the dynamic theory applies directly to the high frequencies at which the static theory approaches the limit of its qualitative applicability, and the static theory handles space charge of such amount as to seriously complicate the dynamic theory. Accordingly, it appears highly probable that the Barkhausen-Kurz type of oscillation arises from a joint action of the two causes.[10]

In the near future I hope to publish the experimental results on which some of the general conclusions cited here are based.

RESEARCH LABORATORY,
GENERAL ELECTRIC CO.,
June 9, 1927.

[8] Gill and Morrell, Phil. Mag. **44,** 161 (1922).

[9] Through an oversight the authors have missed this feature in the behavior of the resistance. Referring to their table, p. 174, there is a region of positive work between $p=\pi/T$ and $p=2\pi/T$.

[10] Other theories have been proposed to account for these oscillations. Van der Pol, Physica **5,** 1 (1925) suggests that an excess of electrons returning through the grid causes a decrease in emission which later causes an excess emission, etc., thus setting up an oscillating condition. Several objections to this theory immediately suggest themselves. First, the frequency of oscillation calculates to one-half the actual value. Second, the electron excess combined with the deficiency would constitute a more nearly normal space charge, tending to decrease rather than accentuate the irregularity. Third, no oscillations could occur when the electron current is emission limited. J. Sahánek, Phys. Zeits. **26,** 368 (1925) has observed certain oscillations and proposes a theory which he believes may, with slight modification, be applicable to the Barkhausen-Kurz type. The theory is difficult to follow. It depends, apparently, upon the voltage drop along the filament. According to it oscillations are possible only when $2<r_C/r_G<5$, and it may give the correct value for the frequency.

ON THE MAGNETIC SUSCEPTIBILITIES OF VAPORS OF ORGANIC LIQUIDS

By V. I. Vaidyanathan

Abstract

The apparatus employed in this investigation consists essentially of a thin closed diamagnetic bulb suspended from one end of the beam of a modified Curie balance. The vapor under investigation surrounds this bulb. The complete balance is in an air-tight chamber of suitable shape. The bulb moves horizontally and at right angles to a non-homogeneous field, causing a twist in the suspension fibre of the balance beam. The diamagnetism of the bulb is compensated as nearly as possible by enclosing the requisite quantity of air, so that at room temperature there is very little magnetic force acting on it, if surrounded by a vacuum. Now if a diamagnetic vapor is introduced, the bulb apparently becomes paramagnetic and is drawn towards the stronger part of the field, and *vice versa* if a paramagnetic vapor be introduced. Values relative to air were obtained in all cases. All the vapors examined were diamagnetic. The molecular susceptibilities determined for the vapor state were in many cases nearly equal to those calculated from the liquid state, but in some cases they appear to be higher. This is specially true in the case of CS_2 and C_6H_6, the molecules of which are known to possess a high degree of magnetic anisotropy[1] in the liquid state. The results for these two substances await confirmation by independent investigations by other methods.

Introduction

NO LITERATURE seems to exist in connection with the magnetic susceptibilities of vapors. In the liquid state the problem has been extensively studied by Pascal, Henrichsen, Koenigsberger, Ishiwara and others. Many interesting conclusions emerged from Pascal's investigations of organic liquids and atomic susceptibility constants were deduced. In the investigation of molecular and atomic structure the diamagnetic susceptibilities of substances in the gaseous form are of greater interest than of those in the liquid state. Furthermore, a comparison of the gaseous and liquid states is of great importance as it might throw light on the still unsolved problem of the nature of the liquid state.

Experimental

The essential parts of the experimental arrangements are shown diagrammatically in Fig. 1. The magnetic balance consists essentially of a hollow glass bulb B, which is sealed and suspended by a silk loop from one end of a light aluminum bar AD, the latter being suspended by a torsion fibre. This bulb is blown out of feebly diamagnetic glass the diamagnetism being compensated as nearly as possible by enclosing within the bulb the requisite quantity of air and sealing its stem. It hangs in a suitable non-homogeneous field. The bulb C attached to the other end of the balance beam counterpoises the weight of B, and in addition its volume is so adjusted that the hydro-

[1] Raman and Krishnan, Proc. Roy. Soc. **A113**, 511 (1927).

static buoyancy due to introducing gases is completely neutralized. The balance chamber has a suitable shape and is perfectly air-tight. The balance is capable of moving within it over a short range without touching the walls. The concave mirror *M* serves in taking deflections of the beam by the usual lamp and scale arrangement. A side-tube attached to the balance chamber near the bulb *B*, carries a delicate thermometer.

When the magnet is excited the bulb *B* is slightly attracted or repelled in vacuum because of the imperfection in compensation and because of the fact that temperature fluctuations change the susceptibility of the contained air. By a proper rotation of the torsion head the beam is adjusted to lie along the axis of the chamber. If we introduce a diamagnetic vapor into the balance chamber, the bulb becomes apparently paramagnetic and is drawn towards the stronger parts of the field. On the other hand, if air or some other paramagnetic gas is introduced, the bulb appears to be diamagnetic to this

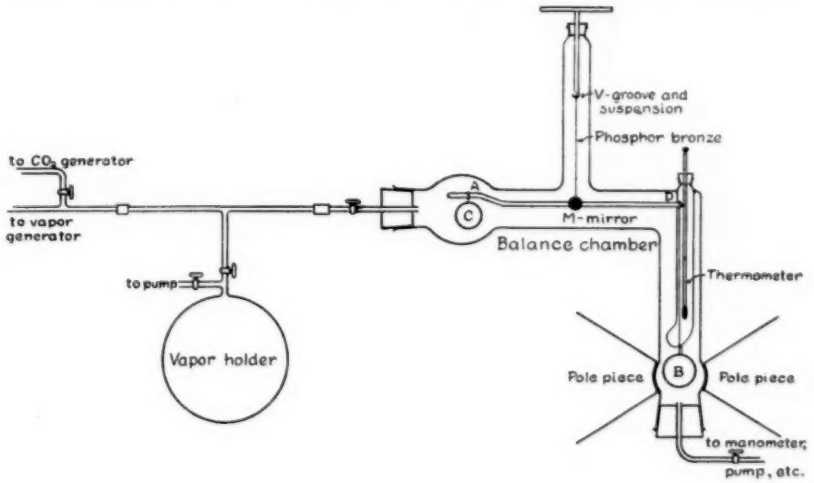

Fig. 1. Diagram of apparatus.

medium and is repelled. Preliminary adjustments were made so that *B* moves in a perfectly horizontal plane and at right angles to the non-homogeneous field causing a twist of the suspension fibre of the balance beam. From the deflections, values relative to air are obtained in all cases.

The sensitiveness was generally such as to produce a deflection of 2 to 4 mm of the spot of light on a scale placed at a distance of 100 cm, corresponding to the change of susceptibility caused by altering the pressure of air by 1 mm. Since in all cases, air was used to calibrate the scale and since the deflections with a diamagnetic gas are oppositely directed to those for air, the rotatable head was so adjusted after an experiment as to make it possible to have the calibration deflections cover the same range as those for the gas. When the sensitiveness was kept low, this adjustment was not found necessary. The field strength was generally about 2000 Gauss.

The vapor was generated from a bulb containing the pure liquid. To displace any trace of air in the vapor holder, carbon dioxide from a Kipp's

apparatus was passed through it for an hour; this was then pumped out and filled many times with the vapor.

The chief source of error is introduced by the rise of temperature due to the heating of the coils of the magnet and a correction is applied for this. There was some difficulty due to the absorption of the vapor by rubber cork surfaces and this was minimized by coating the inside with water glass. There were also oscillations of the balance caused by letting the vapor into evacuated balance chamber. These were reduced by careful manipulation of the taps. To avoid condensation of the vapor on the balance bulbs, the pressures at which measurements were made were less than the saturation pressures at atmospheric temperature.

Results

The results of one calibration are given in Table I.

Table I

Calibration with air.

Temperature	Pressure	Deflection	Temperature correction	Corrected readings
23.5°C	0 mm	300	0	300
23.7	9	271.5	2.4	274
23.9	16	251	4.8	256
24.2	24.5	229	8.4	237
24.5	33	210	12	222
24.7	40.5	194.5	14.4	209

On plotting the observations of the last columns, the gradient of the deflection-pressure curve is obtained and hence the number of divisions corresponding to the change in the volume susceptibility due to a change of 1 mm in pressure of air. This is equal to 2.44 divisions per mm at a mean temperature of 24°C.

The results for hexane vapor are presented in Table II.

Table II

Observations on hexane vapor.

Temperature	Pressure	Deflection	Temperature correction	Change of deflection	Relative pressure change	Change of deflection per mm
23.3°C	0 mm	256		39.1	114 mm	0.343
23.6	114	291.5	3.6			
23.9	14	253.5	−3.6	34.4	100	.344

Generally three experiments were conducted with each vapor, in some cases under different sensitiveness. Taking the volume susceptibility of air as 0.0308×10^{-6} at 0°C and 760 mm according to Také Soné,[2] the volume susceptibility of the vapor at the temperature of observation is obtained after the necessary corrections for the change of volume susceptibility of air according to Curie's law. The volume susceptibility of the vapor for the

[2] Také Soné, Phil. Mag. **39**, 305 (1920).

molar volume is calculated assuming it to obey Boyle's law. This is called the mol. susceptibility in Table III.

TABLE III

Mol. susceptibility of various substances in the vapor and liquid state.

Substance	mol. sus. $\times 10^6$ vapour	mol. sus. $\times 10^6$ liquid*
Methyl acetate	51	45, Pe. 45, A. 53, K.
Ethyl formate	50	45, Pe.
Carbon-tetrachloride	79	70, Hn.
Chloroform	73	70, Ml. 62, Hn.
Ether	70	60, A. 63, Hn.
N. Pentane	82	68, A.
N. Hexane	89	80, A.
N. Heptane	97	92, A.
Methyl formate	38	33, A.
Acetone	34	40, A.
Carbon disulphide	75	45, Hn.
Benzene	83	57, Pe. 56, B and Z.

* In L. B. Tables Hn, Henrichsen; Pe, Pascal; Ml, Meslin; K, Koenigsberger. A, Additive law. B and Z. Berkman & Zocher. Zeits. f. Phys. Chemie. **124**, 318 (1926). The molar susceptibilities are calculated to the nearest numbers from the data given by the authors.

On calculating the value of the susceptibility of the CH_2 group from the difference in the values for $C_3H_6O_2$ and $C_2H_4O_2$ it is found to be 11.2×10^{-6}, nearly the same as was deduced by Pascal from liquid measurements. Because of various experimental difficulties met with in the measurements in the vapor state, the results are accurate only up to about 6 percent.

DISCUSSION OF EXPERIMENTAL RESULTS

The susceptibility per gram molecule determined from the vapor state is in many cases nearly equal to that determined from the liquid state. In the case of CS_2 and C_6H_6 the gram molecular susceptibility in the vapor state appears to be much higher than can be accounted for by experimental errors. The two isomers methyl acetate and ethyl formate have the same susceptibility. In many organic compounds Oxley[3] found a change of susceptibility in passing from the crystalline solid to the liquid state. Honda[4] and Owen[5] found that many elements undergo a change of susceptibility at their melting points. Whether the approach of the neighboring molecules in the liquid state is sufficient to cause any such change as was observed in the cases mentioned above is now uncertain. As such an enormous difference as was observed in CS_2 is difficult to reconcile with our present state of knowledge, arrangements for further investigation by a different method are being made, and it is premature at present to attempt an explanation.

In conclusion I wish to express my gratitude to Professor C. V. Raman, F.R.S., at whose suggestion this problem has been taken up. The investigation was carried out in the Laboratory of the Indian Association for the Cultivation of Science.

CALCUTTA, INDIA,
May, 1927.

[3] A. E. Oxley, Phil. Trans. **A214**, 109 (1914).
[4] Honda, Ann. d. Physik **32**, 1027 (1910).
[5] Owen, Ann. d. Physik **37**, 657 (1912).

THE TROUTON-NOBLE ETHER DRIFT EXPERIMENT

By Carl T. Chase

Abstract

In view of recent theoretical investigations by Epstein which show that the sensitivity of this experiment is less than had been supposed and thus render inconclusive the previous performance of the experiment by the author, the experiment has been repeated once more with still greater sensitivity. The present apparatus should detect a motion in the ether of as low as 3 km/sec. and no such motion is found.

Introduction

If a parallel plate condenser whose plates are in a vertical plane and which is moving with respect to a stationary ether, is charged, there will under certain conditions exist a couple tending to rotate the condenser about a vertical axis. This couple is given by the expression[1,2]

$$K = (CV^2v^2/10\epsilon c^2)\sin 2\psi \sin^2 Z$$

where C is the capacity of the condenser; V, the potential to which it is charged; ϵ, the dielectric constant of the dielectric used in the condenser; v, the velocity of the condenser with respect to the ether; c, the velocity of light; ψ, the azimuthal angle between the direction of motion and the plane of the plates; and Z, the angle between the direction of motion and the vertical direction (the zenith distance of the direction of motion). This expression includes Epstein's correction[1] which made necessary a repetition of the experiment.

If the condenser is suspended by means of a delicate fiber, the angular rotation that will be produced by the couple can be computed when the elastic constants of the fiber are known.

The improvements in the present apparatus over the previous arrangement consist of the following: higher potential, better shielding from both temperature and electrostatic disturbances, finer suspending wires, and more suitable material for these wires. Also, the improved shielding makes possible the use of a greater scale distance.

Apparatus

The apparatus is in general similar to that which was used before, except that in this case the condenser is surrounded by a copper sphere specially spun for the purpose, instead of a cylinder. This sphere is 20 cm in diameter with walls 3 mm thick. The suspending wires (one above and one below the condenser) are of tungsten, 0.0013 cm in diameter and 90

[1] Epstein, Phys. Rev. **29**, 753 (1927).
[2] Chase, Phys. Rev. **28**, 378 (1926).

cm long. Means are provided for accurately and smoothly adjusting the height and angular position of the ends of these wires, either together or separately. The wires are protected by tubes of brass, each 2.5 cm in diameter and 100 cm long with walls 2 mm thick. Cylinders of hard rubber at the outer ends of these tubes insulate the wires from the case. A small mirror for observing deflections is fixed to a piece of No. 14 aluminum wire which is securely fastened to the lower terminal of the condenser. The mirror can be seen through a small hole in the lower tube just below the sphere, the hole being covered with mica.

The condenser is the same one that was used before, having a capacity of 0.04 mf and weighing 10 grams. It is built up of discs of mica and aluminum foil, and is 4 cm in diameter with a thickness of 3 mm. As before, it is wrapped with a coating of foil which connects to the lower terminal and completely covers the condenser except for a small space around the upper terminal. The period of the swinging condenser is 80 seconds, when suspended as described.

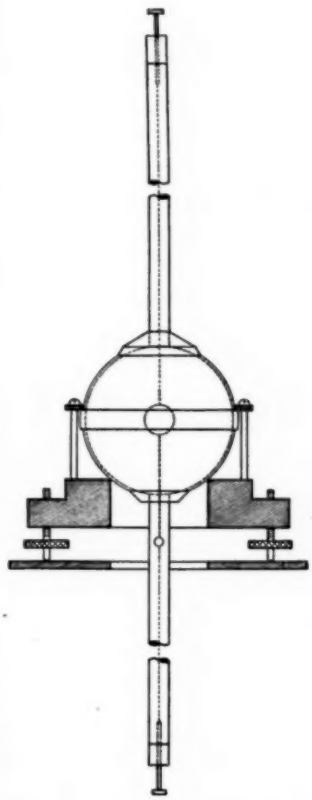

Fig. 1. Diagram of apparatus.

The potential is supplied by a storage battery giving 2420 volts and remained constant within 6 volts during a run. A resistance of 8000 ohms is placed in each battery lead, and the lower suspending wire (and thus the foil wrapping of the condenser) is connected to the case through a resistance of 50,000 ohms. The case is grounded.

The apparatus stands on a tripod made of a piece of boiler plate and three iron pipes. It is set up in the center of a constant temperature room below ground, in which the temperature variation during a run is less than two-tenths of a degree. The room is kept closed during and immediately before a run, observations being made from outside through a small hole in the wall in which a ground glass scale has been inserted. Deflections are observed by reading on this scale the position of the image of a galvanometer lamp as reflected from the mirror attached to the condenser. The scale distance is three meters, and under normal conditions readings can be taken to a tenth of a millimeter with confidence. A thermometer is hung near the instrument and is read from outside the room by means of a telescope.

Method of Observation

Observations were made every ten minutes for twelve consecutive hours. Although there is a certain advantage in continuing the observations for

twenty-four hours at a time, it was found impossible with the increased sensitivity to find twenty-four hours during which there would be no disturbances of sufficient magnitude more than to offset the advantages of the longer run. It was, however, possible to find twelve hour periods during which conditions were quiet enough to give significant results.

The condenser is charged and after a few moments five consecutive turning points of the lamp image are read. The battery is connected to the condenser during the whole time that the condenser is charged, in order that the potential shall remain constant. As soon as these turning points have been read, the condenser is discharged and at the next ten minute point five more turning points are read. Thus the condenser is allowed to swing for about five minutes after the switch has been thrown and before the readings are made, eliminating the effect of any possible shock or ballistic throw that might be caused by charging or discharging (such shocks are largely eliminated by the resistances in the battery leads), and one "resting point" is obtained for each ten minutes, alternately for the condenser charged and discharged. To obtain the deflections resulting from charging the condenser, any three consecutive resting points are used, say two for the condenser discharged and one for the condenser charged. The mean of the two discharged positions is subtracted from the charged position. Thus any zero drift is eliminated from the results, and one deflection is obtained for each ten minutes during the run.

RESULTS

The deflections observed during two of the runs for June, 1927, are plotted against time in Figs. 2 and 3, and a scale of corresponding ether drift velocities as computed by means of the above formula from the constants of the

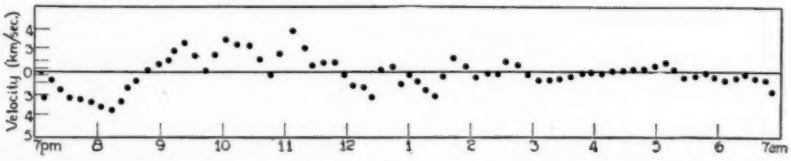

Fig. 2. Observed deflections, 7 P.M. to 7 A.M., E. Std. Time. Condenser in East-West plane.

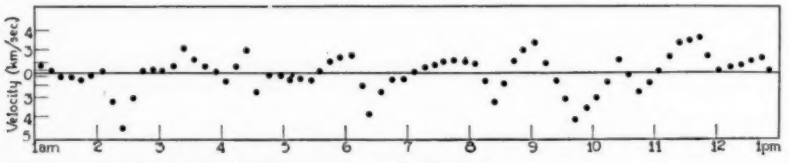

Fig. 3. Observed deflections, 1 A.M. to 1 P.M., E. Std. Time. Condenser in East-West plane.

apparatus is given. A velocity of 3 km/sec. should give a deflection of 5 mm, 6 km/sec. should give 21 mm deflection, and so on. There appears to be no systematic change in the deflections that would correspond to a velocity in a stationary ether of more than 3 km/sec.

Conclusion

Thus the experiment has been repeated with sufficiently increased sensitivity to compensate for theoretical reduction in the sensitivity of the experiment. The apparatus should detect a motion in the ether as small as 3 km/sec., and no motion is detected.

The author wishes to express his thanks to Professor G. W. Pierce for putting the facilities of Cruft Laboratory at his disposal, and for his interest as the work progressed. He also wishes to thank Messrs. E. W. Pike, H. A. Blackmun, D. P. Adams, and F. V. Hunt for their invaluable and voluntary assistance in making the observations.

Cruft High Tension Electrical Laboratory,
Harvard University,
June 28, 1927.

AN OPTICAL DETERMINATION OF AXIAL STRESSES IN LONG RECTANGULAR PLATES UNDER TORSION

By Isay A. Balinkin

Abstract

The use of polarized light is extended to the determination of the distribution and evaluation of axial stresses in long rectangular plates subjected to torsion. The equation connecting the stresses, σ, with the distance from the axis of rotation, r is

$$\sigma = \frac{1}{2}\frac{E\varphi^2}{l^2}\left(r^2 - \frac{l^2}{12}\right),$$

from which it follows that the compression along the central axis is half as large as the tension along the edges. A new photometric method for measuring the stress intensities was employed. As a photometer, a selenium cell with a narrow window was used; and it is suggested that the photo-electric cell may be applied to this purpose with great advantage.

Introduction

A PHOTO-ELASTIC method of determining stresses and their distribution can be successfully used only in case of "two-dimensional" problems. Although the actual problems in elasticity involve three dimensional bodies, it is possible in certain cases to investigate the stress distribution by means of polarized light, as if the stresses were in one plane.

In order to be able to reduce a problem by one dimension we have to assume that the stresses along the direction of the polarized ray do not affect the state of polarization. Also, the type of problem must be such that either the stresses are the same in all vertical parallel planes or for the case of "generalized plane stresses," they are a known function of the distance.

The relative retardation of the two trains of waves, into which a plane polarized beam is decomposed when passing through a transparent specimen under stress, is expressed by

$$R = C\int_0^t (P-Q)dt \qquad (1)$$

where $(P-Q)$ is the difference in the principal stress intensities in the plane perpendicular to the ray of light, C is a constant depending upon the optical characteristics of the material, and t is the thickness of the specimen. It is important to notice from Eq. (1) that stresses along the axis of the propagated ray have no effect on R which is the relative retardation of the two trains of waves with their corresponding electric and magnetic vectors perpendicular to one another.

It would be very desirable to extend the photo-elastic method to problems involving torsion. This field is in great need of an experimental means for

determining shearing components since, although mathematical analysis provides solutions for a number of cases, yet they are limited to the consideration of infinitesimal strains.

The present paper takes up the question of evaluating, by the use of polarized light, the axial stresses produced in long rectangular plates which are subjected to torsion. When a beam of light passes through a plate subjected to torsion and introduced between crossed Nicols, two black parallel lines appear on the screen indicating the position of the neutral axes. These two neutral axes are due to the secondary axial tensional and compressional stresses parallel to the axis of twist. There is also one neutral axis passing through the central points in the cross-sections where the shear stresses are absent. Thus, in a long rectangular plate under torsion, we have to distinguish one neutral axes passing through the points of zero shear, and the other two passing through the points of zero axial stresses in the plane of the twisted plate.

Analytical Theory

When a couple M is applied to one end of a long plate, a shearing strain is created within the body, involving two simple shears at each point. One of these shears is in the plane perpendicular to the axis of rotation and the

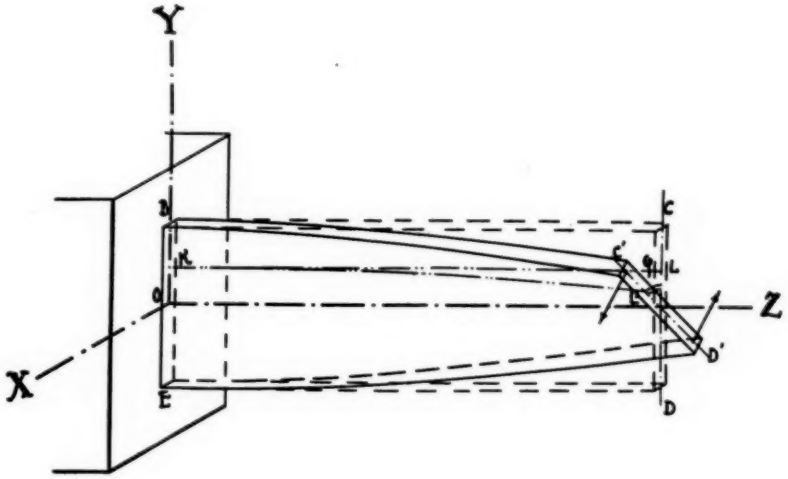

Fig. 1. A long rectangular plate under the action of a turning moment.

other is a longitudional displacement along the centarl axis. The latter produces a distorsion in the non-circular cross-sectional planes.

The following is essentially C. Weber's[1] derivation of axial stresses in terms of the modulus of elasticity E, angle of twist ϕ, and the dimensions of the plate.

When a plate, as in Fig. 1, is twisted through an angle ϕ from the position $BCDE$ into $BC'D'E$ a straight line element, KL, of length l at a distance r

[1] "Die Lehre der Drehungsfestigkeit" Forschungsarbeit Heft 249 des Vereines Deutscher Ingenieure (V. D. I).

from the Z axis is changed into a helix whose length is given by

$$s=(l^2+r^2\phi^2)^{1/2}$$

The increase in length is

$$\Delta l=(l^2+r^2\phi^2)^{1/2}-l$$

and, on expanding the first term and neglecting the higher powers of ϕ and r, we obtain

$$\Delta l=r^2\phi^2/2l$$

The strain due to this elongation is $r^2\phi^2/2l^2$ and therefore the stress

$$\sigma'=E\Delta l/l=Er^2\phi^2/2l^2$$

The total force necessary to retain the elements of the surface $C'D'$ at their original length l from the XY plane is

$$Z'=\int(Er^2\phi^2dA/2l^2)$$

where A is the area of the rectangular section CD. Evaluating this force we get

$$Z'=(E\phi^2/2l^2)\int_{-b/2}^{+b/2}\int_{-h/2}^{+h/2}(x^2+y^2)dx\,dy$$
$$=E\phi^2bh(b^2+h^2)/24l^2$$

Since there is no external force acting at the end of the plate, the stress produced by Z' will be equally distributed over the cross-section bh and we can compute its intensity

$$\sigma''=-Z'/\int dA=-E\phi^2(b^2+h^2)/24l^2$$

Evidently, the final stress intensity parallel to the axis is the summation of σ' and σ''

$$\sigma=\sigma'+\sigma''=\frac{1}{2}\frac{Er^2\phi^2}{l^2}-\frac{1}{24}\frac{E\phi^2}{l^2}(b^2+h^2)$$
$$\sigma=\frac{1}{2}\frac{E\phi^2}{l^2}\left(r^2-\frac{b^2+h^2}{12}\right).$$

Considering σ as a function of r, we can readily see that $\sigma=0$ when

$$r=r_0=\pm\left[(b^2+h^2)/12\right]^{1/2}$$

Thus, at a distance r_0 on either side of the axis Z, the axial stress falls to zero and we have two neutral axes. When r is less than r_0, σ is negative and the central part of the plate is in the state of compression; similarly, places in the plate where r is larger than r_0 must be in a state of tension.

The maximum tension and compression are

$$\sigma(\text{max. compr.}) = E\phi^2h^2/24l^2$$
$$\sigma(\text{max. tens.}) = E\phi^2h^2/12l^2$$

Thus, the maximum tension at the edges of the twisted plate is twice as large as the maximum compression along the z axis and this ratio is independent of the angle of twist, ϕ.

Description of the Apparatus and the Experimental Methods

The experimental proof of the preceding mathematical analysis is shown by the following demonstration. Two Nicol prisms, $2'' \times 1\frac{1}{2}'' \times 5''$ with their principal planes at right angles, were mounted on an optical bench and a "half wave-length plate" method was used to set them exactly at 90°.[3]

A 1000-watt Mazda lamp was used as a light source. On account of the photometric measurements of stresses, it was of considerable importance to maintain the light source at constant intensity. The lamp was connected to a d.c. storage battery, and with a regulating resistance in series, it was possible to keep the voltage constant within one tenth of a volt.

A specimen plate of transparent celluloid, Fig. 2, was fixed between the parallel jaws of two chucks A and B, of which A was stationary and B

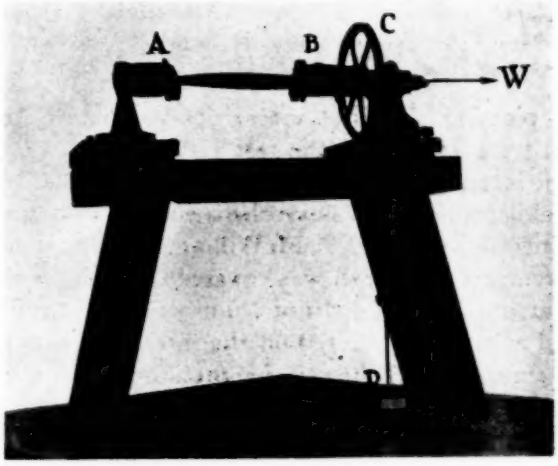

Fig. 2. Apparatus for twisting and examining long plates between crossed Nicols.

could be rotated through an angle measured by a divided circle, C. The first chuck was set back at an angle equal to one half of the final angle of twist so as to leave the central part of the specimen perpendicular to the direction of the ray.

A preliminary investigation of the compressional stresses along the Z axis was first carried out by applying a tensional force, W, and measuring the distances between the two neutral axes. The head A was permanently connected to the table, while B was placed on smooth rollers permitting free

motion along the axis. The effect of applying an axial tension was to reduce the compression in the central part of the plate, and thus shift the two neutral axes nearer to the center. When they were made to coincide the stress due to the outside load, W, was equal to the maximum axial compression. This is clearly shown in Fig. 3.

This method of determining the distribution of axial stresses could be extended also to the part of the plate in tension, by introducing a separate tension piece perpendicular to the axis. It proved, however, to be difficult to record exactly the distances between the neutral axes, since they were not sharply defined. A purely photometric method of measuring the stress distribution was devised and applied successfully to this problem.

When a tensional stress is exerted on a plate placed between two crossed Nichols the field, originally dark, grows brighter with an increasing stress. This suggests that the measure of the light intensity could be utilized for the measurement of the stresses. In the first place a calibration curve was

(*a*) (*b*) (*c*)

Fig. 3. (a) Two neutral axes in a long plate under torsion, when examined between crossed Nicols. (b) The distance between the axes decreases as tension is applied at the ends. (c) One neutral axis is shown when the outside tension is equal to the compression in the central part of the specimen.

constructed, by plotting the light intensities against the measured stress intensities which were applied to the test piece.

A photometric instrument suitable for this purpose must be able to explore a very limited field at a time and have also a comparatively high sensitivity, especially for a low illumination. A McWilliams' selenium cell[3] was adopted for these measurements. The cell was covered completely with black paper leaving only a narrow horizontal slit of 2 mm width. An indicator, attached at the same level as the slit, pointed on the screen the exact place at which the intensity was measured. The cell, mounted on a cathetometer, could be easily set at any desired position in the projection of the specimen on the screen. The resistance of the selenium cell at different positions along the vertical line was measured by means of a Wheatstone bridge. The effect of fatigue was eliminated by taking the mean of the two readings while the load was gradually increased and then decreased.

Calibration Curve

The calibration curve will have to show the relation existing between the intensity of stress and illumination, or in the case of a selenium cell it will be a relation between the stress intensity and the resistance of the cell.

[2] A. Schuster, Theory of Optics, 123, 3rd edition.

[3] McWilliams, Photo-electric cells and amplifying relays catalog number two.

All specimens, including test pieces for the calibration curve, were cut from the same sheet of celluloid in order to assure the uniformity of their elastic characteristics. Acknowledgments and thanks are due to the Du Pont Viscoloid Co. for the supply of remarkably transparent celluloid without initial stresses.

A narrow plate of celluloid was firmly fastened in the chucks A and B, an axial pull applied to it, and the resistance of the cell measured. In the range of the variation of the stress between 0 and 40 kg/cm², it was found that the corresponding variation in the resistance of the cell due to the change in the intensity of illumination was from 510×10^3 to 250×10^3 ohms. From these data a stress-resistance curve was plotted, as shown in Fig. 4.

Results

The curve obtained for the stress distribution will be given only for one case which is taken as the average of a number of plates investigated by the

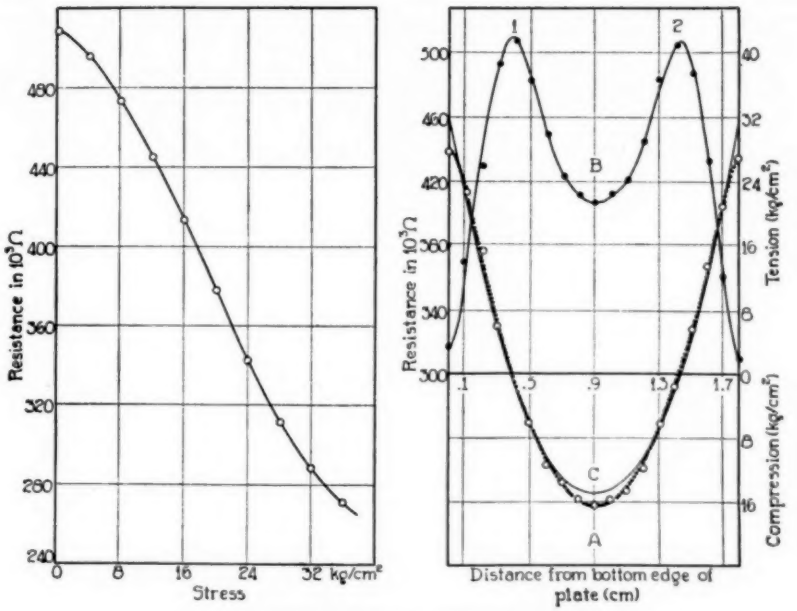

Fig. 4. Stress-resistance calibration curve.

Fig. 5. Curve A represents the axial stresses as determined from curve B by the use of the stress-resistance calibration curve in Fig. 4. Curve C represents the computed stresses.

method described in this paper. The dimensions of the specimen were as follows: length between the jaws $l=14.4$ cm, width $h=1.8$ cm, thickness $b=.195$ cm. Young's modulus $E=21650$ kg/cm², and angle of twist $\phi=60°$.

The curve, B in Fig. 5 gives the values of the resistance of the cell, when its slit was placed at different positions along the width of the plate. Points 1 and 2 of maximum resistance correspond to the two black neutral lines in Fig. 3. Referring back to the calibration curve, Fig. 4, and changing the units of the ordinates into kg/cm² we can plot in the same coordinate plane the actual distribution of stresses, which gives the curve A.

When constants for E, ϕ, l, and h are substituted in the equation

$$\sigma = \frac{1}{2} \frac{E\phi^2}{l^2}\left(r^2 - \frac{h^2}{12}\right),$$

we can plot the relation between the distance r and the axial stress σ. This is shown on the same Fig. 5 by the curve C.

Conclusions

The axial stress distribution as determined by the photo-elastic method shows a close agreement with the stresses calculated by mathematical analysis. This speaks well for the rigor of the latter, and it certainly must increase our confidence in the photo-elastic method of stress determination. The photometric evaluation of the stress intensities was successfully performed by the use of the selenium cell, although some difficulty was experienced because of the effect of fatigue. This difficulty could be overcome by the use of a photo-electric cell.

It is the author's pleasure to express his grateful thanks to Dr. L. T. More and Dr. R. C. Gowdy for guidance received throughout the course of this investigation.

University of Cincinnati,
Graduate School, Physics Department,
July, 1927.

EVAPORATION FROM LAKES

By N. W. Cummings and Burt Richardson

Abstract

Evaporation can be determined by the aid of the first law of thermodynamics in such a way that wind velocity need not enter the calculation. Air temperature and humidity enter only as terms in a correction which can have a relatively small average value under typical conditions. The complete equation is

$$E=(H-S-C)/L(1+R)$$

where E is the evaporation, H the difference between the incoming and outgoing radiation, S the heat stored in a column of water having unit cross-section, C a correction for heat carried by flowing water and leakage of heat through the walls of the vessel, L the latent heat of water, and R is Bowen's ratio. A method of finding the difference between the incoming and outgoing radiation, by means of observations on a well insulated pan is described, and also a method of finding the ratio of sensible heat to latent heat transmitted through the air-water surface. Bowen's theoretical conclusions respecting this ratio were found to be consistent with observations.

The above formula can be used in estimating evaporation from an actual lake whenever the requisite data can be obtained. Although from a physical standpoint the quantity of sensible heat passing through the air-water surface is not strictly negligible, nevertheless is most meteorological and engineering applications, the error caused by neglecting this quantity will be negligible in comparison with other errors that enter the main problem of which evaporation is a part.

Introduction

IT HAS long been customary to estimate evaporation from lakes on the basis of observations on pans in the vicinity, but there has been no means of showing conclusively that the error thus involved is not excessive. Thus, pans of different sizes are known to have different depths of evaporation[1] and this obviously means that the depth of evaporation from a lake cannot in general be the same as that from any particular pan. If the theory described in this paper proves to be correct, substantial progress in the evaluation of evaporation from lakes will have been made.

Theory

Evaporation must obviously be uniquely determined by the energy that is rendered available for that purpose. Expressed as an equation this is

$$E=(I-B-S-K-C)/L \qquad (1)$$

where E is the evaporation expressed in centimeters of depth, I is the incoming radiation per square centimeter of surface, B the back-radiation to thesky, S the heat consumed in warming the water, K a correction due to heat derived from the air or given up to the air as sensible heat, C a combined correction

[1] R. B. Sleight, Jour. Ag. Res. **10**, 209 (1917).

for heat leakage through the walls of the container, expansion of the water, and in the case of a lake, for heat carried by flowing water. It is supposed that all the quantities in the numerator are expressed in gram calories per square centimeter of open water surface and are to be integrated over the same time interval as E.[2] The heat of vaporization of water expressed in gram calories per cubic centimeter is denoted by L.

If it is possible to observe all the elements on the right side of Eq. (1) except K, then to compute K by means of a certain equation derived by Bowen,[3] which will presently be stated, and finally to compare the right side with the observed evaporation placed on the left side, the agreement between the right and left sides will not only constitute a check on Bowen's equation, but it will also show whether or not evaporation can be computed without making any measurements of wind velocities, as the general theory demands. The elimination of wind from evaporation calculations is one of the fundamental ideas previously emphasized by one of the present writers.[4]

Such a comparison of the right hand side of Eq. (1) with the observed evaporation has virtually been made, though in order to avoid the necessity of measuring I and B directly, a slight variant on the above procedure was adopted, as follows:

We first introduce the quantity R as defined by the relation

$$LER = K \tag{2}$$

This means that R is the ratio of sensible heat swept away by the wind to latent heat carried off by the vapor. This ratio has been discussed by Anders Angstrom,[5] the Swedish meteorologist, who finds that it averaged less than 0.10 for the North Atlantic during the forepart of September, 1905. Angstrom concluded that R is in general relatively small, but until now it has been extremely difficult to obtain extensive and reliable information with regard to this quantity. However, Bowen has recently given us an equation which makes it possible to compute R from ordinary atmospheric data, without knowing either the sensible heat or the latent heat separately. His equation is

$$R = 0.46 \frac{t_1 - t_2}{p_1 - p_2} \frac{P}{760} \tag{3}$$

where $(t_1 - t_2)$ is the difference between the temperature of the air and that of the water surface, and $(p_1 - p_2)$ is the difference between the vapor

[2] It may not be obvious that S and C can be thus expressed, but if the total amount of heat stored in the entire lake or entering by the methods to which C refers be divided by the lake surface-area, then a definite part of each of these total quantities of heat will be allocated to a column under each square centimeter. By thus centering attention on a column of water having a square centimeter cross-sectional area and a depth equal to the average depth of the lake we make all the quantities in the numerator comparable and can express them in the same units.

[3] I. S. Bowen, Phys. Rev. **27**, 779 (1926).

[4] N. W. Cummings, Jour. of Electricity **46**, 491 (May 15, 1921).

[5] A. Angstrom, Geografiska Annaler **3**, 13 (1920).

pressure of the moisture in the air and the pressure this would have if the air were saturated at the temperature of the water surface, while P denotes the barometric pressure expressed in millimeters. Eqs. (2) and (3) together serve to eliminate K from Eq. (1) and to express the quantity R in terms of easily measurable magnitudes.

Next, after substituting $L\ E\ R$ for K in Eq. (1), we solve for $(I-B)$, which will hereafter be denoted by H. This is really the difference between the solar and sky radiation which penetrates the water surface, and the energy which the water body radiates back to the sky. For convenience it will be called the *heat budget per square centimeter of surface.*

$$H=I-B=S+LE(1+R)+C \tag{4}$$

Now I must be the same for all water surfaces exposed to the same external conditions whether the water bodies are shallow and heat up rapidly or deep and therefore change slowly in temperature. This equality does not necessarily hold for B, however, because if two bodies of water have different temperatures they must radiate energy at different rates. For two surfaces exposed to the same conditions we can evidently write from Eq. (4) on account of the equality of I_1 and I_2

$$B_1-B_2+S_1+LE_1(1+R_1)+C_1=S_2+LE_2(1+R_2)+C_2 \tag{5}$$

Since Bowen has pointed out that water radiates practically like a black body[6] because it almost completely absorbs low temperature radiation we may compute B_1-B_2 by means of Stefan's law, thus

$$B=49.5\times10^{-10}T^4 \text{ gram calories per sq cm per hour.} \tag{6}$$

Because T_2-T_1 in our application does not exceed 15°C and T_2 and T_1 are always between 0°C and 35°C we may calculate B_1-B_2 with sufficient accuracy if we differentiate Eq. (6) with respect to T and substitute 290 for T, obtaining

$$dB/dT=198\times10^{-10}\times(290)^3=0.5 \text{ calories per sq cm per hour} \tag{7}$$

and then multiply by the difference between the temperatures of the two surfaces. These considerations make it possible to subject Eq. (5) to experimental test.

Experimental Procedure

Some of the experimental work was done in Pasadena and some in Fort Collins, Colorado. At both places two bodies of water were used, one being contained in a tank and the other in a pan, the same pan being used in both cases. The dimensions of the vessels are as follows:

	Pan	Tank Pasadena	Tank Fort Collins
Area	0.37 sq. m.	2.2 sq. m.	520.0 sq. m.
Depth of vessel	0.19 m.	1.47 m.	2.0 m.
Depth of water below rim	0.01 m.	0.02 m.	0.07 m.

[6] See also Abbot, Annals of the Astrophysical Observatory, vol. IV, p. 291.

Both vessels used in Pasadena were thoroughly insulated, but corrections were applied to take account of such small quantities of heat as did leak through the walls. At Fort Collins the tank was so large as to render insulation unnecessary

The evaporation loss was determined by observing the amount of make-up water required to bring the level back to a predetermined height defined by a wire projecting upward from below the surface The error of this measurement lay between one tenth and two hundredths of a millimeter. The surface temperature of each body of water was measured by means of a mercury in glass thermometer graduated in tenths, but for the change in temperature, a Beckman instrument readable to one thousandth of a degree centigrade was used. The water was stirred before reading the volume temperature. The air temperature and absolute humidity were obtained by an Assmann psychrometer.

Since Eq. (3) was derived for instantaneous values of the variables, continuous records for the entire time interval should be used, but in this work hourly readings were used, which prove to be a good substitute.

Bowen's value of K was checked experimentally by many runs: one especially interesting run was made Oct. 24, 1925 when the pan was maintained for seven hours at 30°C by a measured amount of electric energy, and when this injected energy was deducted a value of H was obtained which agreed well with the one computed from the tank by the aid of the theory.

TABLE I.

The number of gram calories per square centimeter per day making up each term of Eq. (1).

Pasadena, California June 23, 1926–July 3, 1926.										
Day	1	2	3	4	5	6	7	8	9	10
Tank Evaporation (E)	376.8	339.3	343.4	379.1	426.1	439.0	470.8	446.9	436.1	425.5
" Warming (S)	40.1	−8.3	100.2	154.3	15.3	108.0	−31.0	−69.7	−85.0	15.4
" Convection (K)	64.4	80.3	54.0	−2.8	5.4	15.7	51.5	91.4	83.4	80.4
" Heat Budget ($I-B$)	481.3	411.3	497.6	530.6	446.8	562.7	491.3	468.6	434.5	521.3
Pan Evaporation	393.6	394.2	399.0	507.3	489.1	436.6	500.2	359.8	343.8	445.8
" Warming	34.8	−7.5	−32.1	−56.7	18.6	−9.8	46.8	65.9	−28.9	−64.6
" Convection	60.9	57.8	60.7	45.3	16.1	2.6	2.1	50.9	62.5	72.5
B_1-B_2	−27.7	−37.8	−32.7	−20.7	−8.3	−9.4	−1.0	−17.0	−23.5	−10.2
Pan Leakage (C)	30.1	27.5	29.8	24.8	14.1	4.8	10.2	28.1	30.8	34.8
" Heat budget	491.7	434.2	424.7	500.0	529.8	424.8	558.3	487.4	384.7	478.3

Fort Collins, Colorado September 15–25, 1926.										
Day	1	2	3	4	5	6	7	8	9	10
Tank Evaporation	171.7	145.3	127.0	134.1	124.3	231.1	224.6	155.4	291.9	246.1
" Warming	85.0	79.9	13.6	83.3	−57.8	44.3	78.2	11.8	−168.3	−333.2
" Convection	3.5	4.6	29.3	27.6	40.1	−10.2	−7.9	39.3	69.2	142.5
" Heat budget	260.2	229.8	169.9	245.0	106.6	265.2	294.9	206.5	192.8	55.4
Pan Evaporation	272.3	237.5	166.9	191.3	119.7	345.5	322.1	223.8	309.5	131.9
" Warming	2.4	41.2	−21.8	49.7	−19.6	5.4	27.3	−58.1	−130.5	−80.0
" Convection	7.2	−22.4	13.1	15.8	28.2	−46.0	−37.5	41.7	26.2	66.5
B_1-B_2	−22.5	−23.8	−20.7	−24.7	−41.5	−16.1	−20.3	−15.4	−62.6	−140.2
Pan Leakage	10.0	−0.7	16.1	18.1	18.8	−14.6	−7.9	33.7	31.4	48.8
" Heat budget	269.4	231.8	153.6	250.2	105.6	274.2	283.7	225.7	174.0	26.8

Two runs of ten days each were made under quite dissimilar circumstances, the first in Pasadena June, 1926 and the second in Fort Collins September, 1926. The results of these experiments indicate the relative importance of each factor in the evaporation equation.

Comparison with Theory

Eq. (4) was used to compute H, the heat budget, or the resultant radiation for each body of water. The correction $B_1 - B_2$ was calculated by means

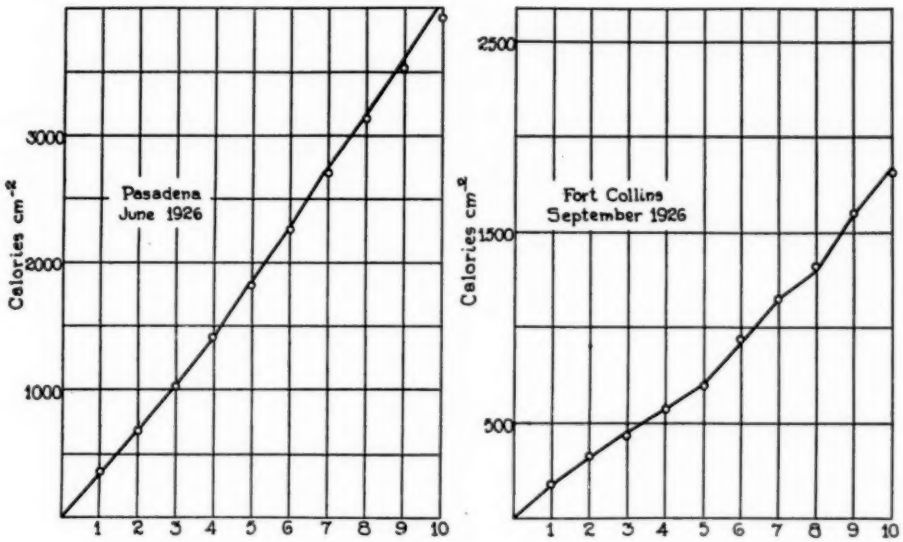

Fig. 1. Ten day summation curves for Pasadena, June, 1926, and Fort Collins, September, 1926, where solid lines represent the observed tank evaporation in calories per sq cm and the lines of circles indicate the tank evaporation calculated from the pan data.

of Eq. (7) and applied to the budget of the pan in order to reduce H of the pan to the temperature of the tank as indicated by Eq. (5). This process

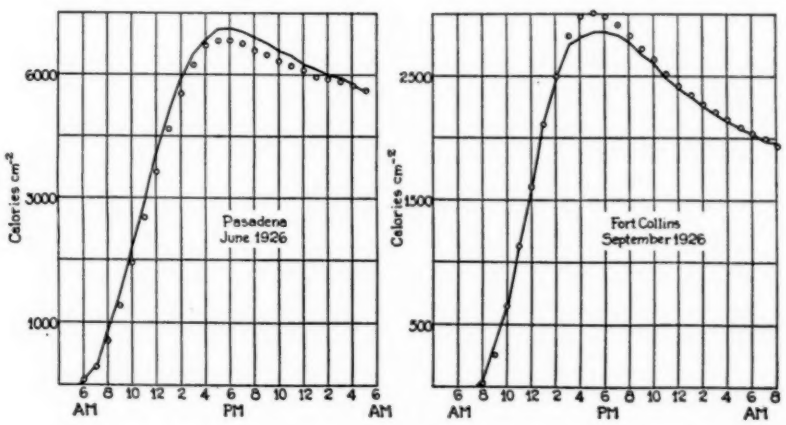

Fig. 2. Summation curves for Pasadena, June, 1926, and Fort Collins, September, 1926. The solid lines represent the heat budget of the tank for a particular hour measured on ten consecutive days, and the lines of circles indicate the same for the pan.

should then have brought the two budgets into agreement, which it did. For the purpose of comparison, cumulative heat budgets (obtained by a

process of continued summation for each body of water) were used. Table I gives the numerical values of the various terms of the evaporation equation as they were determined by the ten day runs at Pasadena and Fort Collins.

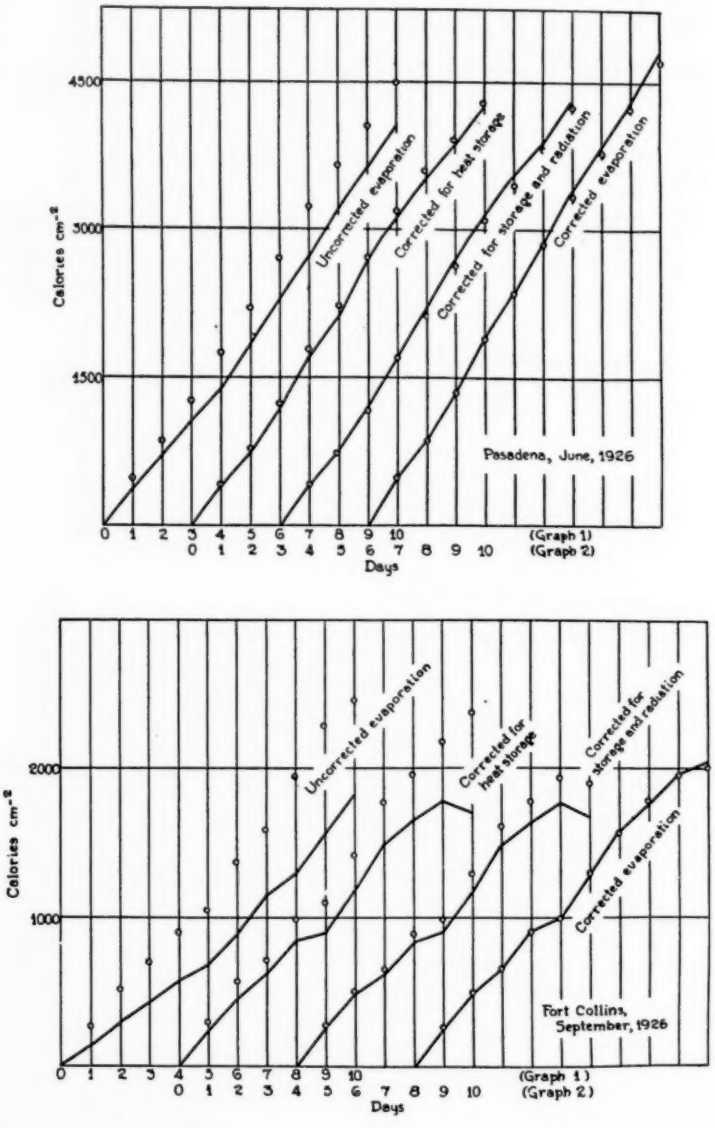

Fig. 3. Curves which indicate the marked improvement in the correspondence of the tank (solid lines) and pan (lines of circles) evaporations upon the introduction of corrections for heat storage, back radiation and convection losses.

Fig. 1 presents the Pasadena and Fort Collins runs where the observed and calculated evaporations have been plotted against time.

Fig. 2 presents Pasadena and Fort Collins summation curves of the tank and pan heat budgets of a particular hour of the day; here the budgets of

such an interval of time—say from 9 to 10 A.M.—have been computed on ten consecutive days and added. The slopes of these curves show that radiant energy starts to produce an effect upon a body of water at an early hour in the morning, increases until noon (point of maximum slope), and then decreases until evening, after which time and during the night the body of water radiates to the sky.

Fig. 3 shows for Pasadena and Fort Collins respectively the relative value of each of the correction terms in the evaporation equation. It is evident that the uncorrected evaporations disagree widely in all cases. In Pasadena the most important correction was heat-storage while in Fort Collins it was back-radiation.

Fig. 4 shows the record of a thermo-electric pyranometer and the heat budgets of the tank and pan plotted against time over a ten day period in Pasadena.

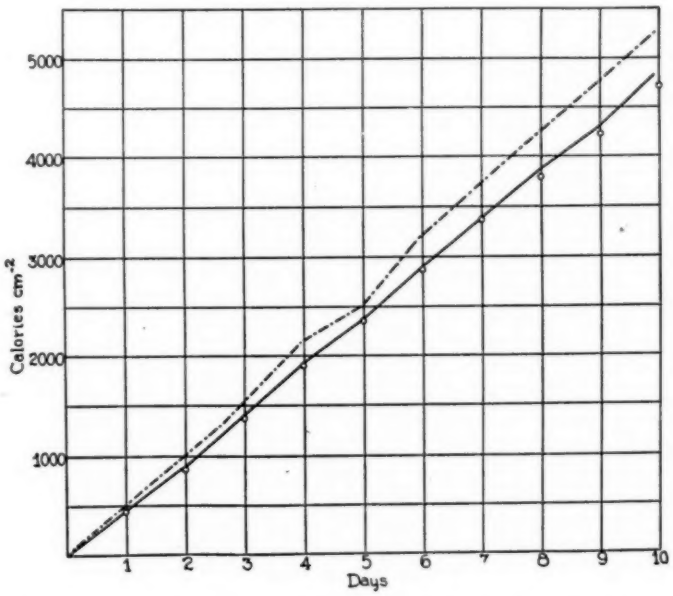

Fig. 4. Pasadena, June, 1926. Curves show the record of a thermo-electric pyranometer (broken line) and the summation heat budgets of the tank (solid line) and pan (line of circles) over a ten day period.

From a study of the graphs and Table I it is seen that by using Bowen's theory we bring into agreement the two heat budgets which we believe on the basis of the conservation of energy ought to agree. In other words, the theory works, and on this ground it is justified. The foregoing is therefore a correct method of computing H. It follows that we can take the pan to a lake, compute H as has been done here, and, after making the B_1-B_2 correction, apply this H to the lake. We may then determine S, R, and C for the lake and compute E by the following equation

$$E=(H-S-C)/L(1+R) \tag{8}$$

which is obtained from Eq. (1) on substituting $L\ E\ R$ for K and solving for E. It will be seen that wind-velocity does not enter this equation.

This can be taken as the primary standard for calibrating all other methods of determining lake evaporation. Other equations such as that of Dalton contain certain empirical constants which can only be evaluated when a series of real lake evaporations are known. The procedure outlined herein furnishes the only method thus far devised for ascertaining these required lake evaporations with satisfactory precision and reliability. Like most primary standards this method is difficult to apply because of the necessity of hourly readings. However, for many purposes where great accuracy is not required the work can be shortened considerably by adopting empirical constants.

On superficial examination it might appear that this research is nothing but a comparison of evaporation from two vessels of different dimensions, with certain corrections applied. As a matter of fact it is more than that. While it is true that H has been determined by means of observations on the pan, nevertheless this was merely an expedient that had to be resorted to because as yet no technique has been developed for measuring B with satisfactory precision and convenience. If such a technique ever is developed, then lake evaporation can be found without using any pan and without making measurements of wind velocity. Moreover, if it turns out that the effect of the atmosphere in causing a transfer of sensible heat really is small under conditions that might be called normal—which is not unlikely—then air temperature and humidity need enter the calculations only as terms in a relatively small correction which for many purposes may be neglected entirely. Obviously then it is worth while to accumulate as much information as possible in regard to the value which R assumes at various places and various times of the year. This can be done by means of Bowen's equation, when the requisite wet and dry bulb and water temperatures become available.

In conclusion the writers wish to express their appreciation of the many helpful suggestions they have received from Dr. Millikan and other members of the California Institute faculty, and of the assistance given by Paul Richardson in carrying out the observations. Also thanks are extended to R. L. Parshall of the U. S. Department of Agriculture for making possible the use of certain tanks at Fort Collins, Colorado.

Norman Bridge Laboratory of Physics,
California Institute of Technology,
Pasadena, California,
May 16, 1927.

BOOK REVIEWS

Atomic Theory. ARTHUR HAAS, PH. D.—Translated from the German by T. Verschoyle, Ph. D. As the translator says, the text of this book is practically identical with that of Part 3, Vol. II of the author's "Introduction to Theoretical Physics." It covers the whole field of atomic theory about as it was known in 1924. A few notes are added to bring the subject matter up to date, but generally speaking, the extremely interesting recent developments are not included. Among the most important errors may be noted the statement on page 185, than an n-quantum atom can only assume $2n$ positions in a magnetic field. The note on page 160 describing methods of predicting the spectral terms of atoms having several valence electrons is in some ways misleading. The translation is an excellent one and the book will be extremely useful to many persons approaching the subject for the first time. It is interesting to note in connection with the treatment of the hydrogen atom a fact which is often overlooked, —that the author obtained a derivation of the Balmer formula using the Thomson atom, in 1910, correct in all respects except for a numerical factor multiplying the Rydberg constant R. Pp. 222+xiv, 114 figs. D. Van Nostrand Company, New York, 1927. Price $3.50.

ARTHUR E. RUARK

Molecular Spectra in Gases. EDWIN C. KEMBLE, RAYMOND T. BIRGE, WALTER F. COLBY, F. WHEELER LOOMIS, LEIGH PAGE. Bulletin of the National Research Council, Vol. 11, Part 3, Number 57.—This Report deals comprehensively with the quantum theory interpretation of the spectra of diatomic molecules in the gaseous state. Hitherto only comparatively brief accounts of the subject have existed (cf. Report, p. 70), *e. g.*, the excellent chapter in Sommerfeld's Atombau, and the Report therefore fills what was a serious gap in the literature. In addition to being a review and compilation, it contains much material not previously published, especially in the chapters by Kemble and Birge. There are numerous helpful figures, and reproductions of spectra. The lack of an index is however unfortunate. The opportunity of obtaining this work bound in cloth will be appreciated by many.

Chapter I, by Kemble, is an instructive brief historical discussion of the development of the quantum theory of band spectra. Chapter II, by Page, is an account of the (old) quantum theory and its application to the rotator and anharmonic oscillator, including correspondence principle, selection rules, and band spectra. In Chapter III, Colby treats first the subject of infra-red absorption bands of diatomic molecules (halogen halides, CO), then, developing the theory for polyatomic molecules having a symmetry axis, discusses the infra-red spectra of CH_4, NH_3, HCN, CO_2, and H_2O. The treatment is good but rather brief. This is the only chapter in which polyatomic molecules are discussed.

Chapter IV, on "Electronic Bands," by Birge, constitutes more than half the Report. Sections 1–5 will be especially helpful to the experimentalist. Empirical relations and their theoretical interpretation are carefully distinguished. The methods by which quantum numbers are assigned and molecular energy levels are determined are fully discussed, with the help of many figures. Three methods for accurately evaluating molecular constants, for a band whose structure is known, are presented in section 5B (pp. 169–175). The analysis of several typical band spectra is critically discussed in section 5 (but the reader should note that later developments have considerably clarified the interpretation of these spectra; this is in part suggested in the footnotes).

The table of molecular constants with bibliography (section 7, pp. 230–2; cf. also pp. 132–3), the data in part newly computed by Birge, contains a mass of information. Energy level diagrams for CO, NO, O_2, and NO (but cf. p. 252) are given on p. 244. Vibrational intensity types (pp. 134–43) and their theoretical interpretation (pp. 248–9; and cf. Kemble, pp. 296–8) are discussed. Rotational intensity distribution is treated in section 6, but it should be men-

tioned that the subject is now in a much clearer state than when section 6 was written. Section 8 and many important footnotes elsewhere were added in order to bring the discussion as far as possible up to date. Section 8 includes on pp. 235–7 (cf. also pp. 112–113 and 173–4, and Chap. 7, pp. 293 et seq.) a discussion of the determination, from empirical molecular constants, of the effective law of force governing nuclear vibrations and rotations; on pp. 243–7, a brief review of the recent important work on the determination of heats of dissociation from band spectra; and on pp. 238–43 and 250 a discussion of recent work on molecular states and band structure (cf. also Chapter VII, especially pp. 326–31). Chapter IV might well have contained a fuller discussion of absorption spectra and a brief treatment of electronic bands of polyatomic molecules. In Chapter V Loomis gives a good discussion of the isotope effect in band spectra, and in Chapter VI, "Fluorescent Band Spectra," discusses in detail, as a typical example, the analysis of the visible "resonance spectrum" of iodine. A brief discussion of other fluorescent spectra, e. g. of the ultra-violet iodine resonance series (Oldenberg) and of the Na_2 bands, might well have been included here.

In Chapter VII Kemble first discusses the nature of the forces which hold molecules together (pp. 293–310), beginning with an analysis of the continuous distortion of electronic frequencies during the vibration of a molecule, with applications to the problem of vibrational intensity distribution in electronic band spectra. He then discusses the Kramers and Pauli molecular model (top with rigidly mounted gyroscope) and objections to it; then shows how the motions in an actual diatomic molecule can be treated by perturbation theory; then, develops the theory for a model with elastically mounted gyroscope (pp. 310–26). Pp. 326–31 contain an excellent review of Hund's important paper on molecular electronic state and band structure. There follows (pp. 331–53) a valuable discussion of the Zeeman effect in band spectra, with much new material (intensities of Zeeman components, theory of magnetic rotation in iodine bands, theory of CN doublets and their behavior in a magnetic field), and on pp. 353–6 a discussion of the Stark effect in band spectra and of dielectric constants of diatomic gases.

The faults of the Report are chiefly due to its having had the bad luck to be completed (1925–6) just before the advent of important advances. These may be classed under two heads (1) results of the application of the quantum mechanics (2) systematization of band structure types as a function of definite types of initial and final electronic states. As a result of these advances, many of the uncertainties and difficulties indicated in the Report have been removed; this the reader should bear in mind in using the Report. In the hope of assisting the reader, some of the main items of recent progress will be briefly indicated under the above two heads.

(1) The quantum mechanics, as is well known, introduces important new methods and view-points in the theory. It accounts for the apparent half quantum numbers (vibrational, rotational), but has brought no radical changes in respect to numerical values of molecular constants or energy levels. It gives at last a satisfying explanation (Heisenberg and Hund, see Hund, Zeits. f. Physik **40,** 742 and **42,** 93 (1927)), leading incidentally to interesting conclusions in regard to a possible nuclear spin, of the long puzzling phenomenon of alternating intensities in band lines. As Hund has shown in two extremely important papers (*l. c.*) it also permits a great step forward toward a solution of the problems of molecular structure,—specifically, toward an understanding of the electronic states of a molecule and of their relation to the electronic states of the constituent atoms.

(2) It now appears possible, on the basis of intensity relations, missing lines, number and nature of branches, etc. (provided the band structure can be sufficiently resolved), to classify band spectra of diatomic molecules under definite types each characteristic of a particular combination of initial and final electronic states (e. g. $^1P \rightarrow {}^1S$, $^2D \rightarrow {}^2D$, $\cdots$), for which rotational, vibrational, and (in part) electronic quantum numbers can be unambiguously specified. This development is foreshadowed in the Report (Chapter IV, section 8 and footnotes elsewhere; chapter VII, pp. 326–31, 345–6, etc.; cf. also articles by Kemble and the reviewer, Phys. Rev. 1926–7).

Pp. 358, numerous plates and figures. National Research Council, Washington, D. C. Price $4.00 (paper), $4.50 (cloth). ROBERT S. MULLIKEN

Handbuch der Physikalischen Optik. Edited by E. GEHRCKE. Vol. II, Second Half, First Part.—This part of volume II continues the treatment of modern or quantum optics. The first section is on band spectra. This seems to be too brief in view of the great recent activity in this field. It has, however, a good bibliography of 376 references to work published since 1909. These references are also tabulated according to the elements or compounds studied. The second section is on x-ray spectroscopy. It deals with the various experimental methods and gives tables of wave-lengths of lines and absorption edges observed in the K, L, and M series of many elements. The theory of x-ray spectra is discussed. The section on gamma rays also summarizes the recent numerical data and theories on the subject. The Zeeman effect is treated in masterly fashion by Zeeman and de Bruin. Some fine illustrations are given. It is unfortunate that the Faraday rotation and the transverse double refraction are not discussed for it seems that they will be omitted from the entire work. A section on the Stark effect naturally follows and the book closes with a discussion of atomic theories. This includes an introduction to the new matrix and wave mechanics and illustrates the latter by some simple applications. This volume provides a set of excellent summaries of the newer developments in physical optics, and it will be of great service to students and teachers of this subject. Pp. 388+vi, 112 Figs. Verlag von Johann Ambrosius Barth, Leipzig, 1927. Price 28RM. unbound. JOSEPH VALASEK

Spektoskopie und Kolorimetrie. I. LIFSCHITZ. Handbuch der Physikalischen Chemie, edited by George Bredig, Vol. V.—This volume gives a good practical account of spectrum analysis with emphasis on its application to chemical problems. The first section explains the various kinds of spectroscopes used for the different regions of the spectrum. Methods for measuring wave-lengths and intensities (spectrophotometry) are explained. The second section deals with the emission spectra of gases, liquids, and solids, and includes thermal radiation, fluorescence, and phosphorescence. The regularities observed in line and band spectra are discussed and the quantum theory of their origin is briefly reviewed. Methods of chemical analysis based on analysis of emission spectra are given. The third section deals with absorption spectra of gases, liquids, solutions, and solids. Much space is devoted to the interesting subject of the dependence of selective absorption on chemical constitution of organic as well as inorganic compounds. As the author points out, there is much work yet to be done before this problem is solved. The last section explains the principles and methods of colorimetry and nephelometry. For the physical chemist, especially, this will prove to be a good laboratory reference book. Pp. 325, 112 Figs., 1 Plate. Verlag von Johann Ambrosius Barth, Leipsig, 1927. Price 27RM. bound. JOSEPH VALASEK

X-rays Past and Present. V. E. PULLIN and W. J. WILTSHIRE.—This book has been written neither for the physicist nor for the x-ray specialist. The purpose of the book is well expressed by quoting from the authors' preface: "We have set out to tell the story of x-rays for the benefit of the interested and enquiring layman because we believe that no general account of this fascinating branch of science is so far available to him. We have attempted to sketch a panoramic view of the subject. . . ."

With the exception of the equation connecting wave-length, frequency and velocity and the Einstein photo-electric equation there is a complete absence of mathematical equations and formulas. The book is written in popular and entertaining style and, with few exceptions, the technical terms used are as familiar to the layman as those of modern radio. The exceptions occur when the authors discuss transfer of energy by means of radiation and so are led into using the terms of the quantum theory.

The scope of the book is best inferred from the table of contents: Chapter I, The Beginnings of Radiology; Chapter II, Röentgen's Discovery; Chapter III, The Nature of Visible Light; Chapter IV, Early X-Ray History; Chapter V, "Weighing" the Electron; Chapter VI, X-Rays in Progress; Chapter VII, X-Rays and the Atom; Chapter VIII, Remarks on Energy; Chapter IX, X-Rays and Crystals; Chapter X, Application of X-Ray Spectroscopy; Chapter XI, Early X-Ray Apparatus; Chapter XII, Early Applications of X-Rays; Chapter XIII, Modern

X-Ray Apparatus; Chapter XIV, Modern X-Ray Tubes; Chapter XV, X-Rays in Medicine and Surgery; Chapter XVI, X-Rays in Practice; Chapter XVII, X-Rays in Industry; Chapter XVIII, At Random; Index.

The last few chapters are concerned with the applications of x-rays in medicine and surgery and in industry. Several suggestions of new applications in industry are made. The book might well be read by the layman seeking a general knowledge of x-rays, by the medical man desiring to know more of the physical properties of x-rays, and by the industrialist and engineer seeking for new applications in industry. Pp. 229, 43 figs. Van Nostrand Company, New York, 1927. $4.50. G. E. M. JAUNCEY